(2)

AFWAL-TR-88-2025

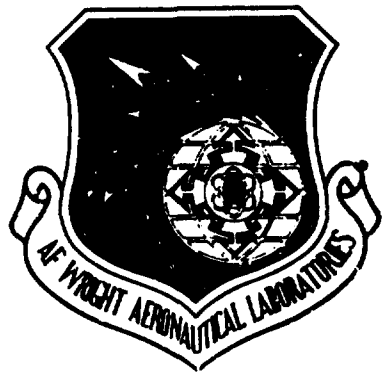

EXPERIMENTAL DETERMINATION OF THE FREQUENCY RESPONSE OF 0.020 INCH INSIDE DIAMETER TUBES AND VALIDATION OF A THEORETICAL MODEL

1Lt Larry A. Coleman
Technology Branch
Turbine Engine Division

April 1987

Final Report for Period February 1985 - April 1986

AERO PROPULSION LABORATORY
AIR FORCE WRIGHT AERONAUTICAL LABORATORIES
AIR FORCE SYSTEMS COMMAND
WRIGHT-PATTERSON AIR FORCE BASE, OHIO 45433-6563

NOTICE

WHEN GOVERNMENT DRAWINGS, SPECIFICATIONS, OR OTHER DATA ARE USED FOR ANY PURPOSE OTHER THAN IN CONNECTION WITH A DEFINITELY GOVERNMENT-RELATED PROCUREMENT, THE UNITED STATES GOVERNMENT INCURS NO RESPONSIBILITY OR ANY OBLIGATION WHATSOEVER. THE FACT THAT THE GOVERNMENT MAY HAVE FORMULATED OR IN ANY WAY SUPPLIED THE SAID DRAWINGS, SPECIFICATIONS, OR OTHER DATA, IS NOT TO BE REGARDED BY IMPLICATION, OR OTHERWISE IN any MANNER CONSTRUED, AS LICENSING THE HOLDER, OR ANY OTHER PERSON OR CORPORATION; OR AS CONVEYING ANY RIGHTS OR PERMISSION TO MANUFACTURE, USE, OR SELL ANY PATENTED INVENTION THAT MAY IN ANY WAY BE RELATED THERETO.

THIS REPORT HAS BEEN REVIEWED BY THE OFFICE OF PUBLIC AFFAIRS (ASD/PA) AND IS RELEASABLE TO THE NATIONAL TECHNICAL INFORMATION SERVICE (NTIS). AT NTIS IT WILL BE AVAILABLE TO THE GENERAL PUBLIC INCLUDING FOREIGN NATIONS.

THIS TECHNICAL REPORT HAS BEEN REVIEWED AND IS APPROVED FOR PUBLICATION.

Norman D. Poti

NORMAN D. POTI
TAM, Compressor Test Group
Technology Branch

Francis R. Ostdiek

FRANCIS R. OSTDIEK
Chief, Technology Branch
Turbine Engine Division

FOR THE COMMANDER

James S. Petty

JAMES S. PETTY
Acting Deputy for Technology
Turbine Engine Division
Aero Propulsion & Power Laboratory

IF YOUR ADDRESS HAS CHANGED, IF YOU WISH TO BE REMOVED FROM OUR MAILING LIST, OR IF THE ADDRESSEE IS NO LONGER EMPLOYED BY YOUR ORGANIZATION PLEASE NOTIFY WRDC/POTX, WRIGHT-PATTERSON AFB, OH 45433-6563 TO HELP MAINTAIN A CURRENT MAILING LIST.

COPIES OF THIS REPORT SHOULD NOT BE RETURNED UNLESS RETURN IS REQUIRED BY SECURITY CONSIDERATIONS, CONTRACTUAL OBLIGATIONS, OR NOTICE ON A SPECIFIC DOCUMENT.

SECURITY CLASSIFICATION OF THIS PAGE

REPORT DOCUMENTATION PAGE

Form Approved OMB No. 0704-0188

1a REPORT SECURITY CLASSIFICATION: UNCLASSIFIED	1b. RESTRICTIVE MARKINGS
2a SECURITY CLASSIFICATION AUTHORITY	3. DISTRIBUTION/AVAILABILITY OF REPORT: APPROVED FOR PUBLIC RELEASE: DISTRIBUTION UNLIMITED
2b DECLASSIFICATION/DOWNGRADING SCHEDULE	
4 PERFORMING ORGANIZATION REPORT NUMBER(S): AFWAL-TR-88-2025	5. MONITORING ORGANIZATION REPORT NUMBER(S)
6a. NAME OF PERFORMING ORGANIZATION: AERO PROPULSION LABORATORY; 6b. OFFICE SYMBOL (If applicable): AFWAL/POTX	7a. NAME OF MONITORING ORGANIZATION
6c. ADDRESS (City, State, and ZIP Code): AIR FORCE WRIGHT AERONAUTICAL LABORATORIES, WRIGHT-PATTERSON AFB, OHIO 45433	7b. ADDRESS (City, State, and ZIP Code)
8a. NAME OF FUNDING/SPONSORING ORGANIZATION: AERO PROPULSION LABORATORY; 8b. OFFICE SYMBOL (If applicable): AFWAL/POTX	9. PROCUREMENT INSTRUMENT IDENTIFICATION NUMBER
8c. ADDRESS (City, State, and ZIP Code): AERO PROPULSION LABORATORY, AIR FORCE WRIGHT AERONAUTICAL LABORATORIES, WRIGHT-PATTERSON AFB, OHIO 45433	10. SOURCE OF FUNDING NUMBERS: PROGRAM ELEMENT NO. 62203F; PROJECT NO. 3066; TASK NO 17; WORK UNIT ACCESSION NO. 54

11 TITLE (Include Security Classification)
EXPERIMENTAL DETERMINATION OF THE FREQUENCY RESPONSE OF 0.020-INCH INSIDE DIAMETER TUBES AND VALIDATION OF A THEORETICAL MODEL

12. PERSONAL AUTHOR(S)
1LT COLEMAN, LARRY A.

13a. TYPE OF REPORT	13b. TIME COVERED	14. DATE OF REPORT (Year, Month, Day)	15. PAGE COUNT
FINAL	FROM Feb 85 TO Apr 86	87 April	231.

16. SUPPLEMENTARY NOTATION

17 COSATI CODES			18. SUBJECT TERMS (Continue on reverse if necessary and identify by block number)
FIELD	GROUP	SUB-GROUP	FREQUENCY RESPONSE, PHASE SHIFT, AMPLITUDE RESPONSE, DYNAMIC PRESSURE MEASUREMENT, CRF/F100 Test, Compressor

19. ABSTRACT (Continue on reverse if necessary and identify by block number)

The Compressor Research Facility (CRF) of the Aero Propulsion Laboratory's Turbine Engine Division at Wright-Patterson AFB, Ohio will perform a rig test of an F100 High-Pressure Compressor in 1987. One of the highlights of this test will be the acquisition of post-stall performance data. Close-coupled and high-response instrumentation will be used to make the necessary dynamic pressure measurements.

This report describes the experimental effort to determine the frequency response of the close-coupled pressure instrumentation on the CRF/F100 compressor rig. Experiments were conducted on various lengths of the 0.020-inch-inside-diameter steel tubing used to connect the test article pressure probes to Scanivalve ZOC14 pressure transducers. From these experiments, transfer functions were obtained describing the amplitude response and phase shift characteristics for several tube lengths as a function of the input pressure oscillaton frequency.

After obtaining experimental results for these small-diameter tubes a comparison was (back)

20 DISTRIBUTION/AVAILABILITY OF ABSTRACT	21. ABSTRACT SECURITY CLASSIFICATION
☒ UNCLASSIFIED/UNLIMITED ☐ SAME AS RPT ☐ DTIC USERS	UNCLASSIFIED

22a NAME OF RESPONSIBLE INDIVIDUAL	22b. TELEPHONE (Include Area Code)	22c. OFFICE SYMBOL
LARRY A. COLEMAN	(513) 255-4141	AFWAL/POTX

DD Form 1473, JUN 86 — Previous editions are obsolete. — SECURITY CLASSIFICATION OF THIS PAGE

made between the experimental data and the frequency response predictions based on the theory developed by Bergh and Tijdeman. Comparisons were favorable, indicating that the theory can predict the amplitude response of 0.020-inch inside diameter tubes within 12 to 15 percent, and phase shift within approximately 10 to 15 degrees, depending on the tube length and the mean pressure in the tube.

Given the excellent correlation of experimental and theoretical results, the theory is suitable for estimating the frequency response characteristics of all tube lengths used on the CRF/F100 rig. This is very important to the posttest analysis of the CRF/F100 data, since transfer functions could not be determined experimentally for every tube length or for every environmental operating condition. Thus the theory, which has been validated experimentally, can be used with a high degree of confidence to estimate the frequency response behavior of the CRF/F100 close-coupled pressure measurement instrumentation.

FOREWORD

This report documents an in-house experimental effort conducted in support of Work Unit 30661754, "CRF/F100 Test." This test of a highly instrumented F100 High-Pressure Compressor will be conducted in the Compressor Research Facility (CRF) by personnel of the Compressor Technology Branch (POTX). This report describes our effort to determine the frequency response characteristics of the close-coupled pressure measurement instrumentation on the CRF/F100 compressor rig. Experimental information on the response characteristics of this instrumentation will be used in conjunction with theoretical predictions to analyze the dynamic pressure measurements to be taken during poststall testing of the rig in the CRF.

The work reported in this document was performed during the period 1 February 1985 to 1 April 1986 by the author, 1Lt Larry A. Coleman (AFWAL/POTX), Project Engineer. The author submitted the report in April 1987.

The author wishes to thank Mr Douglas C. Rabe and Mr William W. Copenhaver for their technical assistance and direction at the outset of the project, particularly in the areas of defining the scope of the effort and outlining the objectives required. Special thanks to Capt Jeffery M. Dierksen for his invaluable technical guidance and advice throughout this project. Thanks also to these gentlemen for their technical review of this report.

Also, thanks to Mr Rich Delgado, Mr Paul Dunigan, and Mr Glen Boggs of the Technical Support Group for their assistance in preparing the equipment used in the experiments. In addition, thanks to Ms Kristine Webb for her clerical assistance in preparing this report, and to Mr John Cole (AAMRL) and Mr Keith Kettler (University of Dayton Research Institute) for the use of AAMRL equipment and facilities for portions of the experimental work.

TABLE OF CONTENTS

TABLE OF CONTENTS (cont.)

LIST OF ILLUSTRATIONS

LIST OF ILLUSTRATIONS (cont.)

LIST OF ILLUSTRATIONS (cont.)

LIST OF ILLUSTRATIONS (cont.)

LIST OF ILLUSTRATIONS (cont.)

LIST OF ILLUSTRATIONS (cont.)

LIST OF ILLUSTRATIONS (cont.)

LIST OF ILLUSTRATIONS (cont.)

LIST OF ILLUSTRATIONS (cont.)

LIST OF TABLES

LIST OF TABLES (cont.)

LIST OF TABLES (cont.)

SECTION I

INTRODUCTION

1. GENERAL

This report describes an in-house experiment conducted in support of Work Unit 30661754, "CRF/F100 Test." One of the primary objectives of the CRF/F100 High Pressure Compressor rig test is to obtain in-stall performance data. The interstage pressure measurement instrumentation has been designed to provide total pressure data that will characterize rotating stall in the rig. To accurately measure the nonsteady pressures which will be encountered during rotating stall, the interstage pressure instrumentation must have a frequency response on the order of 250 to 300 hertz or higher. This frequency response requirement is based on an expected rotating stall fundamental frequency of 50 to 60 hertz, and an estimate that the fundamental and first five harmonics of the dynamic pressure time history must be recorded during testing to allow for adequate characterization of the pressure during postprocessing. In the context of this report, the frequency response of the pressure measurement system is synonomous with the transfer function for the dynamic pressure, where the transfer function describes the amplitude response and phase shift associated with the system as a function of the pressure oscillation frequency.

Ideally, for the best frequency response possible, the pressure transducer would be placed right at the pressure measurement location. However, since this method is physically impractical for the CRF/F100 rig, the pressure transducers will be close-coupled to the measurement probes instead. With this method,the pressure transducers will be connected to the interstage

pressure probes using the shortest possible length tubing. The actual length of tubing needed to connect a given probe will depend on the routing of the tube within the compressor rig from the probe to the instrumentation boss on the outer case. These internal tube lengths were measured within plus or minus one-half inch by Air Force personnel during rig build-up. The length of tubing required external to the compressor rig will be minimized by optimum placement of the Scanivalve Zero-Operate-Calibrate (ZOC) pressure transducers. The expected range of overall tube lengths is 10.0 to 24.0 inches.

Inserting a length of tubing between the pressure probe and the pressure transducer alters the dynamic pressure signal. Depending on the length and diameter of the tube, the measured pressure signal may either be amplified or attenuated as it passes through the tube. A phase lag is also incurred due to the tube length. Therefore, the dynamic pressure signal at the transducer end of the tube is not, in general, the same pressure signal sensed originally at the probe end of the tube.

Theoretical methods have been developed to predict the effects of tube length on dynamic pressure signals. Using information provided by these theoretical predictions, it is possible to convert the modified or distorted pressure signal present at the transducer back into the actual pressure signal sensed by the pressure probe. A method such as this will be needed for the CRF/F100 test to eliminate the effects of the tubing used to close-couple the interstage pressure probes and transducers. Only then will the interstage pressures be determined accurately enough to characterize rotating stall in the compressor rig.

Of course, the accuracy of the theoretical prediction for the frequency response behavior of a given tube is critical to the successful transformation of a pressure signal back into its original form. Therefore, the work described in this report was performed to experimentally determine the effects of various lengths of 0.020-inch inside diameter tube lengths inserted between an input pressure source and a pressure transducer. The results of these experiments were used, in turn, to assess the validity of the theoretical prediction method intended for use in the CRF/F100 test program.

2. OBJECTIVES

The objectives of this experimental program are threefold. The first objective is to obtain experimental data describing the effects various lengths of 0.020-inch-inside-diameter tubing have on a dynamic pressure signal. From the experimental data obtained for each tube length tested, we generated a transfer function which provides the relationship between the sinusoidal input pressure signal and the output pressure signal at the transducer end of the tube.

Similar work has been done in this area by several investigators including Bergh and Tijdeman (Ref 1), Nyland, et al. (Ref 2), Gerlach and Johnson (Ref 3), and Chapin (Ref 4). Even though the previous experimental work was general in nature and several tube lengths, tube diameters, and transducer volumes were tested, none of these experiments tested the 0.020-inch-inside-diameter tube which is of particular interest to the CRF/F100 test program. Consequently, the experimental program described in this report focuses on satisfying the need for experimental data for this specific tube diameter.

The second objective of the experiment is to determine the validity of theoretical predictions of frequency response in small diameter tubes. The analytical model with which the experimental data is compared is a computer program written by NASA and published in the report by Nyland, et al. (Ref 2). The calculations performed by the program are based on the frequency response theory developed by Bergh and Tijdeman (Ref 1). Bergh and Tijdeman reported favorable comparison between experimental data and theoretical predictions for tube diameters of 0.0394 to 0.0984 inch with tube lengths ranging from 19.69 to 153.94 inch. Also, Nyland reported excellent agreement between theory and experiment for tubes 1 inch in length with diameters of 0.063 and 0.128 inch. These results indicate that agreement between theoretical predictions and experimental data is possible over a fairly wide range of tube geometry. The specific objective in the current experiment was to determine the validity of the computer program predictions for a fixed diameter of 0.020 inch, over a range of lengths from 10.0 to 24.0 inches.

The final objective of the experiment is to develop an accurate model for the ZOC transducer which can be used in the NASA program. Early attempts to compare theory with experimental data revealed the sensitivity of the theoretical results to transducer geometry--particularly internal volume. For the Scanivalve ZOC transducer used in the experiment, the published values for volume, and internal tubing diameter and length, were inadequate for use in the computer program. Whenever these values are used as inputs to the program, comparisons to experimental data are generally poor. On the other hand, if the experiment is repeated using a different type of transducer for which the volume and internal geometry are accurately known, comparison with the experimental data is favorable. For example, for a 10.0-inch tube with a

pressure ratio of 1.8349, the experimental peak amplitude ratio, using the ZOC transducer, is 1.19 at a frequency of 120 hertz. Using the manufacturer's specifications to model the ZOC, the theory predicted an amplitude ratio of 1.35 for the same frequency, for a difference of 13 percent. However, when repeating the experiment using a DRUCK test transducer the difference between the experimental and theoretical values at the peak amplitude ratio frequency is only 4.4 percent. Thus, it seemes the specifications published by the manufacturer for the ZOC transducer are obviously not appropriate for frequency response considerations. As a result, the final objective of this experiment is to identify a combination of transducer internal geometry that will accurately model the Scanivalve ZOC transducer.

SECTION II

THEORETICAL PREDICTION OF FREQUENCY RESPONSE

1. GENERAL

Analytical prediction of the frequency response of the small diameter tubes tested in this experiment is based on the theory developed by Bergh and Tijdeman (Ref 1). In their report, the authors develop a general recursion formula for the dynamic response of a set of tubes and transducer volumes connected in series, as shown in Figure 1. The recursion formula is obtained from a linearized solution of the Navier-Stokes equations, the continuity and energy equations, and an equation of state. The solution is based on a tube/volume system with a sinusoidal pressure input. The assumptions used to linearize the flow equations are (1) very small sinusoidal pressure disturbances, (2) a small internal tube diameter in comparison to tube length, and (3) laminar flow throughout the system. The detailed mathematical derivation of the recursion formula is treated in Reference 1.

The formula derived by Bergh and Tijdeman for the prediction of frequency response in a set of series-connected tubes and volumes was converted into a set of FORTRAN subroutines by NASA (Ref 2). Driven by the steering program developed in-house to provide the necessary inputs for each experimental case, the NASA subroutines perform all the calculations necessary to produce a theoretical prediction of the frequency response.

2. NASA COMPUTER PROGRAM

The subroutines written by NASA, together with the steering program used to implement these subroutines, will be referred to throughout the remainder

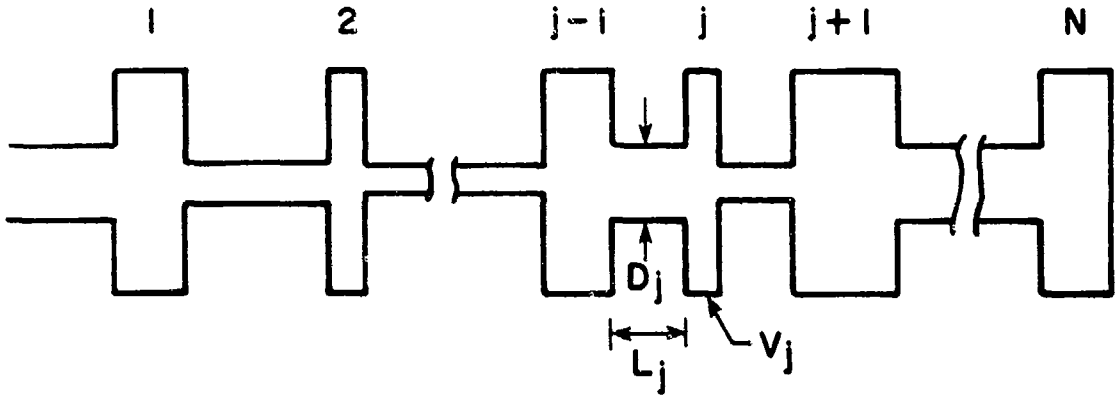

L_j - LENGTH OF jth TUBE

D_j - DIAMETER OF jth TUBE

V_j - VOLUME OF jth TRANSDUCER

FIGURE 1. Series Connection of Tubes and Volumes for Use with the General Recursion Formula

of this report as simply "the NASA program." The NASA program represents the FORTRAN source code necessary to solve the Bergh and Tijdeman recursion relation, which is given by

$$\frac{P_j}{P_{j-1}} = \left[\cosh(\phi_j L_j) + \frac{V_{vj}}{V_{tj}}(1+\sigma_j) n_j \phi_j L_j \sinh(\phi_j L_j) + \frac{D_{j-1}^2 \phi_{j-1} J_2(\alpha_{j-1}) J_0(\alpha_j) \sinh(\phi_j L_j)}{D_j^2 \phi_j J_0(\alpha_{j-1}) J_2(\alpha_j) \sinh(\phi_{j-1} L_{j-1})} \left(\cosh(\phi_{j-1} L_{j-1}) - \frac{P_{j+1}}{P_j} \right) \right]^{-1} \quad (1)$$

where the variables , , and n are defined as

$$\phi_j = \frac{\omega}{\left(\frac{\gamma P_s}{\rho_{sj}}\right)^{\frac{1}{2}}} \left(\frac{J_0(\alpha_j)}{J_2(\alpha_j)} \right)^{\frac{1}{2}} \left(\frac{\gamma}{n_j} \right)^{\frac{1}{2}} \quad (2)$$

$$\alpha_j = i^{\frac{3}{2}} \left(\frac{\omega D_j^2 \rho_{sj}}{4 \mu_j} \right)^{\frac{1}{2}} \quad (3)$$

$$n_j = \frac{1}{1 + \frac{\gamma - 1}{\gamma} \cdot \frac{J_2(\alpha_j \sqrt{Pr})}{J_0(\alpha_j \sqrt{Pr})}} \quad (4)$$

The variables used in Equation (1) are defined in Table 1 together with their equivalent FORTRAN variable names.

Inputs to the program for a particular experimental case are provided in the steering program through two labelled common blocks and the call to subroutine AMPPHS. Labelled common block GEOMTY contains four one-dimensional arrays of 10 elements each. These arrays are used to specify the tube diameter (D), tube length (XL), transducer volume (V), and transducer volumetric displacement (DVDP) for a maximum system of 10 tubes and volumes.

The thermodynamic properties are input through labelled common block THERMO. The ratio of specific heats (GAMMA) and the mean pressure in the tube (AMPRES) are passed to the other subroutines through this common block. In addition, the Prandtl number (P), fluid density (RHO), and dynamic viscosity (VIS) are 10 element, one-dimensional arrays contained within the THERMO common block.

Table 1. Definition of Variables used in Equation (1)

Variable in EQN (1)	FORTRAN Variable Name	Definition
J	I	Number of the tube or volume
ω	-	Angular frequency (2 f)
f	FREQ	Frequency of the input pressure oscillations
D	D	Tube diameter
J_n	-	Bessel function of the first kind of order "n"
L	XL	Tube length
p	-	Amplitude of the pressure oscillations
Pr	P	Prandtl number
P_s	AMPRES	Mean pressure in the tube
V_t	-	Tube volume
V_v	V	Transducer volume
γ	GAMMA	Ratio of specific heats
μ	VIS	Dynamic viscosity
ρ_s	RHO	Air density
σ	DVDP	Dimensionless increase in transducer volume due to internal wall deflection
-	N	Total number of tube/volume combinations

The only other inputs needed in the program are provided in the call to subroutine AMPPHS. The call statement is

```
CALL AMPPHS (FREQ,A,PA,I,N)
```

The arguments are the pressure oscillation frequency (FREQ), the number of the tube/volume combination for which frequency response information is desired (I), and the total number of tube/volume combinations making up the system (N). Subroutine AMPPHS returns the solution of the Bergh-Tijdeman equation for the Ith tube and volume through the variables A and PA. A is the pressure ratio or amplitude ratio, P(I)/P(0), where P(0) is the amplitude of the sinusoidal input pressure at the inlet of the first tube, and P(I) is the amplitude of the pressure disturbance in the Ith tube/volume. PA is the phase angle between the pressure signal at the input of the first tube and that of the Ith tube/volume.

Using the steering program to provide the inputs just described, the frequency response of a given tube/volume combination can be determined from a single call of subroutine AMPPHS. AMPPHS makes all the subsequent calls to the other subroutines and function subprograms needed to produce the final result. A listing of the steering program and NASA subroutines used to provide the theoretical frequency response predictions contained in this report is given in Appendix A.

For the purposes of this project, we assumed a Prandtl number of 0.7 and the ratio of specific heats set at 1.4 for all cases. We assumed a transducer volumetric displacement of zero. This is a valid assumption as long as the diaphragm deflection is a very small part of the total transducer volume. The

fluid viscosity was calculated in the steering program for each experimental case from Sutherland's equation, using room temperature as the input. We determined the density for each case by treating the air in the tube as a perfect gas. The reference temperature used in Sutherland's equation and the perfect gas equation of state was 530 degrees Rankine.

The steering program determined the frequency response characteristics of a given tube/volume configuration over a specific frequency range of interest. We accomplished this by placing a statement to increment the oscillation frequency inside a DO loop, followed by the call to subroutine AMPPHS. For most of the cases in this experiment, the loop was set to provide a frequency range from 10 to 200 hertz in increments of 10 hertz. This provided theoretical frequency response information at frequencies matching those for which the experimental data was taken. Thus, it was possible to make a direct comparison between experimental data and theoretical predictions for a given test condition and tube/volume configuration.

Before using the NASA program for comparison with experimental data, we compared the program with the results of another theoretical approach based on characteristic impedances. The sample case used for this comparison was reported in Reference 6. The development of the theory based on characteristic impedances is treated in Reference 3.

The comparison was made for a 6.0 inch tube length with an inside diameter of 0.030 inch. The predictions from each theoretical approach are shown in Figure 2. Essentially identical results were obtained from both theoretical methods. The excellent comparison between these two theoretical approaches provided a high degree of confidence in the Bergh and Tijdeman theory, and its implementation in the NASA program.

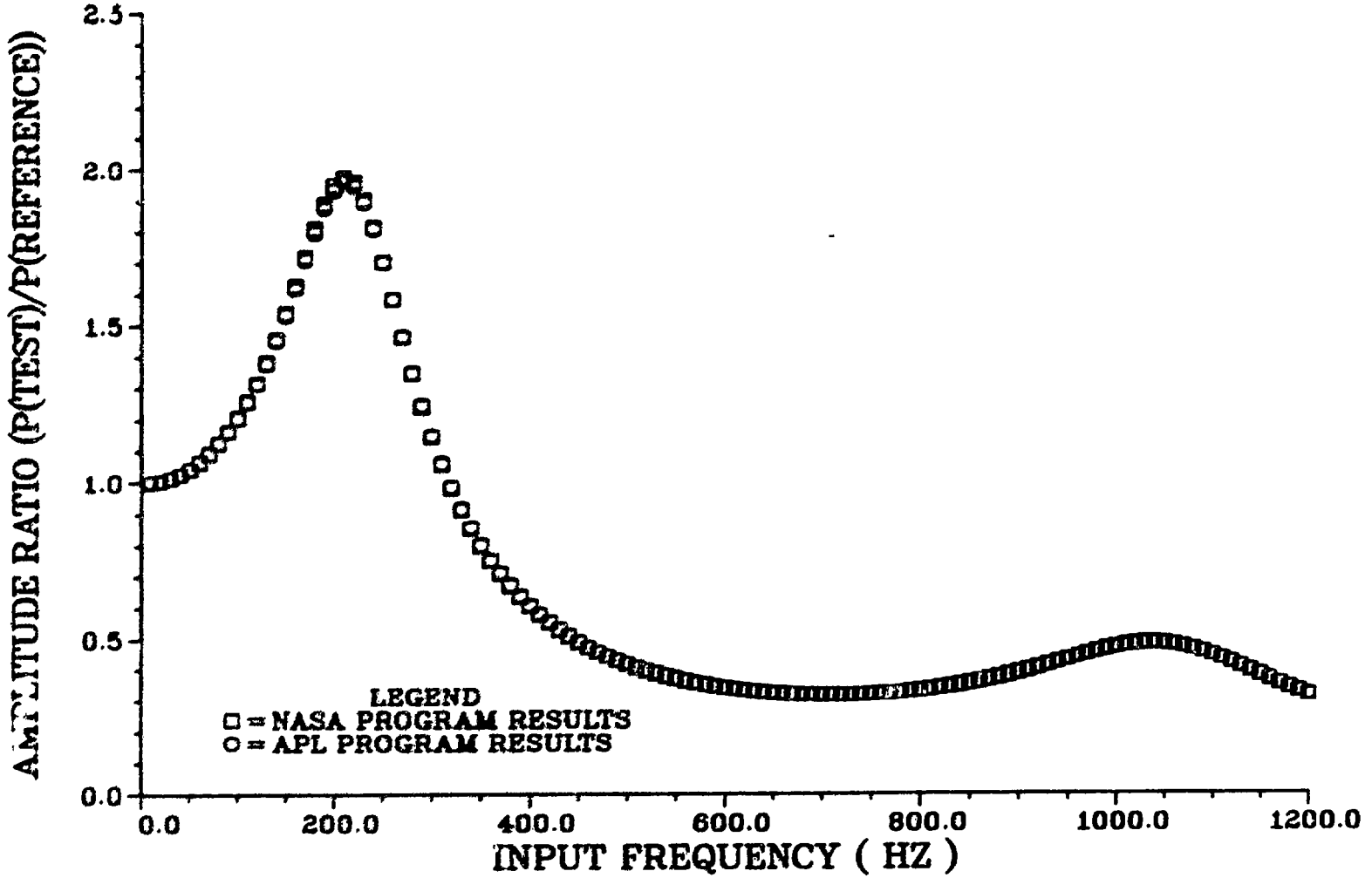

FIGURE 2. COMPARISON OF NASA AND APL PROGRAM RESULTS—PREDICTION OF THE FREQUENCY RESPONSE OF A 6.0 IN LONG, .030 IN ID TEST TUBE

SECTION III

EXPERIMENTAL DETERMINATION OF FREQUENCY RESPONSE - PHASE 1

1. GENERAL

The experimental work for this project was carried out in two phases. The source used to produce the oscillating pressure input signal was different for each phase. In fact, the second phase of the experimental work was undertaken to overcome some of the limitations of the oscillating pressure source and other apparatus used during the first phase of the experimental effort.

The objective of both experimental phases was the same, however--to determine the transfer function describing the relationship between input and output dynamic pressure signals in various lengths of 0.020-inch-inside-diameter tubing. This experimental data describing the gain and phase shift for a given tube was then compared to the theoretical predictions of frequency response generated by the NASA program. This comparison was made to validate the ability of the NASA program to accurately predict the frequency response behavior of 0.020-inch-inside-diameter tubes.

In the sections that follow, we describe the experimental setups used in both phases of the project. We discuss problems we encountered during the experiments, and the results from each experimental setup.

2. PHASE 1 EXPERIMENTAL SETUP

The first phase of the experimental work was conducted in Room 24, Building 18 of the Aero Propulsion Laboratory. A description of the experimental setup used for the experiments in Room 24 follows.

a. Experimental Apparatus and Data Acquisition Equipment

A block diagram of the basic experimental setup used in the Room 24 experiments is shown in Figure 3. The photograph in Figure 4 shows the actual hardware and data acquisition equipment. A close-up of a typical tube and transducer arrangement is shown in Figure 5.

In these experiments the oscillating pressure input signal was provided by the Fluidics Model AT31A Signal Generator. This device converts an electrical input signal into a pneumatic signal. The electrical input signal drives an electromechanical torque motor which in turn drives two flapper nozzles. By opening and closing the flapper nozzles, the air pressure supplied to the signal generator is modulated at the input frequency and an oscillating pneumatic signal is generated. For the experiments in Room 24, a Wavetek Model 134 oscillator was used to provide a sine wave input to the Fluidics signal generator over the frequency range from 10 to 200 hertz.

A DRUCK model PDCR 22 transducer with a range of 0 to 15 psig was connected to the output of the pneumatic signal generator to measure the input or reference pressure. The transducer in this location is referred to as the "reference transducer." The total distance from the output of the pneumatic signal generator to the reference transducer face is referred to as the "reference length" throughout the rest of this report.

Ideally the reference length should be zero to prevent any distortion of the pressure signal before it reaches the reference pressure measurement location. In the Room 24 experimental setup it was not possible to completely eliminate the reference length. This length was minimized, however, through the use of a modified DRUCK zero volume adapter.

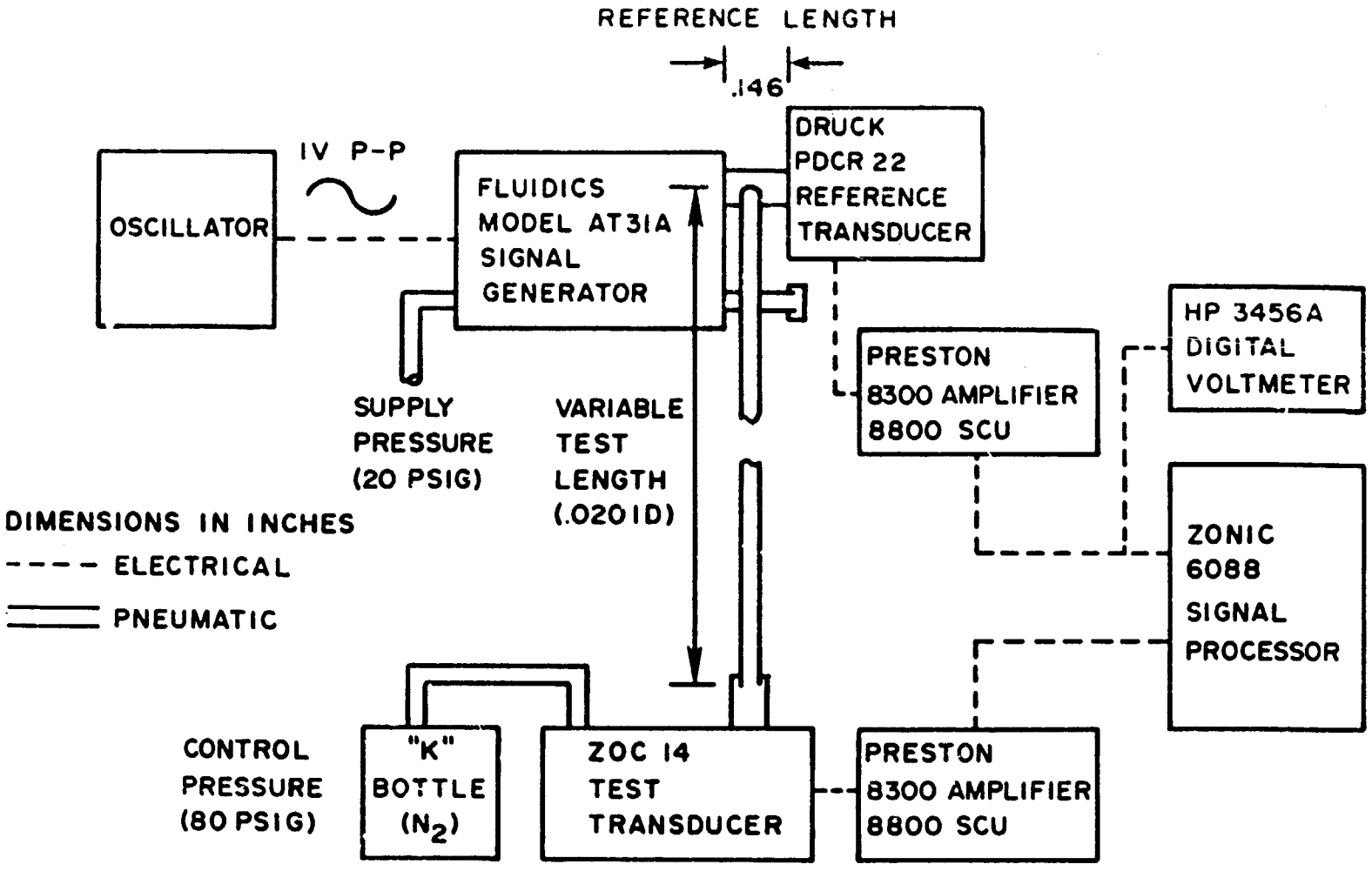

FIGURE 3. Schematic of the Room 24 Experimental Set-Up

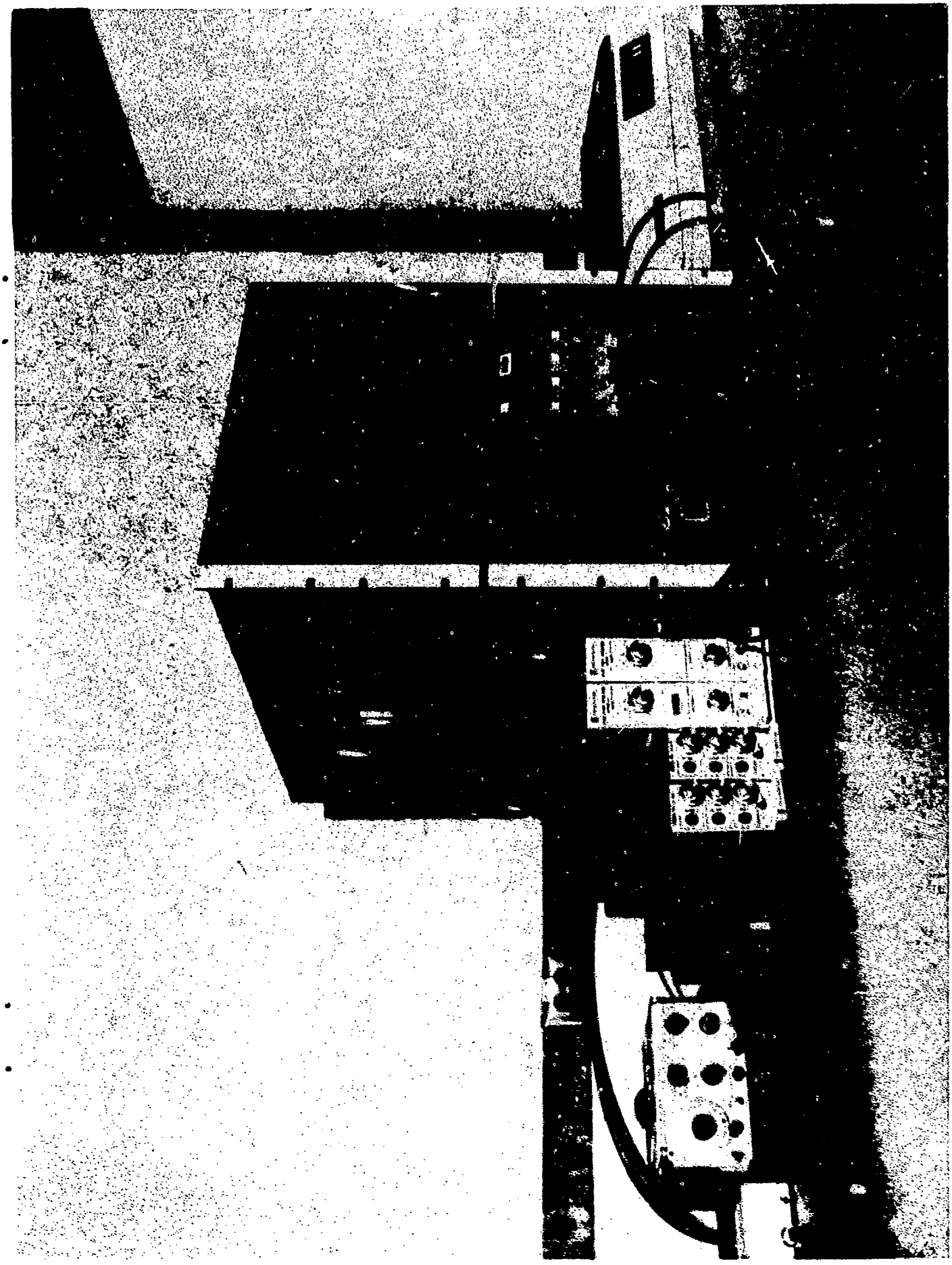

Figure 4. Hardware and Data Acquisition Equipment Used in the Room 24 Experiments

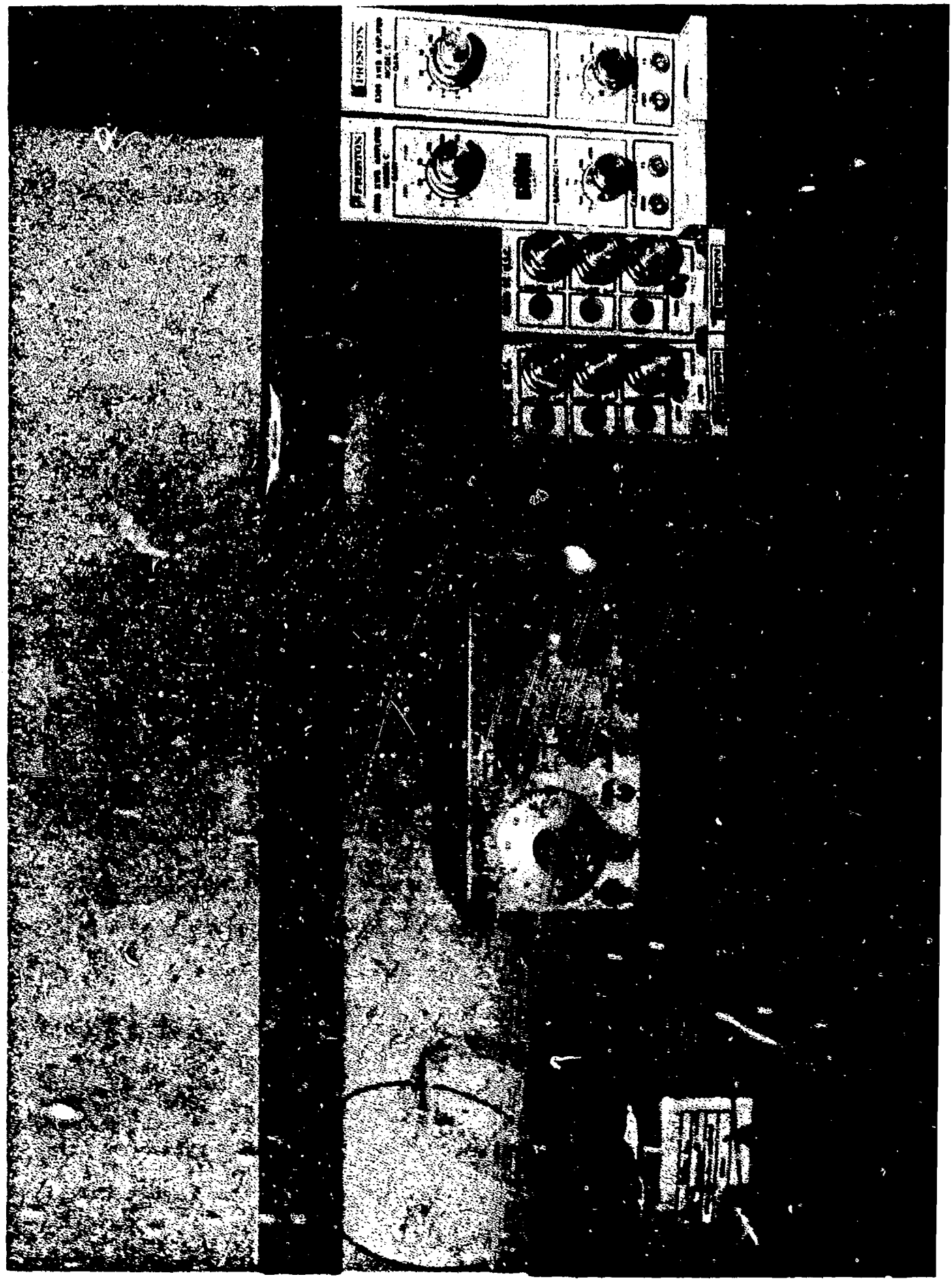

Figure 5. Typical Tube and Transducer Arrangement

The modified adapter is shown in Figure 6. The threaded end of the adapter screwed into one of the Fluidics signal generator output ports. The boss between the zero volume adapter housing and the threaded stud was drilled through on one side to provide a tee connection for the 0.020-inch-inside-diameter test tube. Figure 7 shows the details of the tee. The housing itself contained the DRUCK reference transducer. With this adapter the total reference length was less than 0.15 inch.

The length of 0.020-inch-inside-diameter tubing to be tested in the experiment was connected to the pneumatic signal generator output through the tee connection. This connection was sealed using epoxy glue. For most of the experiments the opposite end of the test tube was connected to one of the pressure measurement ports of a Scanivalve ZOC14 transducer. The range of the ZOC transducer was 0 to 5 psig. Near the end of the project a few experiments were conducted using a DRUCK transducer with a range of 0 to 15 psig in place of the ZOC. In both instances, heat shrink tubing was used to seal the connection at this end of the tube. The transducer at this end of the test tube is referred to as the "test transducer."

Another connection was made to the ZOC transducer to provide the necessary control for the transducer. A bottle of pressurized nitrogen was connected to the ZOC's Px CTL port, providing the 80 psig control pressure necessary to switch the transducer from calibrate mode to operate mode.

The electrical output of each reference and test transducer was connected to individual Preston 8300XWB Amplifiers and 8800SC Universal Signal Conditioners. The signals leaving the amplifier/signal conditioner arrangement were then connected to both the HP3456A digital voltmeter and the ZONIC 6088 Signal Processor. The HP3456A digital voltmeter was used to take

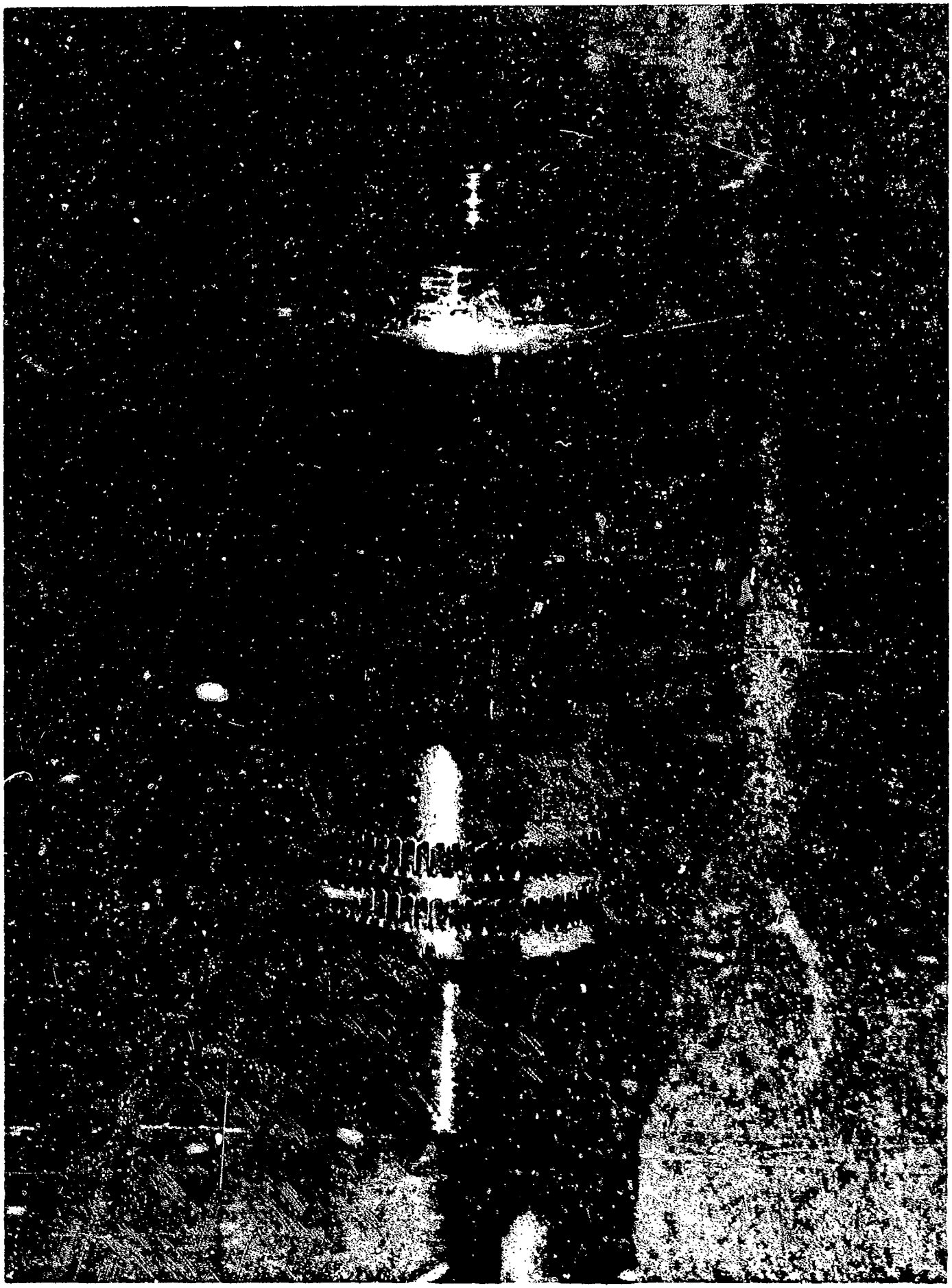

Figure 6. Modified DRUCK Zero Volume Adapter

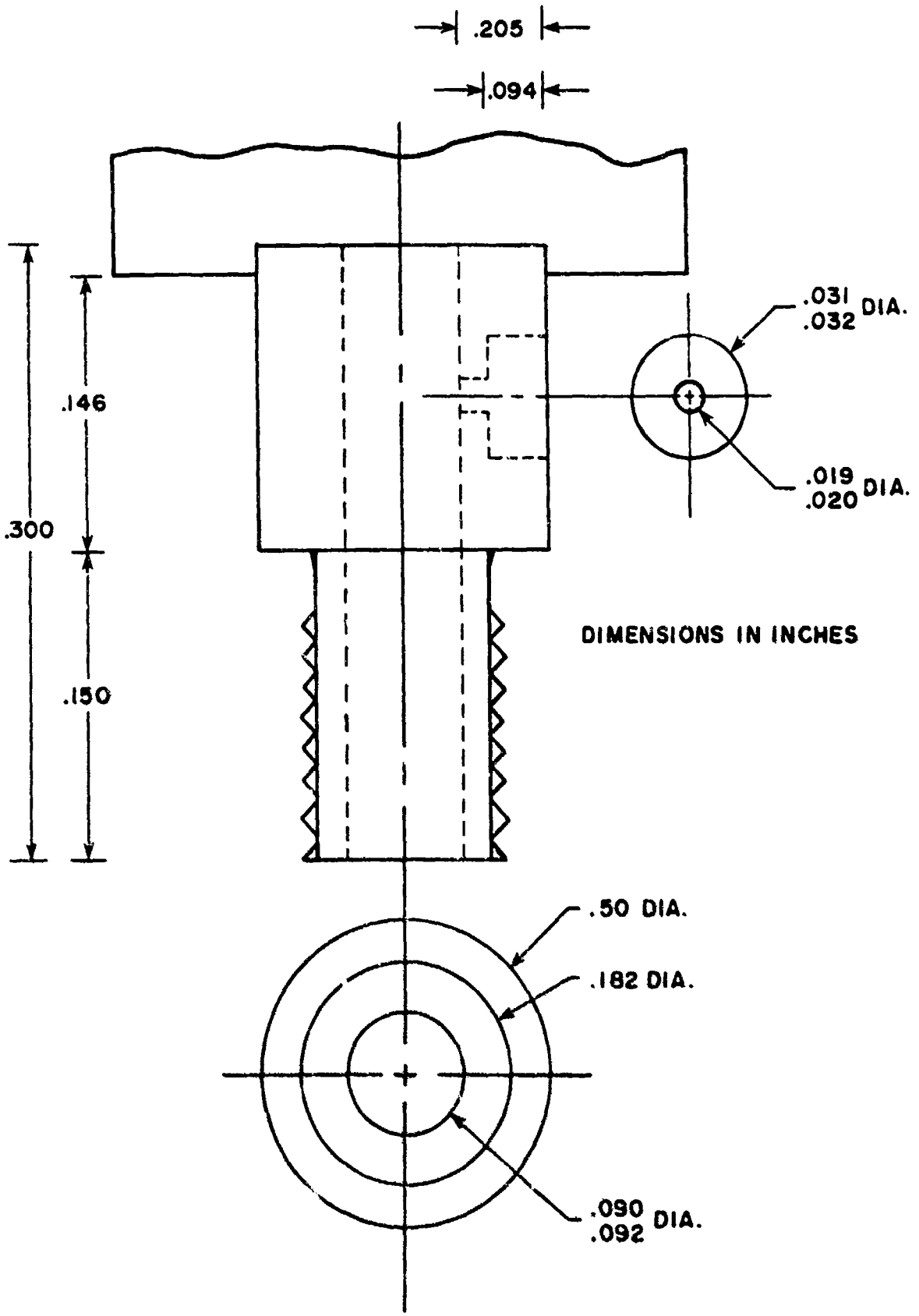

FIGURE 7. Schematic of the Modified Zero Volume Adapter

readings of the ac and dc output voltages of both transducers. The transducer outputs were also ac-coupled to the ZONIC 6088 signal processor for generating the transfer function.

The HP3456A digital voltmeter is capable of measuring both dc voltage and true RMS voltage, and it can perform several math functions as well. It can also be programmed to take a specified number of readings for each trigger input. These features were all used during the experiments. The voltmeter was set to take 50 readings per trigger and compute the average of these readings. This was done for both the ac and dc voltages from each transducer for every data point. The dc voltage readings provided a measure of the mean pressure in the tube, while the ac voltages indicated the RMS level of the dynamic pressure signal.

The ZONIC 6088 signal processor was used to determine the transfer function between the signals from the reference and test transducers. The transfer function was determined from an average of 10 ensembles of input data. Each ensemble of data represents a block of 1024 data samples of the respective transducer output voltage. For input frequencies up to 120 hertz the sampling rate is 320 samples per second per channel. For input frequencies from 130 to 200 hertz the sampling rate is 640 samples per second per channel. Data samples from the reference transducer are labelled as "Block 1 data" and data from the test transducer are denoted as "Block 2 data."

Before these blocks of time domain data are averaged, a weighting function is applied and a fast-Fourier transform (FFT) is performed to transform the data from the time domain to the frequency domain. This weighting function, also known as windowing, is applied to reduce the smearing

of the actual data which is likely to occur if there are large differences between the amplitudes of the first and last data points within a block. This smearing of the energy in the actual data into adjacent frequencies is termed "leakage." The weighting function which is applied to the actual data helps reduce the leakage inherent when data is transformed into the frequency domain. A complete discussion of the windowing technique used by the ZONIC signal processor can be found in Ref 7.

After the weighting function is applied, a FFT is performed. In this process, the two data blocks, each of which contain 1024 samples of time domain data, are transformed into 512 complex pairs of frequency domain data per block. As a final step in preparing the data for averaging, the signal processor calculated the autospectrum for Blocks 1 and 2, and the cross spectrum of Block 2 to 1. These three functions are used to calculate the averaged values. This entire process is repeated for 10 ensembles of input data.

Once the data averaging is completed for a given input frequency, the signal processor determines the transfer function, which is defined as

$$\text{Transfer function} = \frac{\text{Cross Spectrum of Block 2 to 1}}{\text{Autospectrum of Block 1}} \qquad (5)$$

where these spectra represent the averages for the 10 data ensembles. This transfer function can be displayed as a plot of amplitude ratio and phase shift versus frequency. A sample plot of the transfer function is shown in Figure 8. The signal processor also generates a table of the amplitude ratio

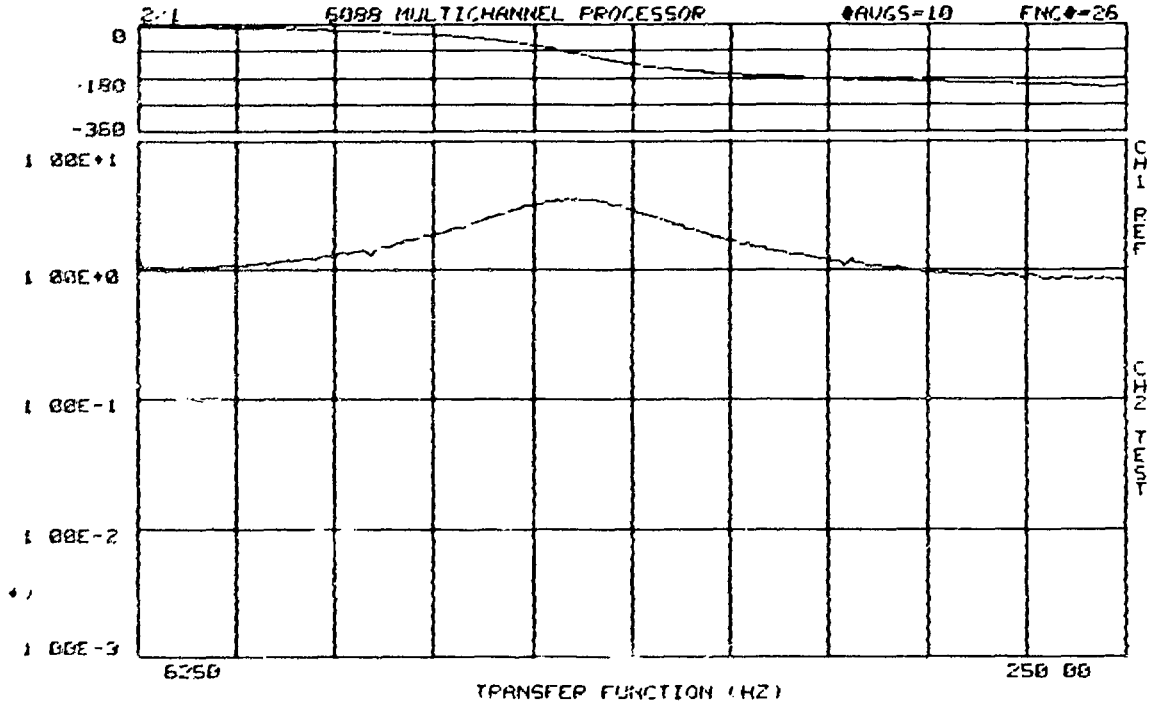

FIGURE 8. A Typical Transfer Function Display from the ZONIC Signal Processor

and phase shift values as a function of frequency. These features were both used during the experiments to determine the magnitude and phase shift of the transfer function at the given input frequency.

b. Experimental Procedures

Before acquiring any experimental data, two preliminary tasks were completed. First, the reference and test transducers were calibrated to determine the slope and zero offset for each transducer. In addition to this initial calibration, both transducers were calibrated again later in the project. The details of the calibration procedure are provided in Appendix B along with listings of the calibration data and plots of the calibration curves. Another preliminary task was the development of a program to automate the repetitive process of acquiring data with the ZONIC signal processor. We began the experimental work after completion of these preliminary details. Each experiment was conducted as follows:

1. Air pressure was applied to the Fluidics signal generator input. All experiments were done twice; once with a 20 psig input pressure and again with a 10 psig input pressure. The 20 psig input pressure was the upper limit for the Fluidics signal generator.

2. The amplitude of the oscillator sine wave output was adjusted to one volt RMS. This was the maximum allowable input signal level for the signal generator. This level was chosen because the RMS pressure level exhibited a tendency to fall off with increasing frequency. By choosing the maximum allowable input signal level, an adequate RMS pressure level could be maintained out to the upper frequency limit of 200 hertz.

3. The oscillator was adjusted to the desired frequency. The exact frequency of the oscillator signal was determined with the ZONIC signal processor from a display of the autospectrum for the reference transducer. A typical reference transducer spectrum is shown in Figure 9.

4. Once the input frequency was set, the data acquisition process was started by executing the control program written for the ZONIC. This program acquired and averaged the data, and then determined the transfer function. The transfer function was displayed on the screen momentarily for visual inspection. Then a table of the values comprising the transfer function was displayed. From this table the amplitude ratio and phase shift values for the given input frequency were selected and recorded.

5. The entire process was repeated for input frequencies from 10 to 200 hertz, using a 10 hertz increment.

6. After completing the experiments at both input pressures for a given tube length, one end of the tube was removed from the experimental apparatus and the tube was cut back to the next desired length. Initially, the tube was removed at the signal generator adapter by breaking the tube free from the epoxy glue. After this process was repeated a few times, however, the remaining length of tubing became quite bent from the force required to break the glue joint. To avoid this problem, the tube was removed at the test transducer end for subsequent experiments by simply removing the heat shrink tubing.

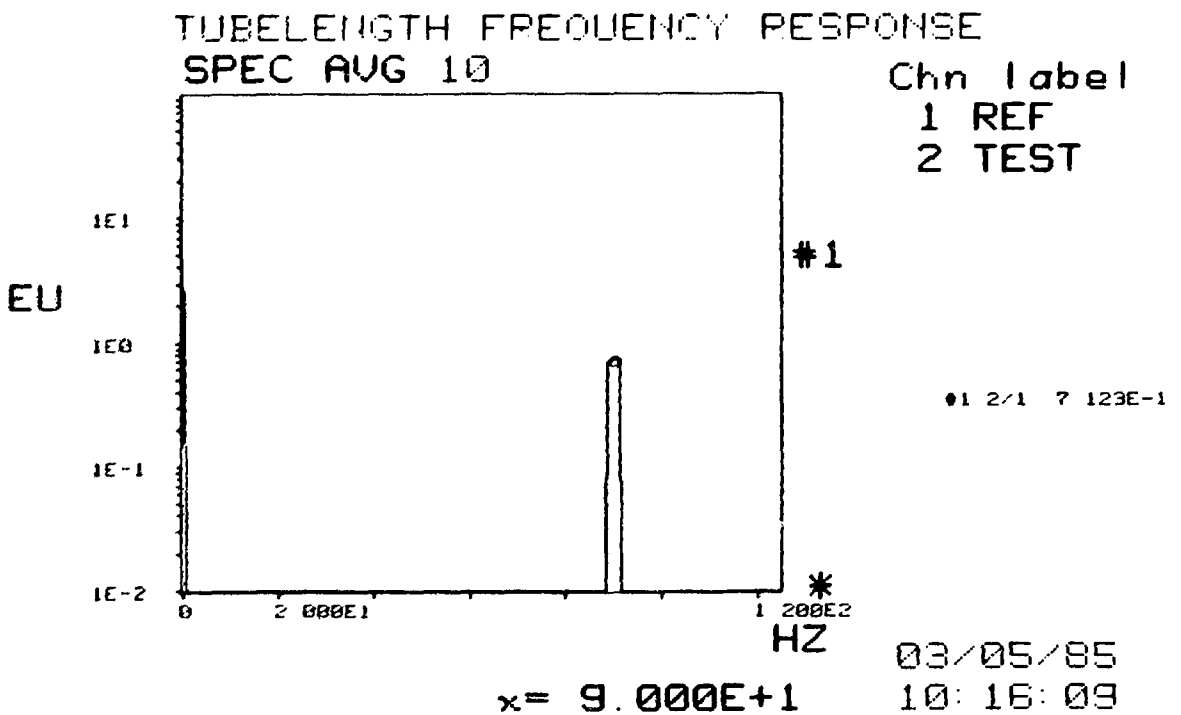

FIGURE 9. A Typical Average Spectrum Display for the Reference Transducer

c. Experimental Results and Comparison to Theoretical Predictions

During this phase a total of 18 experiments were completed. The individual test cases and test conditions are summarized in Table 2. The first 16 of these experiments were conducted using a ZOC14 transducer as the test transducer, while the last two experiments were completed using a DRUCK PDCR22 as the test transducer.

Table 2. Summary of the Phase 1 Experiments

Date	Tube Geometry			Pressure Ratio	Transducer Type	Tube Stock
	Ref Length (inches)	Length (inches)	Diameter (inches)	Mean Tube Pressure (psig)			
23 May 85	0.146	10.0	0.020	11.755	1.8244	ZOC	Original
24 May 85	0.146	10.0	0.020	5.54	1.3879	ZOC	Original
28 May 85	0.146	16.375	0.020	11.95	1.8383	ZOC	Original
28 May 85	0.146	16.375	0.020	5.632	1.3951	ZOC	Original
31 May 85	0.146	15.5	0.020	11.645	1.8250	ZOC	Original
31 May 85	0.146	15.5	0.020	5.519	1.3910	ZOC	Original
3 Jun 85	0.146	15.0	0.020	11.95	1.8395	ZOC	Original
4 Jun 85	0.146	15.0	0.020	5.695	1.3976	ZOC	Original
4 Jun 85	0.146	14.5	0.020	12.311	1.8598	ZOC	Original
4 Jun 85	0.146	14.5	0.020	5.722	1.3996	ZOC	Original
10 Jun 85	0.146	15.0	0.020	12.017	1.8405	ZOC	New
10 Jun 85	0.146	15.0	0.020	5.668	1.3964	ZOC	New
25 Jun 85	0.146	10.0	0.020	11.987	1.8349	ZOC	New
25 Jun 85	0.146	10.0	0.020	5.717	1.3982	ZOC	New
25 Jul 85	0.146	16.375	0.020	12.128	1.8486	ZOC	New
25 Jul 85	0.146	16.375	0.020	5.625	1.3936	ZOC	New
30 Aug 85	0.146	10.0	0.020	12.194	1.8531	DRUCK	New
24 Sep 85	0.146	24.0	0.020	12.248	1.8514	DRUCK	New

Test tube lengths were cut from two separate sources of tubing. Test lengths for the first ten experiments were cut from a 6.0 foot length of tubing which was on hand at the outset of the project. Later, a new supply of tubing stock was received and it was used to provide the test tube lengths for the remaining 8 experiments. To avoid confusion concerning the source of tubing used, the tubing used in the first ten experiments is referred to as the "original" tubing, while that used in the remainder of the experiments is denoted as the "new" tubing.

For each experiment, the NASA program was used to calculate the theoretical frequency response for the given tube and test conditions. In the presentation of results which follows the Room 24 experimental data is compared with the NASA program predictions.

(1) Experimental Results Using the ZOC14 Test Transducer

Experiments were conducted for test lengths of 10.0, 14.5, 15.0, 15.5, and 16.375 inches using the original tubing. The results of these experiments are shown in Figures 10-19. There are two plots for each tube length--one plot to display the amplitude ratio versus input frequency, and another plot showing the phase shift as a function of the input frequency. Note also that the experimental results for both the high pressure input and the low pressure input are shown on the same plot for a given tube length. This can be seen from the pressure ratio (PR) values given in the legend for each plot. The pressure ratio is defined as

$$PR = \frac{\text{Average gage pressure in tube + atmospheric pressure}}{\text{atmospheric pressure}} \quad (6)$$

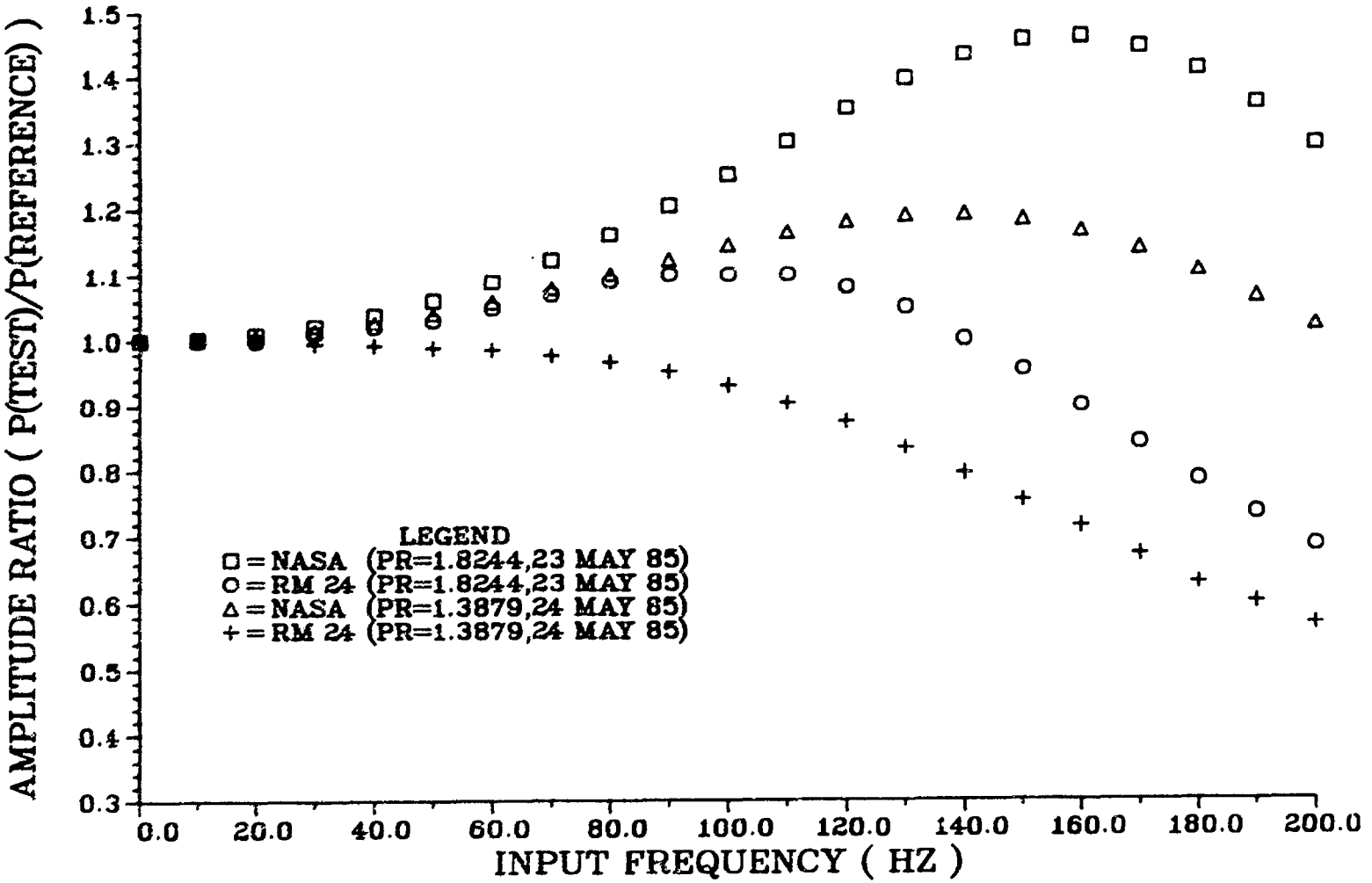

FIGURE 10. COMPARISON OF RM 24 EXPERIMENTAL DATA TO NASA PROGRAM FREQUENCY RESPONSE PREDICTIONS FOR A 10.0 IN. TUBE WITH .020 IN. ID

FIG10

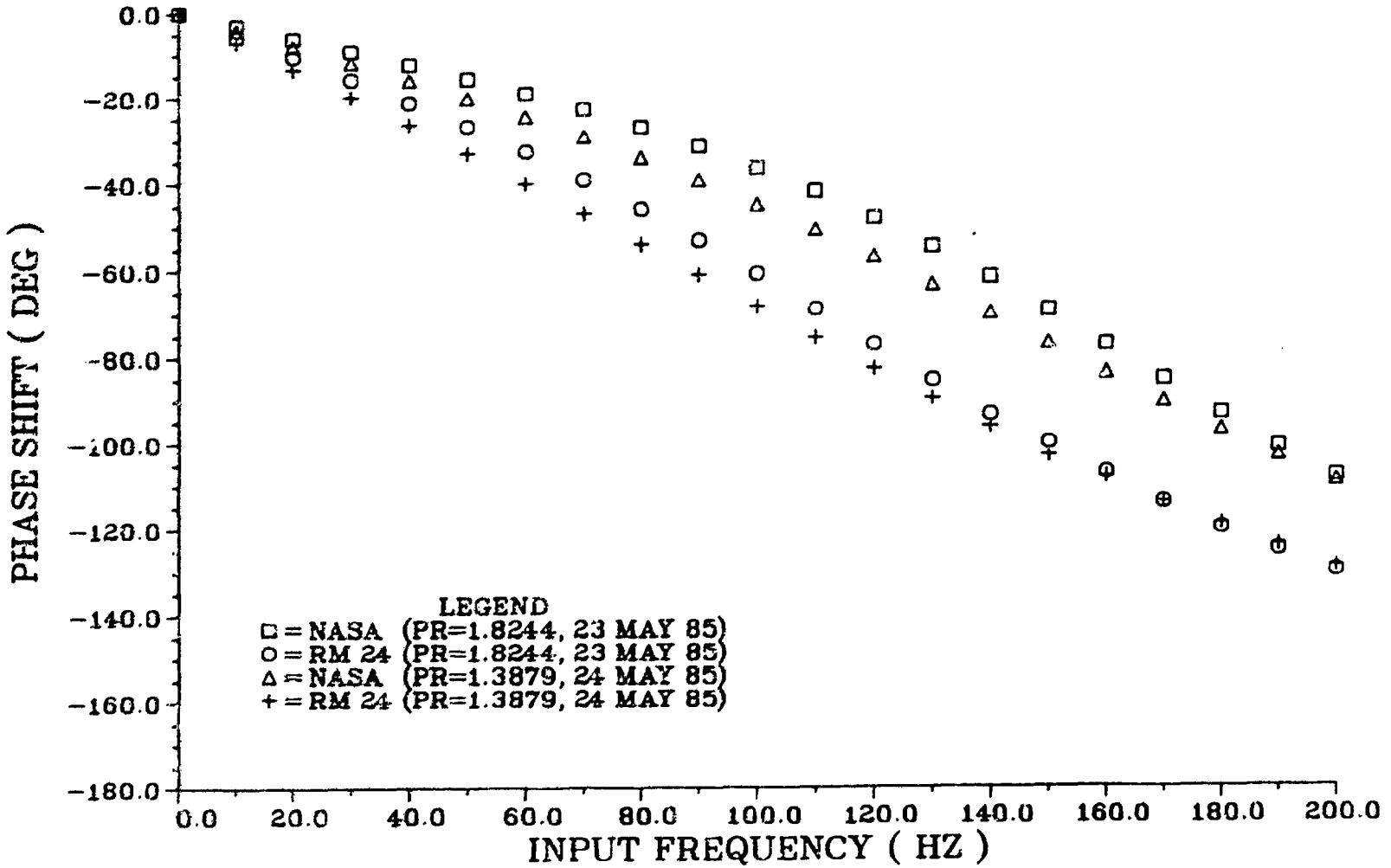

FIGURE 11. COMPARISON OF RM 24 EXPERIMENTAL DATA TO NASA PROGRAM FREQUENCY RESPONSE PREDICTIONS FOR A 10.0 IN. TUBE WITH .020 IN. ID

FIG11

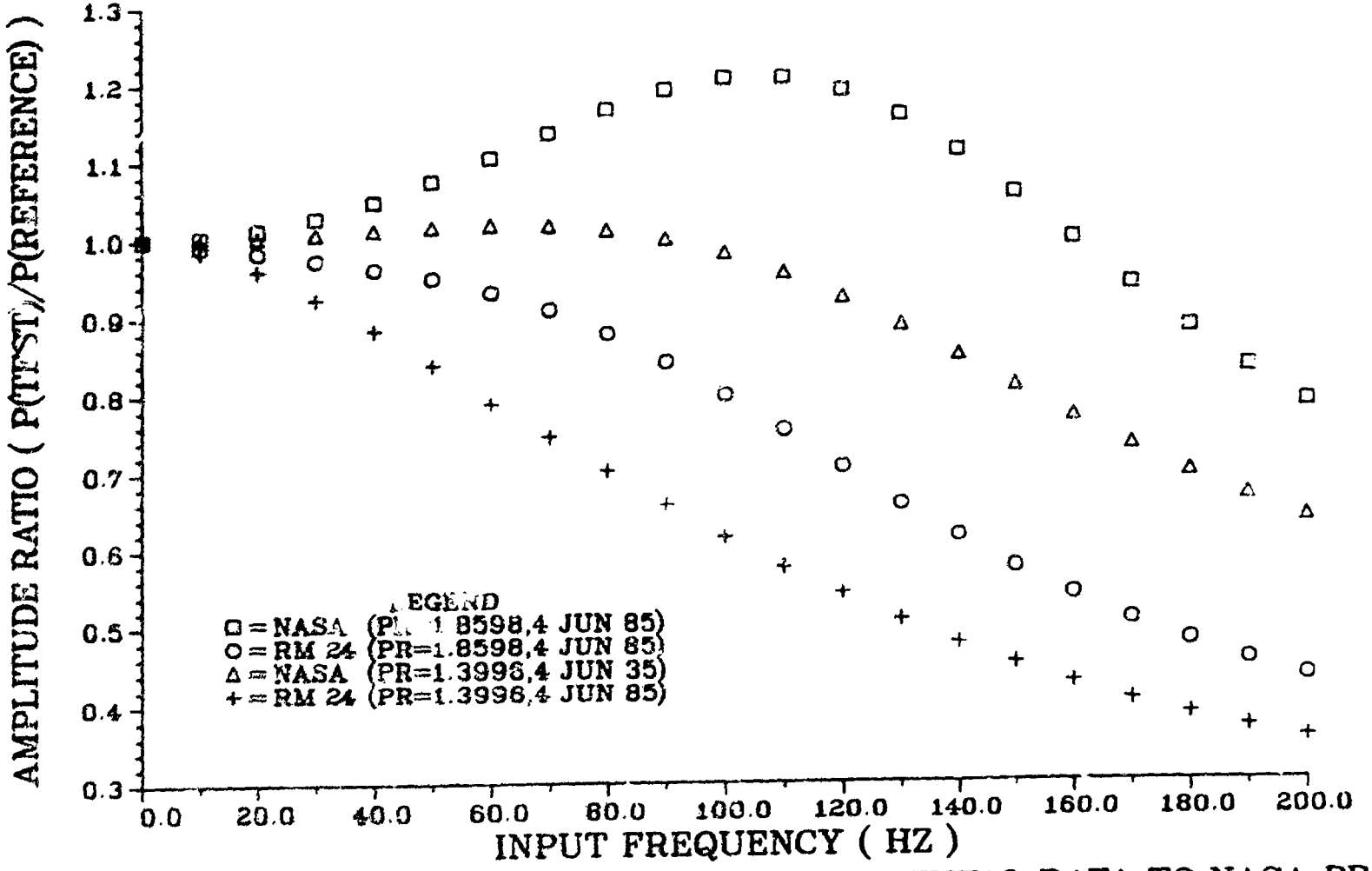

FIGURE 12. COMPARISON OF RM 24 EXPERIMENTAL DATA TO NASA PROGRAM FREQUENCY RESPONSE PREDICTIONS FOR A 14.5 IN. TUBE WITH .020 IN. ID

FIG12

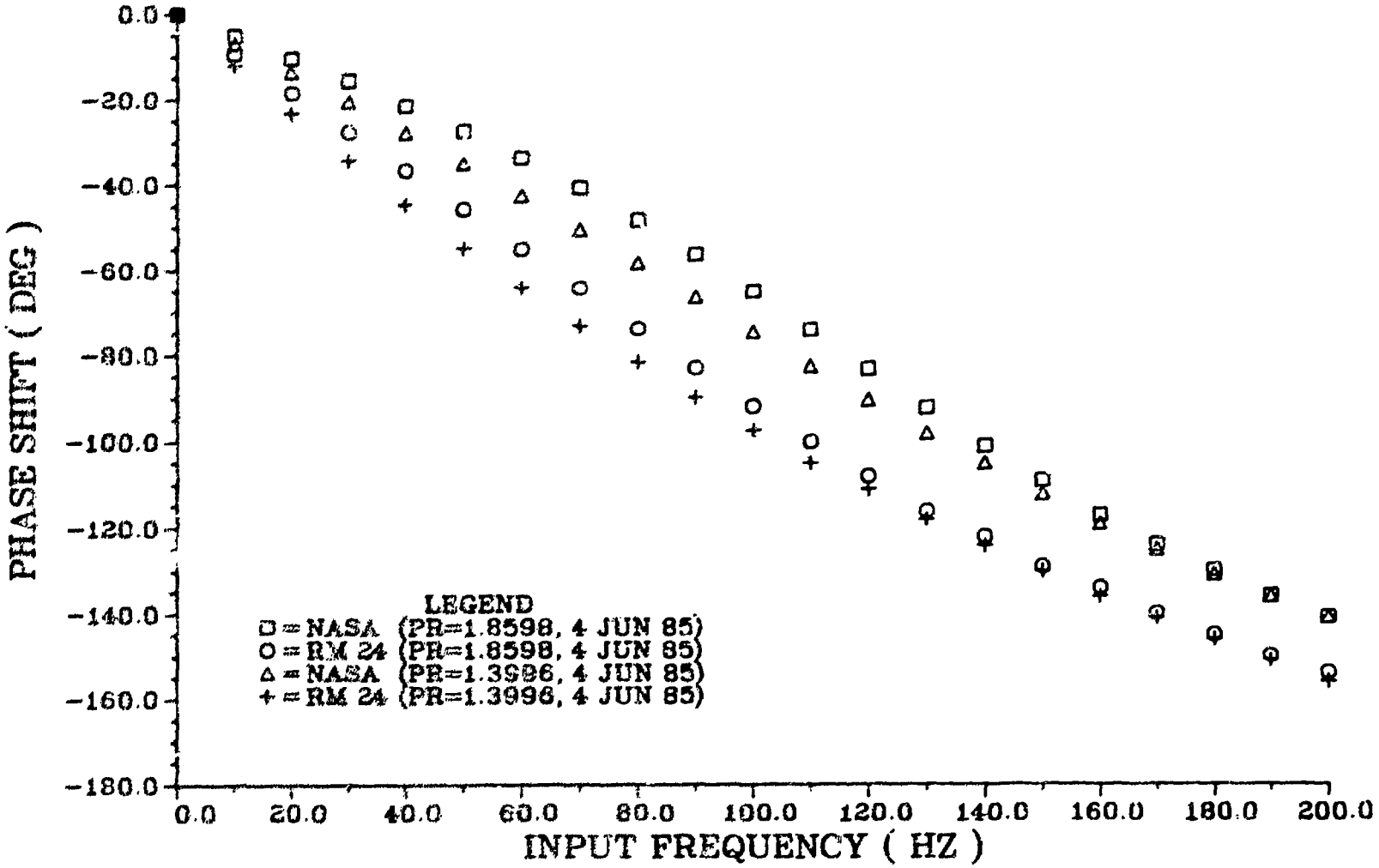

FIGURE 13. COMPARISON OF RM 24 EXPERIMENTAL DATA TO NASA PROGRAM FREQUENCY RESPONSE PREDICTIONS FOR A 14.5 IN. TUBE WITH .020 IN. ID

FIG13

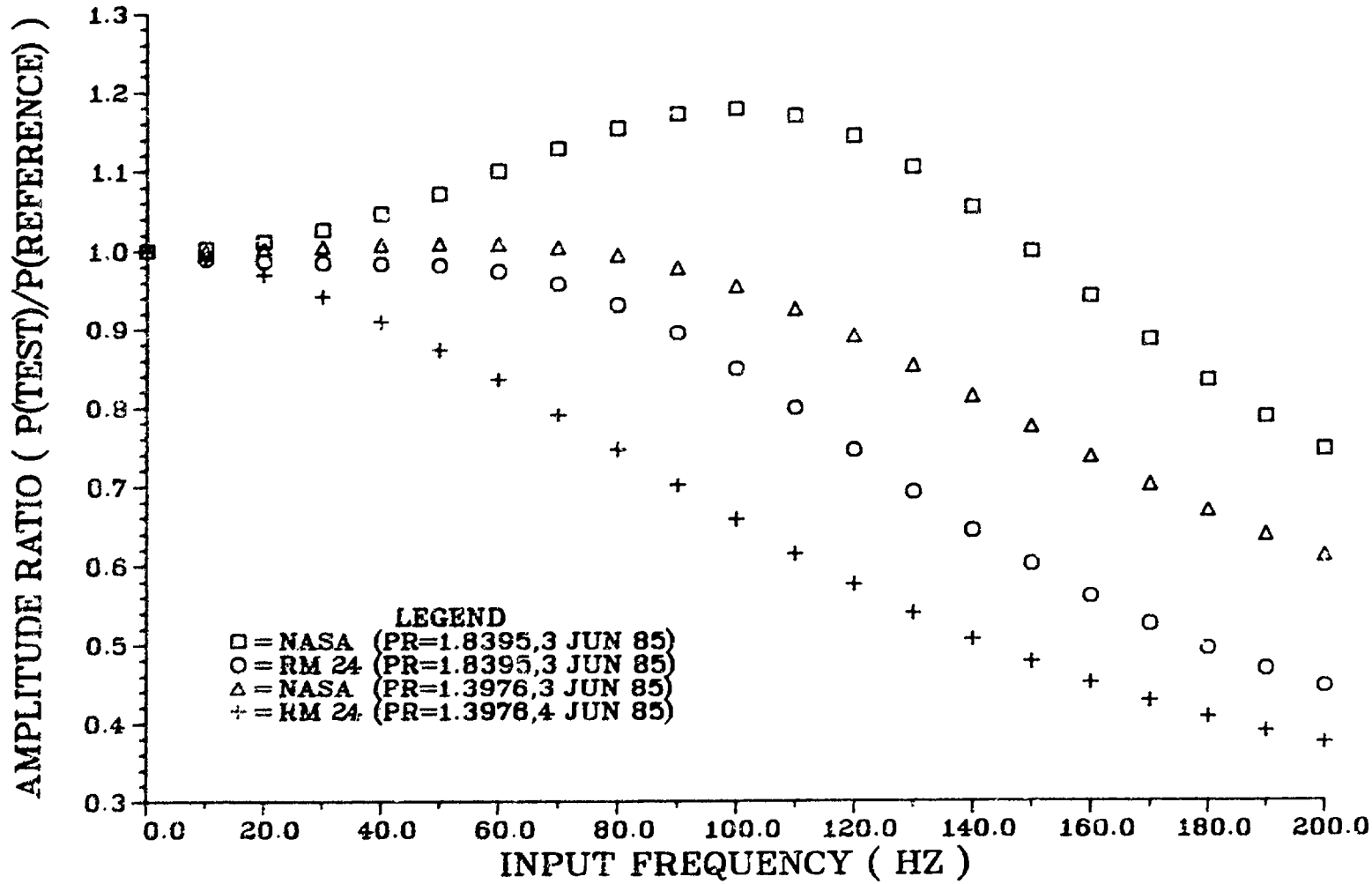

FIGURE 14. COMPARISON OF RM 24 EXPERIMENTAL DATA TO NASA PROGRAM FREQUENCY RESPONSE PREDICTIONS FOR A 15.0 IN. TUBE WITH .020 IN. ID

FIG14

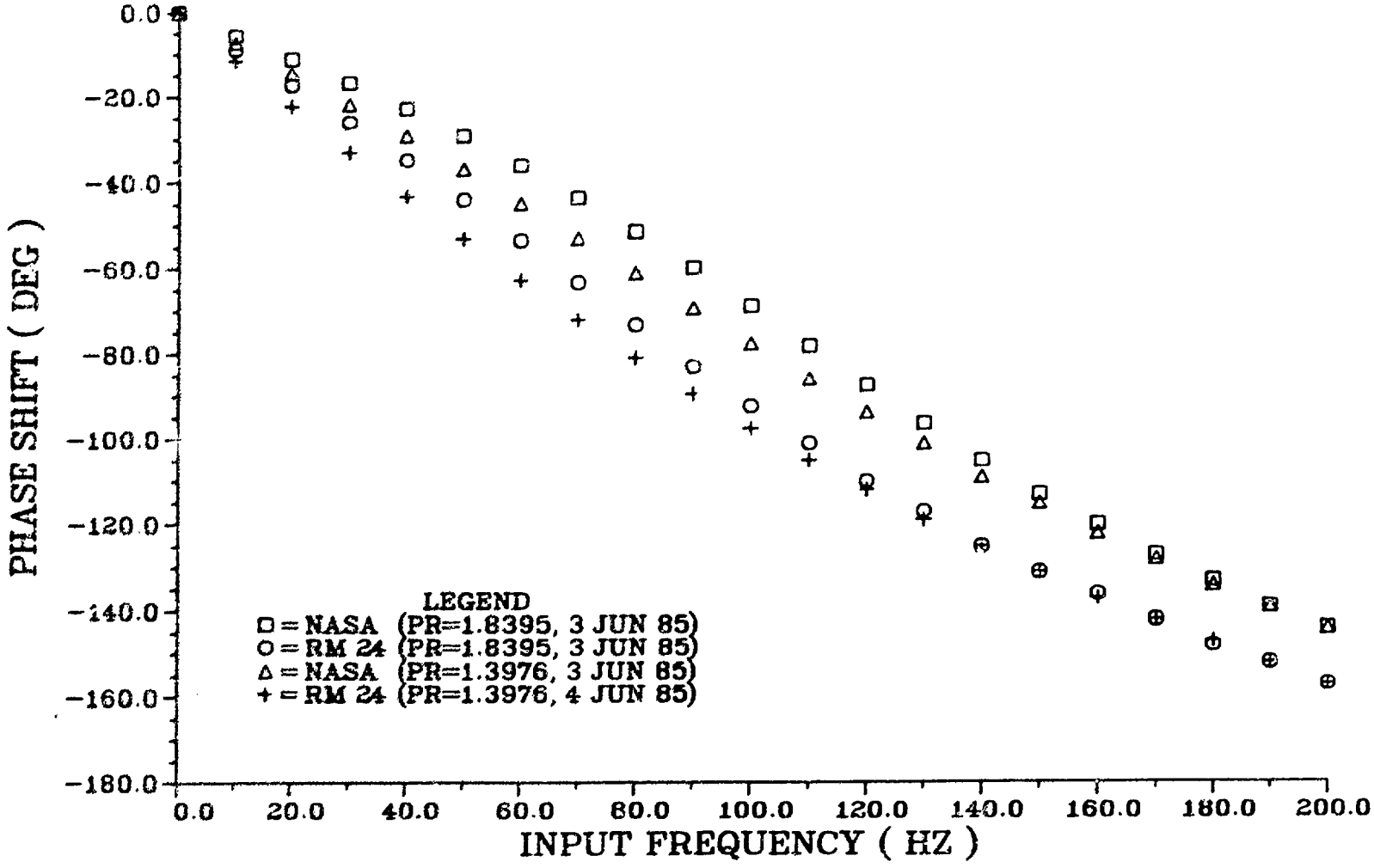

FIGURE 15. COMPARISON OF RM 24 EXPERIMENTAL DATA TO NASA PROGRAM FREQUENCY RESPONSE PREDICTIONS FOR A 15.0 IN. TUBE WITH .020 IN. ID

FIG15

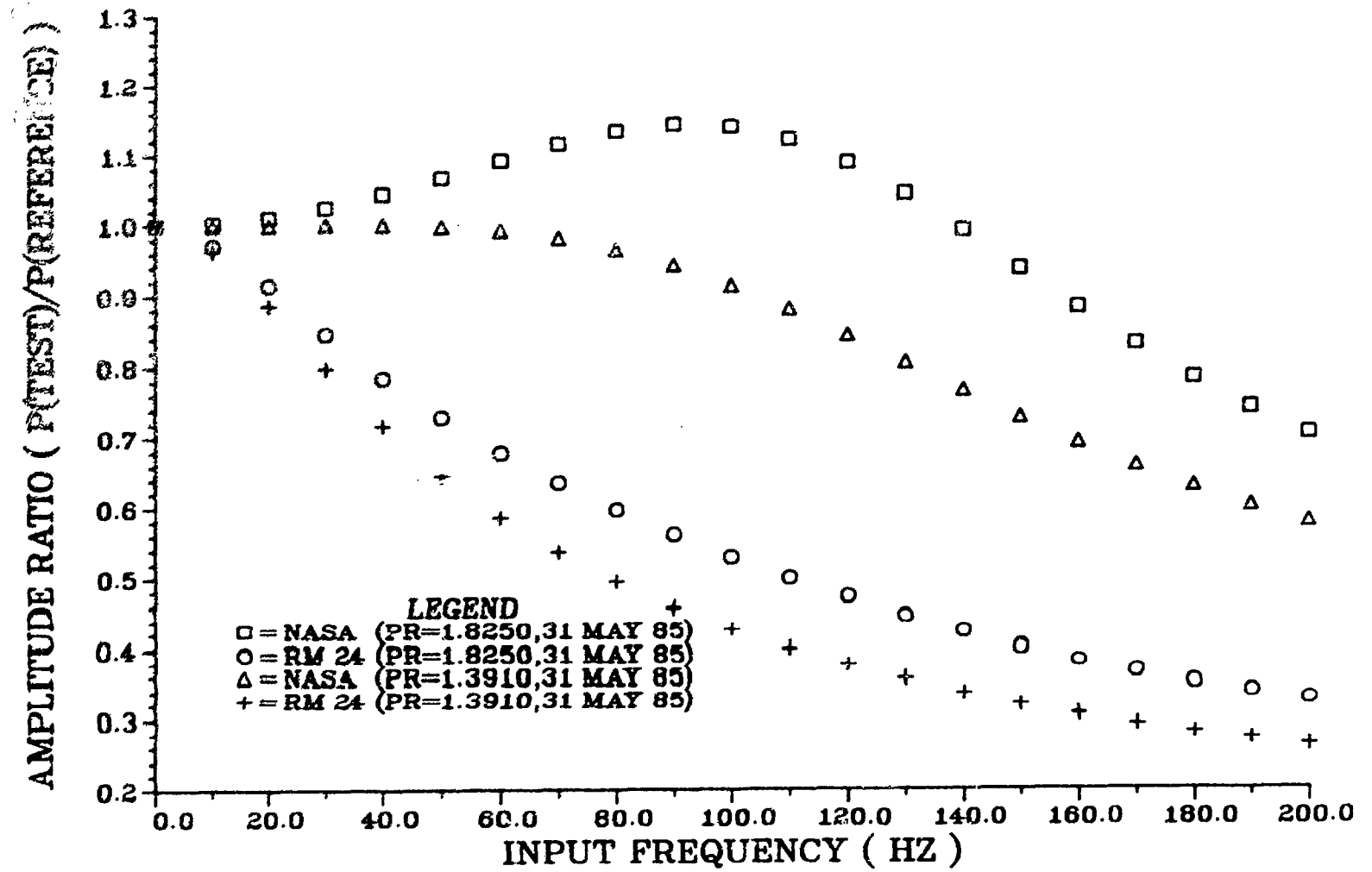

FIGURE 16. COMPARISON OF RM 24 EXPERIMENTAL DATA TO NASA PROGRAM FREQUENCY RESPONSE PREDICTIONS FOR A 15.5 IN. TUBE WITH .020 IN. ID

FIG16

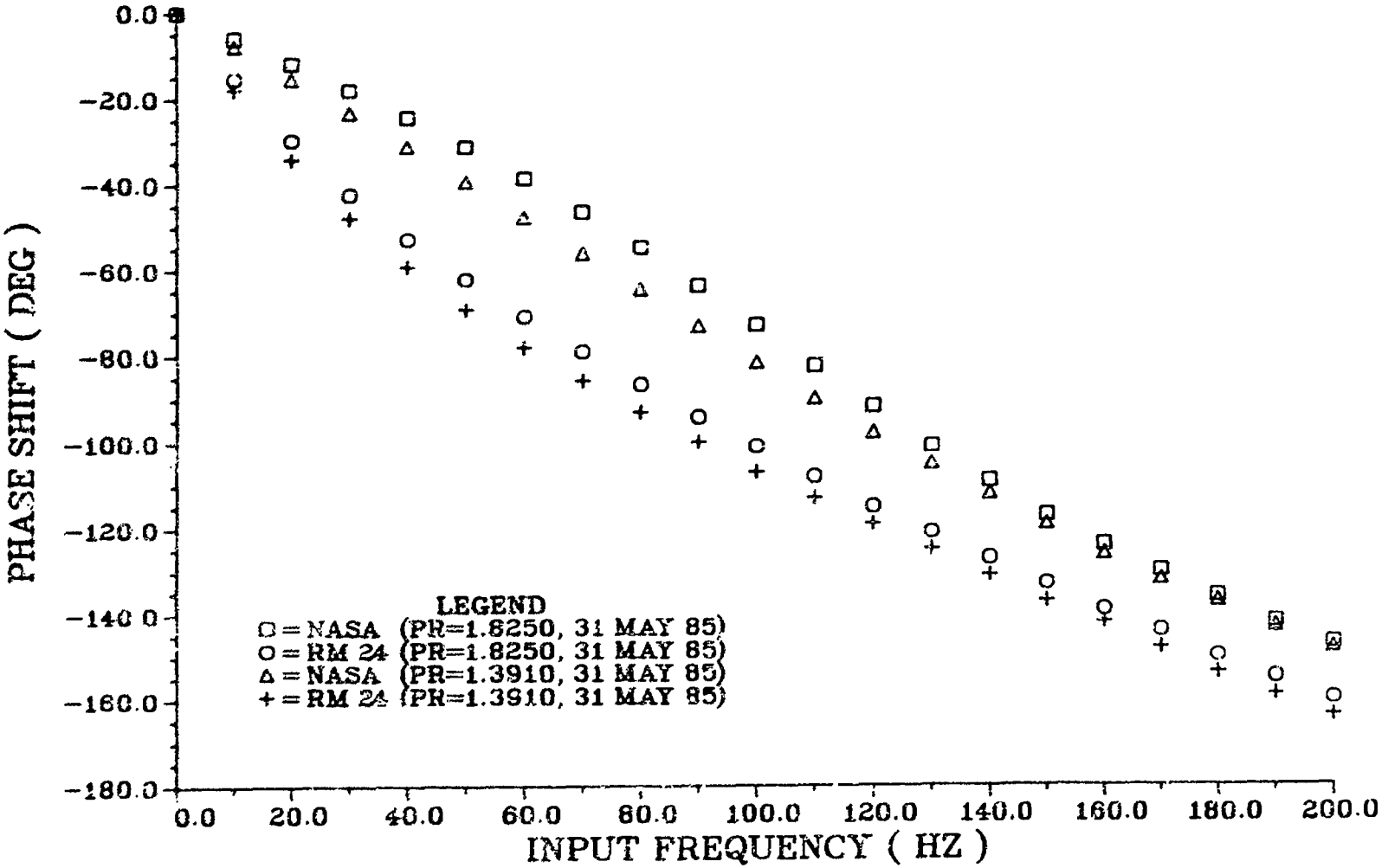

FIGURE 17. COMPARISON OF RM 24 EXPERIMENTAL DATA TO NASA PROGRAM FREQUENCY RESPONSE PREDICTIONS FOR A 15.5 IN. TUBE WITH .020 IN. ID

FIG17

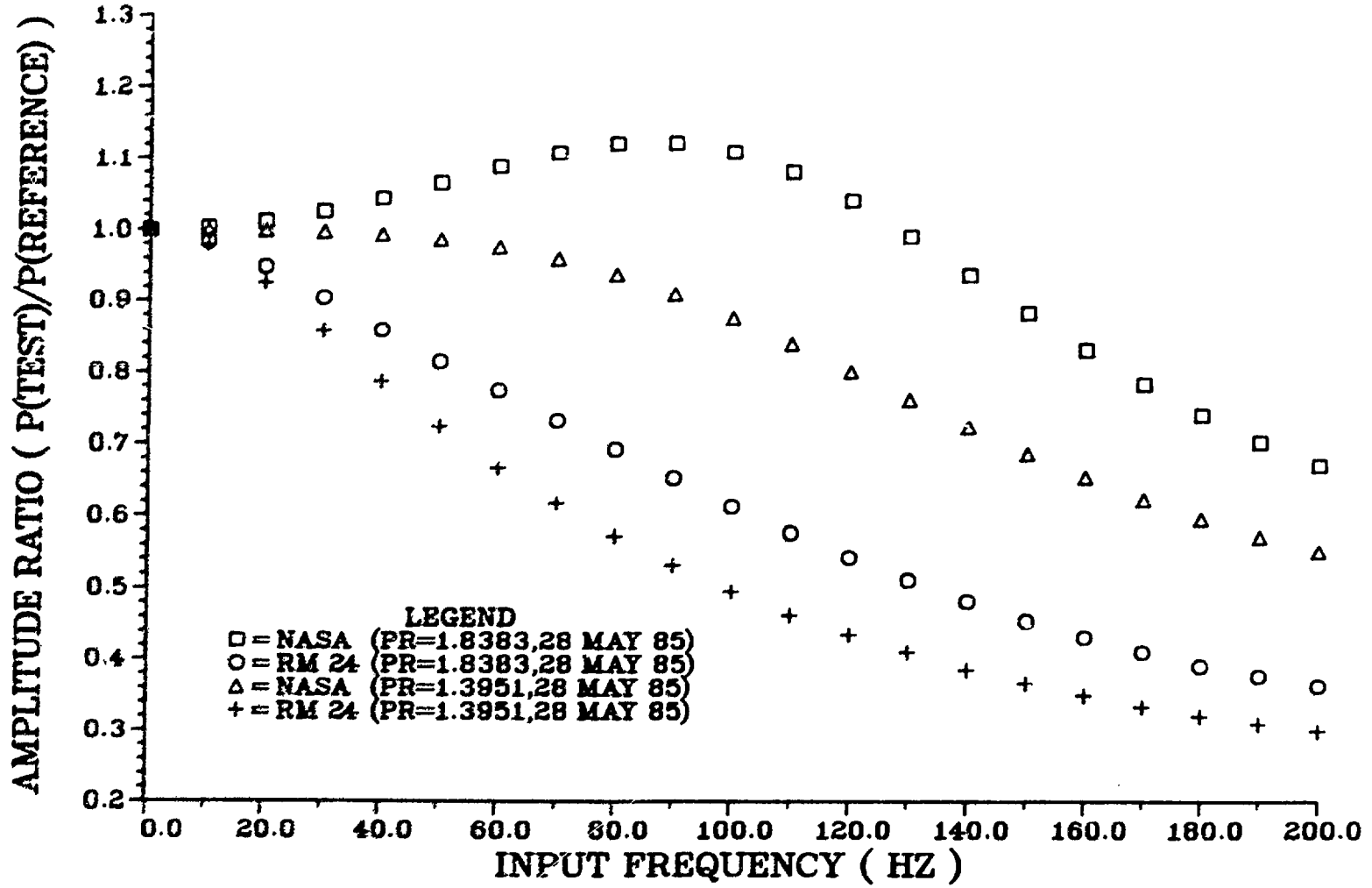

FIGURE 18. COMPARISON OF RM 24 EXPERIMENTAL DATA TO NASA PROGRAM FREQUENCY RESPONSE PREDICTIONS FOR A 16.38 IN. TUBE WITH .020 IN. ID

FIG18

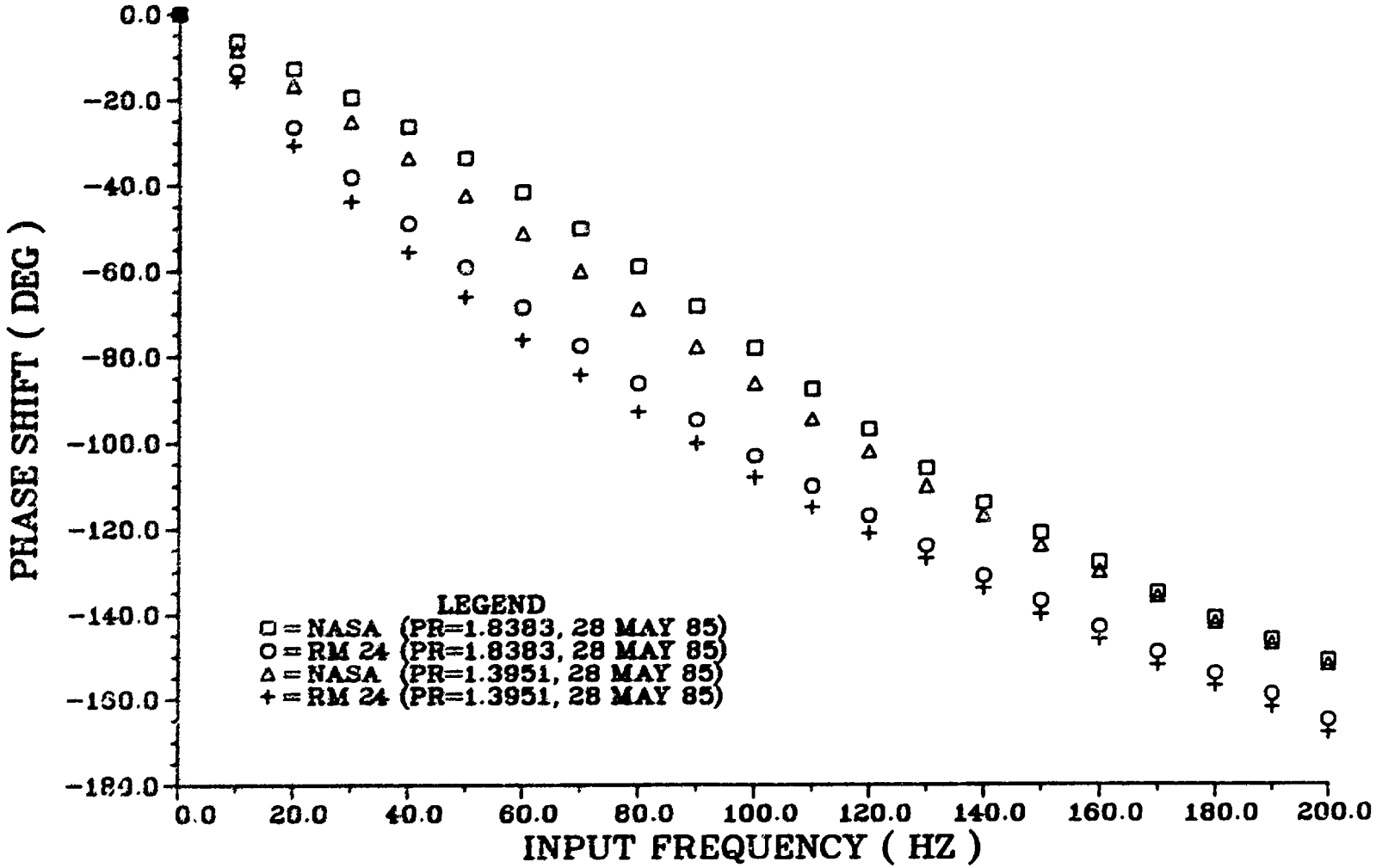

FIGURE 19. COMPARISON OF RM 24 EXPERIMENTAL DATA TO NASA PROGRAM FREQUENCY RESPONSE PREDICTIONS FOR A 16.38 IN. TUBE WITH .020 IN. ID

FIG19

The comparison between experimental results and theoretical predictions for this series of experiments was generally encouraging insofar as the trends in the Room 24 data were similar to those of the smallest diameter tubes tested by Bergh and Tijdeman. Their experiments covered a range of tube diameters from 0.039 inch (0.49mm) to 0.086 inch (1.09mm) with lengths ranging from 19.7 inches (500mm) to 153.9 inches (3910mm). In general, they found a greater mismatch between theory and experiment as the tube diameter decreased. In their comparison for the 0.039 and 0.041-inch-inner-diameter tubes, the theory predicted a resonant peak both higher in amplitude and at a higher frequency than that exhibited by the experimental data. This same trend can be seen in the comparison of the theory with the Room 24 experimental data.

While the similarity in general trends was encouraging, the specific match between the theory and the Room 24 experimental data was not as good as expected. The correlation of the amplitude ratios was the best for the shortest tube, becoming progressively worse as the tube length increased. But even for the best match, which occurred for the 10.0 inch tube with a pressure ratio of 1.8244 (Fig. 9), the experimental data differs from the theoretical predictions by 1 percent at only 30 hertz, and by more than 5 percent at 80 hertz. As the first resonant peak is approached the comparison is even worse. For the longer tubes tested, reasonable correlation between the experimental results and theory only extended to about 30 hertz. Based on the comparisons reported by Bergh and Tijdeman for larger diameter tubes, these correlations were considered inadequate. Therefore, the focus of the remaining effort was to investigate ways to improve the experimental setup and modelling of the experimental apparatus in the NASA program.

The first attempt to improve the experimental setup was to conduct a series of experiments using test lengths cut from the new 0.020 inch tubing stock. The results of these experiments, for tube lengths of 10.0, 15.0, and 16.375 inches, are shown in Figures 20-25. Using this new tubing, a modest improvement was seen in the comparison between the data and theory. For example, the experimental data for the amplitude ratio was within 5.8 percent of the theory up to 100 hertz, as opposed to about 80 hertz with the original tubing.

This improvement in the comparison is due to the slightly different diameter of the new tubing. The diameter of the original tubing was between 0.019 and 0.020 inch while that of the new tubing was 0.020 inch. Bergh and Tijdeman's results showed that a larger diameter tube will have a resonant peak which is higher in amplitude and which occurs at a slightly higher frequency than that of a smaller diameter tube of the same length, given that the tube mean pressures, temperatures, and transducer volumes are the same. Figure 26 shows the results of the experiments for the two 15.0-inch tubes which were cut from different tubing stock. Note that the pressures are nearly the same for each case. The same transducer was used in each experiment as well. Therefore, the different results for each tube can be attributed to differences in the tube diameters.

The modest improvement achieved by using different tubing still did not yield correlations comparable to those reported by Bergh and Tijdeman. Therefore, two additional sources of potential improvement were investigated. These were the effects of the signal generator adapter upstream of the reference transducer, and the method of modelling the EOC test transducer in the NASA program.

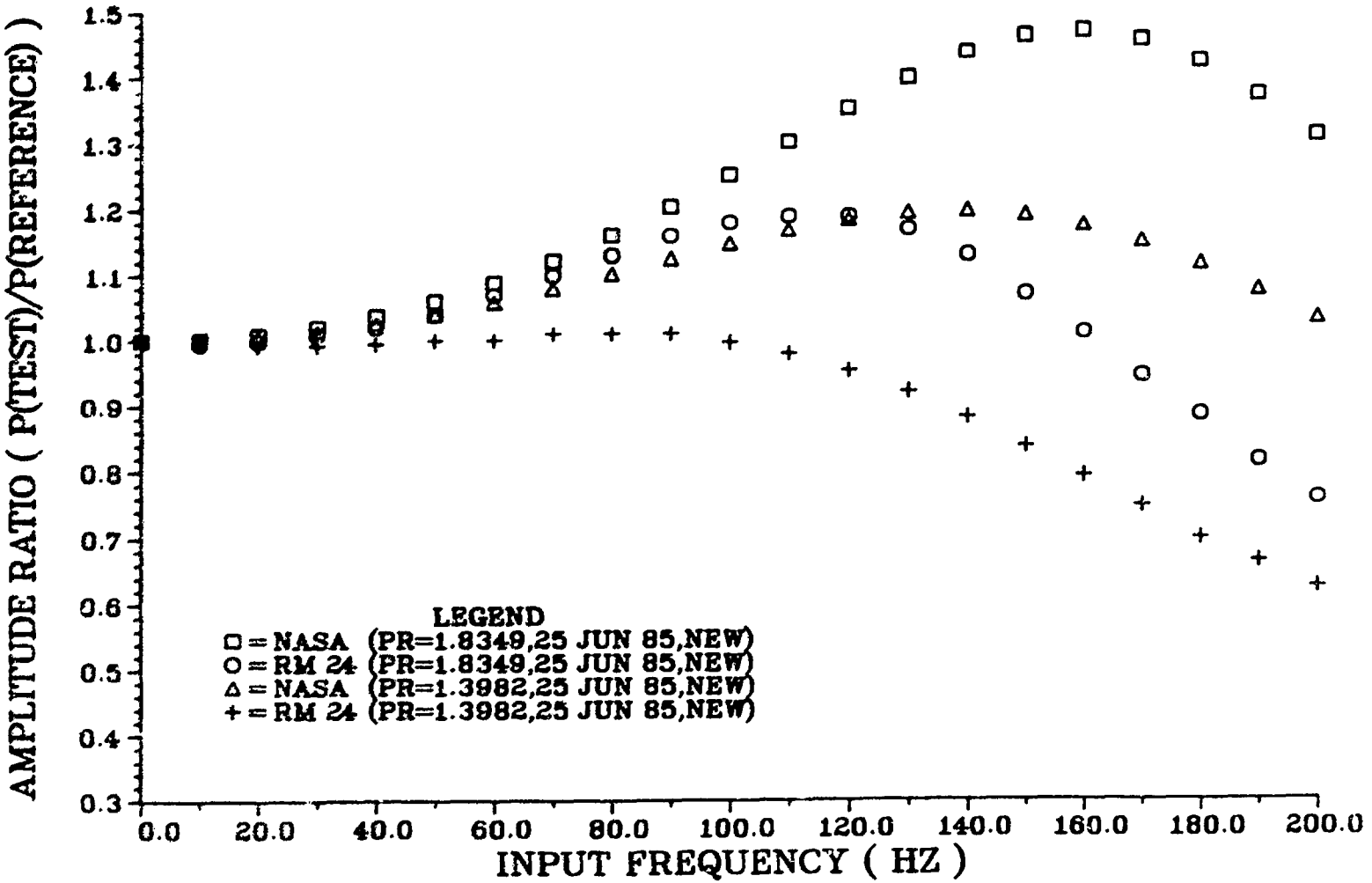

FIGURE 20. COMPARISON OF RM 24 EXPERIMENTAL DATA TO NASA PROGRAM FREQUENCY RESPONSE PREDICTIONS FOR A 10.0 IN. TUBE WITH .020 IN. ID

FIG20

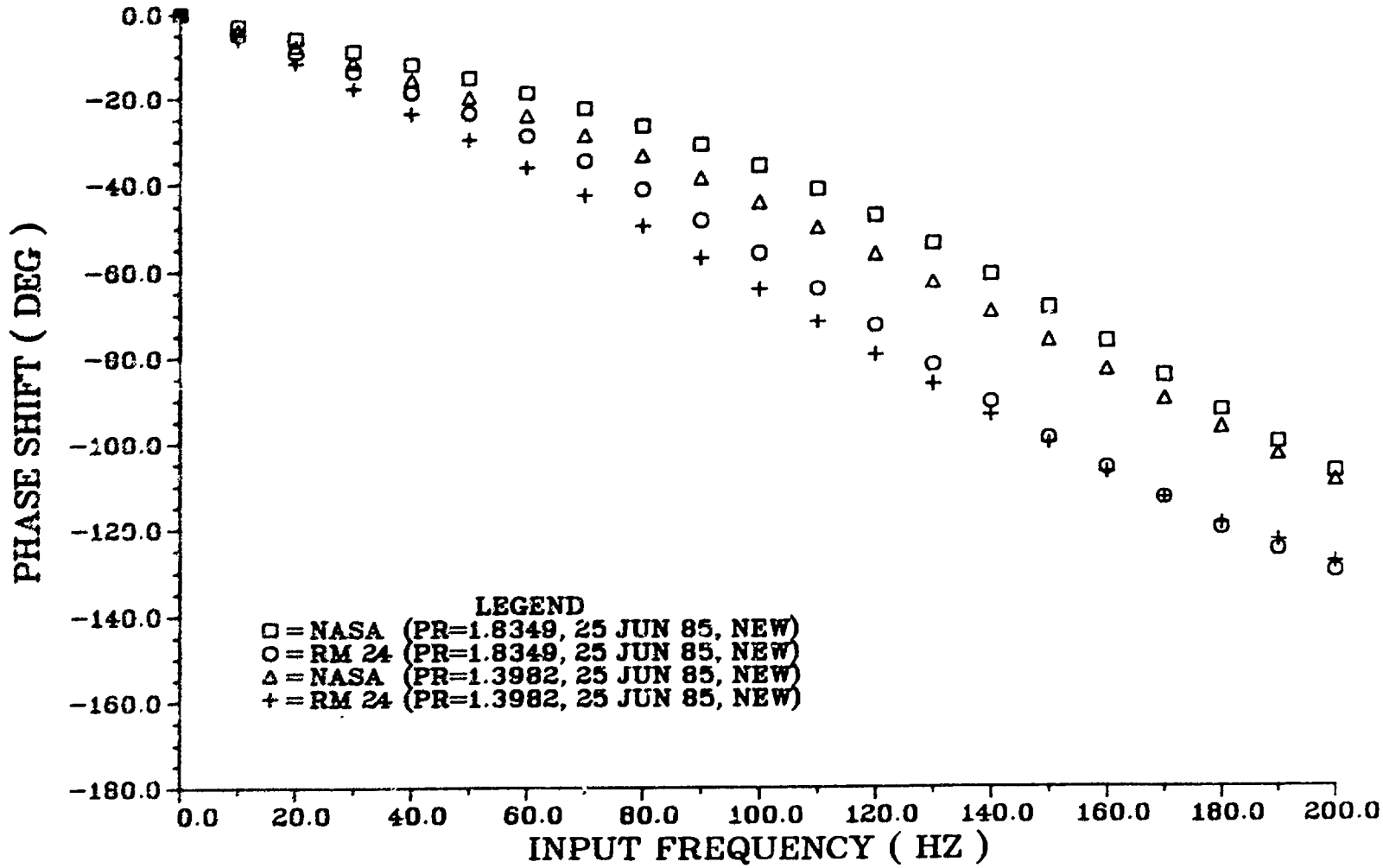

FIGURE 21. COMPARISON OF RM 24 EXPERIMENTAL DATA TO NASA PROGRAM FREQUENCY RESPONSE PREDICTIONS FOR A 10.0 IN. TUBE WITH .020 IN. ID

FIG21

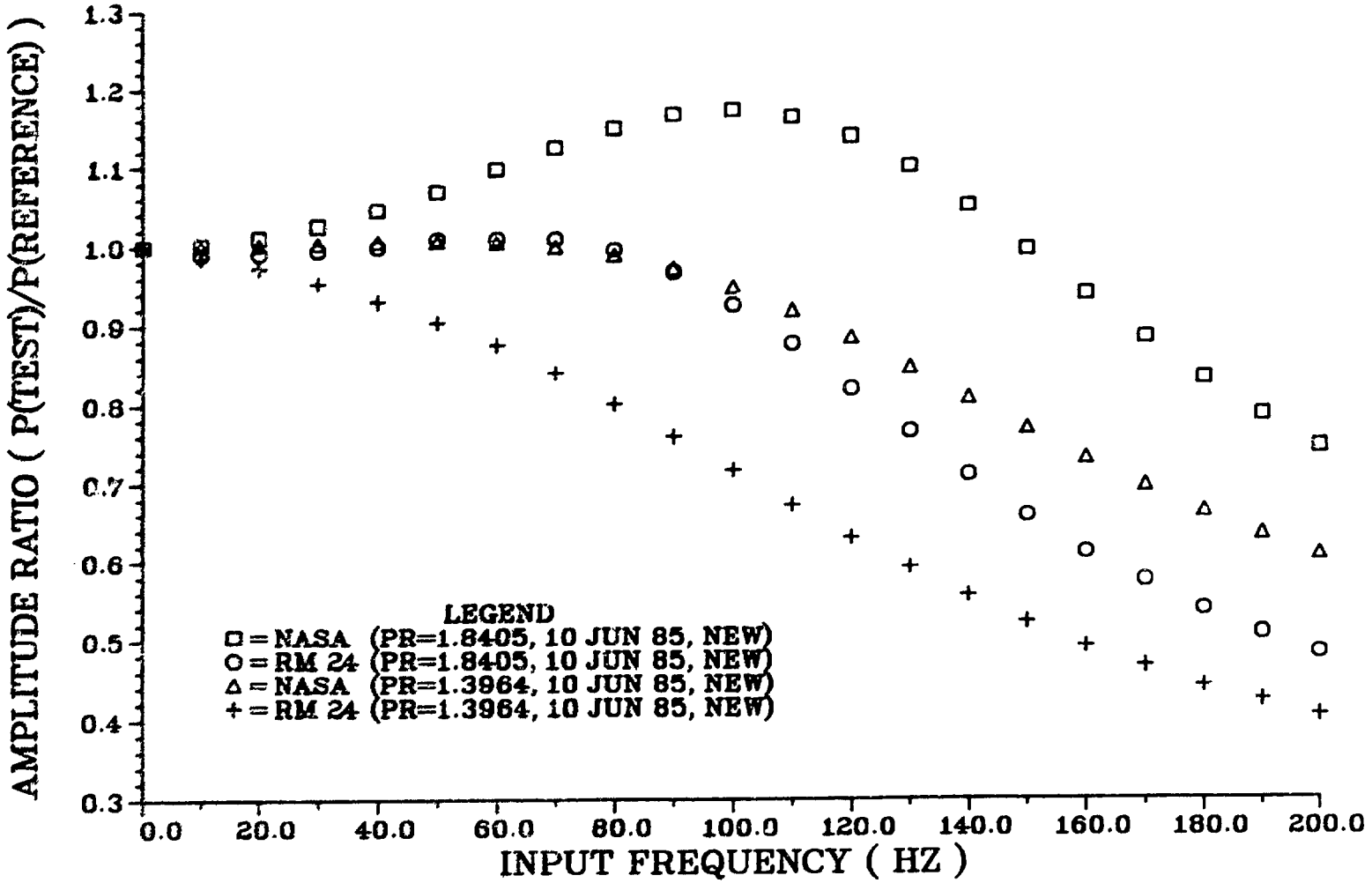

FIGURE 22. COMPARISON OF RM 24 EXPERIMENTAL DATA TO NASA PROGRAM FREQUENCY RESPONSE PREDICTIONS FOR A 15.0 IN. TUBE WITH .020 IN. ID

FIG22

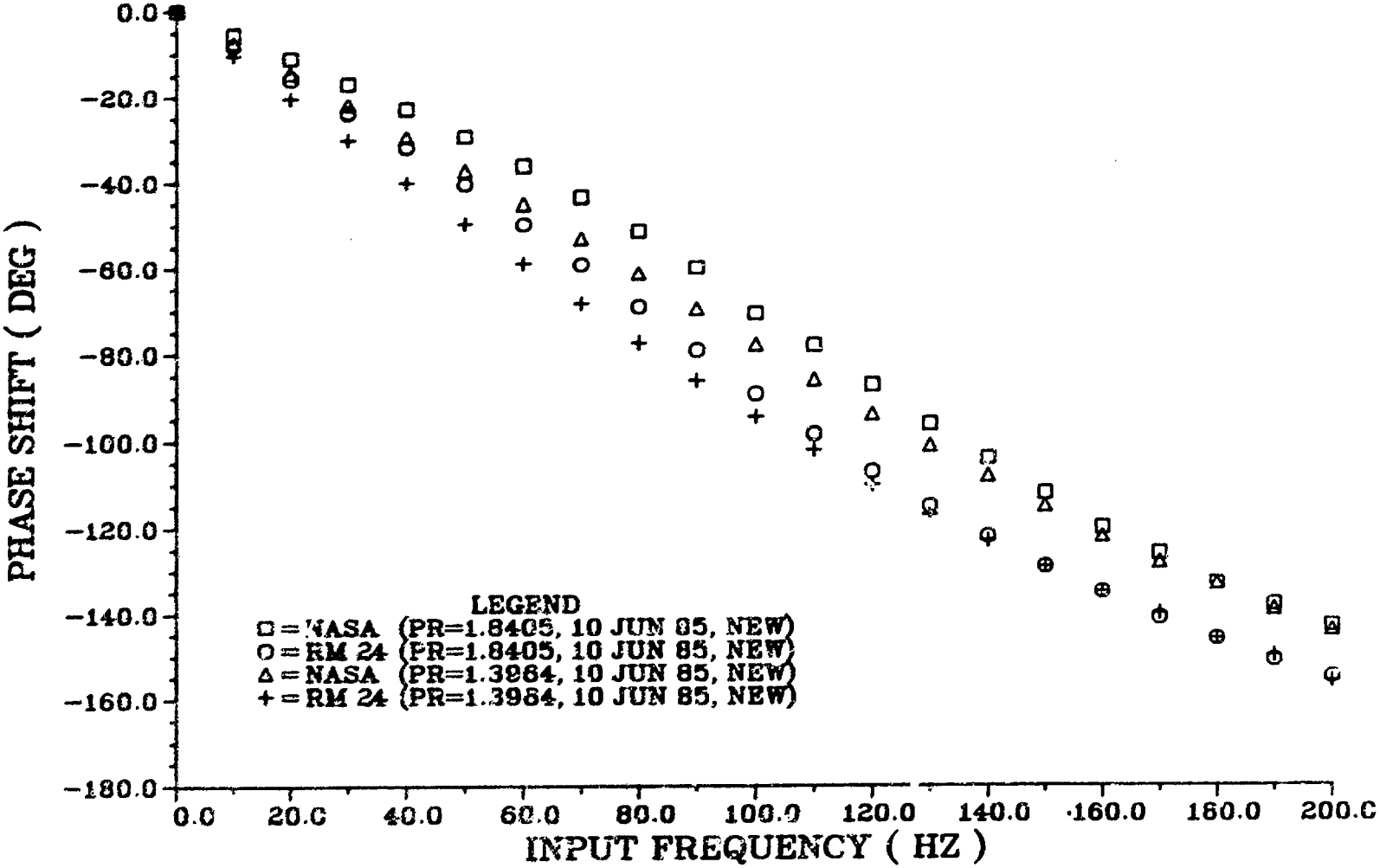

FIGURE 23. COMPARISON OF RM 24 EXPERIMENTAL DATA TO NASA PROGRAM FREQUENCY RESPONSE PREDICTIONS FOR A 15.0 IN. TUBE WITH .020 IN. ID

FIG23

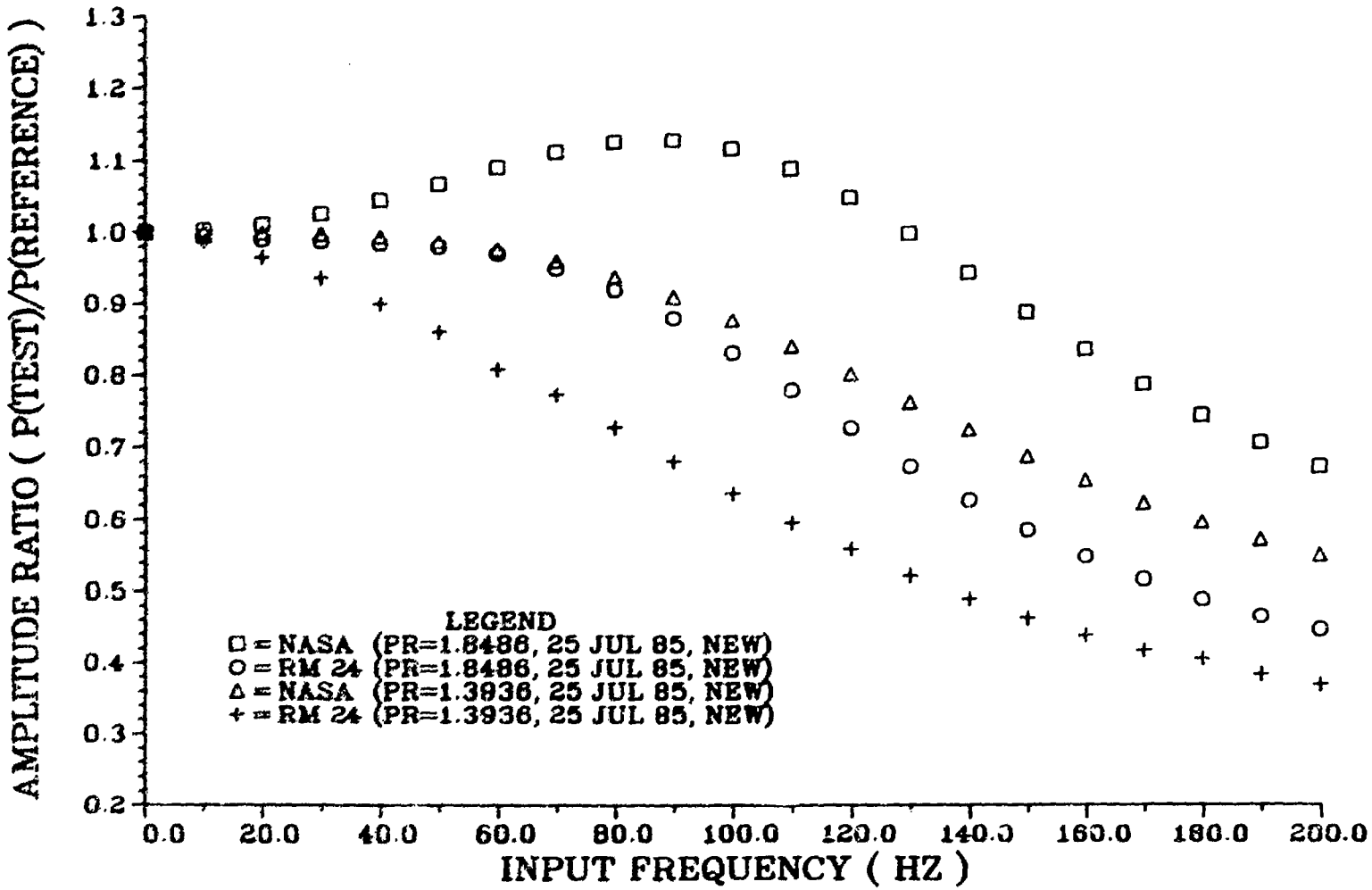

FIGURE 24. COMPARISON OF RM 24 EXPERIMENTAL DATA TO NASA PROGRAM FREQUENCY RESPONSE PREDICTIONS FOR A 16.38 IN. TUBE WITH .020 IN. ID

FIG24

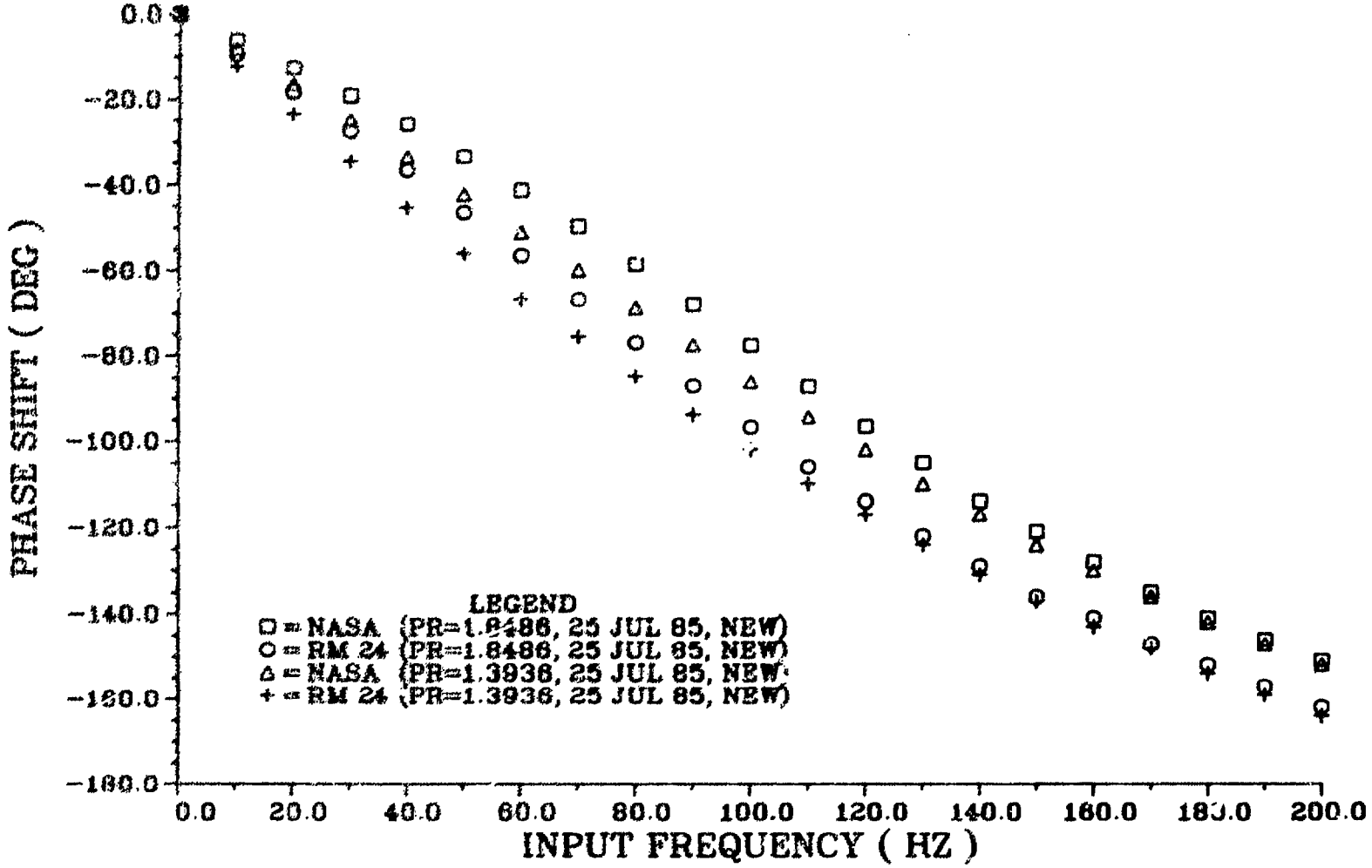

FIGURE 25. COMPARISON OF RM 24 EXPERIMENTAL DATA TO NASA PROGRAM FREQUENCY RESPONSE PREDICTIONS FOR A 16.38 IN. TUBE WITH .020 IN. ID

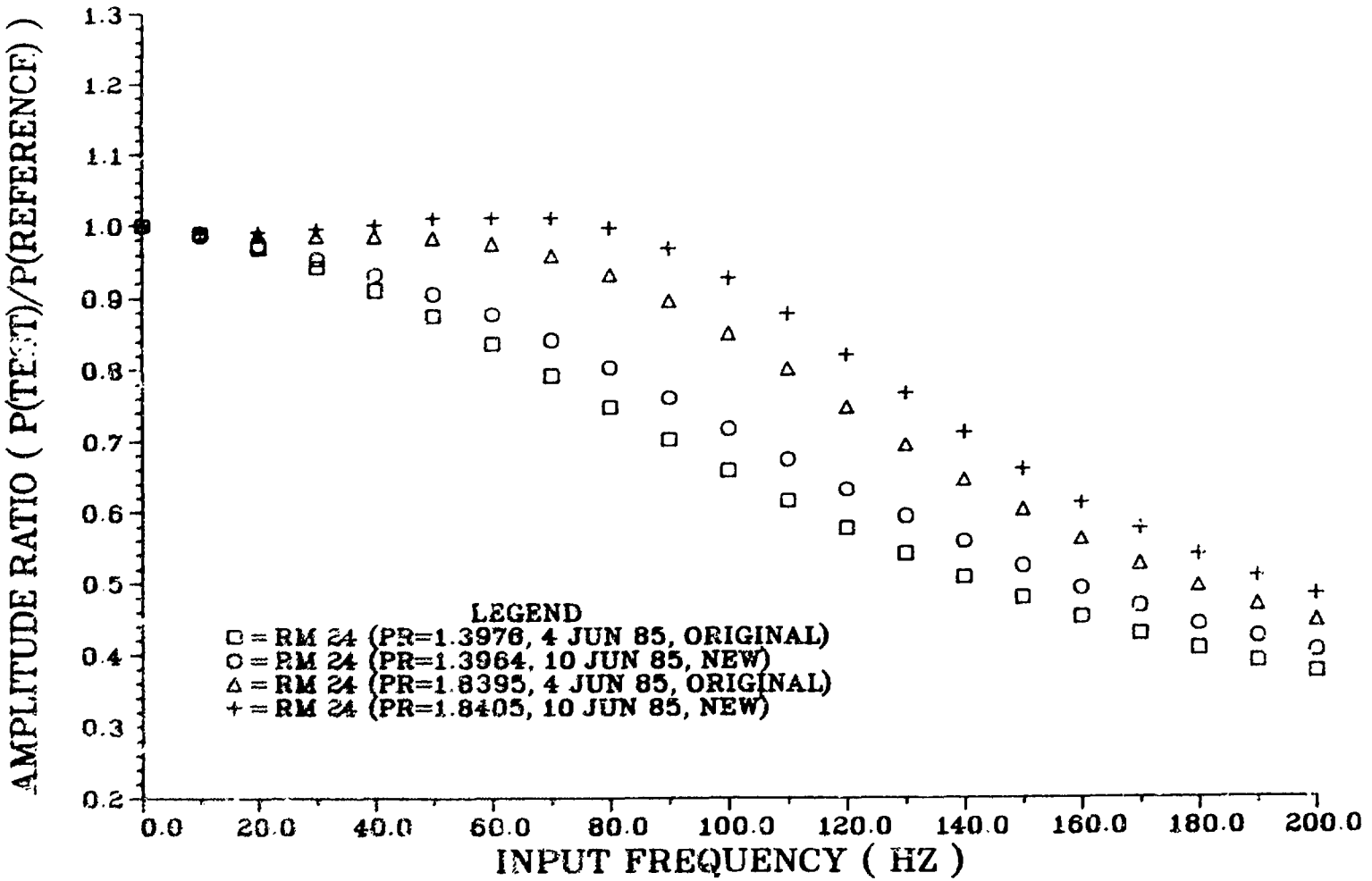

FIGURE 26. COMPARISON OF RM 24 EXPERIMENTAL DATA FOR TUBE LENGTHS FROM THE ORIGINAL AND NEW STOCK (15.0 IN. LENGTHS OF 0.020 IN. ID)

FIG26

Up to this point the tubing system was being modelled for the NASA program as two series connected tubes and volumes, as shown in Figure 27. Note that the discontinuity in tube diameters at the junction of the test tube and test transducer is treated as a zero volume, as there is no physical volume associated with the change in tube diameters. Also, the dimensions used for the ZOC14 test transducer are equivalent values quoted by the manufacturer--not the actual internal tubing lengths and volume for the transducer. These equivalent values are determined by the manufacturer from an analysis of the pressure drop versus flowrate curves for the actual transducer internal hardware.

This model for the tubing system does not include the signal generator adapter at all. The model assumes the test tube length is connected directly to the signal generator output. In addition, this model neglects the short distances that the test tube is inserted into the signal generator adapter at one end and into the ZOC measurement port at the other. To improve this model and account for the presence of the signal generator adapter, the adapter was modelled in four different ways. Each version of the new model was combined with the test conditions for one of the 10.0-inch tube experiments, and the NASA program was run with each version of the model to generate the results shown in Figure 28. The first curve in this figure is just a plot of the NASA program results using the original model in which the signal generator adapter and length adjustments were neglected. It is the baseline against which the various signal adapter models can be compared.

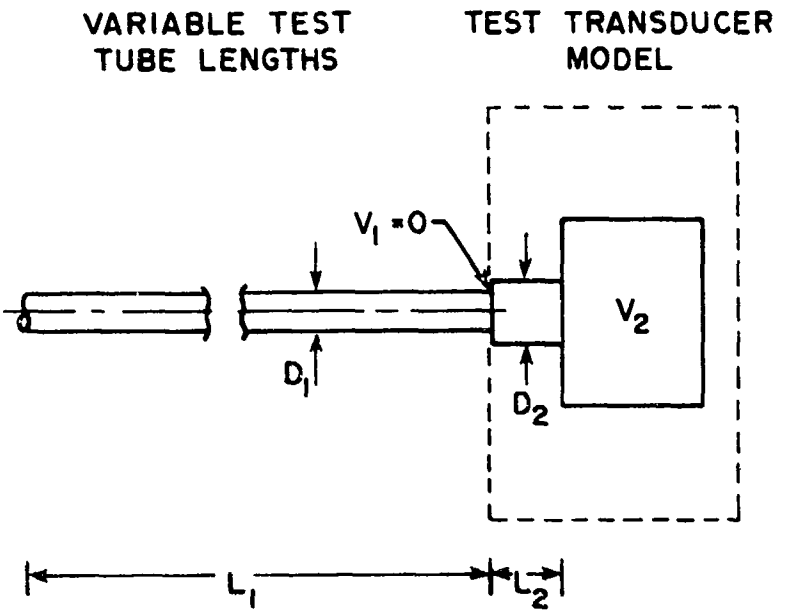

SYMBOL	DESCRIPTION	DIMENSION
L1	TEST TUBE LENGTH	10.0 – 16.375 IN.
D1	TEST TUBE INNER DIAMETER	0.020 IN.
V1	TEST TUBE TERMINATION VOLUME	0 $IN.^3$
L2	TEST TRANSDUCER EQUIVALENT LENGTH	2.0 IN.
D2	TEST TRANSDUCER EQUIVALENT DIAMETER	0.029 IN.
V2	TEST TRANSDUCER EQUIVALENT VOLUME	0.0002 $IN.^3$

FIGURE 27. Initial Model of the Tubing System Used for the NASA Program

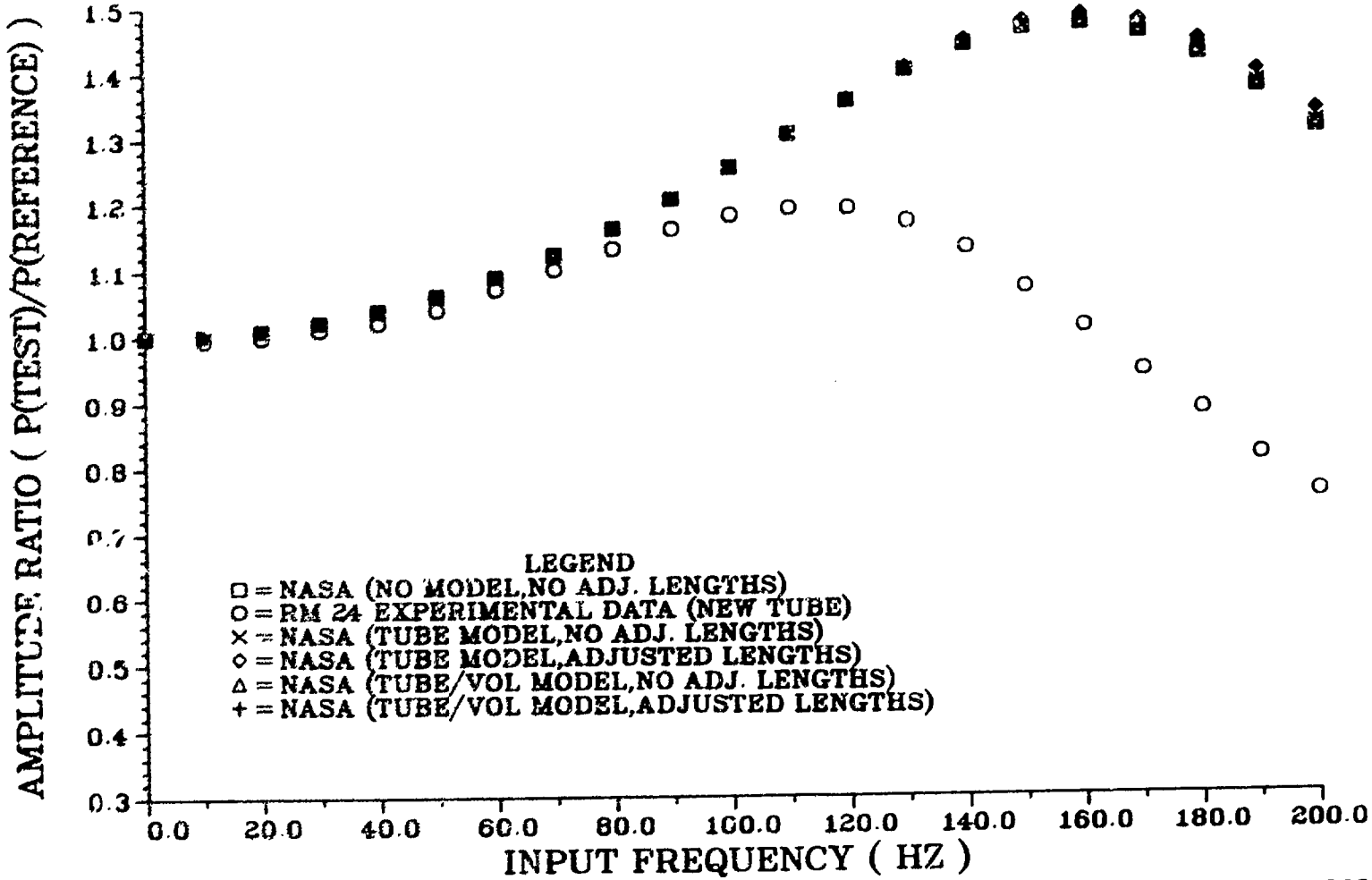

FIGURE 28. EFFECT OF VARIOUS ADAPTER MODELLING METHODS ON NASA FREQUENCY RESPONSE PREDICTIONS FOR A 10.0 IN. TUBE WITH .020 IN. ID

FIG28

Each of the signal generator adapter models was an attempt to model the actual interconnection of hardware shown in Figure 29. The dimensions for the signal generator adapter are shown in Figure 7. In the first model for the signal generator adapter, the portion of the adapter internal to the signal generator body was treated as a tube length (cross-hatched area in Figure 29), and the remainder of the flowpath to the reference transducer was considered to be a volume. In this model the insertion lengths of the test tube into the signal generator adapter and the ZOC transducer were neglected. This model resulted in the tubing system description shown in Figure 30, with dimensions as listed under the column heading, "DIMENSIONS (NO ADJUSTED LENGTHS)." In Figure 28, the curve labelled "NASA (TUBE/VOL MODEL, NO ADJ. LENGTHS)" shows the NASA predictions based on this model.

In the next version, the test tube length was increased by 0.111 inch to account for the added length of the signal generator adapter, and the test transducer equivalent length was decreased by 0.125 inch to account for the insertion of the test tube into the transducer output port by this amount. The resulting dimensions are shown in the last column in Figure 30. The NASA program results based on this model are labelled as "NASA (TUBE/VOL MODEL, ADJUSTED LENGTHS)" in Figure 28.

In the next two versions of the signal generator adapter model, the entire adapter flowpath was modelled as a tube only, with and without adjusted lengths as before. Figure 31 is a schematic of the model and the dimensions for each of these versions. The NASA program results based on these two models are shown in Figure 28 as the curves labelled "NASA (TUBE MODEL, NO ADJ. LENGTHS)" and "NASA (TUBE MODEL, ADJUSTED LENGTHS)."

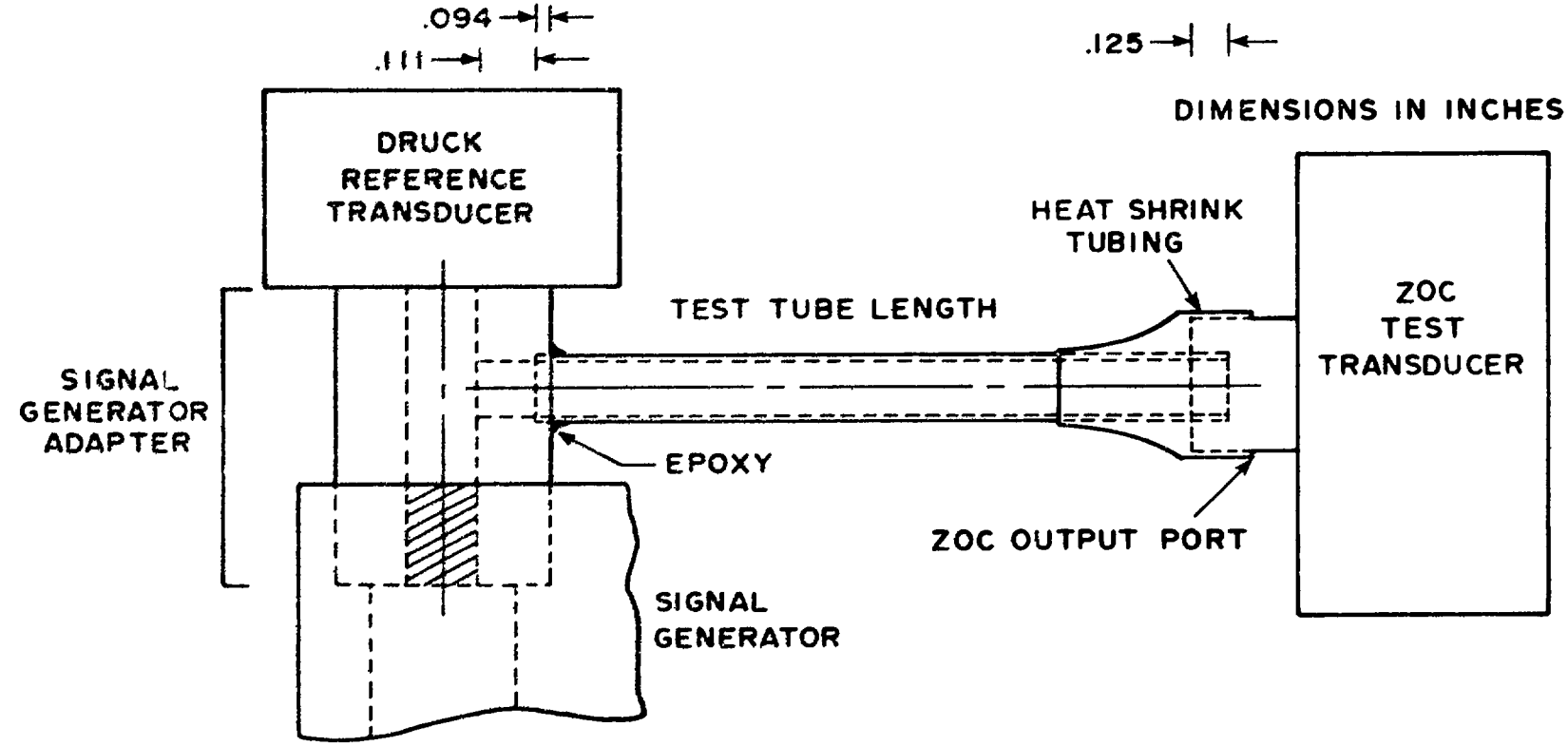

FIGURE 29. Tubing System Interconnections

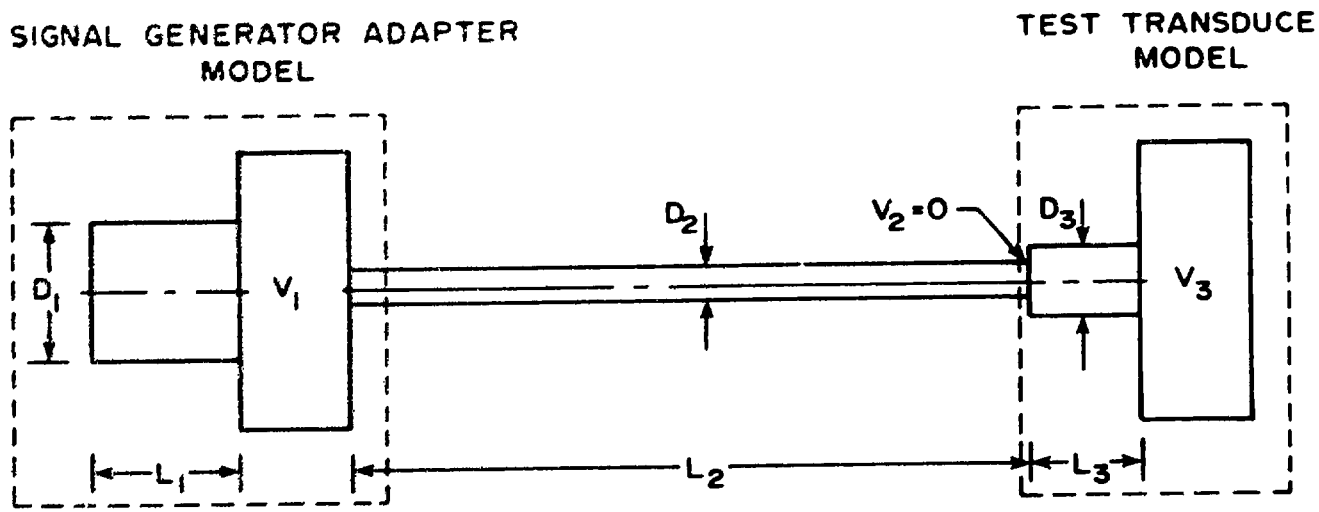

SYMBOL	DIMENSIONS (NO ADJUSTED LENGTHS)		DIMENSIONS (WITH ADJUSTED LENGTH)	
L_1	.150 IN.		.150 IN.	
D_1	.090 IN.		.090 IN.	
V_1	.00095 IN^3		.00095 IN^3	
L_2	10.0 IN.		10.111 IN.	
D_2	.020 IN.		.020 IN.	
V_2	0		0	
	ZOC	DRUCK	ZOC	DRUCK
L_3	2.0 IN.	.6 IN.	1.875 IN.	.46 IN.
D_3	.029 IN.	.041 IN.	.029 IN.	.041 IN.
V_3	.0002 IN^3	1.22×10^{-6} IN^3	.0002 IN^3	1.22×10^{-6} IN^3

FIGURE 30. Modelling the Signal Generator Adapter as a Tube and Volume

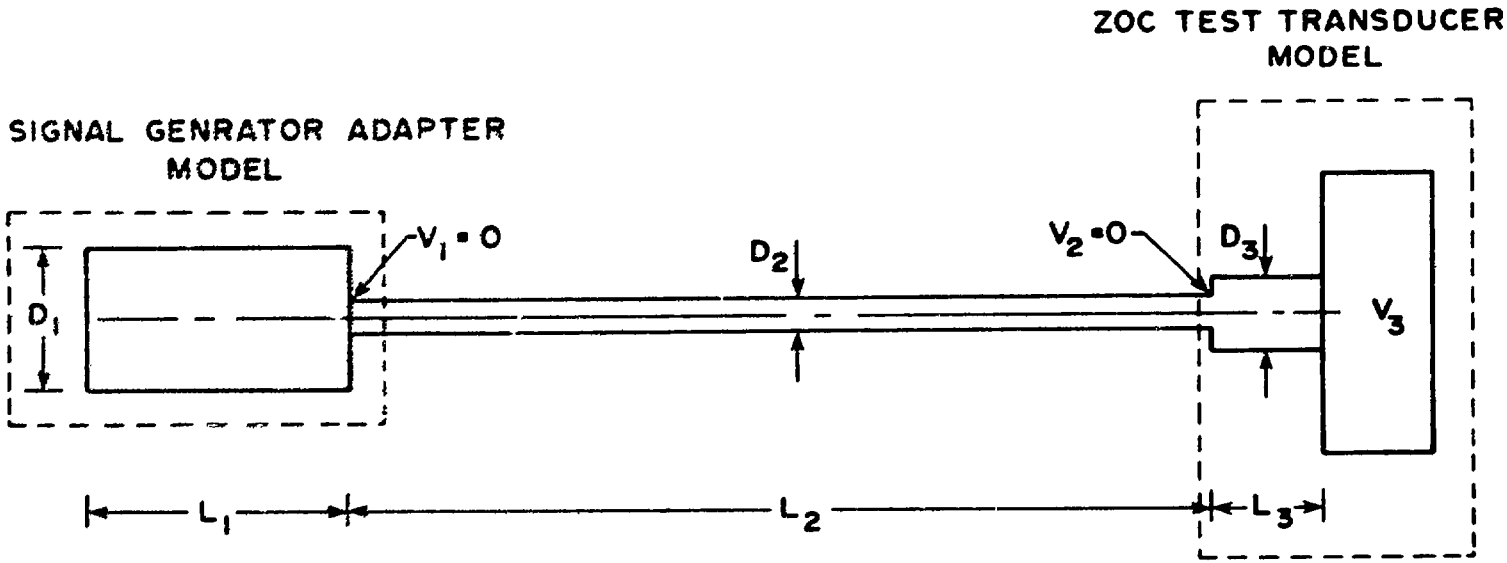

SYMBOL	DIMENSIONS (NO ADJUSTED LENGTHS)		DIMENSIONS (WITH ADJUSTED LENGTH)	
L_1	.300 IN.		.300 IN.	
D_1	.090		.090 IN.	
V_1	0		0	
L_2	10.0 IN.		10.111 IN.	
D_2	.020 IN.		.020 IN.	
V_2	0		0	
	ZOC	DRUCK	ZOC	DRUCK
L_3	2.0 IN.	.6 IN.	1.875 IN.	.46 IN.
D_3	.029 IN.	.041 IN.	.029 IN.	.041 IN.
V_3	.0002 $IN.^3$	$1.22 \times 10^{-6} IN.^3$	.0002 $IN.^3$	$1.22 \times 10^{-6} IN.^3$

FIGURE 31. Modelling the Signal Generator Adapter as a Tube Only

Figure 28 shows that the various methods of modelling the signal generator adapter had a negligible effect on the theoretical predictions of the frequency response for the 10.0-inch tube. The predictions with signal generator adapter models are virtually the same as those in which the adapter was not modelled. Therefore, previous omission of a signal generator adapter model from the tubing system description for the NASA program did not significantly alter the theoretical predictions.

Once the influence of the signal generator adapter on the theoretical results was found to be minimal, the focus of the effort to improve the comparison between experiment and theory shifted to the ZOC14 test transducer. The primary concern with this transducer was the use of published equivalent values of internal tubing geometry to model the ZOC in the NASA program. The equivalent values were used because they were available, and we did not know the actual internal geometry of the ZOC. To determine the effect of using the equivalent values to model the transducer, it was necessary to repeat some experiments using the DRUCK transducer as the test transducer instead of the ZOC. With the DRUCK transducer the actual geometry was known, so the transducer could be modelled in the NASA program using actual rather than equivalent values. A description of the experiments using the DRUCK test transducer is presented in the following section.

(2) Experimental Results Using the DRUCK PDCR 22 Test Transducer

Experiments were conducted with 10.0 and 24.0-inch tubes. A DRUCK transducer with a standard zero volume adapter was used as the test transducer. The actual internal dimensions of the zero volume adapter were known, so no equivalent values were needed with this transducer.

For the 10.0-inch tube experiment, the NASA program was run five times to calculate the theoretical predictions based on each of the different signal generator adapter models, as before. The dimensions for the DRUCK test transducer with and without adjusted lengths are shown in Figures 30 and 31. The results of the single experiment with the 10.0-inch tube are presented in Figures 32 and 33.

These results clearly indicate the importance of knowing the actual dimensions for the test transducer, so that the transducer can be modelled accurately in the NASA program. When this is done, the experimentally determined amplitude ratio agrees with the theoretical predictions to within 3 percent up to a frequency of 170 hertz. At this frequency the experimental data has reached the first resonant peak while the theoretical predictions have not. As a result, the data and theory differ significantly at higher frequencies. Nonetheless, these results are a significant improvement over the comparison obtained earlier with the ZOC test transducer. It is apparent from these results that using the equivalent values to model the ZOC in the NASA program is ineffective.

Once again, the various signal generator adapter models have very little effect on the NASA program predictions. In fact, the predictions are essentially the same regardless of the type of model used, as long as the lengths are not adjusted to account for the 0.020-inch-diameter passage in the adapter and the insertion of the test tube into the test transducer port. When these adjustments are factored in, the predictions are still within 1 percent of the others up to 180 hertz, and only differ by 2.8 percent at 200 hertz.

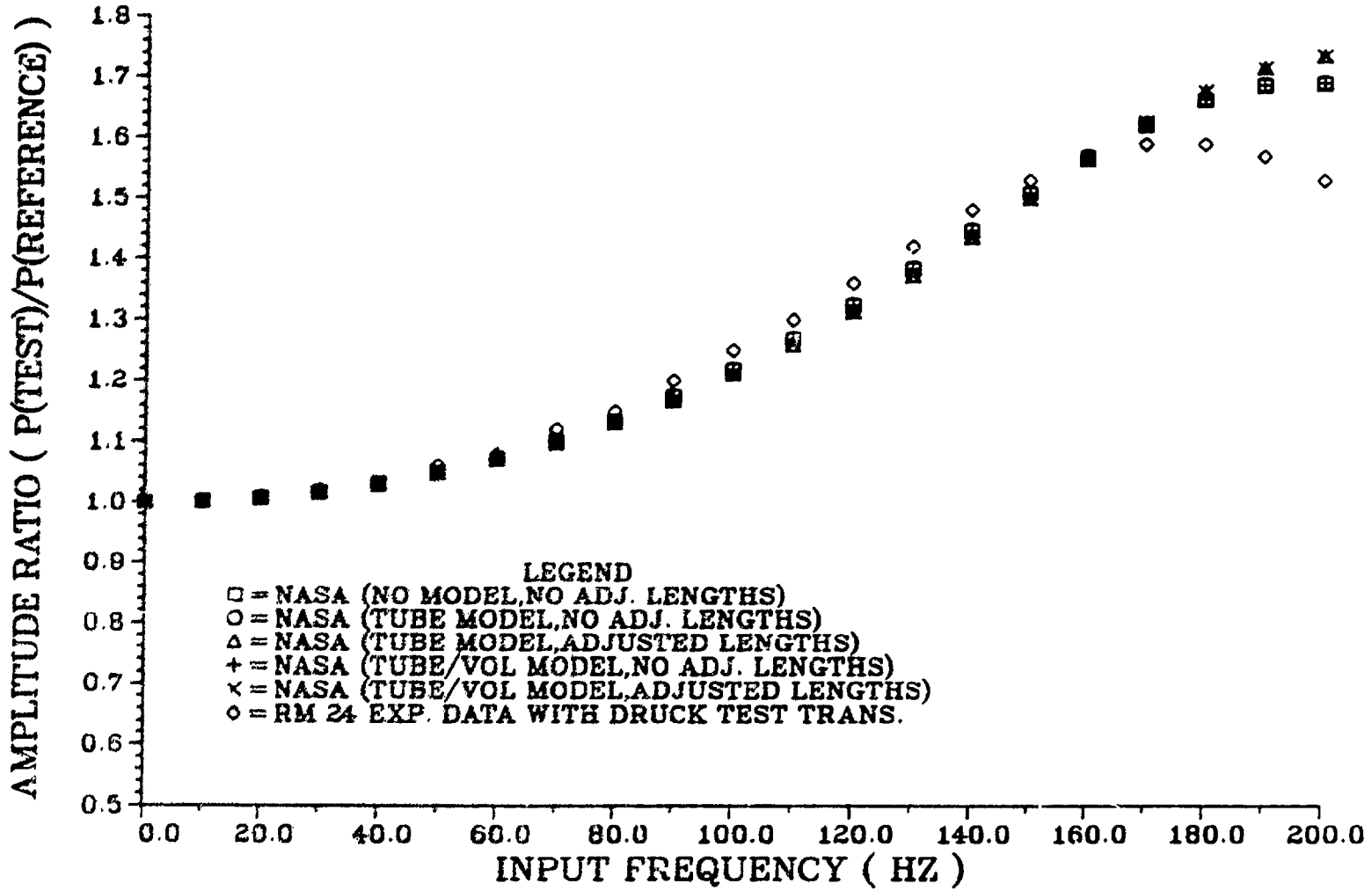

FIGURE 32. EFFECT OF VARIOUS ADAPTER MODELLING METHODS ON NASA FREQUENCY RESPONSE PREDICTIONS FOR A 10.0 IN. TUBE WITH .020 IN. ID

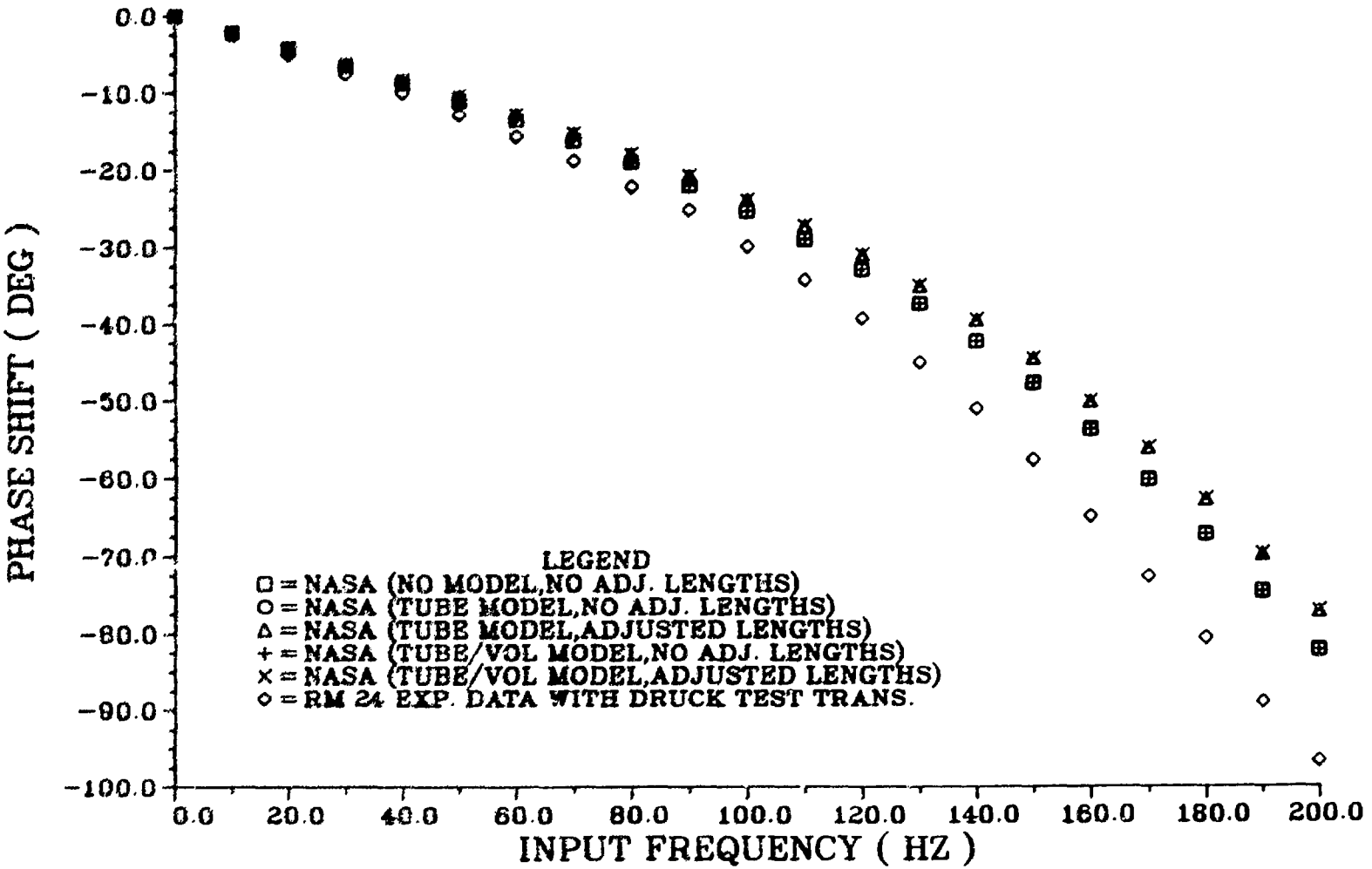

FIGURE 33. EFFECT OF VARIOUS ADAPTER MODELLING METHODS ON NASA FREQUENCY RESPONSE PREDICTIONS FOR A 10.0 IN. TUBE WITH .020 IN. ID

Figure 33 shows the comparison of the phase shift results for the 10.0 inch tube. The phase shift does not compare as favorably as the amplitude ratio. The difference between data and theory increases steadily with frequency. The predicted phase shift is the same as the experimental value only up to 20 hertz. At 100 hertz the difference is up to about 6 degrees, and at 200 hertz the difference has increased to 13.5 degrees. The theoretical predictions are also conservative in that the predicted phase shift is consistently lower than that seen in the experimental data.

Another experiment with the DRUCK test transducer was conducted for a 24.0 inch tube. The results are presented in Figures 34 and 35. The signal generator adapter models were not used in the NASA program for this experiment since their effect on the theoretical results in previous experiments was minimal.

For this tube length, the theoretical predictions of amplitude ratio are consistently greater than the experimental data by as much as 11.8 percent. The trend for both curves is essentially the same, however, throughout the frequency range. The difference between the experimental and predicted values is nearly constant over most of the frequency range. The phase shift comparison, shown in Figure 35, is excellent for this tube. Both curves are nearly linear, with a difference of no more than 7 degrees over the entire frequency range.

The results of these experiments with the DRUCK test transducer were very promising. They showed that the Bergh-Tijdeman theory could be successfully applied to tubes with an inside diameter of 0.020 inch, as long

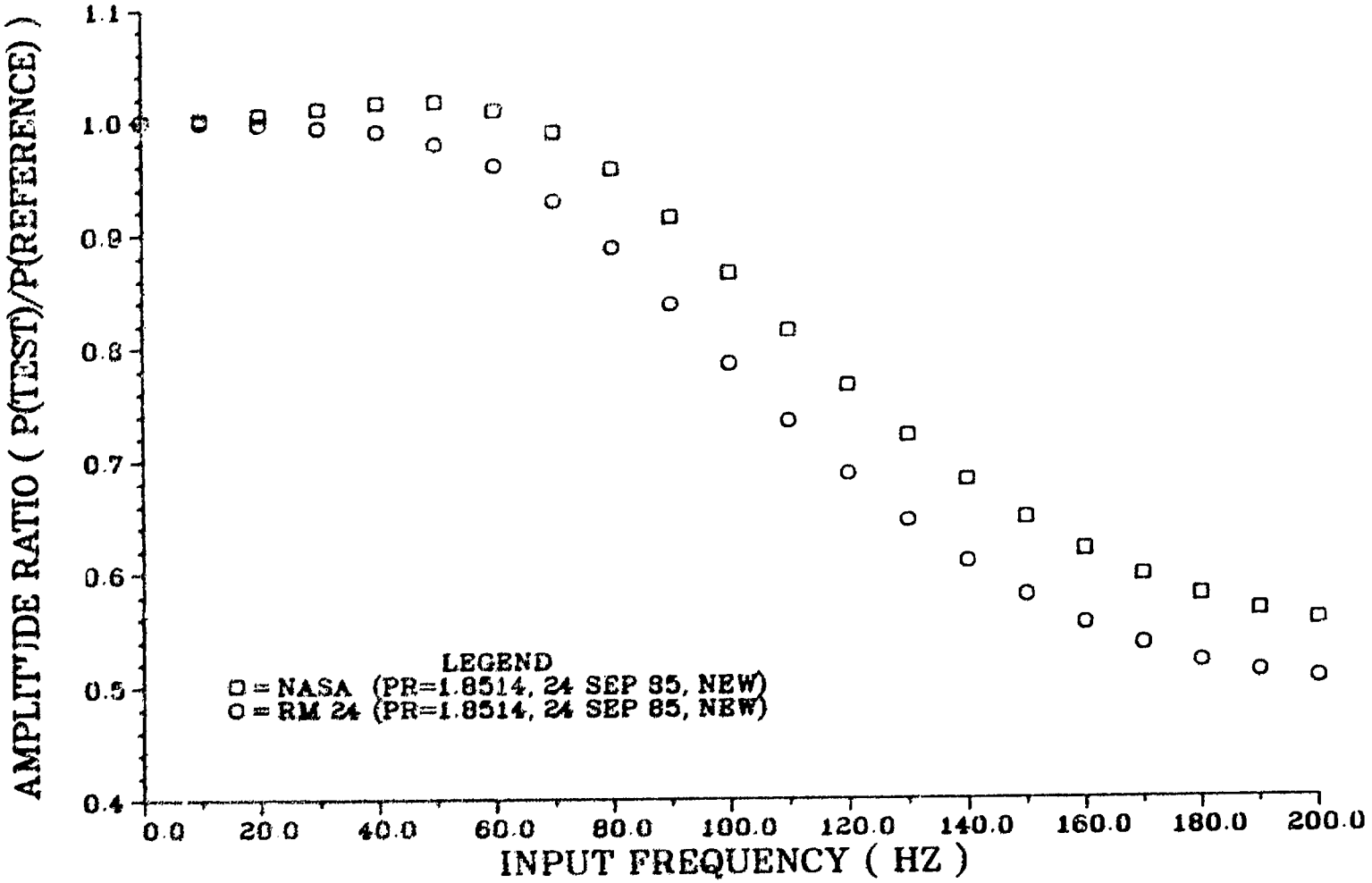

FIGURE 34. COMPARISON OF RM 24 EXPERIMENTAL DATA TO NASA PROGRAM FREQUENCY RESPONSE PREDICTIONS FOR A 24.0 IN. TUBE WITH .020 IN. ID

FIG34

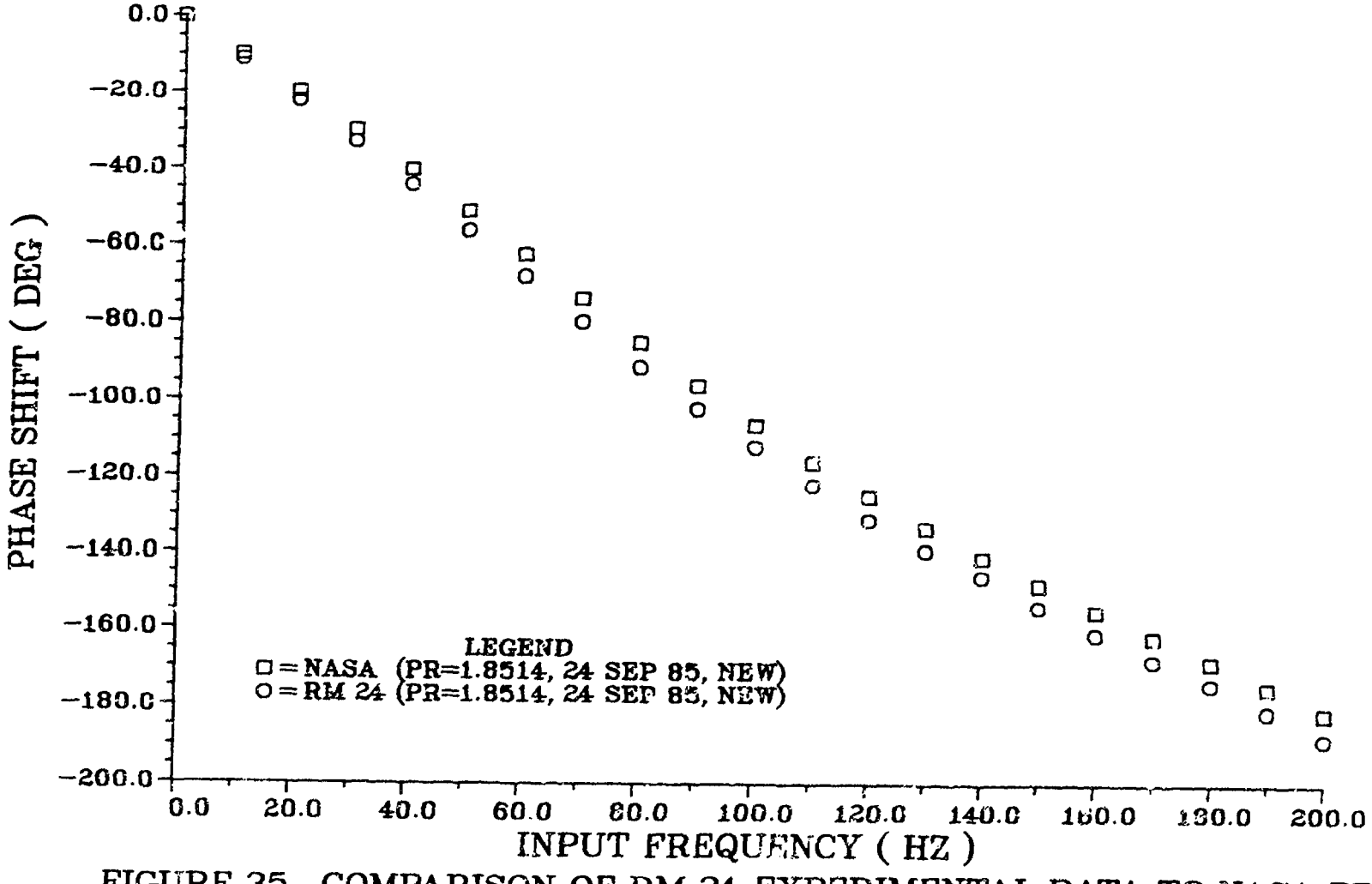

FIGURE 35. COMPARISON OF RM 24 EXPERIMENTAL DATA TO NASA PROGRAM FREQUENCY RESPONSE PREDICTIONS FOR A 24.0 IN. TUBE WITH .020 IN. ID

FIG35

as the test transducer could be accurately described. Using the DRUCK test transducer, the NASA program had produced frequency response predictions that were sufficiently accurate for the purposes of the CRF/F100 program.

3. CONCLUSIONS

The results of the Phase 1 experimental work established the feasibility of using the NASA program to predict the frequency response behavior of the 0.020-inch-inside-diameter tubing on the CRF/F100 test article. Comparisons of the experimental data acquired with a DRUCK test transducer to the NASA program results showed that the theoretical predictions of the gain for a 10.0 inch tube were within 3 percent of the experimental values up to a frequency of 170 hertz, although above this frequency the comparison is worse. For a 24.0 inch tube length, the comparison was within 12 percent over the 200-hertz frequency range. With a 10.0 inch tube, the NASA program predicted the phase shift to within 14 degrees of the experimental value over the 200-hertz range, while for the 24.0-inch tube the comparison was within 7 degrees.

In contrast, the comparison of the experimental data acquired with the ZOC test transducer to the NASA program results was generally poor. There were large differences between the experimental and theoretical values of amplitude ratio and phase shift for all tube lengths tested. For example, with the 10.0 inch tube the theoretical and experimental amplitude ratios differed by 13 percent at the frequency of the experimental peak, and the phase shift differed by over 25 degrees. The primary reason for the disparity was the dimensions being used to model the ZOC transducer in the NASA program. The equivalent geometry values quoted by the manufacturer were simply unacceptable for modelling the ZOC in the NASA program.

Various methods of modelling the signal generator adapter were found to have minimal effect on the theoretical predictions of the frequency response for the tubes tested in the Phase 1 experiments. However, the effects of this adapter on the experimental data, if any, were not determined in the Phase 1 experimental work.

SECTION IV

EXPERIMENTAL DETERMINATION OF FREQUENCY RESPONSE - PHASE 2

1. GENERAL

The results obtained from the Phase 1 experiments, and their comparison with the theory, strongly indicated the need for further investigation in two areas.

First of all, it was necessary to determine what effect, if any, the signal generator adapter may have had on the experimental data acquired in the Phase 1 experiments. The ideal situation would be to have no adapter at all, with the reference transducer mounted directly to the pressure signal source. This arrangement was not possible with the Room 24 experimental setup, but the adapter had been made as short as possible to minimize any distortion of the pressure signal before it reached the reference transducer location. However, any effect the adapter may have had on the data could not be accounted for in the Phase 1 experimental setup. Therefore, a series of experiments was needed using a new experimental setup in which the signal generator adapter was eliminated altogether. Then by comparing the data acquired from the setups with and without the adapter, it would be possible to quantify the effect of the adapter on the Phase 1 experimental data. The details of this effort are presented in this section.

A second area requiring further investigation was the choice of internal geometry to be used in modelling the ZOC test transducer for the NASA program. The equivalent values for the internal geometry which were used in the Phase 1

experiments proved to be invalid. Therefore, it was necessary to determine a set of values for the internal geometry that would provide an accurate model of the transducer for the NASA program. The development of the values for this model is described in Section V.

2. PHASE 2 EXPERIMENTS

In this phase of the experimental work, a new experimental setup was used to overcome the limitations encountered during the Phase 1 experiments. The main problem with the Phase 1 setup was the reference length between the signal generator output and the reference transducer. Other limitations with the setup were: (1) the tee connection in the signal generator adapter required for interconnecting the test tube, (2) a variation in dynamic pressure level with frequency due to limitations of the Fluidics signal generator, (3) an upper limit on the mean pressure in the tube of approximately 1.85 atmospheres due to input pressure level restrictions for the signal generator, and (4) the inability to change the mean level of the dynamic pressure signal, which was needed to investigate larger perturbation pressure effects.

To eliminate these problems, a new dynamic pressure source was used, along with a new interface for the test tube and reference transducer. The pressure source used was a Multilevel Pistonphone Calibrator, provided by the Environmental Acoustics Branch of the Armstrong Aeromedical Research Laboratory (AAMRL) here at Wright-Patterson AFB. The Phase 2 experiments were conducted at the AAMRL.

Using the pistonphone calibrator and specially fabricated adapter hardware, a series of experiments was conducted at the AAMRL for both 10.0 inch and 24.0 inch tubes. With this experimental setup, many of the limitations noted for the Phase 1 setup were eliminated.

Using the calibrator it was possible to run tests with tube mean pressures both lower and higher than the levels attainable in Phase 1. The first series of experiments using this setup were run at atmospheric chamber pressure. In the Phase 1 experiments, the lowest average pressure in the tube was about 5 psig. The next set of Phase 2 experiments were run with the calibrator chamber pressurized. In one instance, the pressure was set to about 1.85 atmospheres. This pressure was chosen to match the highest level achieved in the Phase 1 experiments. Matching the mean pressure levels was done to allow direct comparison of the experimental results. The final pressurized tests were run at approximately 2.5 atmospheres. This pressure was chosen because it was the expected mean pressure level within the CRF/F100 rig during rotating stall. Data at this pressure level could not be obtained in Phase 1 because of the input pressure restrictions of the signal generator.

a. Experimental Apparatus and Data Acquisition Equipment

A photograph of the AAMRL experimental setup is shown in Figure 36. The pistonphone calibrator is shown on the portable cart. A close-up of the calibrator is shown in Figure 37, with the adapter, containing the reference transducer and test tube, mounted in one of the calibrator's test chambers. Details of the adapter used to mount the reference transducer and test tube into the various pistonphone calibrator chambers can be seen in Figures 38 and 39. Figure 38 shows the top of the adapter, detailing the mounting of the reference transducer and test tube. In Figure 39, the inner face of the

Figure 36. Hardware and Data Acquisition Equipment Used in the AAMRL Experimental Set-Up

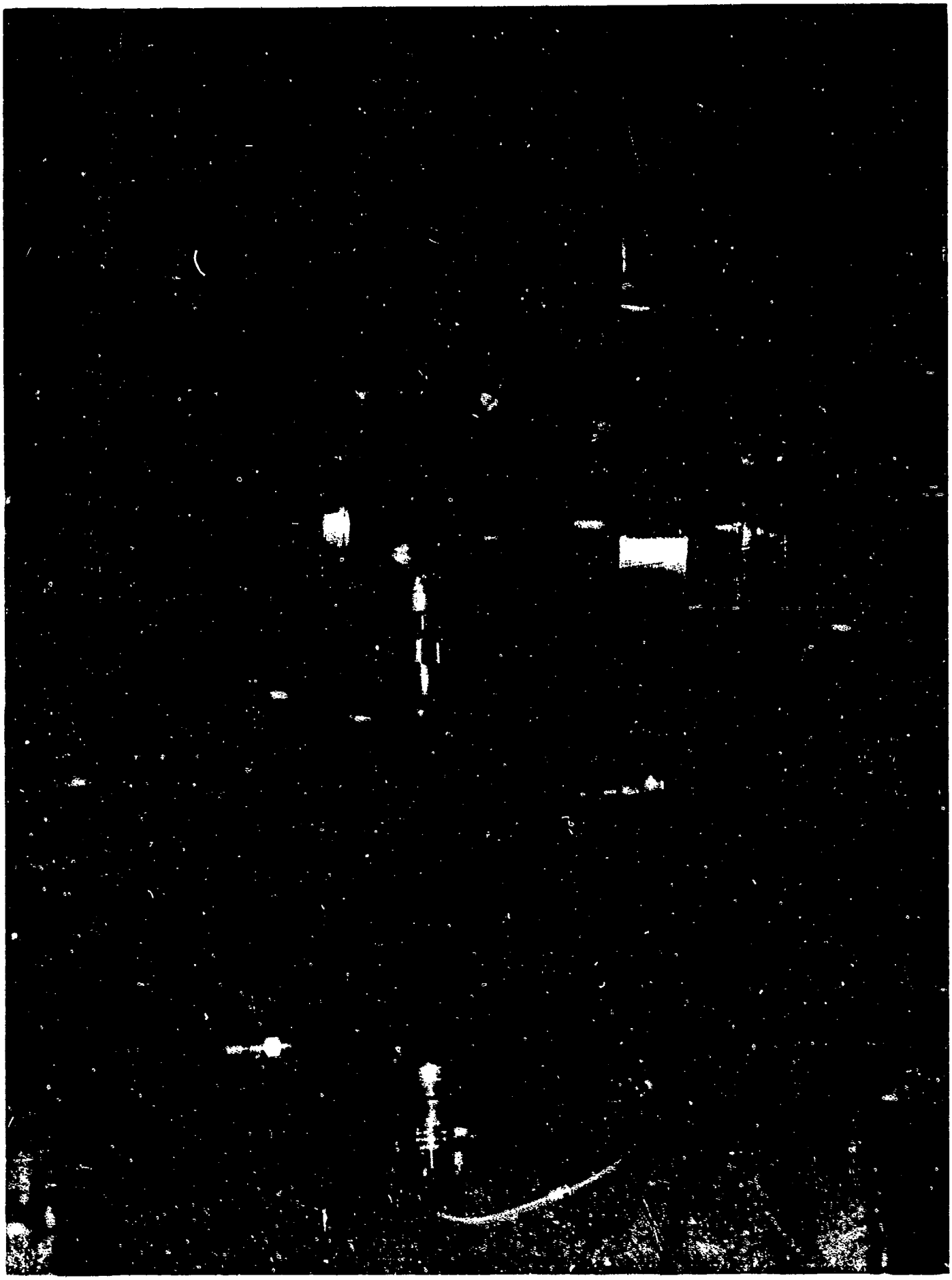

Figure 37. Multilevel Pinstonphone Calibrator with Adapter Installed

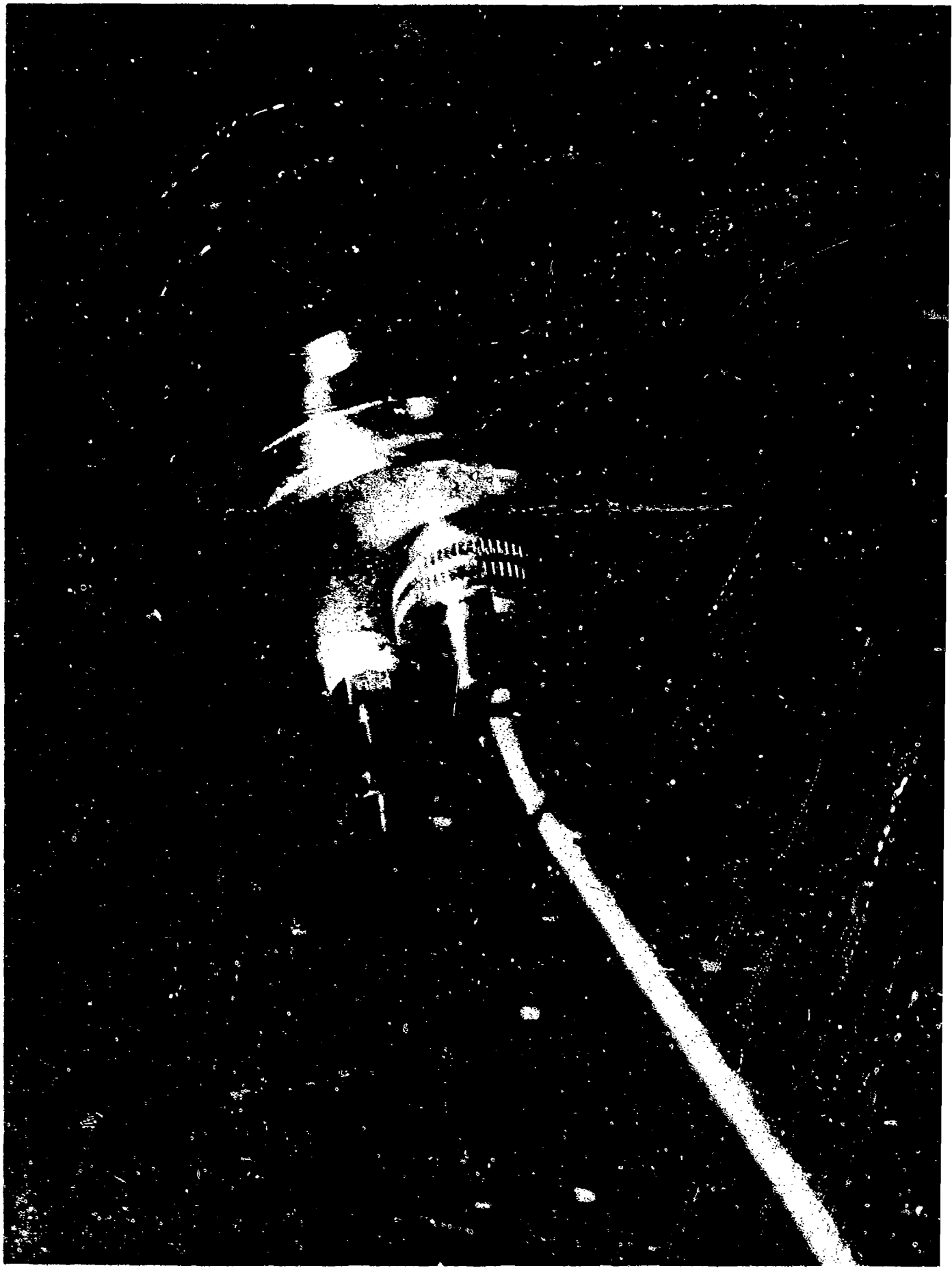

Figure 38. Pistonphone Calibrator Adapter Showing Mounting Details

Figure 39. Pistonphone Calibrator Adapter, Inner FAce

adapter is shown. Notice that with this adapter both the test tube and the reference transducer are flush-mounted at the adapter inner face, thereby eliminating the reference length and tee connection present in the Phase 1 experimental setup. A block diagram of the AAMRL experimental setup is shown in Figure 40.

The test tube length and reference transducer were mounted at the top of a given calibrator chamber via the adapter shown in Figures 38 and 39. A schematic of the adapter hardware is shown in Figure 41. The DRUCK reference transducer was mounted by threading the outer sleeve of the transducer into the adapter. An O-ring was installed as near to the inner face of the adapter as possible to provide a seal for the transducer without altering the volume of the chamber. The test tube was mounted in a Swagelok fitting. To prevent crimping of the 0.020-inch-inside-diameter tube, a sleeve of larger diameter tubing was placed over the 0.020-inch-inside-diameter tubing within the fitting. This sleeve was soldered to the inner tube to seal the connection. The placement of the sleeve was such that one end of the 0.020-inch-inside-diameter tube was flush with the inner face of the adapter. Two of these tubes and fittings were made--one with an overall tube length of 24.0 inches, and the other with an overall length of 10.0 inches. Figure 42 is a photograph of the 24.0 inch tube and fitting. Figures 43 and 44 show the details of the connection at each end of the tube. Teflon tape was applied to the threads on the fitting to seal the connection at the adapter.

The adapter was held in place atop the chamber with two arms which were rotated to clamp over the outer lip of the adapter. Silicone grease was applied to the adapter prior to installation in the chamber to provide a seal at the adapter/chamber interface.

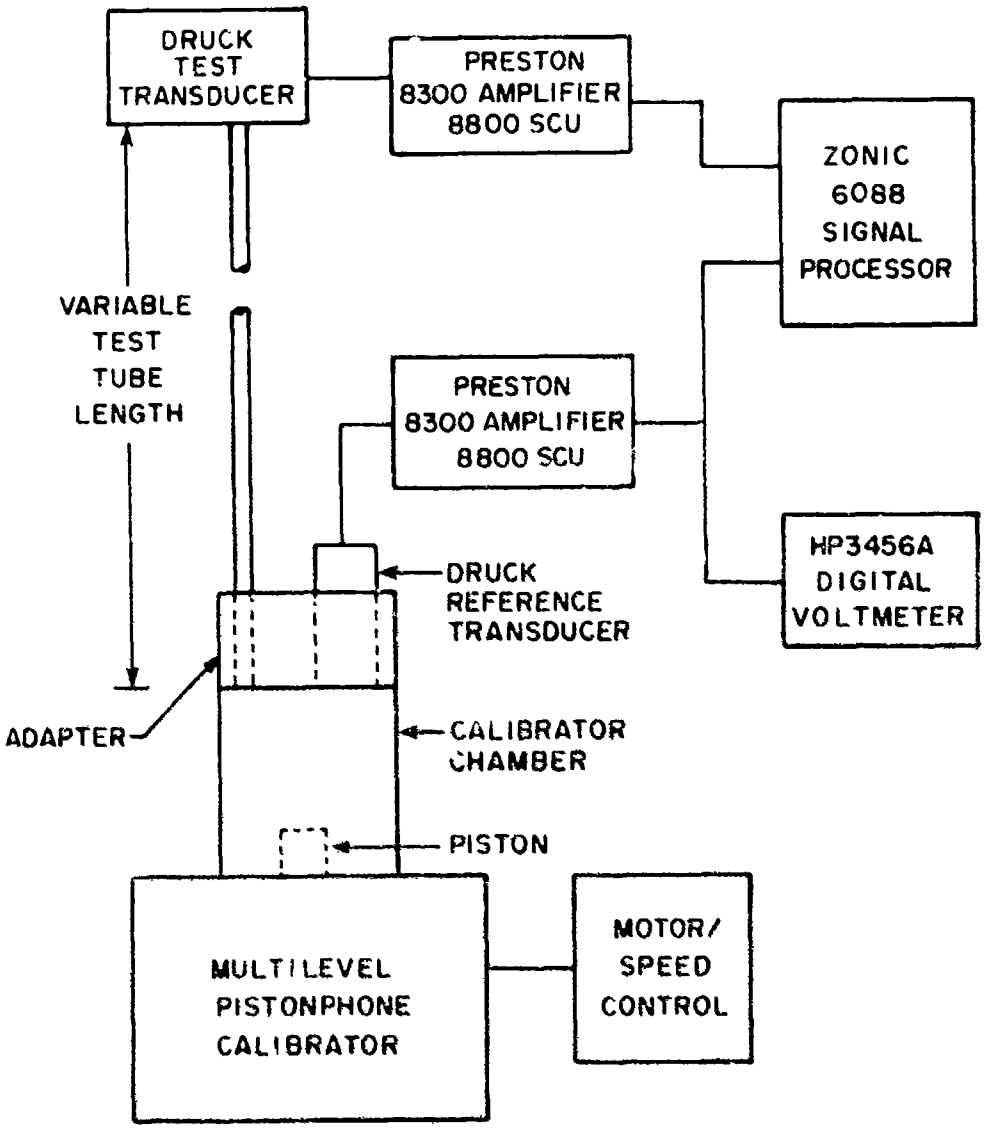

FIGURE 40. Block Diagram of AAMRL Experimental Set-Up

MATERIAL: BRASS DIMENSIONS: INCHES

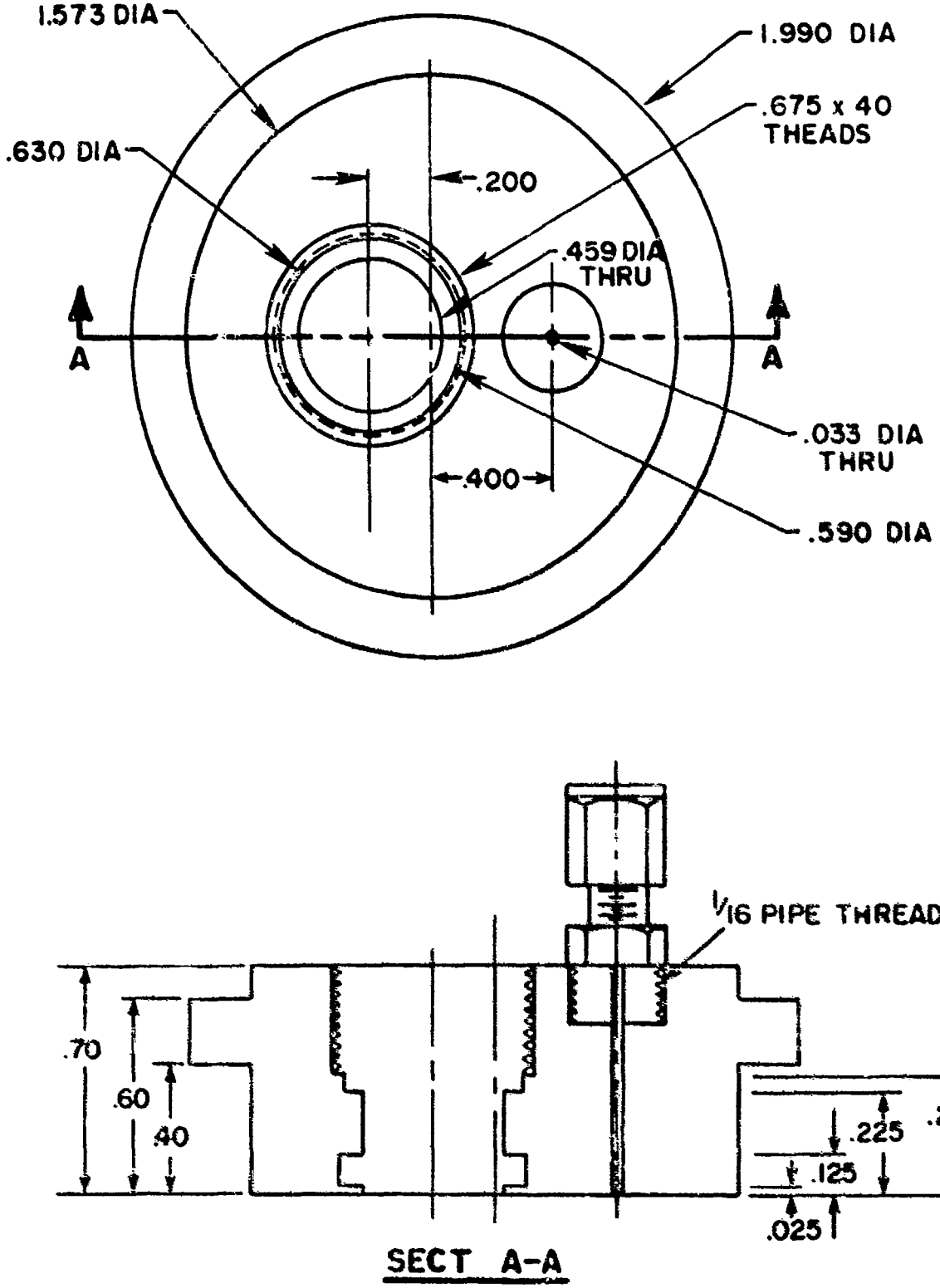

FIGURE 41. Schematic of the Pistonphone Calibrator Adapter

Figure 42. 24.0-inch Tube and Fitting

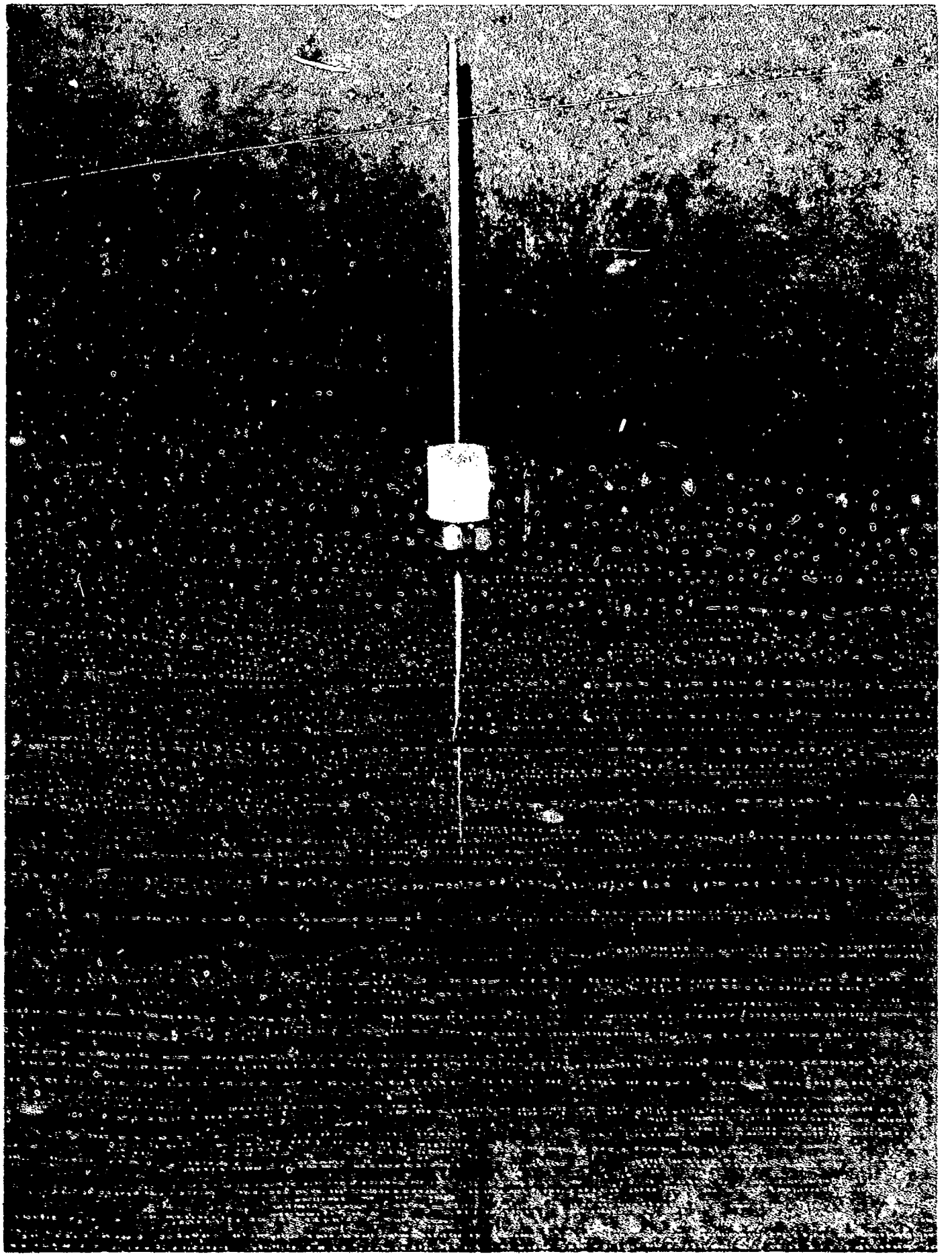

Figure 43. 24.0-Inch Tube-Adapter Fitting End

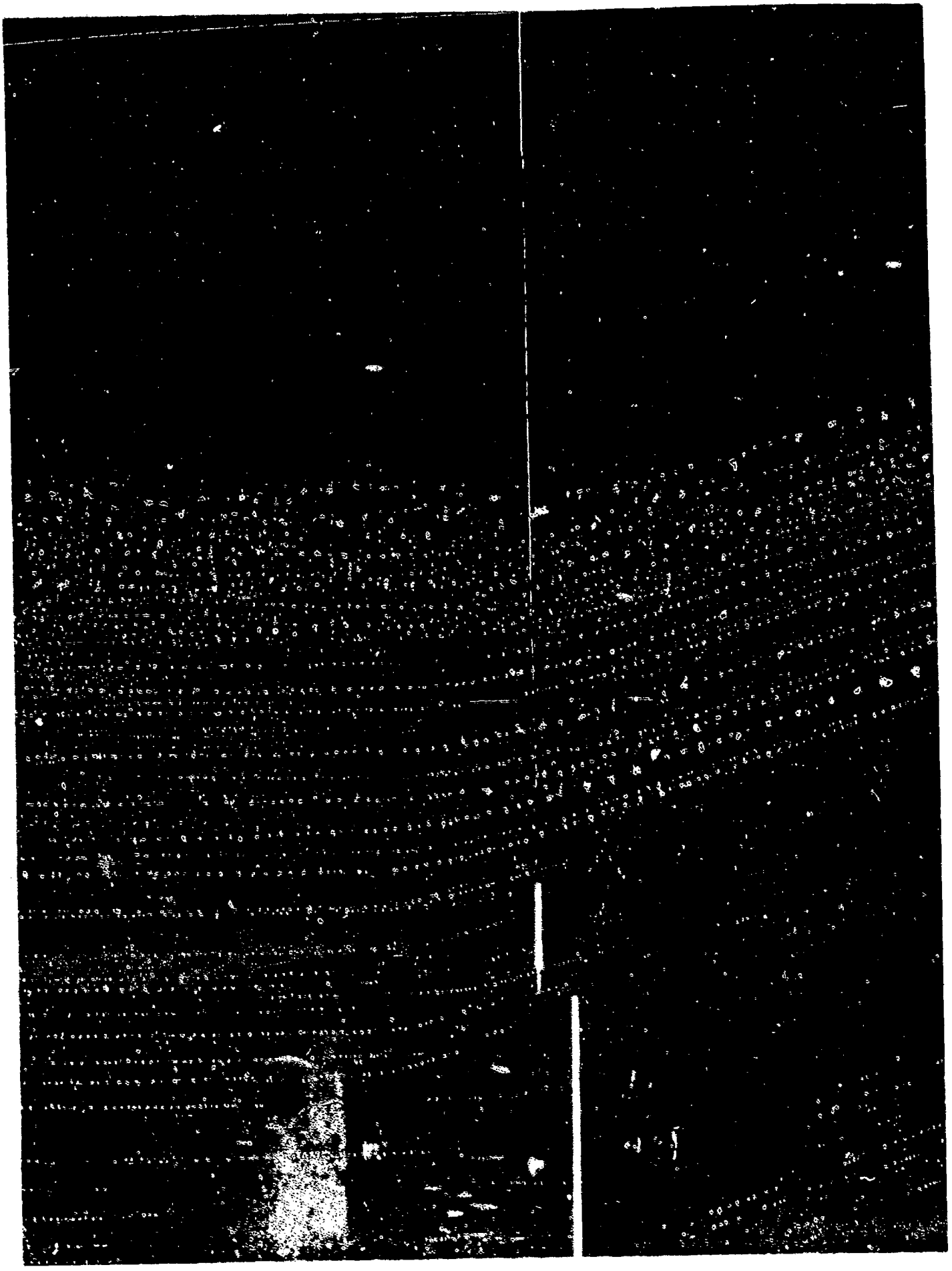

Figure 44. 24.0-Inch Tube-Transducer Fitting End

One of the advantages of the calibrator was that tests could be done at higher pressure ratios than could be achieved in the Phase 1 experiments. To do this, it was necessary to increase the mean pressure in the calibrator chamber. This was accomplished by using one of the two bleed ports on each of the chambers. A hollow bleed screw was fabricated for this purpose. This hollow screw could be attached to a bottle of pressurized nitrogen and then threaded into one of the chamber bleed ports when it was necessary to pressurize the chamber.

Another feature of the calibrator is the ability to change the dynamic pressure level. A piston moving in and out of a fixed volume chamber produces the oscillating pressure signal. The calibrator has two different size pistons and four chambers of different volume. Various combinations of piston and chamber sizes can be used to produce 8 discrete dynamic pressure levels, from a low of 109 dB to a high of 175 dB. With a reference pressure level of 2.9E-9 psi these dB levels correspond to 8.17E-4 psi and 1.45 psi, respectively. These dynamic pressures can be produced over a frequency range from 0.5 to 90 hertz. In addition, the dynamic pressure level is essentially constant over the frequency range.

An electric motor with a rheostat control is used to drive the piston. The piston crankshaft is connected to the motor using pulleys and a drive belt. A flywheel is also connected to the piston crankshaft for speed stabilization. An optical transducer is used to measure the flywheel speed. An oscilloscope was used to monitor this signal. The signal was also fed into a frequency counter to measure the flywheel period, from which the piston frequency was determined.

A DRUCK transducer was used as the test transducer for these experiments. It was connected to the 0.020-inch-inside-diameter tubing using heat shrink tubing, as before. The calibration data for this transducer is in Appendix B.

The remaining data acquisition equipment was the same as that used previously in the Phase 1 experiments. The transducer signals were routed through the Pacific amplifier and signal conditioner units, and monitored with the HP3456A Digital Voltmeter and ZONIC 6088 Signal Processor, as before.

b. Experimental Procedures

The experimental procedures for these tests were similar to those used previously in Phase 1. Each experiment was carried out as follows:

1. The appropriate piston and chamber was selected to give the desired dynamic pressure. The chamber adapter, with the reference transducer and test tube in place, was mounted on the chamber. If a pressurized chamber was needed, one of the standard chamber bleed screws was replaced with the hollow bleed screw. A line from the nitrogen bottle was connected to the hollow bleed screw to provide the pressure needed.

2. The speed of the electric motor was adjusted to produce a piston frequency in the range from 10 to 90 hertz. This frequency was checked, as before, by examining a spectrum display of the reference transducer with the ZONIC signal processor.

3. The chamber was pressurized if needed. The chamber pressure was calculated from the dc voltage output of the reference transducer.

4. To take the raw data, average it, and display the results, the ZONIC control program was executed. A brief display of the transfer function for the tube was shown, followed by a table of values for the amplitude ratio and phase shift. The values for the current input frequency were then recorded. The data acquisition and averaging scheme used in Phase 1 was also used in these experiments.

5. The piston frequency was increased in increments of 10 hertz and a new set of data was acquired.

6. The entire process was repeated until all test cases for both tube lengths were completed.

c. Experimental Results and Comparison to Theoretical Predictions

During this phase of the project a total of 11 experiments were completed. The individual test cases and test conditions are shown in Table 3. All of the experiments for the 10.0 inch tube were completed as originally planned. Not shown in the table are the experiments originally planned for the 24.0 inch tube with a pressurized test chamber. These tests were attempted but finally abandoned due to problems with the pistonphone calibrator. Experiments with an atmospheric chamber pressure were completed for the 24.0 inch tube instead.

(1) Experiments with a 10.0-Inch Tube

For the 10.0-inch tube with an atmospheric chamber pressure, experiments were conducted with dynamic pressure levels of 130, 145, 159, and 175 dB. The results of these experiments are plotted in Figures 45-52. Plots of the amplitude ratio and phase shift are shown together with the NASA program theoretical predictions.

The comparison of this data with the theory is very good. The theoretical prediction for the amplitude ratio is within 8 percent of the

Table 3. Summary of the Phase 2 Experiments

Tube Geometry					
Length (inches)	Diameter (inches)	Chamber Pressure (Atmospheres)	Dynamic Pressure (dB)	(Psi)	Dynamic/Chamber Pressure Ratio (%)
10.0	0.020	1.0	130	0.00917	0.0641
10.0	0.020	1.0	145	0.0516	0.3606
10.0	0.020	1.0	159	0.256	1.808
10.0	0.020	1.0	175	1.63	11.41
10.0	0.020	1.85	130	0.00917	0.0347
10.0	0.020	1.85	145	0.0516	0.1950
10.0	0.020	1.85	175	1.63	6.166
10.0	0.020	2.5	175	1.63	4.562
24.0	0.020	1.0	130	0.00917	0.0641
24.0	0.020	1.0	138	0.0230	0.1611
24.0	0.020	1.0	175	1.63	11.41

experimental data for each of the four cases shown. The greatest discrepancy in each case occurs at the highest frequencies. As with the Phase 1 experiments, the predicted amplitude ratio is consistently greater than the actual measured value. Changing the dynamic pressure level appears to have no effect on the data. For the four cases shown in Figures 45-52, the dynamic pressure level was increased from a low of 130 dB (0.009 psi) to a high of 175 dB (1.45 psi). At least over this range, there is no trend in the data to indicate that the dynamic pressure level is a factor in the frequency response of the tube.

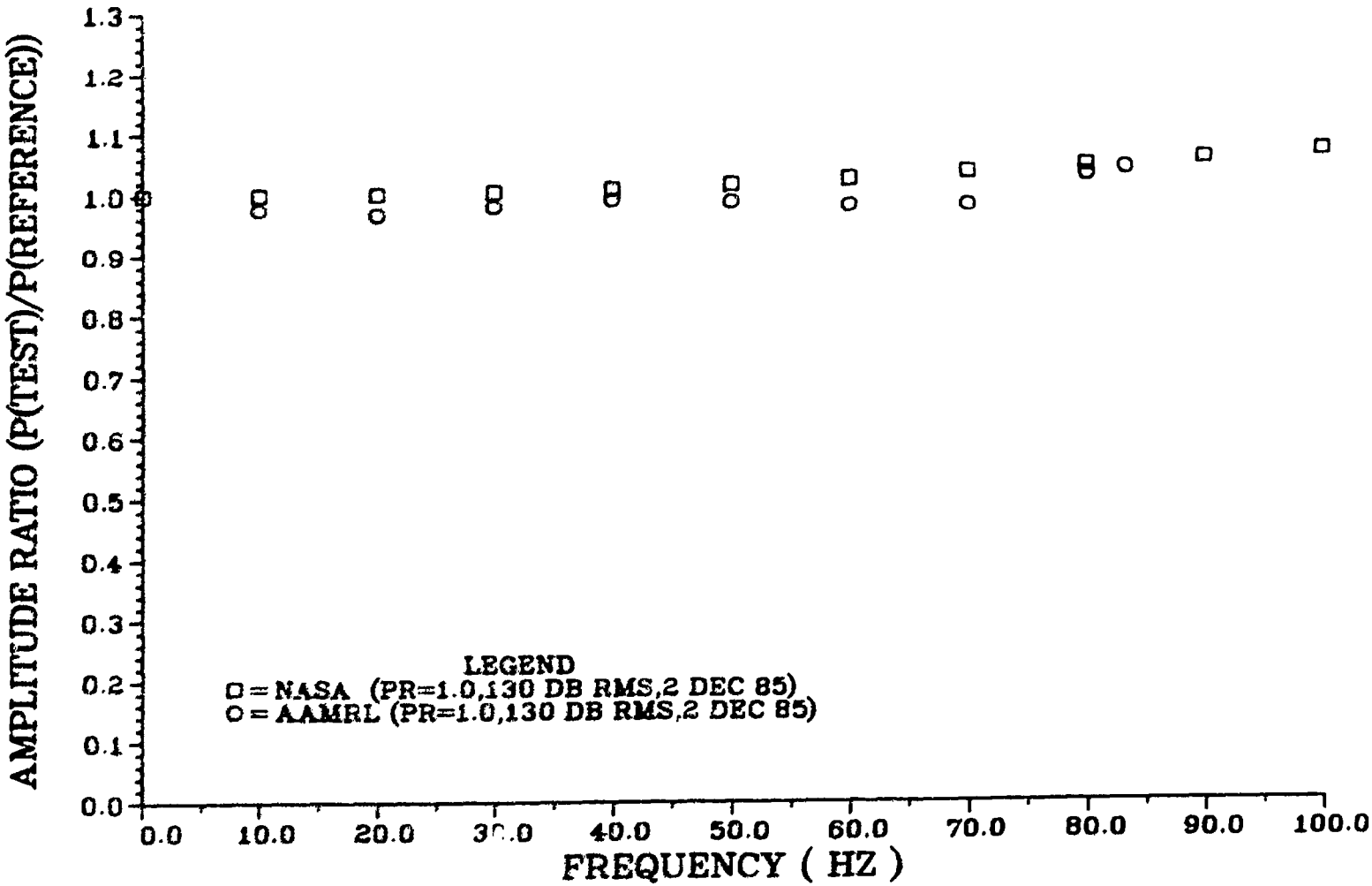

FIGURE 45. COMPARISON OF AAMRL EXPERIMENTAL DATA TO NASA PROGRAM FREQUENCY RESPONSE PREDICTIONS FOR A 10.0 IN. TUBE WITH .020 IN. ID

FIG45

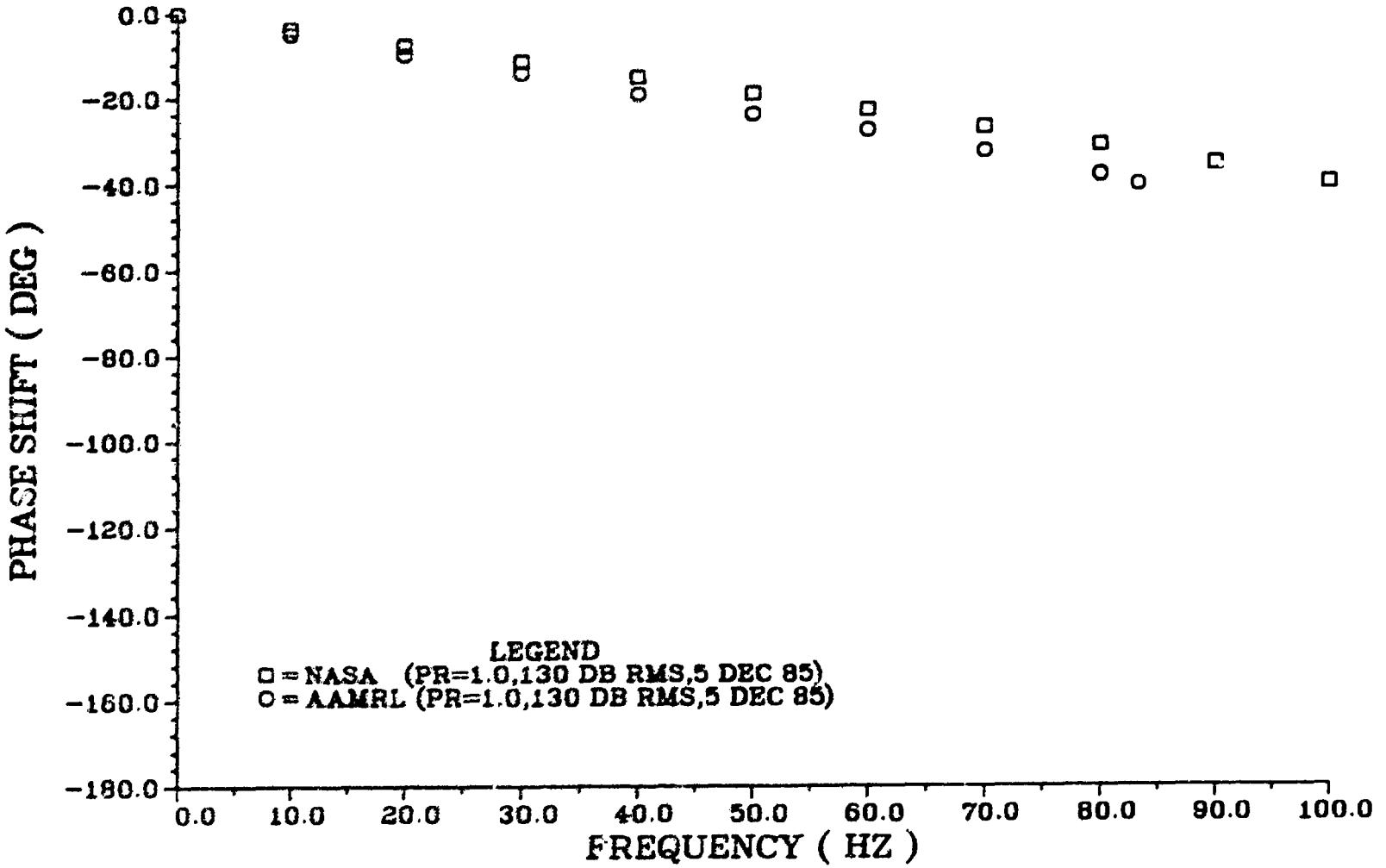

FIGURE 46. COMPARISON OF AAMRL EXPERIMENTAL DATA TO NASA PROGRAM FREQUENCY RESPONSE PREDICTIONS FOR A 10.0 IN. TUBE WITH .020 IN. ID

FIG46

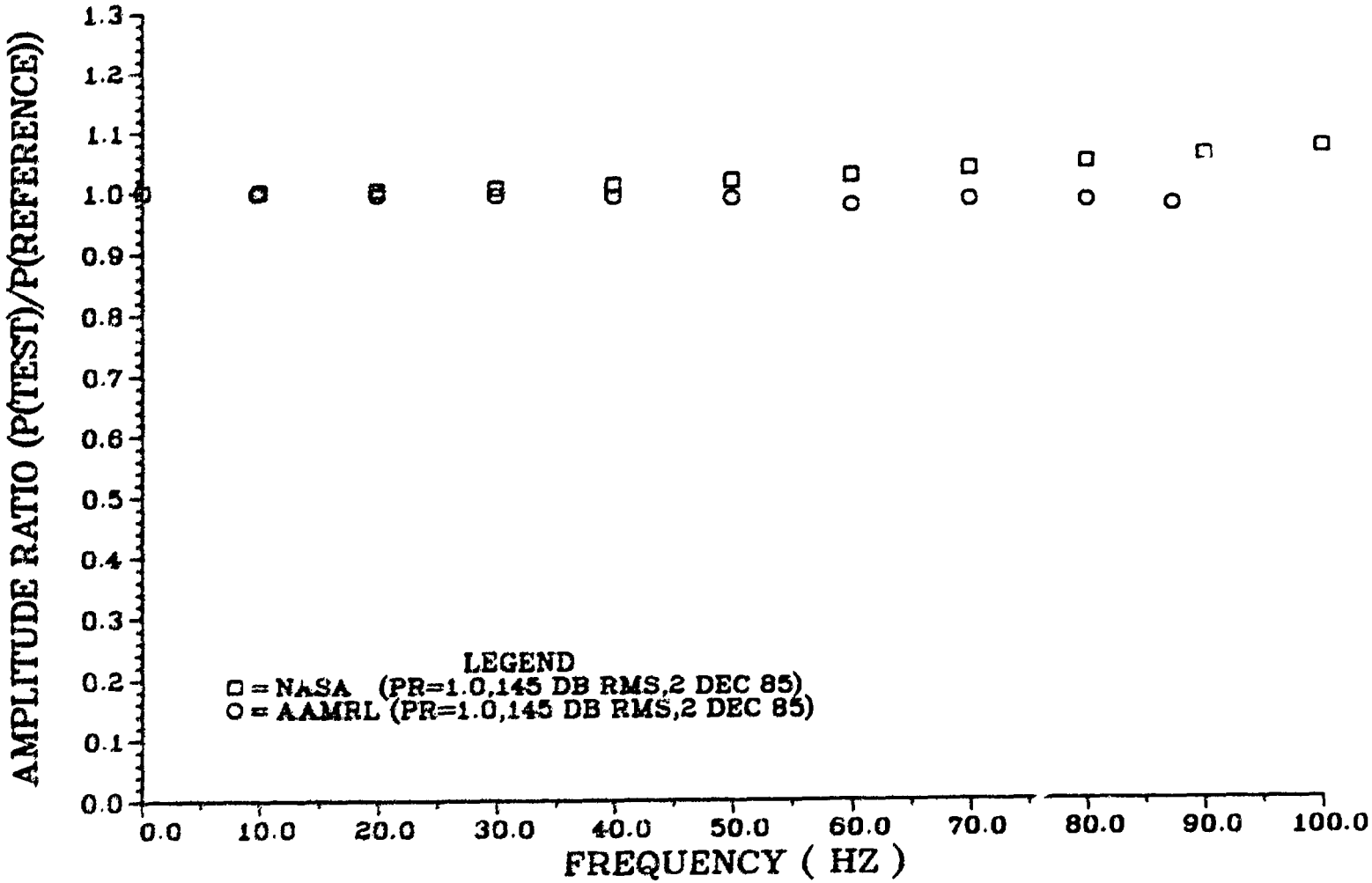

FIGURE 47. COMPARISON OF AAMRL EXPERIMENTAL DATA TO NASA PROGRAM FREQUENCY RESPONSE PREDICTIONS FOR A 10.0 IN. TUBE WITH .020 IN. ID

FIG47

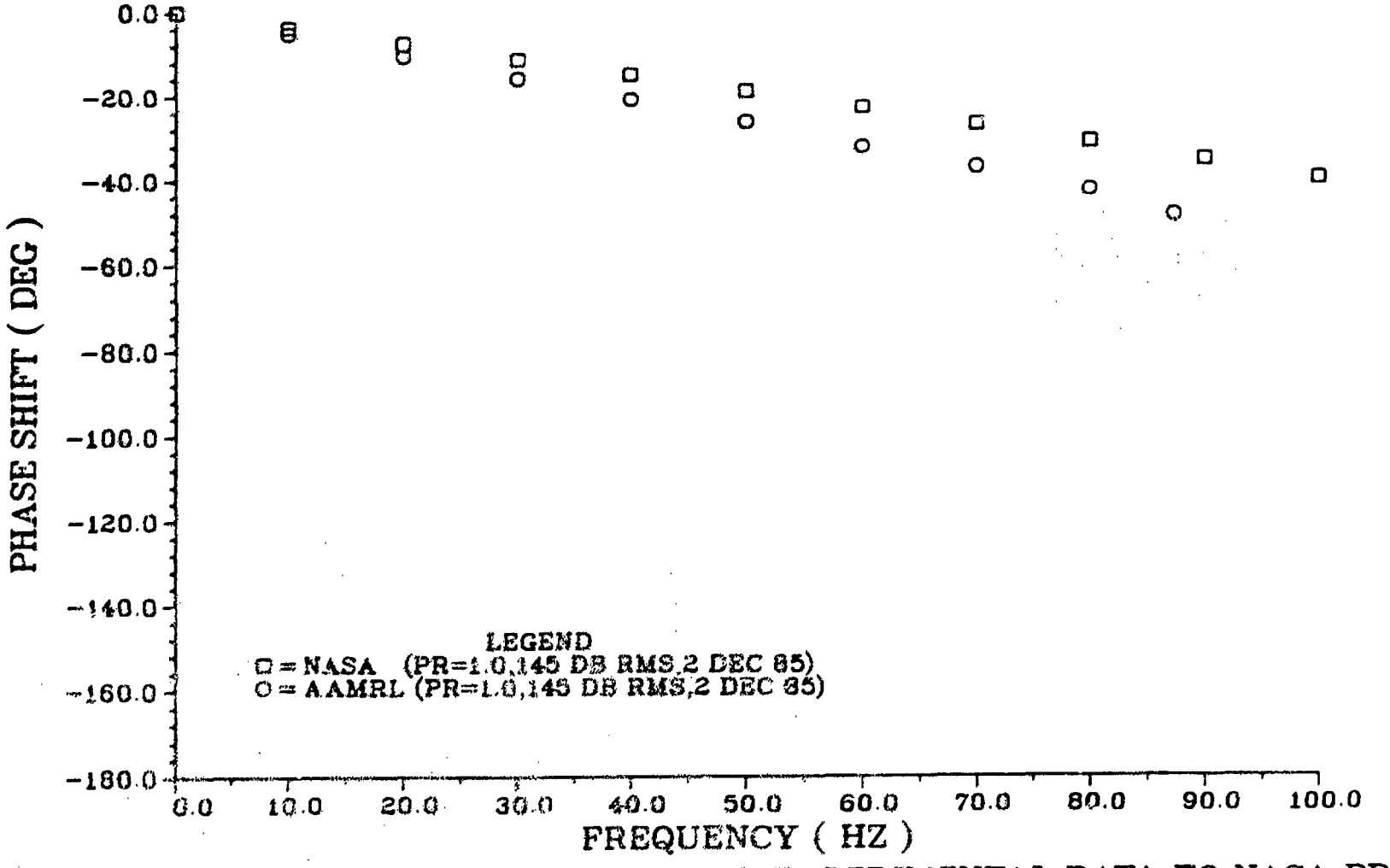

FIGURE 48. COMPARISON OF AAMRL EXPERIMENTAL DATA TO NASA PROGRAM FREQUENCY RESPONSE PREDICTIONS FOR A 10.0 IN. TUBE WITH .020 IN. ID

FIG48

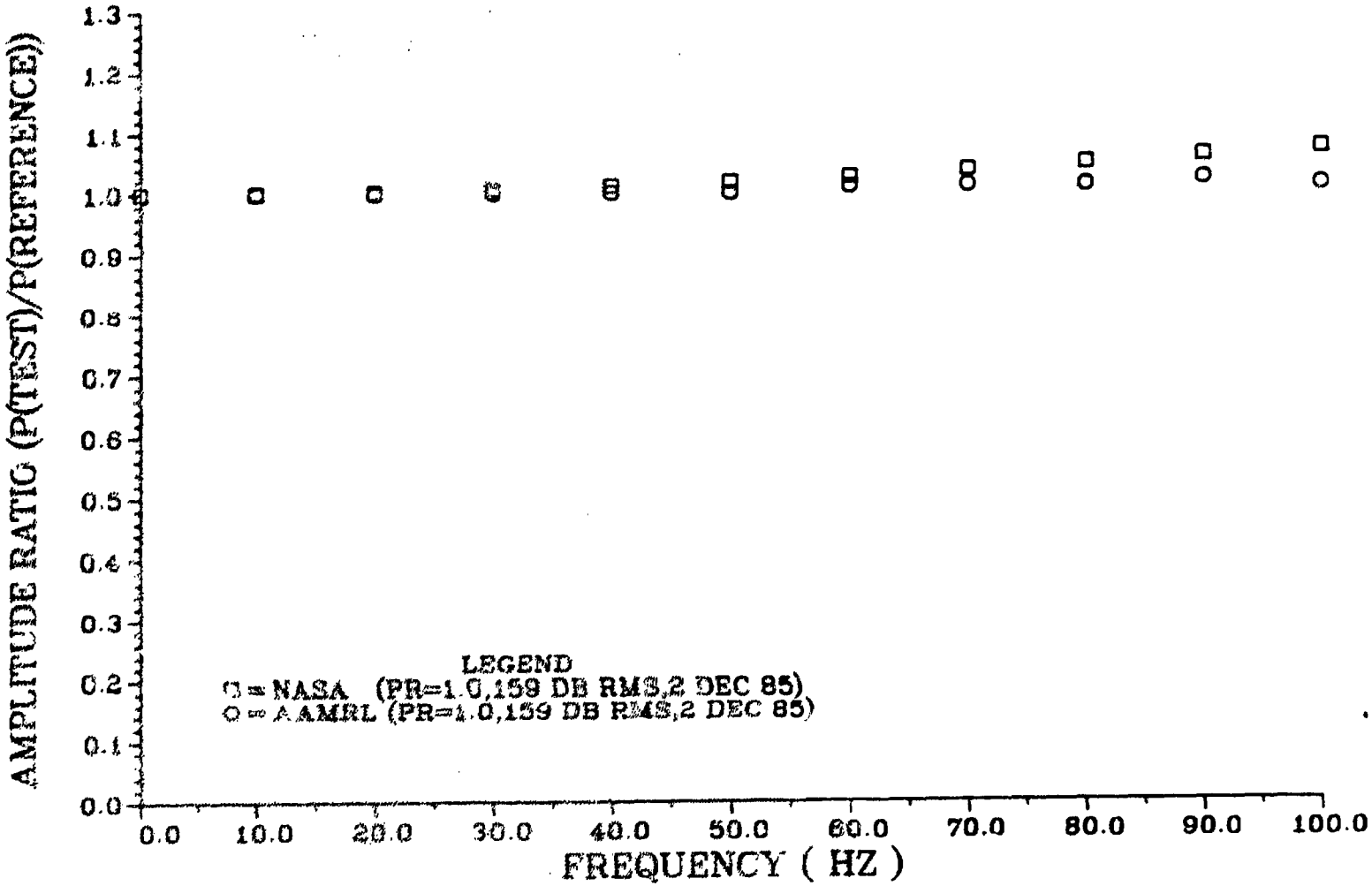

FIGURE 49. COMPARISON OF AAMRL EXPERIMENTAL DATA TO NASA PROGRAM FREQUENCY RESPONSE PREDICTIONS FOR A 10.0 IN. TUBE WITH .020 IN. ID

FIG49

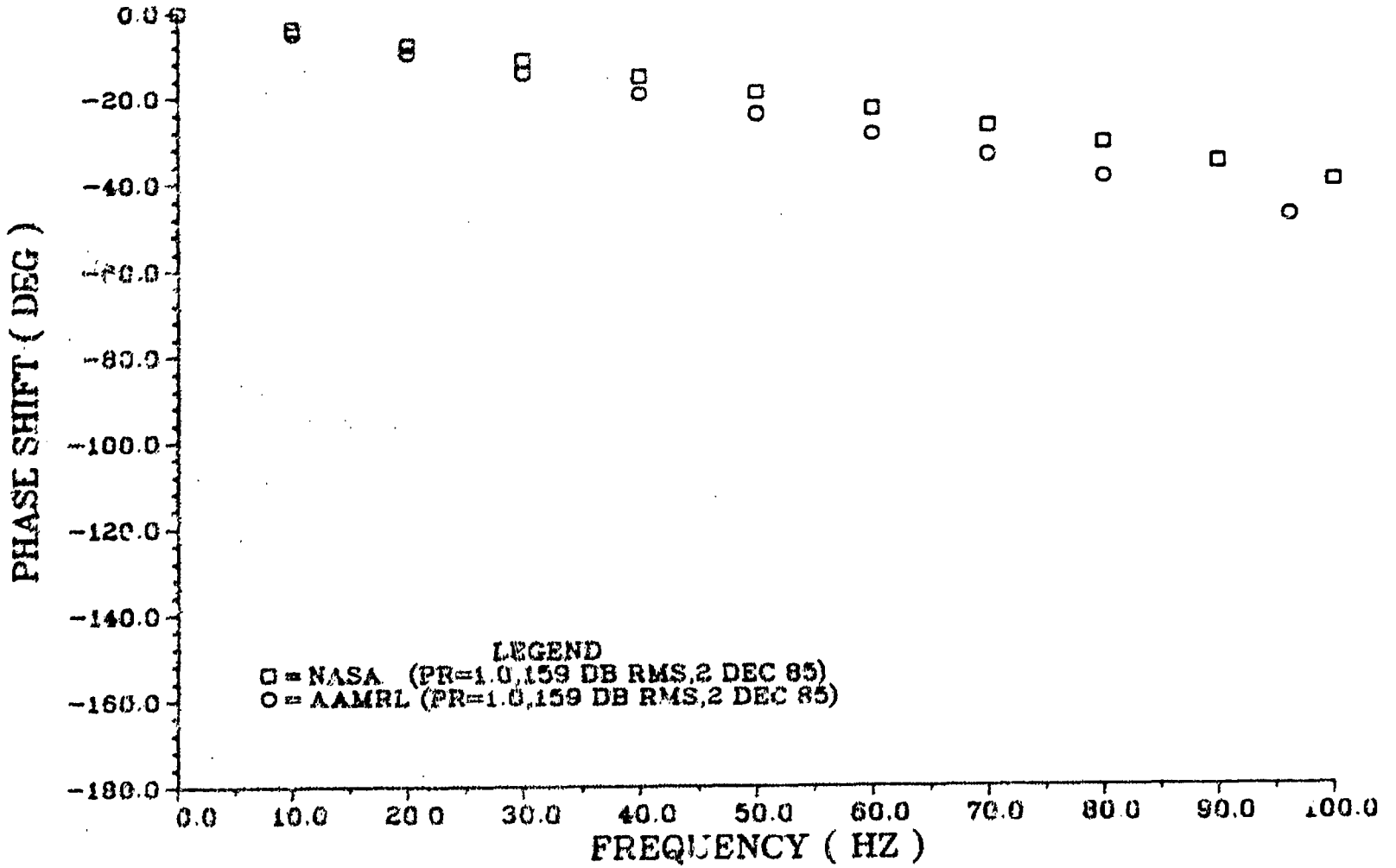

FIGURE 50. COMPARISON OF AAMRL EXPERIMENTAL DATA TO NASA PROGRAM FREQUENCY RESPONSE PREDICTIONS FOR A 10.0 IN. TUBE WITH .020 IN. ID

F1C50

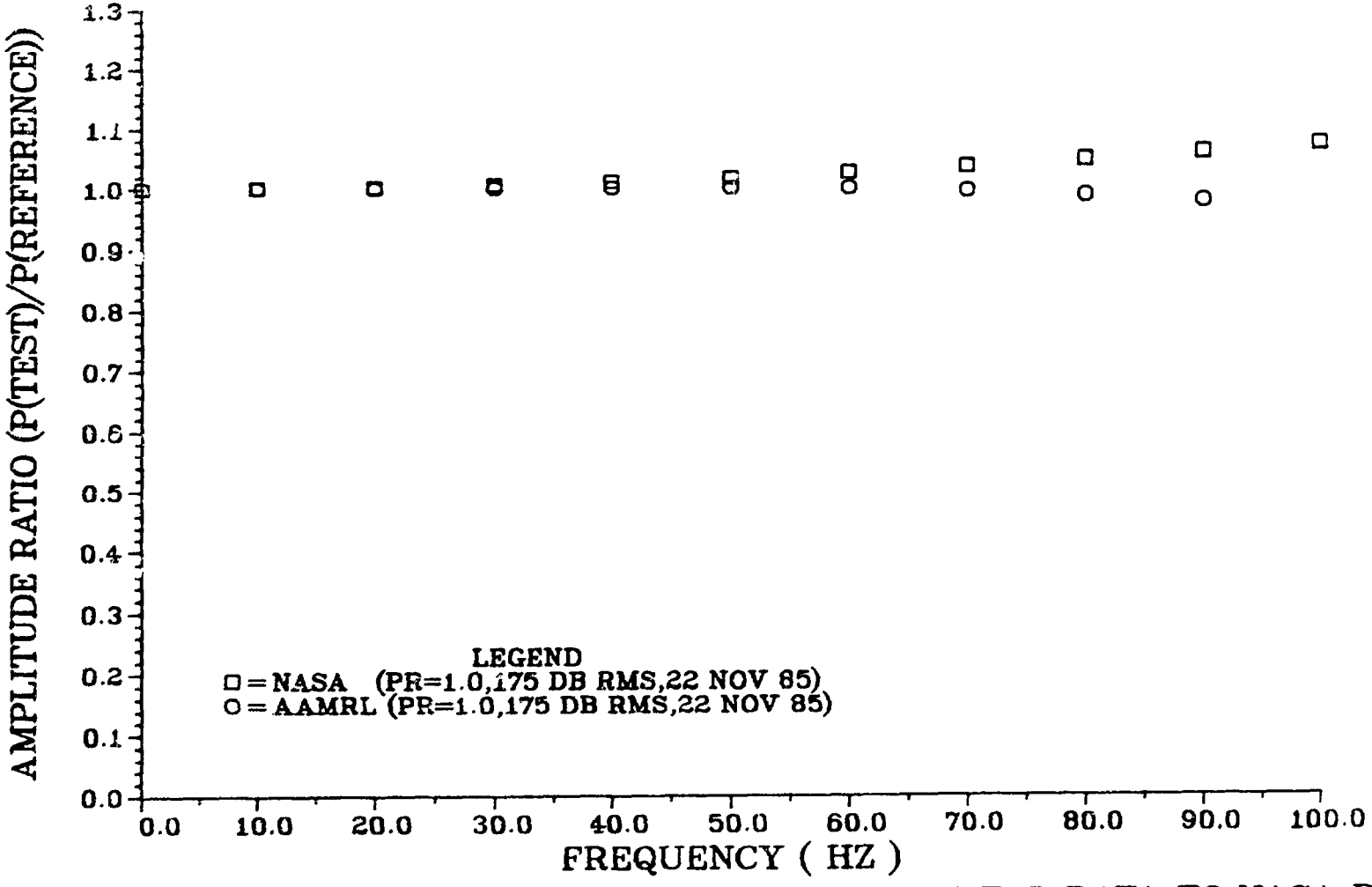

FIGURE 51. COMPARISON OF AAMRL EXPERIMENTAL DATA TO NASA PROGRAM FREQUENCY RESPONSE PREDICTIONS FOR A 10.0 IN. TUBE WITH .020 IN. ID

FIG51

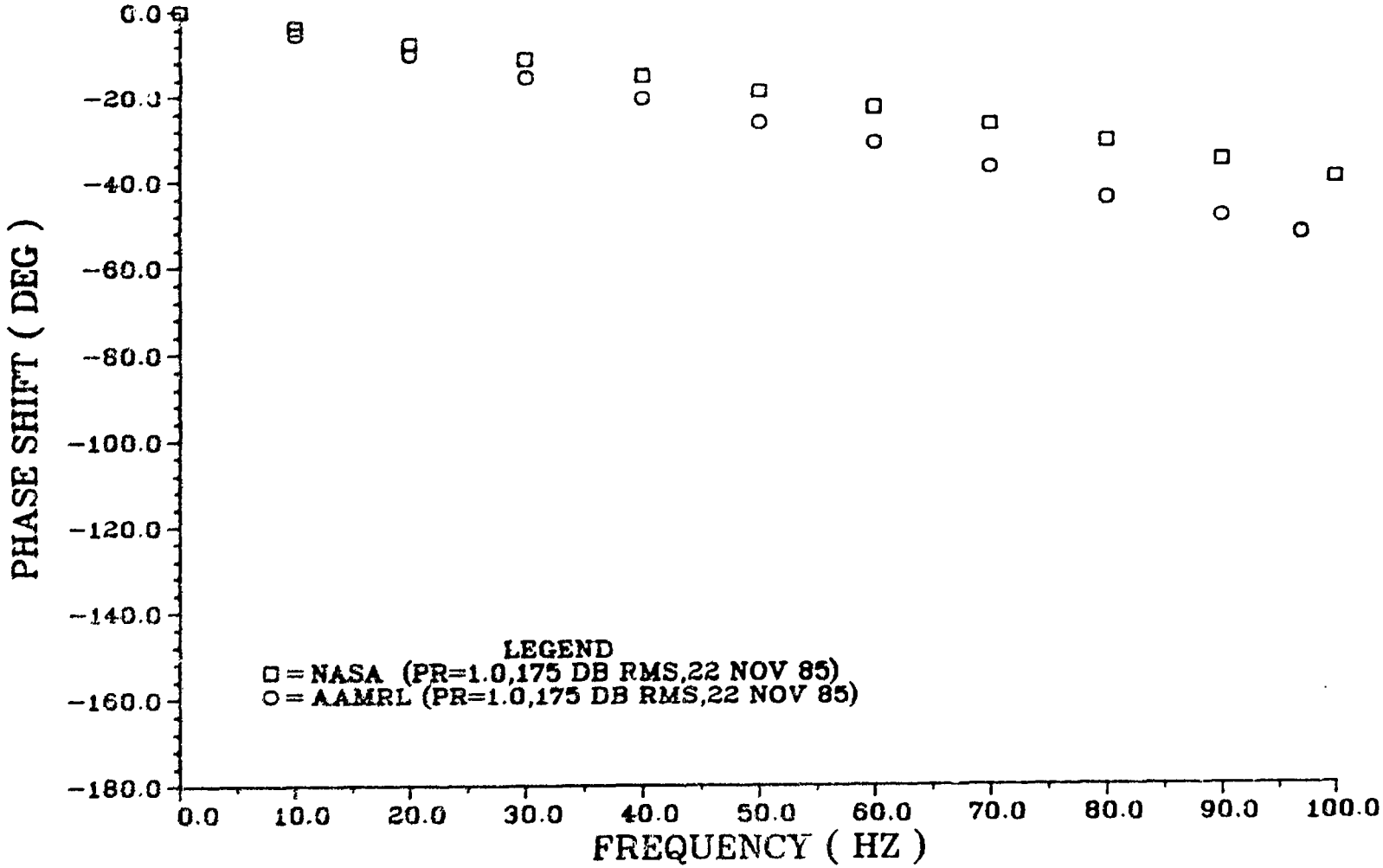

FIGURE 52. COMPARISON OF AAMRL EXPERIMENTAL DATA TO NASA PROGRAM FREQUENCY RESPONSE PREDICTIONS FOR A 10.0 IN. TUBE WITH .020 IN. ID

FIG52

The same general trends can be seen in the phase shift data. The predicted phase shift is consistently less than the actual phase shift, just as it was in the Phase 1 experiments. The correlation between the experimental data and theory is best at the low frequencies. The differences between the values increases as the frequency is increased. The largest difference between experimental and predicted values of the phase shift was 13 degrees, which occurred at 90 hertz for the test with a dynamic pressure level of 175-dB. For the 159-dB test case a maximum difference of 8.8 degrees occurred at 90 hertz. For the 145-dB and 130-dB tests, the maximum differences were 11 degrees and 5.9 degrees, respectively, with the maximum difference occurring at 80 hertz in each case. Again, there is no pattern suggesting that the different dynamic pressure levels had any effect on the experimental data.

During the next set of experiments with the 10.0-inch tube, the chamber was pressurized to about 1.85 atmospheres. This chamber pressure was chosen to match as nearly as possible the pressure in the tubes during the Phase 1 experiments. By matching the pressure in each experiment, it is possible to compare the two sets of experimental data directly, and thereby determine the effect of changing to the Phase 2 experimental setup.

While attempting to pressurize the chamber for the first time, we discovered that the silicone grease did not provide an adequate seal around the chamber adapter or the bleed screws. Teflon tape was applied to the bleed screw threads to eliminate the leaks past the screws. By tightening the two arms holding the adapter in place, the amount of air leaking around the

adapter was reduced, but a perfect seal was never achieved. Thus, the mean pressure in the chamber did vary slowly with time. It was impossible to maintain a constant pressure.

In the experiment for a dynamic pressure of 130-dB, the lowest chamber pressure was 7.35 psig and the highest was 12.16 psig, for a difference of 4.81 psi. In the 145-dB experiment, the maximum change in mean pressure was 2.35 psi, while in the 175-dB experiment the change was only 1.19 psi. The amount of change during the course of an experiment was a function of how well the adapter could be sealed with a particular chamber.

The mean pressure in the tube will affect the frequency response of the tube. In these tests, a nominal chamber pressure of 1.85 atmospheres was the target. If the actual chamber pressure is lower than the nominal value, in general the resulting amplitude ratio data will be slightly lower than it would have been at the nominal pressure. Similarly, amplitude ratio data slightly higher than a nominal value can be expected when the actual chamber pressure is higher than the target pressure.

However, Figures 53-55 show that the slight changes in the experimental data due to variations in the chamber pressure are insignificant in comparison to the theoretical predictions. The comparison of the experimental data to the theory is excellent for these experiments. Since the chamber pressure did change during each experiment, the theoretical predictions were calculated using the highest and lowest pressures measured within the chamber during the course of each experiment. These theoretical curves show that the predictions are relatively insensitive to the mean pressure in the frequency range from 0 to 100 hertz. Thus, the experimental data compares favorably with both curves in each experiment.

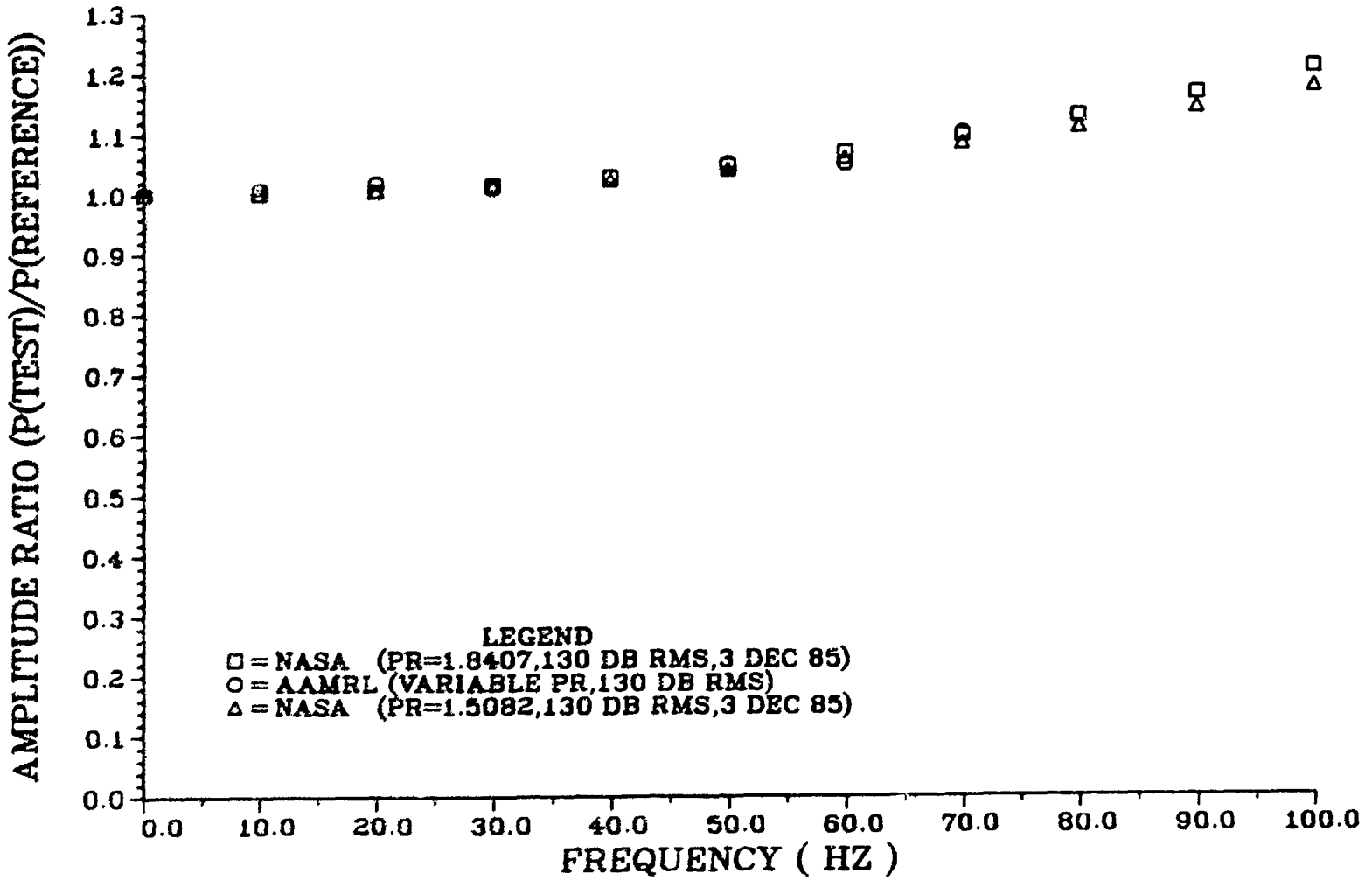

FIGURE 53. COMPARISON OF AAMRL EXPERIMENTAL DATA TO NASA PROGRAM FREQUENCY RESPONSE PREDICTIONS FOR A 10.0 IN. TUBE WITH .020 IN. ID

FIG53

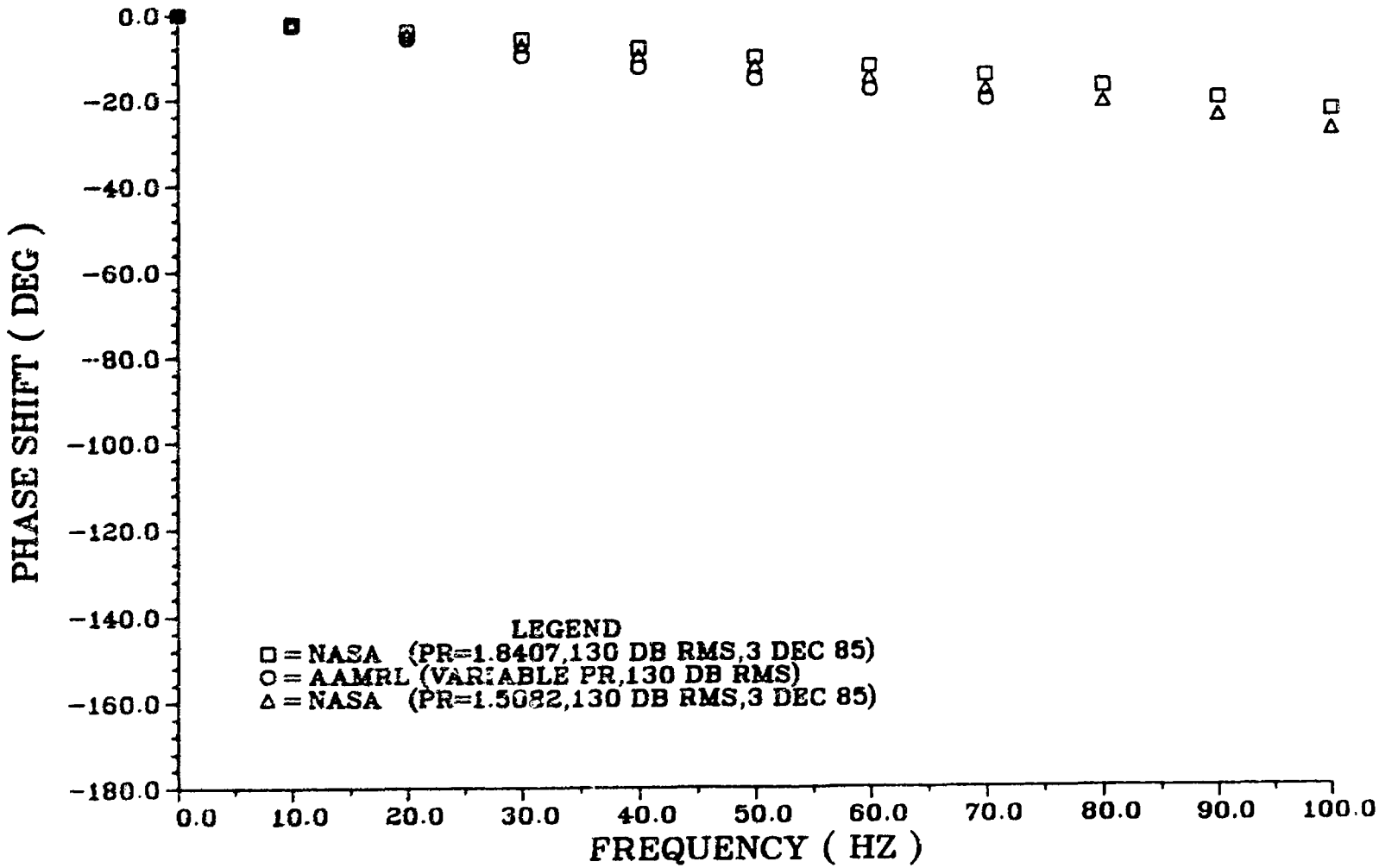

FIGURE 54. COMPARISON OF AAMRL EXPERIMENTAL DATA TO NASA PROGRAM FREQUENCY RESPONSE PREDICTIONS FOR A 10.0 IN. TUBE WITH .020 IN. ID

FIG54

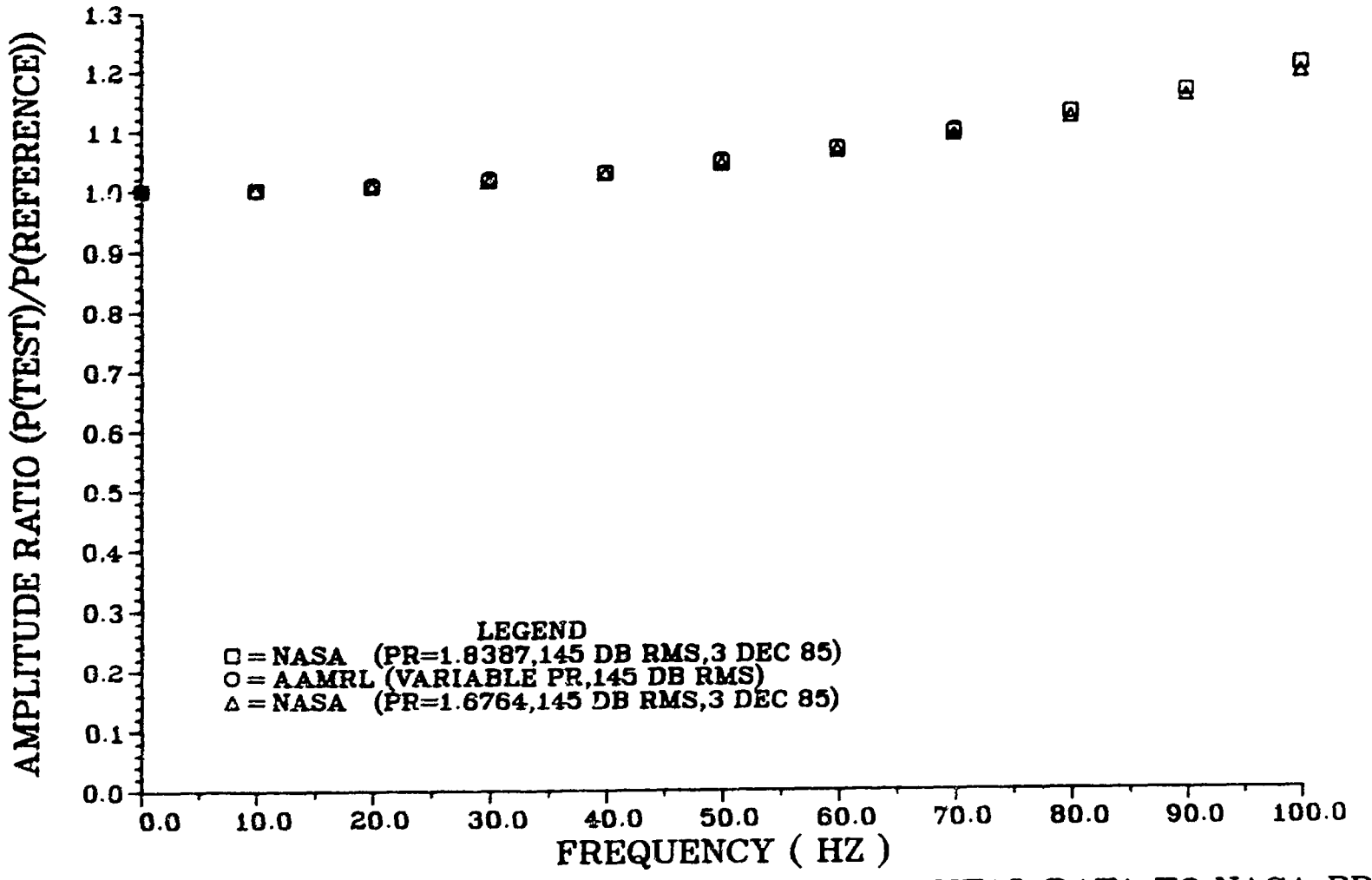

FIGURE 55. COMPARISON OF AAMRL EXPERIMENTAL DATA TO NASA PROGRAM FREQUENCY RESPONSE PREDICTIONS FOR A 10.0 IN. TUBE WITH .020 IN. ID

FIG55

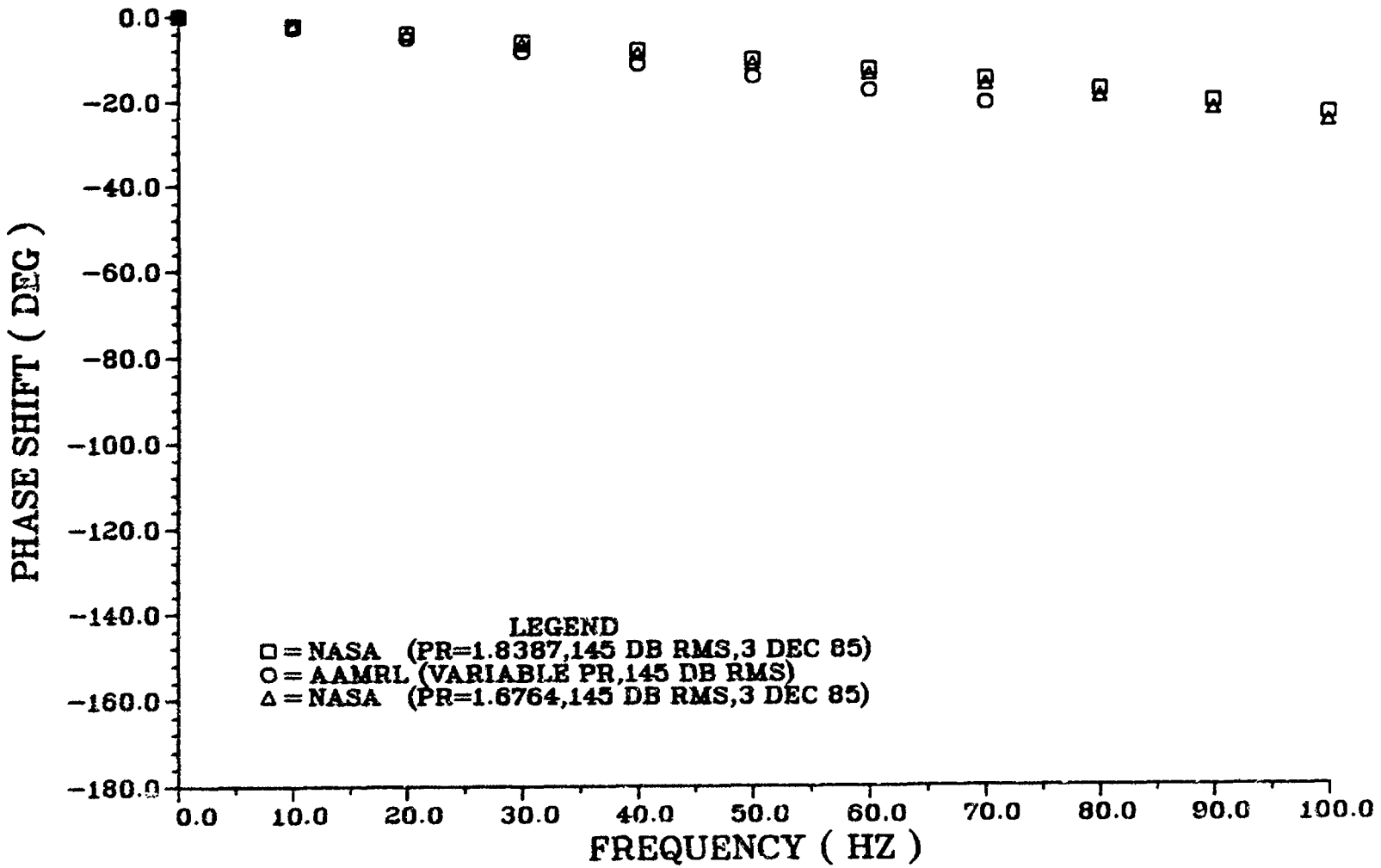

FIGURE 56. COMPARISON OF AAMRL EXPERIMENTAL DATA TO NASA PROGRAM FREQUENCY RESPONSE PREDICTIONS FOR A 10.0 IN. TUBE WITH .020 IN. ID

FIG56

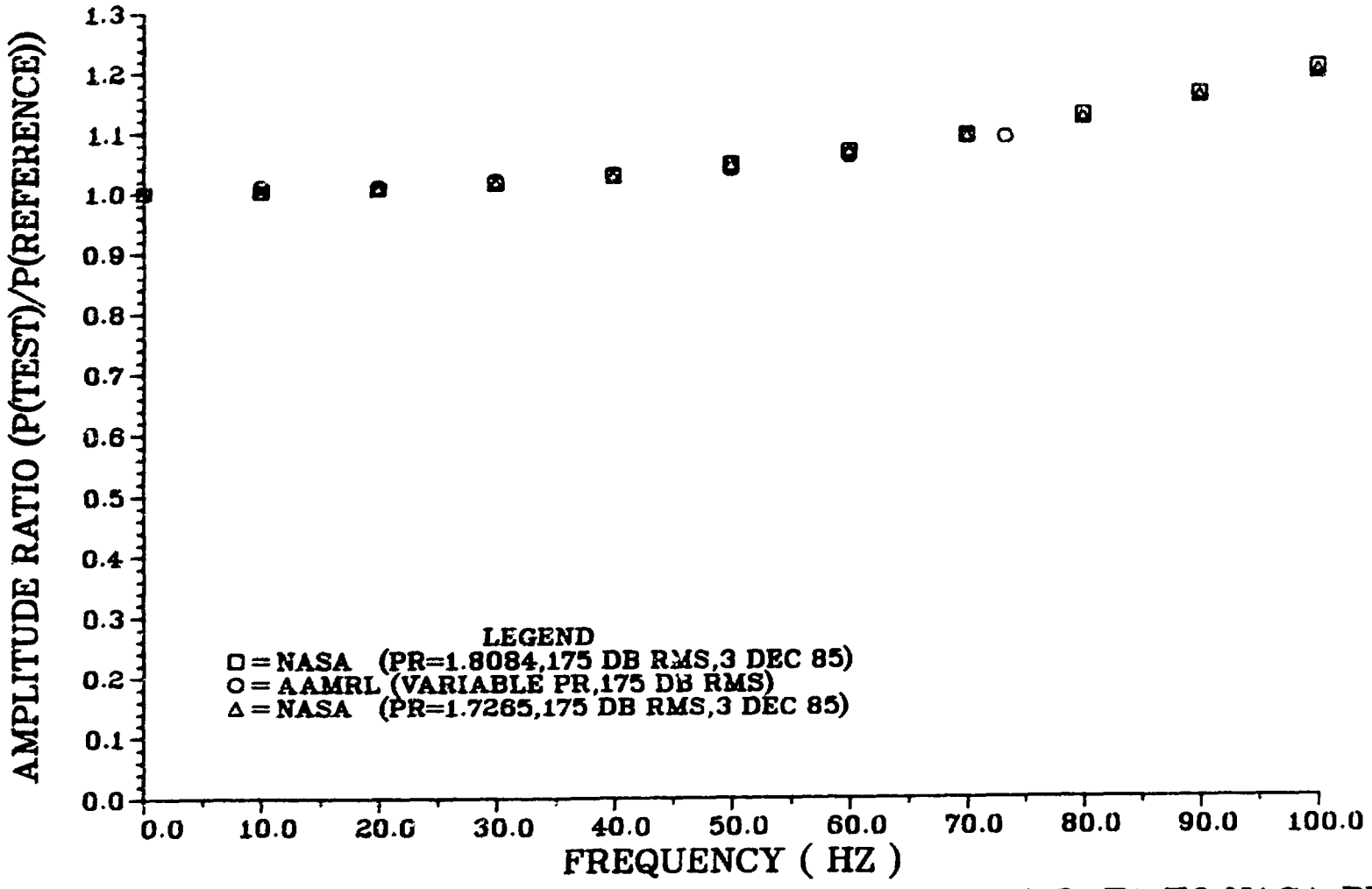

FIGURE 57. COMPARISON OF AAMRL EXPERIMENTAL DATA TO NASA PROGRAM FREQUENCY RESPONSE PREDICTIONS FOR A 10.0 IN. TUBE WITH 0.020 IN. ID

FIG57

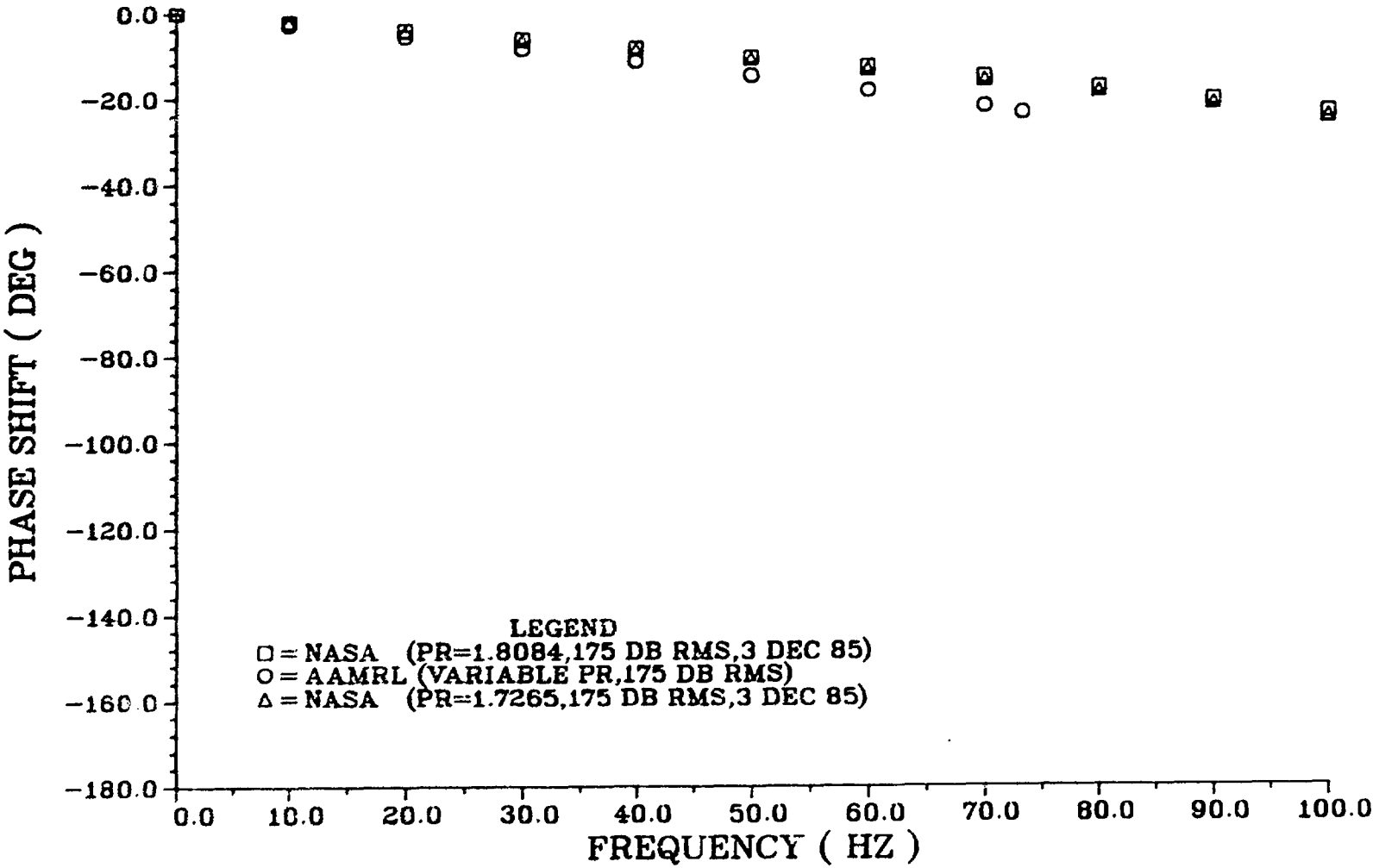

FIGURE 58. COMPARISON OF AAMRL EXPERIMENTAL DATA TO NASA PROGRAM FREQUENCY RESPONSE PREDICTIONS FOR A 10.0 IN. TUBE WITH .020 IN. ID

FIG58

For the experiment with the 130-dB dynamic pressure level, the theoretical predictions of the amplitude ratio are within 2 percent of the experimental data over the frequency range from 0 to 70 hertz. With a pressurized chamber, 70 hertz was the maximum frequency the calibrator could attain. The predicted phase shift was within 6 degrees of the experimental value throughout the frequency range. In the experiments with dynamic pressure levels of 145-dB and 175-dB, there was a difference of less than 1 percent between the experimental and theoretical values of the amplitude ratio. The maximum difference between the experimental and theoretical phase shift values was less than 6 degrees for the 145-dB dynamic pressure level test, and less than 7 degrees for the 175-dB dynamic pressure level case. In all three pressurized tests, the trend was for the difference between the experimental and theoretical phase shift values to increase with increasing frequency.

With data from both experimental setups at nearly the same mean pressure in the 10.0-inch tube, it was possible to determine the effect of changing to the Phase 2 experimental setup. A comparison of the data from each experimental setup is shown in Figures 59 to 60. These figures show that the amplitude ratio and phase shift are essentially the same for both experimental setups out to a frequency of 70 hertz. Therefore, within this limited frequency range, the change to the Phase 2 experimental setup had no effect on the experimental data. This implies that the signal generator adapter used in the Phase 1 experiments did not adversely affect the experimental data, at least not within the 0 to 70 hertz frequency range. Unfortunately, due to the limited operating range of the pistonphone

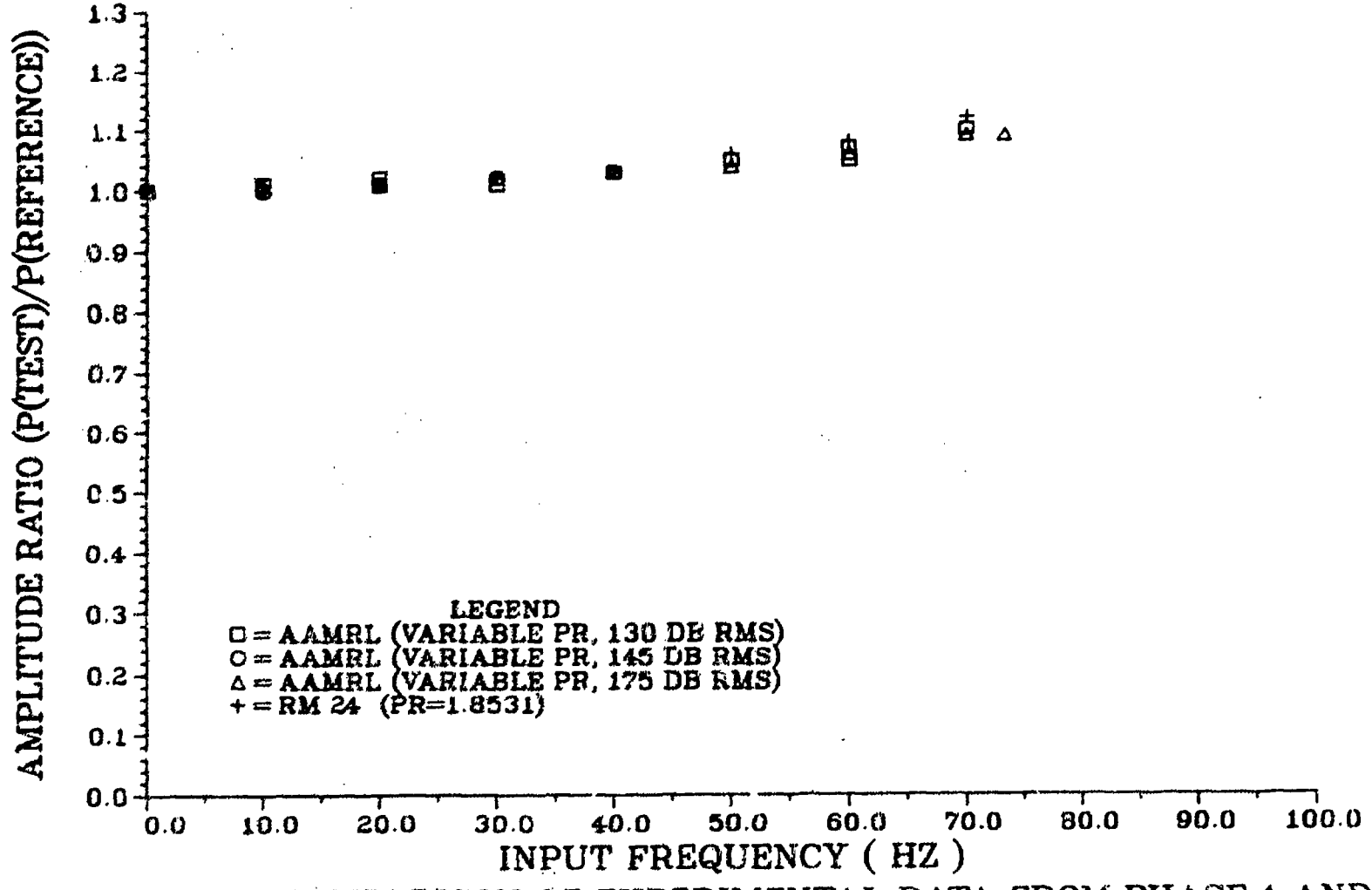

FIGURE 59. COMPARISON OF EXPERIMENTAL DATA FROM PHASE 1 AND PHASE 2 SETUPS FOR A 10.0 IN. TEST LENGTH WITH 0.020 IN. ID

FIG59

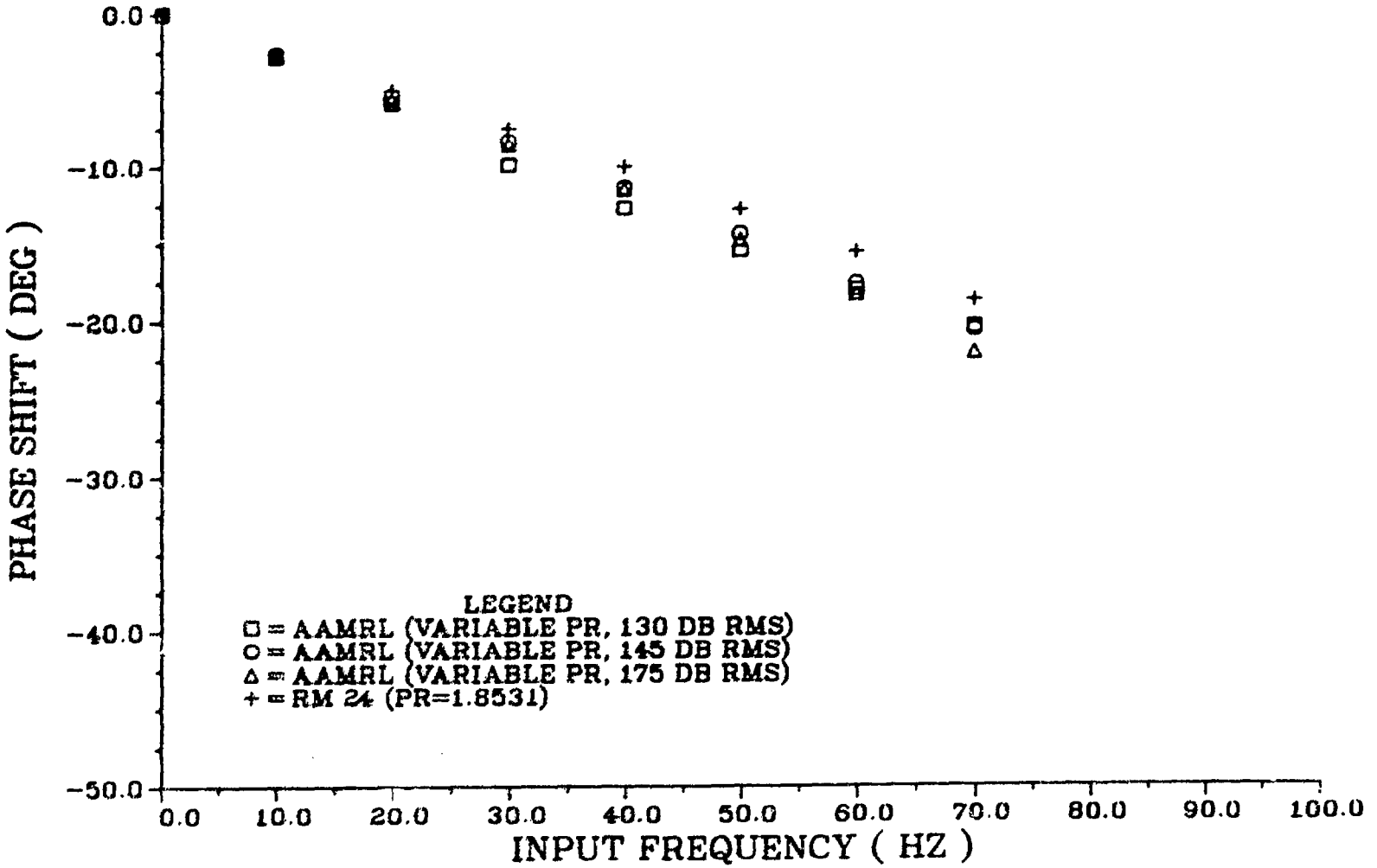

FIGURE 60. COMPARISON OF EXPERIMENTAL DATA FROM PHASE 1 AND PHASE 2 SETUPS FOR A 10.0 IN. TEST LENGTH WITH 0.020 IN. ID

FIG60

calibrator, no higher frequency data could be acquired. As such, the effect of the signal generator adapter, if any, in the frequency range from 70 to 200 hertz could not be determined.

In the final experiment with the 10.0 inch tube, the chamber pressure was increased to approximately 2.5 atmospheres. This is the mean pressure expected in the F100 rig during rotating stall. During this experiment the maximum change in the mean pressure was 3.2 psi. The dynamic pressure level for this test was 175 dB.

The results of the test are shown in Figures 61-62. Again the correlation of the experimental data with the theory is excellent. The experimental amplitude ratio data and the theoretical predictions agree to within less than 1 percent. For the phase shift data, the comparison with theory is within 7 degrees throughout the frequency range.

(2) Experiments with a 24.0-Inch Tube

The initial experiments with the 24.0-inch tube were attempted with a chamber pressure of 1.85 atmospheres. However, none of these experiments could be completed. During the previous experiment in which the chamber pressure was set at 2.5 atmospheres, the piston seal apparently deteriorated slightly. In subsequent experiments for the 24.0-inch tube with the chamber pressurized, oil leaked past the piston seal and began to fill the chamber volume. During two of these experiments with the smallest chamber, both the chamber and the 24.0-inch tube became filled with oil. At this point we abandoned attempts to obtain data with the pressurized chamber. The tube was cleaned with freon to remove the oil film, and then tested with an atmospheric chamber pressure.

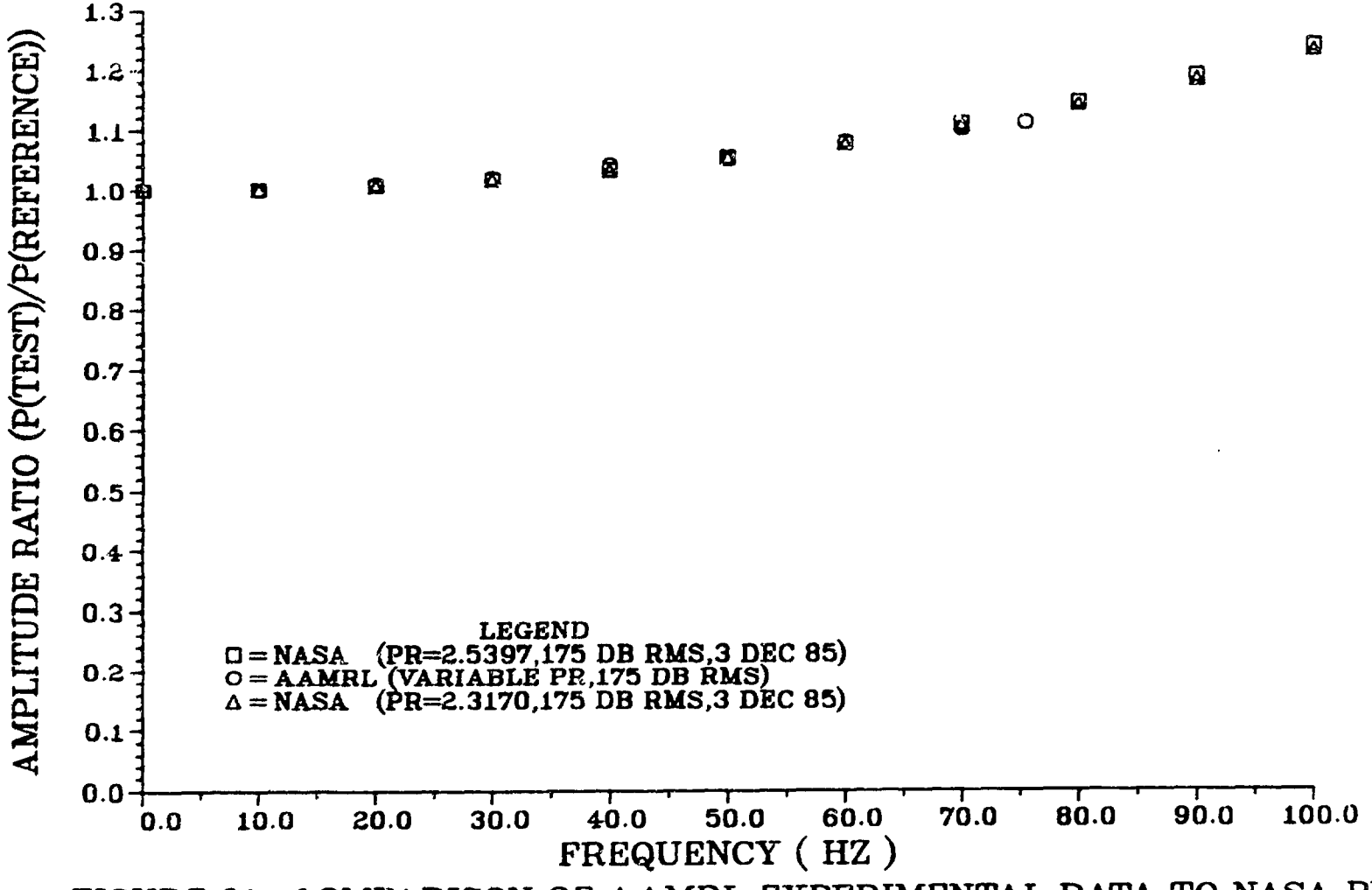

FIGURE 61. COMPARISON OF AAMRL EXPERIMENTAL DATA TO NASA PROGRAM FREQUENCY RESPONSE PREDICTIONS FOR A 10.0 IN. TUBE WITH .020 IN. ID

FIG61

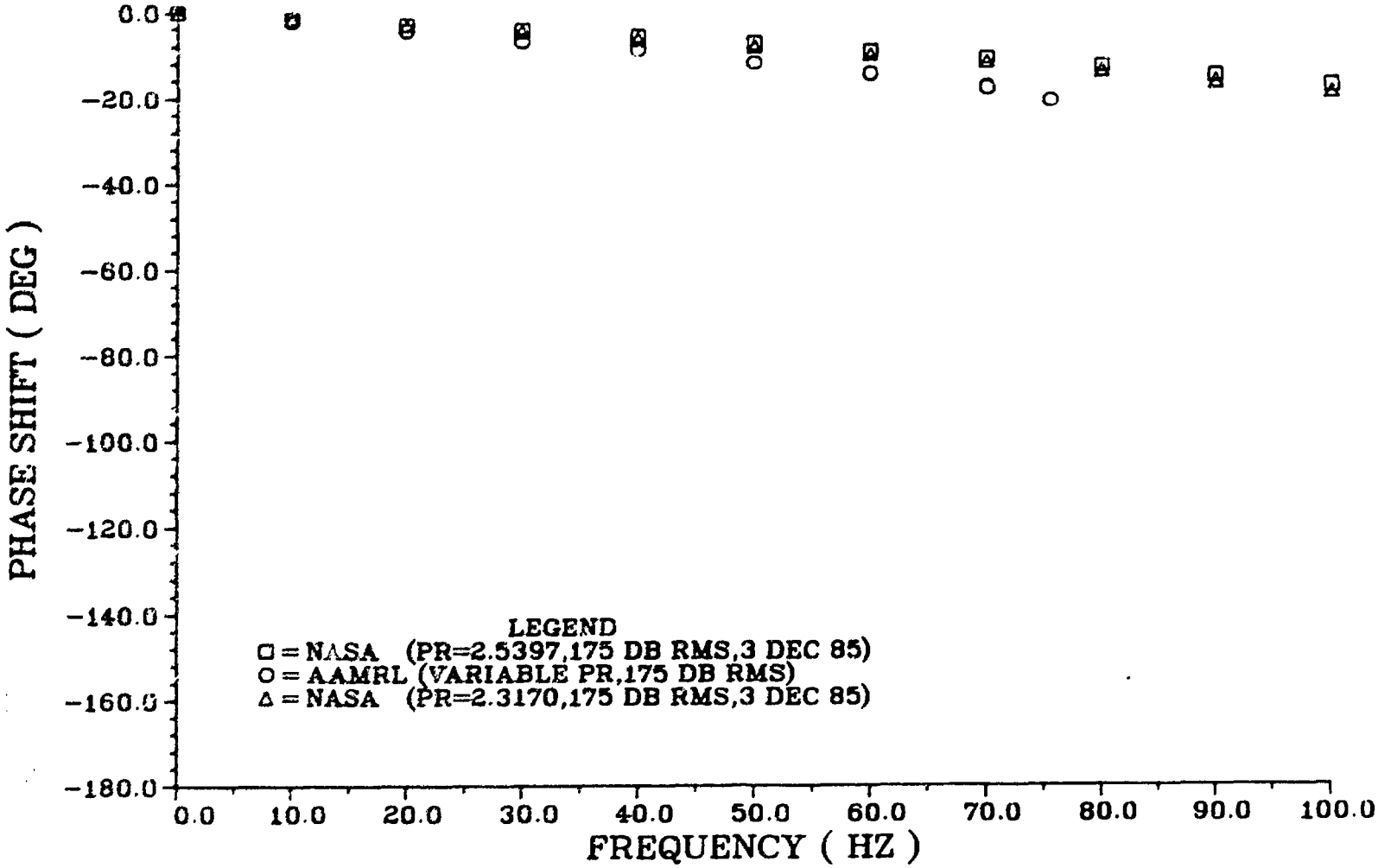

FIGURE 62. COMPARISON OF AAMRL EXPERIMENTAL DATA TO NASA PROGRAM FREQUENCY RESPONSE PREDICTIONS FOR A 10.0 IN. TUBE WITH .020 IN. ID

FIG62

The results of these tests, for dynamic pressure levels of 130, 138, and 175-dB, are shown in Figures 63-68. For these three experiments a maximum frequency of 80 hertz was attained. In the 130-dB dynamic pressure test case, experimental and theoretical values for the amplitude ratio were within 4.5 percent of each other over the frequency range. The predicted phase shift was within 3 degrees of the experimental values. In the 138-dB dynamic pressure experiment, again the amplitude ratio values differed by no more than 4.5 percent, while the greatest difference between the experimental and theoretical phase shift values was 4 degrees. For the experiment at the 175-dB dynamic pressure level, theoretical values of the amplitude ratio were within 8.0 percent of the experimental data, and phase shift predictions were within 6 degrees of the experimental values. Other trends seen in previous experiments were evident in the 24.0-inch tube experimental data as well. The predicted amplitude ratio was always greater than the experimental value, while the predicted phase shift was consistently less.

3. CONCLUSIONS

The results of the Phase 2 experiments substantiated the validity of the Phase 1 experimental data up to a frequency of 70 hertz. Over this frequency range there was very little difference in the experimental data obtained for a 10.0-inch tube from the two setups. This in turn, indicated that the effects of the signal generator adapter used in the Phase 1 experiments were negligible in the low frequency range. But since the frequency range of the calibrator only extended to 70 hertz, the comparison of the data from the two setups is inconclusive. The effect, if any, of the signal generator adapter on the experimental data at frequencies higher than 70 hertz remains unknown.

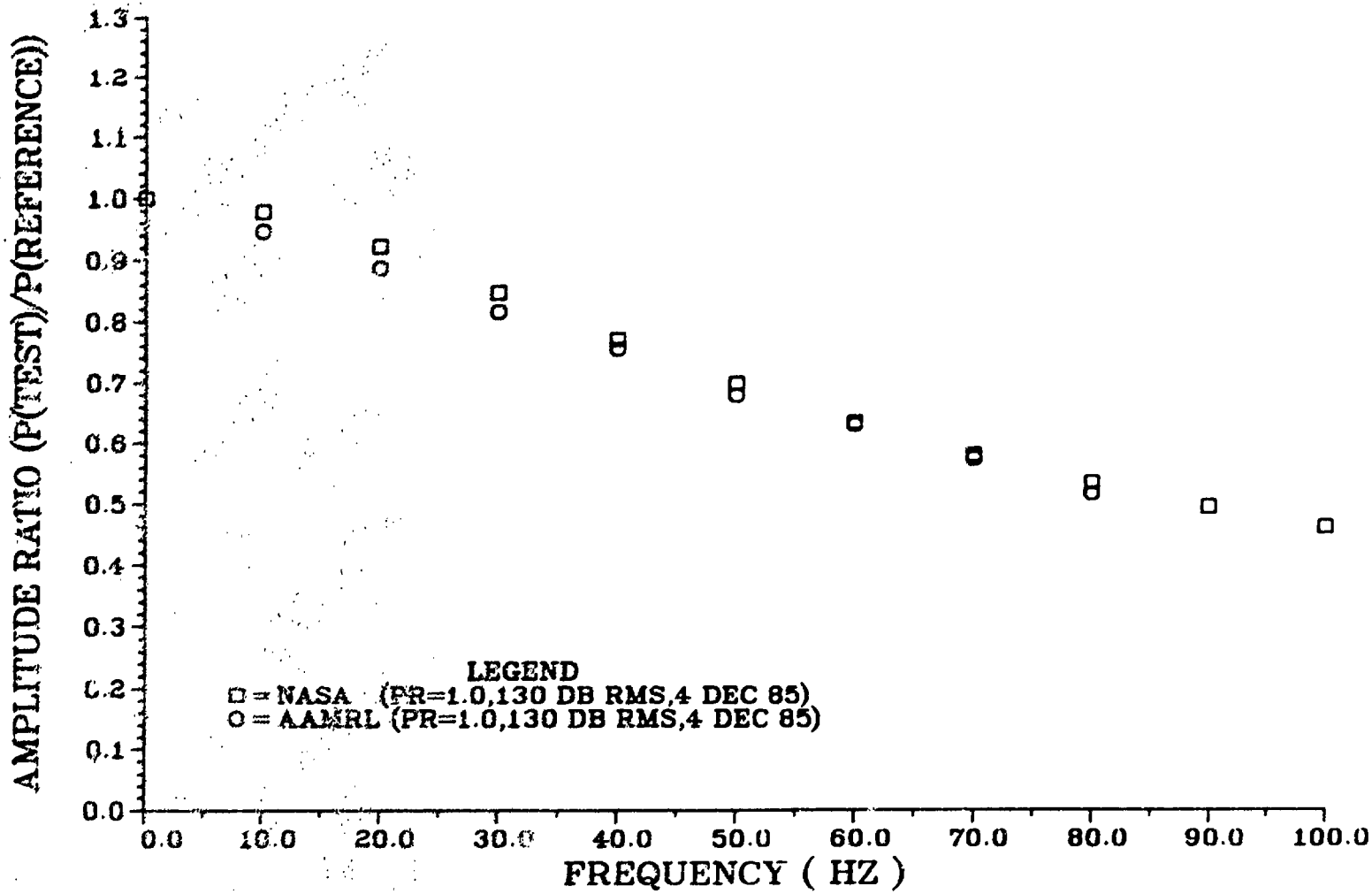

FIGURE 63. COMPARISON OF AAMRL EXPERIMENTAL DATA TO NASA PROGRAM FREQUENCY RESPONSE PREDICTIONS FOR A 24.0 IN. TUBE WITH .020 IN. ID

FIG63

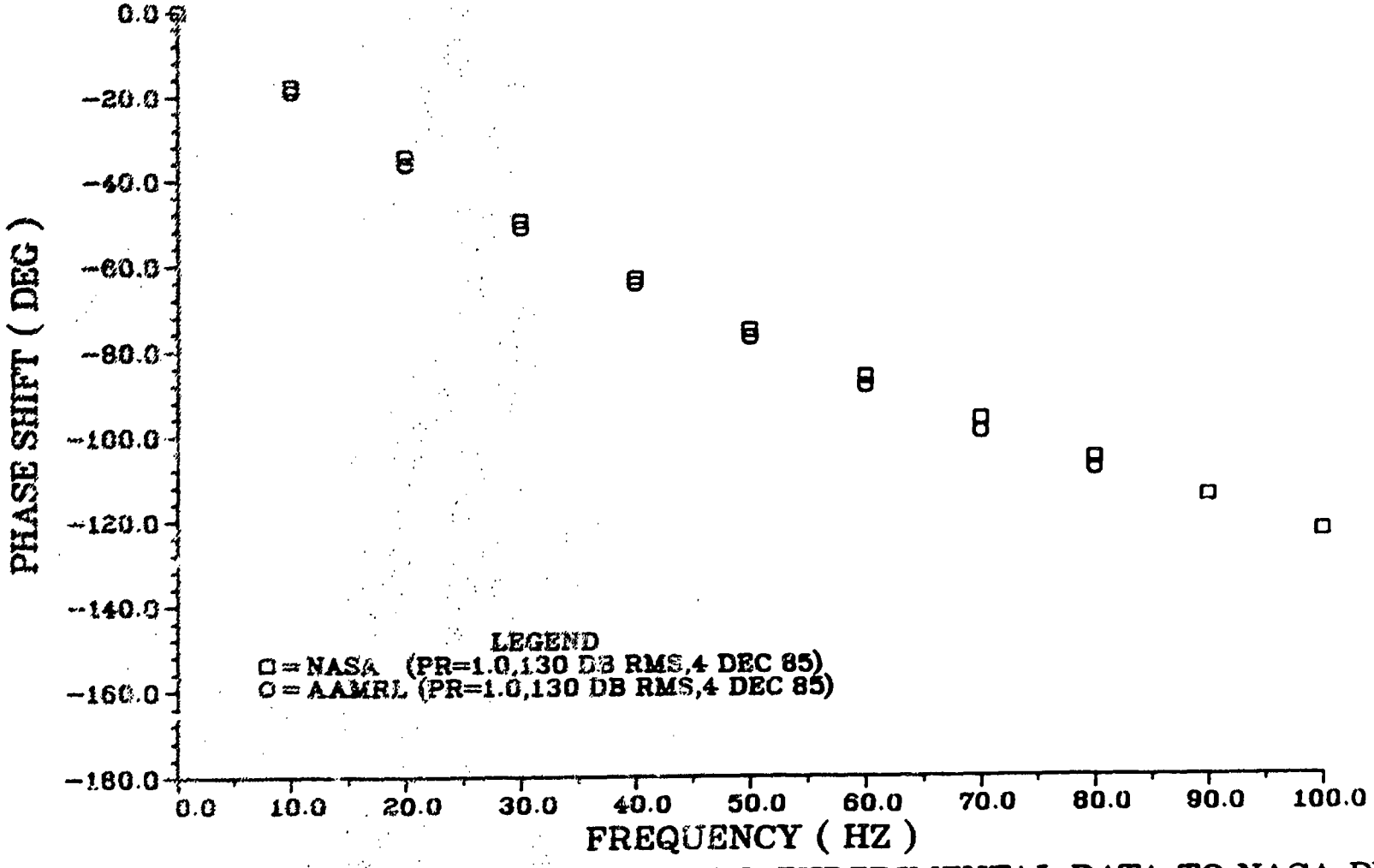

FIGURE 64. COMPARISON OF AAMRL EXPERIMENTAL DATA TO NASA PROGRAM FREQUENCY RESPONSE PREDICTIONS FOR A 24.0 IN. TUBE WITH .020 IN. ID

FIG64

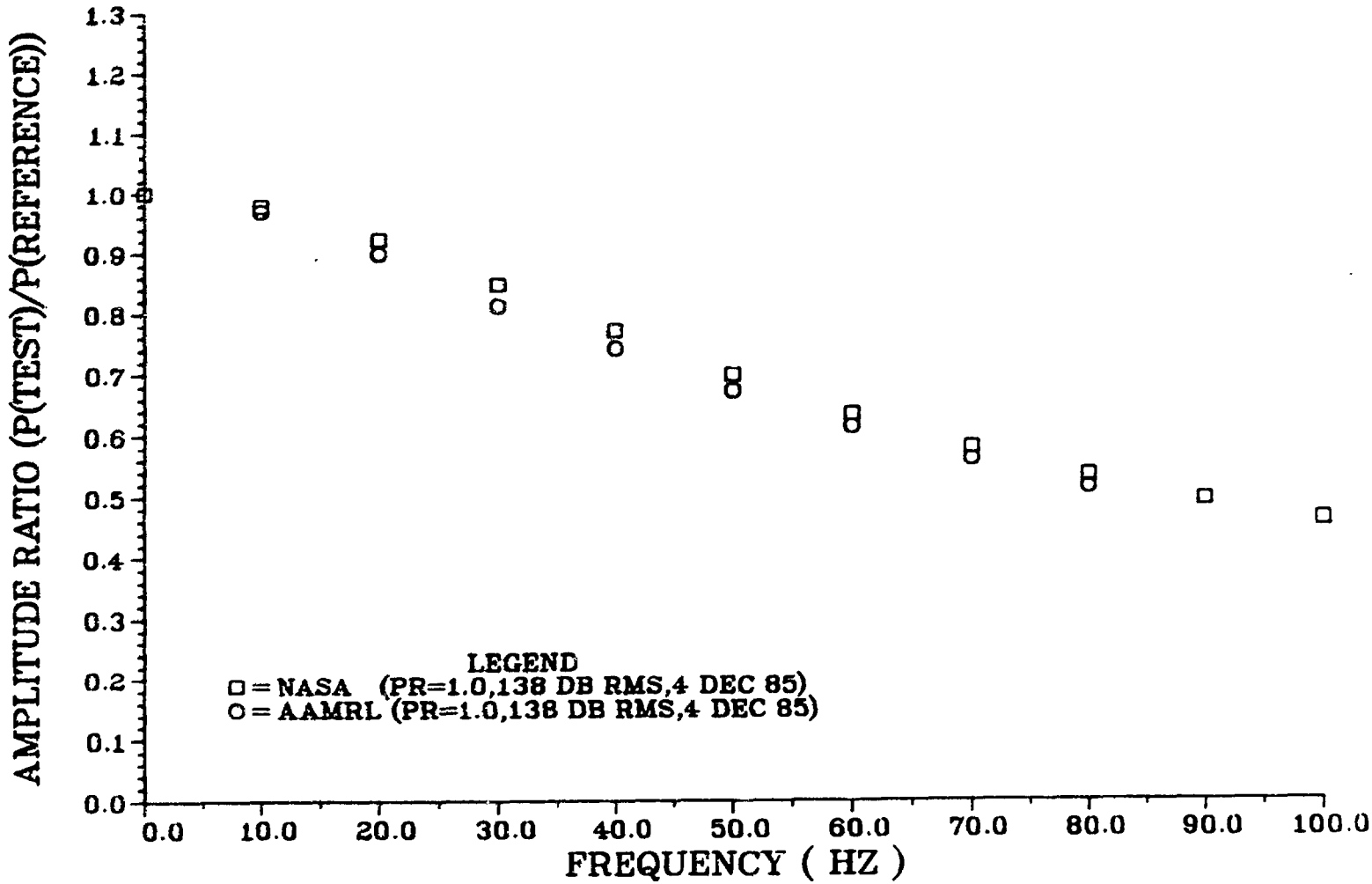

FIGURE 65. COMPARISON OF AAMRL EXPERIMENTAL DATA TO NASA PROGRAM FREQUENCY RESPONSE PREDICTIONS FOR A 24.0 IN. TUBE WITH .020 IN. ID

FIG65

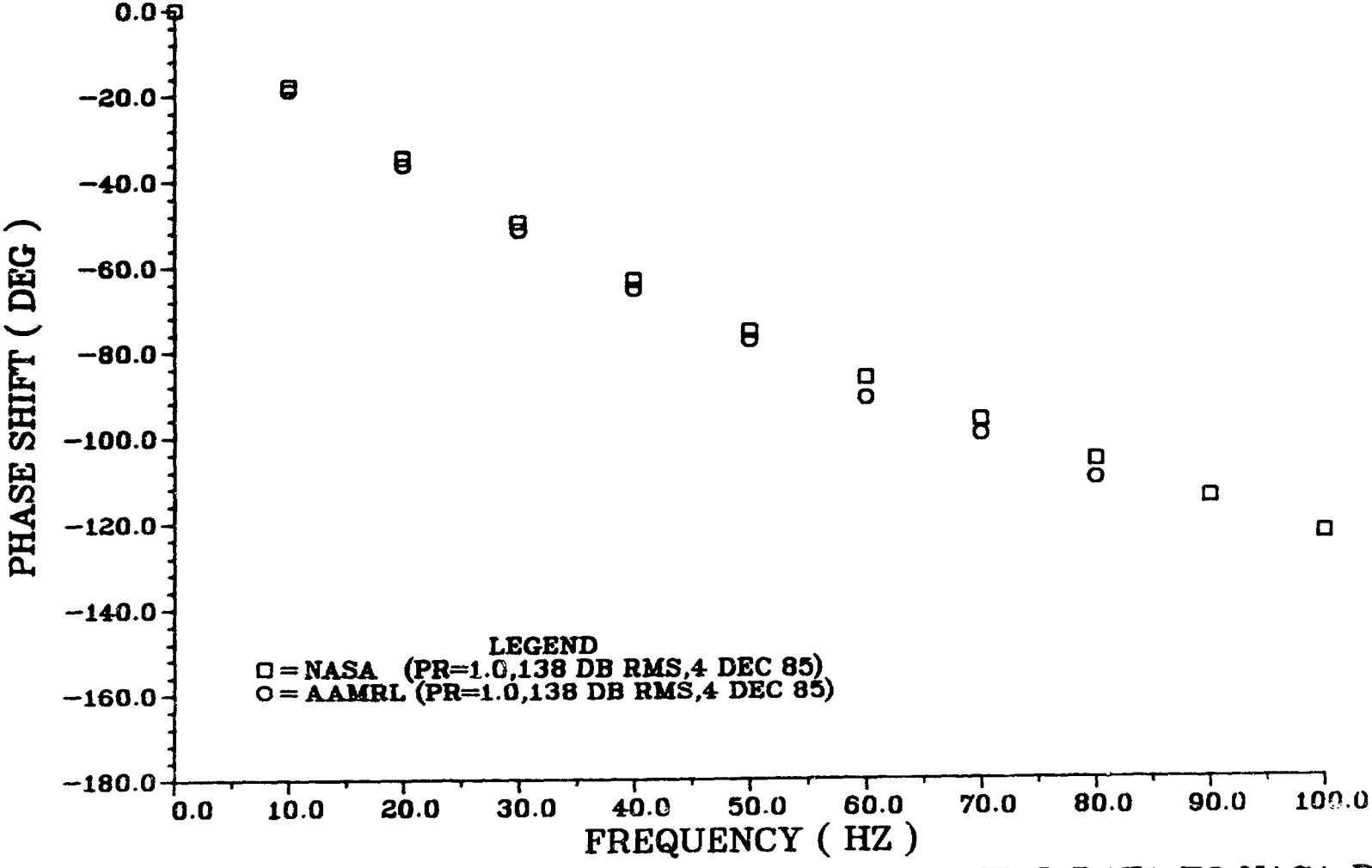

FIGURE 66. COMPARISON OF AAMRL EXPERIMENTAL DATA TO NASA PROGRAM FREQUENCY RESPONSE PREDICTIONS FOR A 24.0 IN. TUBE WITH .020 IN. ID

FIG66

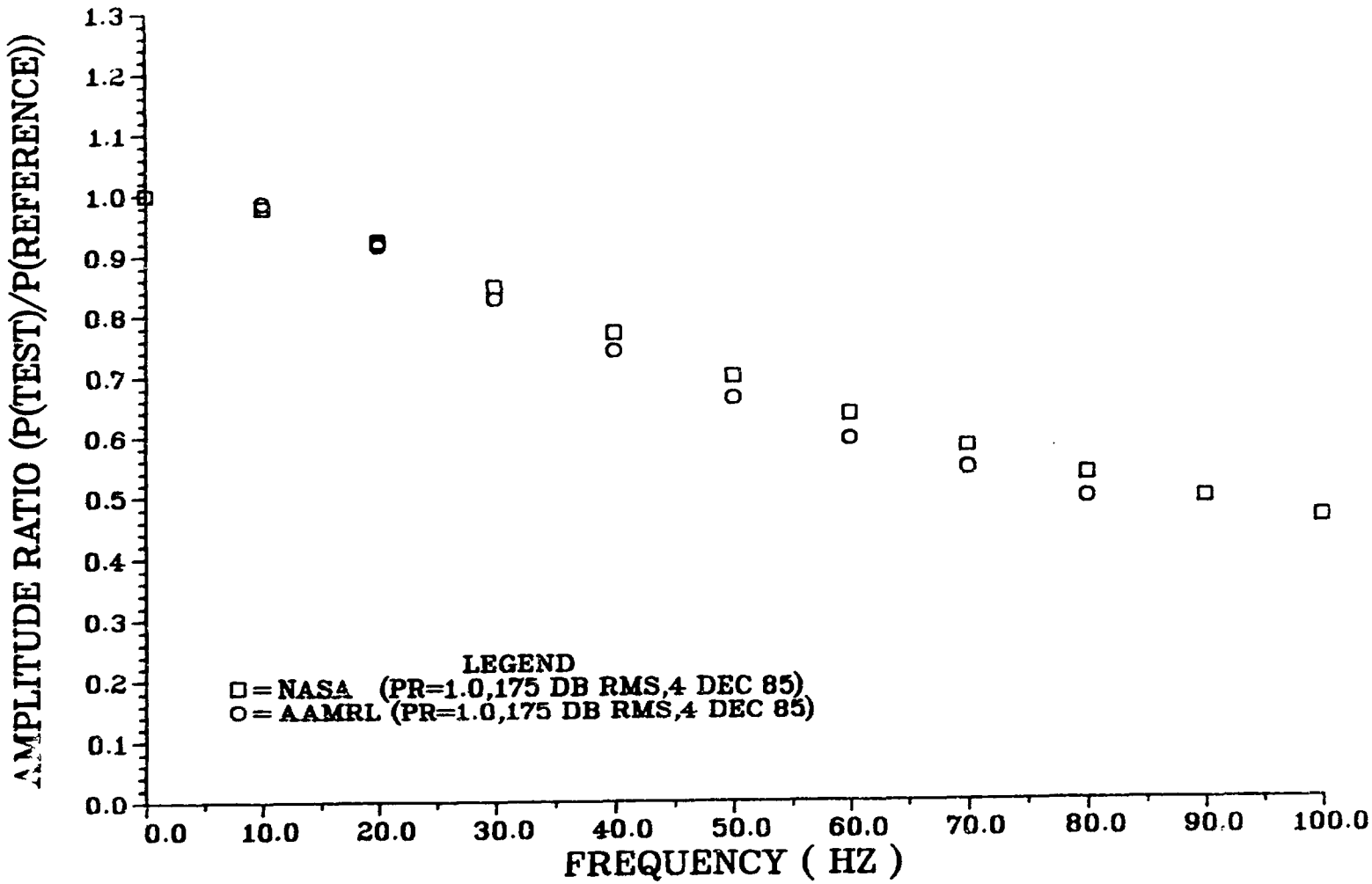

FIGURE 67. COMPARISON OF AAMRL EXPERIMENTAL DATA TO NASA PROGRAM FREQUENCY RESPONSE PREDICTIONS FOR A 24.0 IN. TUBE WITH .020 IN. ID

FIG67

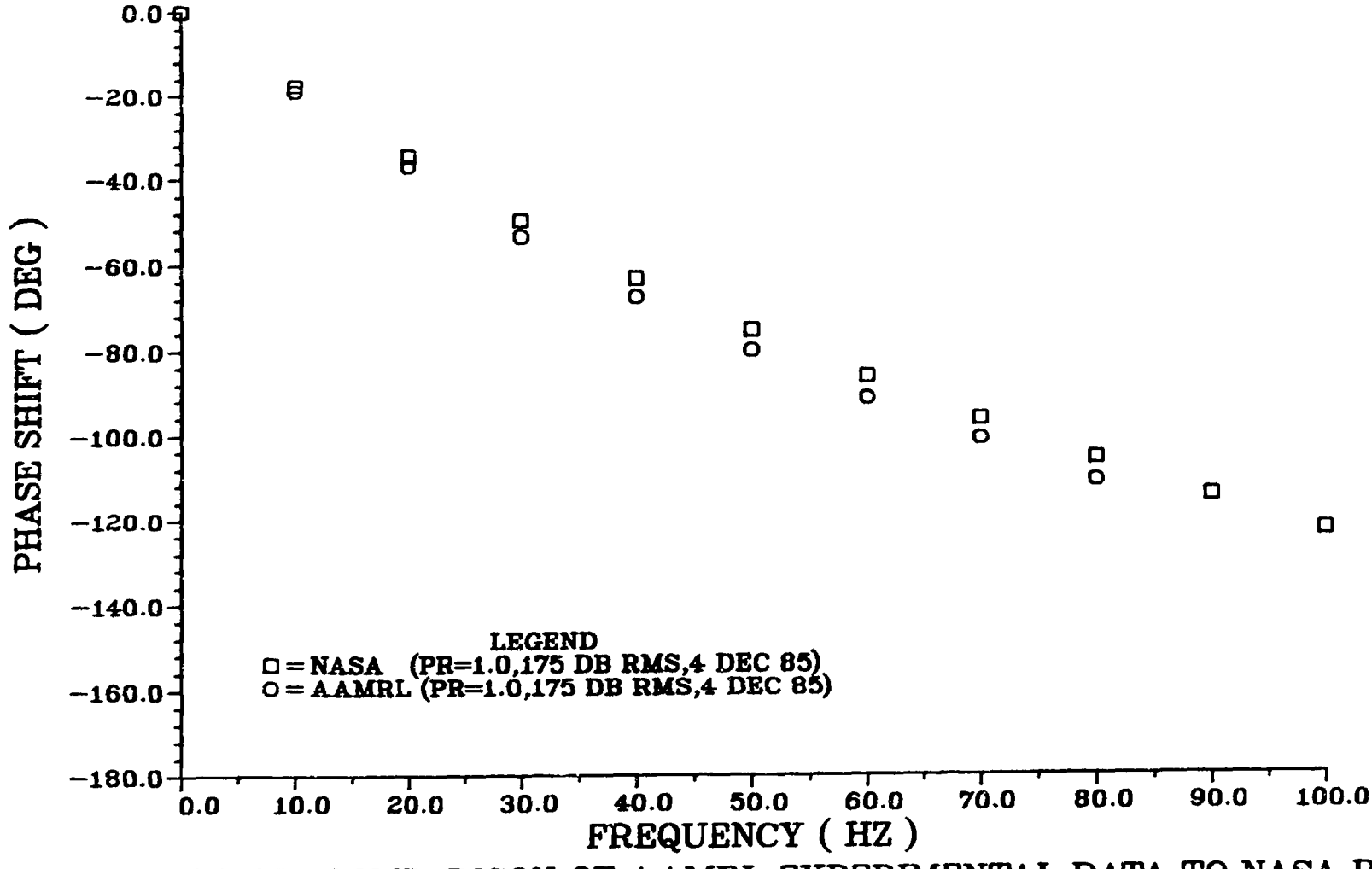

FIGURE 68. COMPARISON OF AAMRL EXPERIMENTAL DATA TO NASA PROGRAM FREQUENCY RESPONSE PREDICTIONS FOR A 24.0 IN. TUBE WITH .020 IN. ID

FIG68

With the Phase 2 experimental setup it was possible to expand on the information gained from the Phase 1 experiments in two ways. Experiments with the 10.0-inch tube were conducted for mean pressures of 1.0 and 2.5 atmospheres, in addition to an experiment at a chamber pressure of 1.85 atmospheres chosen to duplicate the Phase 1 test conditions. The correlation of the experimental data to the theory was excellent for each of these experiments.

In addition to extending the pressure range, the Phase 2 experimental setup made it possible to investigate the effects of various dynamic pressure levels. In the Phase 1 experiments the dynamic pressure decreased steadily with increasing frequency, averaging about 155-dB. With the Phase 2 setup, the dynamic pressure was essentially constant. The results of the Phase 2 experiments showed that the choice of a dynamic pressure level, from within a range of 130-dB (9.17E-3 psi) to 175-dB (1.45 psi), had no effect on the experimental data. This insensitivity to the dynamic pressure level indicates that the variable levels present in the Phase 1 experiments did not adversely affect the experimental data.

Therefore, the objectives of the Phase 2 experiments were met. The effect of the signal generator adapter used in the Phase 1 experiments was found to be negligible up to 70 hertz. Data could not be obtained from the Phase 2 setup at higher frequencies, so the effects of the signal generator adapter in the 70 to 200 hertz frequency range could not be determined. Also, we determined that the variable dynamic pressures encountered in the Phase 1 work were insignificant, as the frequency response of the tube is generally insensitive to changes in dynamic pressure within the 130 to 175-dB range.

4. RECOMMENDATIONS

The results of the Phase 2 experiments eliminated the concerns about the Phase 1 experimental setup and essentially verified the quality of the data acquired during the Phase 1 experiments. And, as in the Phase 1 experiments with the DRUCK test transducer, the agreement between the Phase 2 experimental data and the NASA predictions was excellent. The combined results of both phases of the experimental work establish the NASA program as a useful tool for the prediction of frequency response in the 0.020-inch-inside-diameter tubes on the CRF/F100 rig. Furthermore, the accuracy of these predictions will be sufficient for the purposes of the CRF/F100 test program. Therefore, we recommend that the NASA program be used during the F100 test to characterize the frequency response of the tubing used to close-couple the ZOC transducers.

SECTION V

MODELLING THE SCANIVALVE ZOC14 TRANSDUCER FOR THE NASA PROGRAM

1. GENERAL

For most of the Phase 1 experiments, a Scanivalve ZOC14 transducer was used as the test transducer. In all of these experiments the comparison of the experimental data with the NASA program predictions was generally poor. By substituting a DRUCK transducer for the ZOC and performing additional experiments, an excellent match between experimental data and theoretical results is possible. The primary reason for the difference in the comparison of the data from the two transducers was the manner in which each transducer was modelled in the NASA program.

For the DRUCK transducer with a zero volume adapter, the actual dimensions of the adapter and transducer were known. The adapter, shown in Figure 69, has an input tube 0.6 inches long, with an inside diameter of 0.041 inches. The volume between the inner face of the adapter and the transducer sensor is 1.22E-6 cubic inches. There are no other internal tube lengths or volumes. These dimensions were used to model the transducer in the NASA program and good results were obtained.

In contrast, the actual internal dimensions of the ZOC14 were unknown. Instead, the manufacturer's specifications quoted equivalent dimensions which were determined from measurements of pressure drop versus flow rate through the actual internal hardware. The equivalent dimensions consist of an internal tube with a length of 2.0 inches and an inside diameter of 0.029 inch, and an internal volume of 0.0002 cubic inch. The use of these values in the NASA program produced unsatisfactory results.

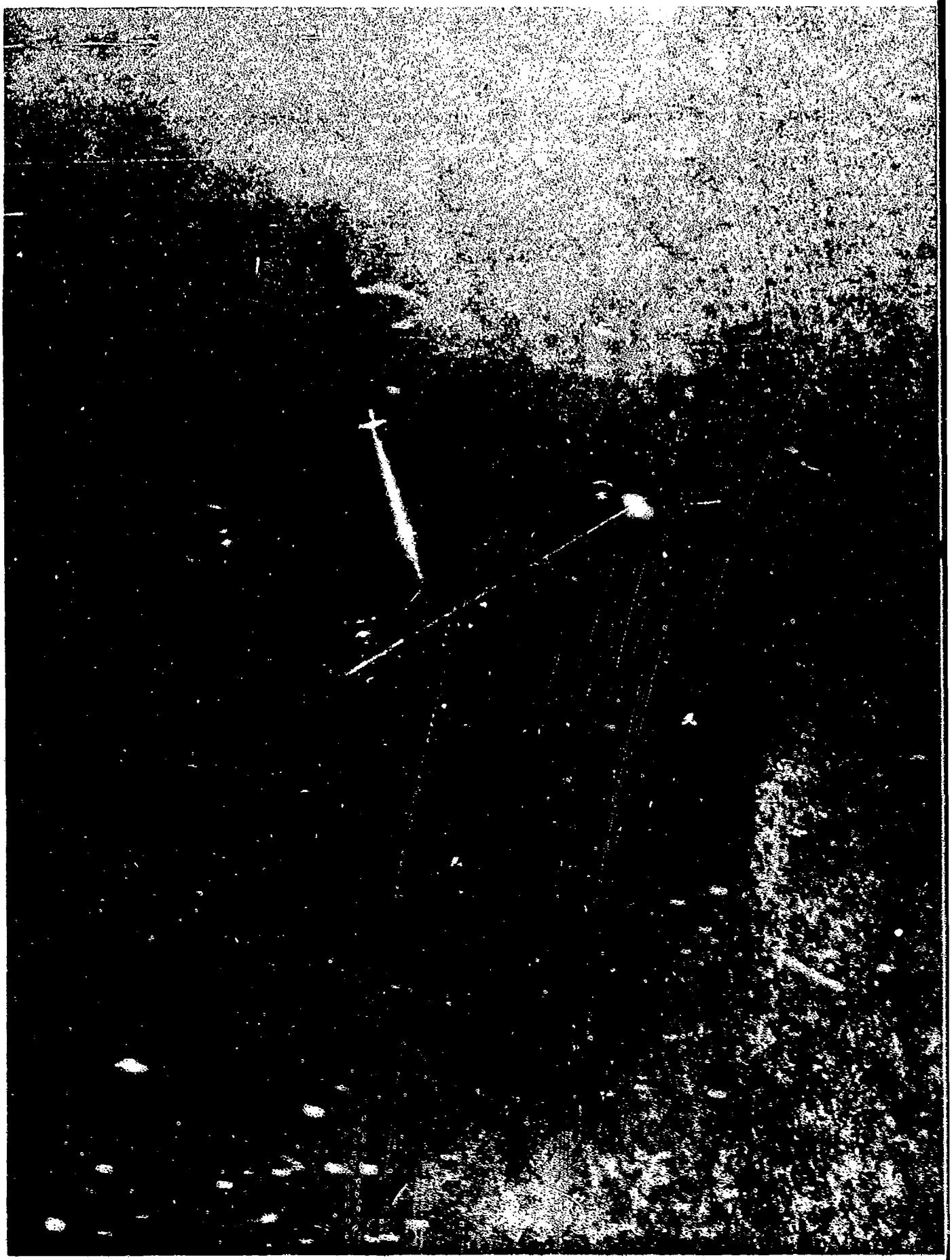

Figure 69. Standard Zero-Volume Adapter

To improve the theoretical predictions, a more accurate set of internal dimensions was needed for the ZOC transducer. The effect of various transducer dimensions on the frequency response of a single tube system was investigated with the aid of a computer program written to iterate on the transducer variables.

2. COMPUTER PROGRAM DEVELOPMENT

A modified version of the steering program described in Section II was used in conjunction with the NASA subroutines to isolate a set of transducer dimensions best suited for modelling the ZOC transducer. Modifications to the original steering program included the addition of loops to perform the iteration on the transducer volume, diameter, and length. Variables were added to specify the minimum and maximum values for each transducer dimension and to set the increment or step size within each loop.

Previous experience with the NASA program indicated that the theoretical results were more sensitive to changes in transducer volume than changes in either the internal length or diameter. Therefore, in stepping through the range for each transducer variable, the volume was incremented first, followed by the internal tube diameter, and finally the internal tube length.

The tube diameter and length were incremented by the addition of a relatively small constant value to the previous diameter or length for each iteration. The increment was specified for each case through the variables INCDIA for the tube diameter, and INCXL2 for the tube length.

Because of the sensitivity to changes in transducer volume, provision was made for using either a coarse or a fine increment for this variable. The logical variable COARSE was used to control the program flow. With this variable set to a true condition, the coarse increment was used. With this increment the transducer volume was increased by multiplying the current volume by a constant factor, specified through the variable DV. For example, setting DV equal to five increased the transducer volume by a factor of five on each iteration.

With the COARSE variable set to the false condition, the fine volume increment was used. In this instance the volume was incremented the same way as the length and diameter variables. That is, for each iteration the volume was increased by adding a relatively small constant value to the previous volume. The value of this increment was specified through the variable INCVOL.

The initial selection of ranges and step sizes for the transducer variables was arbitrary. The initial range for the length was 0.25 to 12.0 cm, with a step size of 0.25 cm. For the diameter, an initial range of 0.0005 to 0.1060 cm was chosen along with a step size of 0.005 cm. The initial volume range was 1.0E-7 to 0.1 cubic cm, with a coarse step size of a factor of five.

Subsequent choices for the range and step size of each transducer dimension were based on the optimum geometry identified during a previous execution of the program. In general, the range for each variable was adjusted to evenly bracket the previous optimum dimension. In some instances

the step sizes were changed also. In addition, the transducer volume increment was switched from coarse to fine once the lowest relative error was attained for a given set of ranges and step sizes, thereby refining the optimum transducer volume.

To gauge the effect of various internal dimensions on the overall system response it was necessary to compare the theoretical results for each set of geometry with experimental data. The experimental data for the 10.0-inch tube with pressure ratios of 1.8349 and 1.3982 were used for this comparison. The method used to make the comparison between the theoretical results and experimental data during each iteration was based on the results of the Phase 1 experimental work. The comparison of the theory with this data shows that the greatest discrepancies between the theoretical and experimental amplitude ratios occurred when the resonant peaks were not at the same frequency. When the peaks were not aligned, considerable error existed at frequencies above the peak. Therefore, the peak amplitude ratio was chosen as the single point of comparison between the theoretical and experimental curves. The objective of the steering program was to identify the transducer geometry which would result in a theoretical resonant peak at the frequency of the experimental peak, and for which the difference in the amplitudes of the two curves was minimum.

The program performed this task for a given set of transducer dimensions by first calling the NASA subroutines to calculate the theoretical amplitude ratio at 10 hertz intervals over a range of 10 to 200 hertz. Logic was added within this loop to identify the peak amplitude ratio and its frequency.

These values were then compared to the experimental peak amplitude ratio and peak frequency. The difference between the peak frequencies was calculated along with the relative error between the amplitudes of the peaks. The relative error was defined as

$$\text{Relative Error} = \frac{\text{Experimental Peak AR} - \text{Theoretical Peak AR}}{\text{Experimental Peak AR}} \quad (7)$$

which can be expressed as the percent relative error by

$$\% \text{ Relative Error} = \text{Relative Error} \times 100 \quad (8)$$

where AR is an abbreviation for Amplitude Ratio. If the peak frequencies were the same, then the current relative error was compared to the lowest previous value. The geometry resulting in the least relative error was identified in this manner as the iteration proceeded, and the values were saved to be printed out at the end of the iteration process. The program then printed out the transducer dimensions, the theoretical peak amplitude ratio and its frequency, the relative error, and the difference between peak frequencies. Next the appropriate variable or variables was incremented and the entire process repeated.

Upon completion of the iteration process for a given set of ranges and step sizes, the end result was a set of transducer dimensions which optimized the match between the theoretical and experimental curves at one frequency. Of course, satisfying the condition of minimum relative error at a single

frequency does not guarantee good correlation throughout the rest of the frequency range. To examine this correlation the theoretical amplitude ratio and phase shift curves, generated using the transducer geometry identified with the program, were plotted versus the experimental data over the entire 200 hertz range. The relative error between the theoretical and experimental results was also calculated to provide a quantitative estimate of the match between the curves. These curves were ultimately used to select the geometry which produced the closest match between the theoretical and experimental amplitude ratio and phase shift throughout the frequency range.

3. ZOC INTERNAL GEOMETRY OPTIMIZATION RESULTS

The search for an ideal set of geometry with which to model the ZOC transducer was accomplished using the computer program described in the previous section. The program was run for a total of 11 cases. Seven of these cases were run using a coarse volume increment, and the optimum volumes from four of these cases were further refined using a finer volume increment. The input parameters and results for each case are shown in Table 4.

When running the program for the first time, it was discovered that the length range would have to be reduced from the initial choice of 0.25 to 12.0 cm. The brute force iterative process used in the program turned out to be an extremely time consuming task. With the original length range of 11.75 cm the program took so long to run that timesharing on the CRF's IBM 4341 mainframe was impossible. Therefore, to limit the amount of time required to execute the program, and thereby free up the computer system for other users, the

Table 4. Summary of the IDC Optimization Results

	CASE NUMBER										
	1	2	3	4	5	6	7	8	9	10	11
OPTIMUM GEOMETRY											
LENGTH (CM)	6.0	4.0	6.0	8.5	6.7	3.0	5.5	12.5	3.2	6.0	12.7
DIAMETER (CM)	0.1025	0.0505	0.0505	0.0875	0.0665	0.0255	0.0305	0.0305	0.02925	0.03175	0.03175
VOLUME (CU. CM)	3.125(E-4)	6.25(E-5)	0.0001	0.0001	0.00006	0.020	0.020	0.010	0.026	0.0215	0.0105
MINIMUM RELATIVE ERROR (PERCENT)	2.66	2.36	2.34	2.34	2.27	2.16	1.03	2.38	0.0159	0.002	0.0005
INPUT PARAMETERS											
LENGTH RANGE (CM)	0.25-6.0	6.25-10.0	6.25-12.0	7.0-9.0	6.0-9.0	0.5-5.0	5.5-10.0	10.5-15.0	2.5-3.5	5.0-6.0	12.0-13.0
STEP SIZE (CM)	0.25	0.25	0.25	0.50	0.10	0.50	0.50	0.50	0.10	0.10	0.10
DIAMETER RANGE	.0085-.1060	.0085-.1060	.0085-.1060	.0655-.0955	.0525-.0925	.0055-.1560	.0055-.1560	.0055-.1560	.0205-.0305	.0255-.0305	.0255-.0305
STEP SIZE (CM)	0.005	0.005	0.005	0.001	0.001	0.005	0.005	0.005	0.00125	0.00125	0.00125
VOLUME RANGE (CU. CM)	1.0(E-7)-1.0	1.0(E-7)-1.0	1.0(E-5)-.10	1.0(E-5)-.10	5.0(E-6)-2.0(E-4)	1.0(E-5)-.10	1.0(E-5)-.10	1.0(E-5)-.10	0.01-0.04	0.01-0.04	0.008-0.02
TYPE INCREMENT	COARSE	COARSE	COARSE	COARSE	FINE	COARSE	COARSE	COARSE	FINE	FINE	FINE
STEP SIZE (CU. CM)	NOTE 1	NOTE 1	NOTE 2	NOTE 2	5.0(E-6)	NOTE 2	NOTE 2	NOTE 2	0.0005	0.0005	0.0005

NOTE 1: The volume was incremented by a factor of 5, i.e. NEW VOLUME = OLD VOLUME * 5

NOTE 2: The volume was incremented according to the formula,

V = a*(10**b)*INITIAL VOLUME

where,

V = new volume
a = 2, 4, 6, 8, or 10
b = 0, 1, 2, or 3

length range was segmented into smaller intervals. Thus, two cases were run to cover a 0.25 to 12.0 cm interval early in the optimization process, and later three cases were run to cover an interval of 0.5 to 15.0 cm.

Once the optimization program had been used to identify a potentially optimum set of transducer dimensions, it was necessary to expand the comparison between the theoretical results obtained using this transducer geometry and the experimental data to cover the entire 200 hertz frequency range. The previous description of the optimization criterion program identified the ZOC geometry needed to minimize the relative error between the theoretical and experimental amplitude ratios at only one frequency--the frequency at which the peak amplitude ratio occurred in the experimental data. Based on this criterion alone the Case 11 geometry shown in Table 4 appears to be the best choice, since these dimensions resulted in the smallest relative error. Further examination of the results will show that this is not the best set of geometry, however.

To make the comparison of the theoretical and experimental results throughout the 200-hertz frequency range, it was necessary to run the original NASA program for each case with the ZOC transducer modelled using the optimum dimensions shown in Table 4. These theoretical results were then compared to the experimental data at 10-hertz intervals over the 200-hertz range. The results are presented graphically in Figures 70-81 and the percent relative error between the experimental and theoretical values for each case is shown in Tables 5-26.

Table 5. Comparison of Experimental and Theoretical Results - Case 1
(10.0 inch Tube, PR=1.0349)

FREQUENCY (HZ)	EXPERIMENTAL AMPLITUDE RATIO	THEORETICAL AMPLITUDE RATIO	RELATIVE ERROR (PERCENT)	EXPERIMENTAL PHASE SHIFT (DEG)	THEORETICAL PHASE SHIFT (DEG)	RELATIVE ERROR (PERCENT)
0	1	1	0	0	0	0
10	.995	1.001	-.60	-4.85	-4.425	8.76
20	.999	1.0053	-.63	-9.35	-8.785	6.04
30	1.01	1.015	-.50	-13.8	-13.134	4.83
40	1.02	1.031	-1.00	-18.6	-17.607	5.34
50	1.04	1.0534	-1.29	-23.5	-22.342	4.93
60	1.07	1.0813	-1.06	-28.8	-27.46	4.65
70	1.1	1.1132	-1.20	-34.7	-33.065	4.71
80	1.13	1.1469	-1.50	-41.3	-39.247	4.97
90	1.16	1.1792	-1.66	-48.3	-46.06	4.64
100	1.18	1.2058	-2.19	-55.9	-53.517	4.26
110	1.19	1.2216	-2.66	-64.2	-61.559	4.11
120	1.19	1.2218	-2.67	-72.7	-70.041	3.66
130	1.17	1.2036	-2.87	-81.8	-78.734	3.75
140	1.13	1.1667	-3.25	-90.4	-87.364	3.36
150	1.07	1.1143	-4.14	-98.9	-95.666	3.27
160	1.01	1.0515	-4.11	-106	-103.437	2.42
170	.943	.9838	-4.33	-113	-110.561	2.16
180	.884	.9156	-3.57	-120	-117.001	2.50
190	.814	.8503	-4.46	-125	-122.78	1.78
200	.757	.7897	-4.32	-130	-127.953	1.57

Table 6. Comparison of Experimental and Theoretical Results - Case 1
(10.0 Inch Tube, PR=1.3982)

FREQUENCY (HZ)	EXPERIMENTAL AMPLITUDE RATIO	THEORETICAL AMPLITUDE RATIO	RELATIVE ERROR (PERCENT)	EXPERIMENTAL PHASE SHIFT (DEG)	THEORETICAL PHASE SHIFT (DEG)	RELATIVE ERROR (PERCENT)
0	1	1	0	0	0	0
10	.995	.9992	-.42	-6.12	-5.813	5.02
20	.993	.9978	-.48	-11.8	-11.546	2.15
30	.993	.9975	-.45	-17.7	-17.206	2.79
40	.995	.9995	-.45	-23.6	-22.878	3.06
50	1	1.004	-.40	-29.7	-28.674	3.45
60	1	1.0098	-.98	-36.2	-34.694	4.16
70	1.01	1.0156	-.55	-42.6	-41.003	3.75
80	1.01	1.0193	-.92	-49.6	-47.632	3.97
90	1.01	1.0188	-.87	-57	-54.571	4.26
100	.996	1.0121	-1.62	-64.3	-61.768	3.94
110	.979	.9976	-1.90	-71.8	-69.134	3.71
120	.953	.9749	-2.30	-79.4	-76.549	3.59
130	.921	.9441	-2.51	-86.3	-83.88	2.80
140	.881	.9066	-2.91	-93.6	-90.998	2.78
150	.837	.8643	-3.26	-100	-97.801	2.20
160	.792	.8194	-3.46	-107	-104.216	2.60
170	.746	.7738	-3.73	-113	-110.205	2.47
180	.698	.729	-4.44	-119	-115.76	2.72
190	.663	.6863	-3.51	-123	-120.895	1.71
200	.624	.6463	-3.57	-128	-125.637	1.85

Table 7. Comparison of Experimental and Theoretical Results - Case 2
(10.0 Inch Tube, PR=1.8349)

FREQUENCY (HZ)	EXPERIMENTAL AMPLITUDE RATIO	THEORETICAL AMPLITUDE RATIO	RELATIVE ERROR (PERCENT)	EXPERIMENTAL PHASE SHIFT (DEG)	THEORETICAL PHASE SHIFT (DEG)	RELATIVE ERROR (PERCENT)
0	1	1	0	0	0	0
10	.995	1.0017	-.67	-4.85	-4.397	9.34
20	.999	1.0074	-.84	-9.35	-8.797	5.91
30	1.01	1.0179	-.78	-13.8	-13.242	4.04
40	1.02	1.0339	-1.36	-18.6	-17.822	4.18
50	1.04	1.0556	-1.50	-23.5	-22.646	3.63
60	1.07	1.0825	-1.17	-28.8	-27.827	3.38
70	1.1	1.1132	-1.20	-34.7	-33.469	3.55
80	1.13	1.1457	-1.39	-41.3	-39.661	3.97
90	1.16	1.1769	-1.46	-48.3	-46.462	3.81
100	1.18	1.2025	-1.91	-55.9	-53.885	3.60
110	1.19	1.2178	-2.34	-64.2	-61.874	3.62
120	1.19	1.2181	-2.36	-72.7	-70.289	3.32
130	1.17	1.2005	-2.61	-81.8	-78.988	3.54
140	1.13	1.165	-3.10	-90.4	-87.468	3.24
150	1.07	1.1144	-4.15	-98.9	-95.713	3.22
160	1.01	1.0535	-4.31	-106	-103.445	2.41
170	.943	.9876	-4.73	-113	-110.548	2.17
180	.884	.9212	-4.21	-120	-116.983	2.51
190	.814	.8572	-5.31	-125	-122.77	1.78
200	.757	.7978	-5.39	-130	-127.963	1.57

Table 8. Comparison of Experimental and Theoretical Results - Case 2
(10.0 Inch Tube, PR=1.3982)

FREQUENCY (HZ)	EXPERIMENTAL AMPLITUDE RATIO	THEORETICAL AMPLITUDE RATIO	RELATIVE ERROR (PERCENT)	EXPERIMENTAL PHASE SHIFT (DEG)	THEORETICAL PHASE SHIFT (DEG)	RELATIVE ERROR (PERCENT)
0	1	1	0	0	0	0
10	.995	1	-.50	-6.12	-5.77	5.72
20	.993	1.0003	-.74	-11.8	-11.528	2.31
30	.993	1.0015	-.86	-17.7	-17.29	2.32
40	.995	1.004	-.90	-23.6	-23.105	2.10
50	1	1.008	-.80	-29.7	-29.041	2.22
60	1	1.0126	-1.26	-36.2	-35.17	2.85
70	1.01	1.0167	-.66	-42.6	-41.547	2.47
80	1.01	1.0187	-.86	-49.6	-48.203	2.82
90	1.01	1.0167	-.66	-57	-55.132	3.28
100	.996	1.0089	-1.30	-64.3	-62.289	3.13
110	.979	.9939	-1.52	-71.8	-69.594	3.07
120	.953	.9712	-1.91	-79.4	-76.936	3.10
130	.921	.941	-2.17	-86.3	-84.192	2.44
140	.881	.9046	-2.68	-93.6	-91.244	2.52
150	.837	.8636	-3.18	-100	-97.993	2.01
160	.792	.8201	-3.55	-107	-104.37	2.46
170	.746	.776	-4.02	-113	-110.337	2.36
180	.698	.7326	-4.96	-119	-115.885	2.62
190	.663	.6911	-4.24	-123	-121.026	1.68
200	.624	.6522	-4.52	-128	-125.785	1.73

Table 9. Comparison of Experimental and Theoretical Results - Case 3
(10.0 Inch Tube, PR=1.8349)

FREQUENCY (HZ)	EXPERIMENTAL AMPLITUDE RATIO	THEORETICAL AMPLITUDE RATIO	RELATIVE ERROR (PERCENT)	EXPERIMENTAL PHASE SHIFT (DEG)	THEORETICAL PHASE SHIFT (DEG)	RELATIVE ERROR (PERCENT)
0	1	1	0	0	0	0
10	.995	1.0017	-.67	-4.85	-4.399	9.38
20	.999	1.0074	-.84	-9.35	-8.801	5.87
30	1.01	1.0179	-.78	-13.8	-13.249	3.99
40	1.02	1.0339	-1.36	-18.6	-17.831	4.13
50	1.04	1.0556	-1.50	-23.5	-22.658	3.58
60	1.07	1.0825	-1.17	-28.8	-27.842	3.33
70	1.1	1.1132	-1.20	-34.7	-33.488	3.49
80	1.13	1.1457	-1.39	-41.3	-39.684	3.91
90	1.16	1.1768	-1.45	-48.3	-46.489	3.75
100	1.18	1.2024	-1.90	-55.9	-53.917	3.55
110	1.19	1.2176	-2.32	-64.2	-61.91	3.57
120	1.19	1.2178	-2.34	-72.7	-70.328	3.26
130	1.17	1.2002	-2.58	-81.8	-78.95	3.48
140	1.13	1.1645	-3.05	-90.4	-87.51	3.20
150	1.07	1.1138	-4.09	-98.9	-95.755	3.18
160	1.01	1.0529	-4.25	-106	-103.484	2.37
170	.943	.987	-4.67	-113	-110.585	2.14
180	.884	.9205	-4.13	-120	-117.017	2.49
190	.814	.8566	-5.23	-125	-122.802	1.76
200	.757	.7972	-5.31	-130	-127.992	1.54

Table 10. Comparison of Experimental and Theoretical Results - Case 3
(10.0 Inch Tube, PR=1.3982)

FREQUENCY (HZ)	EXPERIMENTAL AMPLITUDE RATIO	THEORETICAL AMPLITUDE RATIO	RELATIVE ERROR (PERCENT)	EXPERIMENTAL PHASE SHIFT (DEG)	THEORETICAL PHASE SHIFT (DEG)	RELATIVE ERROR (PERCENT)
0	1	1	0	0	0	0
10	.995	1	-.50	-6.12	-5.772	5.69
20	.993	1.0003	-.74	-11.8	-11.534	2.25
30	.993	1.0015	-.86	-17.7	-17.299	2.27
40	.995	1.004	-.90	-23.6	-23.117	2.05
50	1	1.0079	-.79	-29.7	-29.055	2.17
60	1	1.0125	-1.25	-36.2	-35.188	2.80
70	1.01	1.0167	-.66	-42.6	-41.568	2.42
80	1.0	1.0186	-.85	-49.6	-48.227	2.77
90	1.01	1.0166	-.65	-57	-55.159	3.23
100	.996	1.0087	-1.28	-64.3	-62.319	3.08
110	.979	.9937	-1.50	-71.8	-69.625	3.03
120	.953	.9709	-1.88	-79.4	-76.969	3.06
130	.921	.9406	-2.13	-86.3	-84.226	2.40
140	.881	.9042	-2.63	-93.6	-91.278	2.48
150	.837	.8632	-3.13	-100	-98.026	1.97
160	.792	.8197	-3.50	-107	-104.401	2.43
170	.746	.7755	-3.95	-113	-110.367	2.33
180	.698	.7321	-4.89	-119	-115.913	2.59
190	.663	.6906	-4.16	-123	-121.053	1.58
200	.624	.6517	-4.44	-128	-125.811	1.71

Table 11. Comparison of Experimental and Theoretical Results - Case 4
(10.0 Inch Tube, PR=1.8349)

FREQUENCY (HZ)	EXPERIMENTAL AMPLITUDE RATIO	THEORETICAL AMPLITUDE RATIO	RELATIVE ERROR (PERCENT)	EXPERIMENTAL PHASE SHIFT (DEG)	THEORETICAL PHASE SHIFT (DEG)	RELATIVE ERROR (PERCENT)
0	1	1	0	0	0	0
10	.995	1.0019	-.69	-4.85	-4.332	9.44
20	.999	1.0079	-.89	-9.35	-8.797	5.91
30	1.01	1.0187	-.86	-13.8	-13.262	3.90
40	1.02	1.0349	-1.46	-18.6	-17.868	3.94
50	1.04	1.0566	-1.60	-23.5	-22.721	3.31
60	1.07	1.0834	-1.25	-28.8	-27.926	3.03
70	1.1	1.1139	-1.26	-34.7	-33.589	3.20
80	1.13	1.1462	-1.43	-41.3	-39.796	3.64
90	1.16	1.1771	-1.47	-48.3	-46.605	3.51
100	1.18	1.2025	-1.91	-55.9	-54.031	3.34
110	1.19	1.2176	-2.32	-64.2	-62.018	3.40
120	1.19	1.2178	-2.34	-72.7	-70.423	3.13
130	1.17	1.2003	-2.59	-81.8	-79.03	3.39
140	1.13	1.165	-3.10	-90.4	-87.577	3.12
150	1.07	1.1147	-4.18	-98.9	-95.888	3.13
160	1.01	1.0542	-4.38	-106	-103.503	2.36
170	.943	.9888	-4.86	-113	-110.626	2.18
180	.884	.9227	-4.38	-120	-117.059	2.45
190	.814	.8592	-5.55	-125	-122.848	1.72
200	.757	.8	-5.68	-130	-128.047	1.58

Table 12. Comparison of Experimental and Theoretical Results - Case 4
(10.0 Inch Tube, PR=1.3982)

FREQUENCY (HZ)	EXPERIMENTAL AMPLITUDE RATIO	THEORETICAL AMPLITUDE RATIO	RELATIVE ERROR (PERCENT)	EXPERIMENTAL PHASE SHIFT (DEG)	THEORETICAL PHASE SHIFT (DEG)	RELATIVE ERROR (PERCENT)
0	1	1	0	0	0	0
10	.995	1.0002	-.52	-6.12	-5.76	5.88
20	.993	1.0008	-.79	-11.8	-11.5	2.54
30	.993	1.0025	-.96	-17.7	-17.3	2.26
40	.995	1.0054	-1.05	-23.6	-23.2	1.69
50	1	1.0094	-.94	-29.7	-29.1	2.02
60	1	1.0139	-1.39	-36.2	-35.3	2.49
70	1.01	1.0178	-.77	-42.6	-41.7	2.11
80	1.01	1.0195	-.94	-49.6	-48.4	2.42
90	1.01	1.0171	-.70	-57	-55.3	2.98
100	.996	1.009	-1.31	-64.3	-62.5	2.80
110	.979	.9938	-1.51	-71.8	-69.8	2.79
120	.953	.9709	-1.88	-79.4	-77.1	2.90
130	.921	.9408	-2.15	-88.3	-84.4	2.20
140	.881	.9044	-2.66	-93.6	-91.4	2.35
150	.837	.8637	-3.19	-100	-98.1	1.90
160	.792	.8205	-3.60	-107	-104	2.80
170	.746	.7767	-4.12	-113	-110	2.65
180	.698	.7336	-5.10	-119	-116	2.52
190	.663	.6924	-4.43	-123	-121	1.63
200	.624	.6538	-4.78	-128	-126	1.56

Table 13. Comparison of Experimental and Theoretical Results - Case 5
(10.0 Inch Tube, PR=1.8349)

FREQUENCY (HZ)	EXPERIMENTAL AMPLITUDE RATIO	THEORETICAL AMPLITUDE RATIO	RELATIVE ERROR (PERCENT)	EXPERIMENTAL PHASE SHIFT (DEG)	THEORETICAL PHASE SHIFT (DEG)	RELATIVE ERROR (PERCENT)
0	1	1	0	0	0	0
10	.995	1.0019	-.69	-4.85	-4.395	9.29
20	.999	1.008	-.90	-9.35	-8.807	5.81
30	1.01	1.0189	-.88	-13.8	-13.283	3.75
40	1.02	1.0352	-1.49	-18.6	-17.904	3.74
50	1.04	1.057	-1.63	-23.5	-22.77	3.11
60	1.07	1.0837	-1.28	-28.8	-27.991	2.81
70	1.1	1.1141	-1.28	-34.7	-33.667	2.98
80	1.13	1.1463	-1.44	-41.3	-39.886	3.42
90	1.16	1.177	-1.47	-48.3	-46.707	3.38
100	1.18	1.2022	-1.88	-55.9	-54.14	3.15
110	1.19	1.217	-2.27	-64.2	-62.129	3.23
120	1.19	1.217	-2.27	-72.7	-70.536	2.98
130	1 17	1.1994	-2.51	-81.8	-79.14	3.25
140	1.13	1.164	-3.01	-90.4	-87.68	3.01
150	1.07	1.1137	-4.08	-98.9	-95.904	3.03
160	1.01	1.0534	-4.30	-106	-103.618	2.25
170	.943	.988	-4.77	-113	-110.707	2.03
180	.884	.9222	-4.32	-120	-117.134	2.39
190	.814	.8588	-5.50	-125	-122.919	1.66
200	.757	.7999	-5.67	-130	-128.114	1.45

Table 14. Comparison of Experimental and Theoretical Results - Case 5
(10.0 Inch Tube, PR=1.3982)

FREQUENCY (HZ)	EXPERIMENTAL AMPLITUDE RATIO	THEORETICAL AMPLITUDE RATIO	RELATIVE ERROR (PERCENT)	EXPERIMENTAL PHASE SHIFT (DEG)	THEORETICAL PHASE SHIFT (DEG)	RELATIVE ERROR (PERCENT)
0	1	1	0	0	0	0
10	.995	1.0002	-.52	-6.12	-5.77	5.72
20	.993	1.001	-.81	-11.8	-11.5	2.54
30	.993	1.0028	-.99	-17.7	-17.3	2.26
40	.995	1.0057	-1.08	-23.6	-23.2	1.69
50	1	1.0097	-.97	-29.7	-29.2	1.68
60	1	1.0142	-1.42	-36.2	-35.4	2.21
70	1.01	1.018	-.79	-42.6	-41.8	1.88
80	1.01	1.0195	-.94	-49.6	-48.5	2.22
90	1.01	1.0169	-.68	-57	-55.4	2.81
100	.996	1.0085	-1.26	-64.3	-62.6	2.64
110	.979	.9931	-1.44	-71.8	-69.9	2.65
120	.953	.9701	-1.79	-79.4	-77.2	2.77
130	.921	.9399	-2.05	-86.3	-84.5	2.09
140	.881	.9036	-2.57	-93.6	-91.5	2.24
150	.837	.8629	-3.09	-100	-98.2	1.88
160	.792	.8198	-3.51	-107	-105	1.87
170	.746	.7761	-4.03	-113	-111	1.77
180	.698	.7332	-5.04	-119	-116	2.52
190	.653	.6922	-4.40	-123	-121	1.63
200	.624	.6537	-4.76	-128	-126	1.56

Table 15. Comparison of Experimental and Theoretical Results - Case 6
(10.0 Inch Tube, PR=1.8349)

FREQUENCY (HZ)	EXPERIMENTAL AMPLITUDE RATIO	THEORETICAL AMPLITUDE RATIO	RELATIVE ERROR (PERCENT)	EXPERIMENTAL PHASE SHIFT (DEG)	THEORETICAL PHASE SHIFT (DEG)	RELATIVE ERROR (PERCENT)
0	1	1	0	0	0	0
10	.995	1.002	-.70	-4.85	-4.85	0
20	.999	1.0078	-.88	-9.35	-9.75	-4.28
30	1.01	1.0174	-.73	-13.8	-14.8	-7.25
40	1.02	1.0305	-1.03	-18.6	-19.9	-6.99
50	1.04	1.0467	-.64	-23.5	-25.2	-7.23
60	1.07	1.0655	.42	-28.8	-30.8	-6.94
70	1.1	1.086	1.27	-34.7	-36.8	-6.05
80	1.13	1.1072	2.02	-41.3	-43	-4.12
90	1.16	1.1274	2.81	-48.3	-49.5	-2.48
100	1.18	1.145	2.97	-55.9	-56.5	-1.07
110	1.19	1.1579	2.78	-64.2	-63.7	.78
120	1.19	1.164	2.18	-72.7	-71.3	1.93
130	1.17	1.1618	.78	-81.8	-79	3.42
140	1.13	1.1502	-1.79	-90.4	-86.9	3.87
150	1.07	1.1291	-5.52	-98.9	-94.7	4.25
160	1.01	1.0996	-8.87	-106	-102	3.77
170	.943	1.0632	-12.75	-113	-110	2.65
180	.884	1.022	-15.61	-120	-117	2.50
190	.814	.9781	-20.16	-125	-124	.80
200	.757	.9335	-23.32	-130	-131	-.77

Table 16. Comparison of Experimental and Theoretical Results - Case 6
(10.0 Inch Tube, PR=1.3982)

FREQUENCY (HZ)	EXPERIMENTAL AMPLITUDE RATIO	THEORETICAL AMPLITUDE RATIO	RELATIVE ERROR (PERCENT)	EXPERIMENTAL PHASE SHIFT (DEG)	THEORETICAL PHASE SHIFT (DEG)	RELATIVE ERROR (PERCENT)
0	1	1	0	0	0	0
10	.995	1.0003	-.53	-6.12	-6.36	-3.92
20	.993	1.0012	-.83	-11.8	-12.7	-7.63
30	.993	1.0024	-.95	-17.7	-19.2	-8.47
40	.995	1.0036	-.86	-23.6	-25.7	-8.90
50	1	1.0043	-.43	-29.7	-32.4	-9.09
60	1	1.0039	-.39	-36.3	-39.1	-8.01
70	1.01	1.0019	.80	-42.6	-46	-7.98
80	1.01	.9974	1.25	-49.6	-53	-6.85
90	1.01	.99	1.98	-57	-60.2	-5.61
100	.996	.979	1.71	-64.3	-67.3	-4.67
110	.979	.9649	1.51	-71.8	-74.6	-3.90
120	.953	.9454	.80	-78.4	-81.8	-3.82
130	.921	.923	-.22	-86.3	-89	-3.13
140	.881	.8972	-1.84	-93.6	-96.1	-2.67
150	.837	.8699	-3.93	-100	-103	-3.00
160	.792	.8385	-5.87	-107	-110	-2.86
170	.746	.807	-8.18	-113	-116	-2.65
180	.699	.7751	-11.05	-119	-123	-3.36
190	.653	.7432	-13.10	-123	-129	-4.88
200	.624	.712	-14.10	-128	-135	-5.47

Table 17. Comparison of Experimental and Theoretical Results - Case 7
(18.0 Inch Tube, [illegible].8349)

FREQUENCY (HZ)	EXPERIMENTAL AMPLITUDE RATIO	THEORETICAL AMPLITUDE RATIO	RELATIVE ERROR (PERCENT)	EXPERIMENTAL PHASE SHIFT (DEG)	THEORETICAL PHASE SHIFT (DEG)	RELATIVE ERROR (PERCENT)
[illegible]	1	1	0	0	0	0
[illegible]	.995	1.0034	-.74	-4.85	-4.88	-.62
20	.999	1.0096	-1.06	-9.35	-9.82	-5.03
30	1.01	1.0214	-1.13	-13.8	-14.9	-7.97
40	1.02	1.0376	-1.73	-18.6	-20.1	-8.06
50	1.04	1.0578	-1.71	-23.5	-25.6	-8.94
60	1.07	1.0813	-1.06	-28.8	-31.4	-9.03
70	1.1	1.1071	-.65	-34.7	-37.6	-8.36
80	1.13	1.1337	-.33	-41.3	-44.1	-6.78
90	1.15	1.1592	.07	-48.3	-51.1	-5.80
[illegible]	1.18	1.1809	-.08	-55.9	-58.6	-4.83
[illegible]	1.19	1.1962	-.52	-64.2	-66.4	-3.43
120	1.19	1.2023	-1.03	-72.7	-74.5	-2.48
130	1.17	1.1972	-2.32	-81.8	-82.9	-1.34
140	1.13	1.1802	-4.44	-90.4	-91.2	-.88
150	1.07	1.1519	-7.65	-98.9	-99.5	-.61
160	1.01	1.1143	-10.33	-106	-108	-1.89
170	.943	1.07	-13.47	-113	-115	-1.77
180	.884	1.0221	-15.62	-120	-123	-2.50
190	.814	.9731	-19.55	-125	-130	-4.00
200	.757	.9249	-22.18	-130	-136	-4.62

Table 18. Comparison of Experimental and Theoretical Results - Case 7
(10.0 Inch Tube, PR=1.3982)

FREQUENCY (HZ)	EXPERIMENTAL AMPLITUDE RATIO	THEORETICAL AMPLITUDE RATIO	RELATIVE ERROR (PERCENT)	EXPERIMENTAL PHASE SHIFT (DEG)	THEORETICAL PHASE SHIFT (DEG)	RELATIVE ERROR (PERCENT)
0	1	1	0	0	0	0
10	.995	1.0007	-.57	-6.12	-6.4	-4.58
20	.993	1.0029	-1.00	-11.8	-12.8	-8.47
30	.993	1.0061	-1.32	-17.7	-19.4	-9.60
40	995	1.01	-1.51	-23.6	-26	-10.17
50		1.014	-1.40	-29.7	-32.8	-10.44
60	1	1.0171	-1.71	-36.2	-39.8	-9.94
70	1.01	1.0184	-.83	-42.6	-47	-10.33
80	1.01	1.0169	-.68	-49.6	-54.3	-9.48
90	1.01	1.0118	-.18	-57	-61.8	-8.42
100	.996	1.0021	-.61	-64.3	-69.4	-7.93
110	.979	.9874	-.86	-71.8	-77	-7.24
120	.953	.9676	-1.53	-79.4	-84.7	-6.68
130	.921	.943	-2.39	-86.3	-92.2	-6.84
140	.881	.9145	-3.80	-93.6	-99.7	-6.52
150	.837	.8829	-5.48	-100	-107	-7.00
160	.792	.8494	-7.25	-107	-114	-6.54
170	.746	.8149	-9.24	-113	-121	-7.08
180	.698	.7804	-11.81	-119	-127	-6.72
190	.663	.7466	-12.61	-123	-133	-8.13
200	.624	.7141	-14.44	-128	-140	-9.38

Table 19. Comparison of Experimental and Theoretical Results - Case 8
(10.0 Inch Tube, PR=1.8349)

FREQUENCY (HZ)	EXPERIMENTAL AMPLITUDE RATIO	THEORETICAL AMPLITUDE RATIO	RELATIVE ERROR (PERCENT)	EXPERIMENTAL PHASE SHIFT (DEG)	THEORETICAL PHASE SHIFT (DEG)	RELATIVE ERROR (PERCENT)
0	1	1	0	0	0	0
10	.995	1.002	-.70	-4.85	-5.64	-16.29
20	.999	1.008	-.90	-9.35	-11.3	-20.86
30	1.01	1.0179	-.78	-13.8	-17.1	-23.91
40	1.02	1.0313	-1.11	-18.6	-23.1	-24.19
50	1.04	1.0478	-.75	-23.5	-29.3	-24.68
60	1.07	1.0667	.31	-28.8	-35.7	-23.96
70	1.1	1.0871	1.17	-34.7	-42.4	-22.19
80	1.13	1.1079	1.96	-41.3	-49.4	-19.61
90	1.16	1.1274	2.81	-48.3	-56.8	-17.68
100	1.18	1.1441	3.04	-55.9	-64.4	-15.21
110	1.19	1.1561	2.85	-64.2	-72.4	-12.77
120	1.19	1.1617	2.38	-72.7	-80.6	-10.87
130	1.17	1.16	.85	-81.8	-88.9	-8.68
140	1.13	1.1502	-1.79	-90.4	-97.3	-7.63
150	1.07	1.1329	-5.88	-98.9	-106	-7.18
160	1.01	1.1088	-9.78	-106	-114	-7.55
170	.943	1.0795	-14.48	-113	-122	-7.96
180	.884	1.0467	-18.40	-120	-130	-8.33
190	.814	1.0119	-24.31	-125	-137	-9.60
200	.757	.9765	-29.00	-130	-145	-11.54

Table 20. Comparison of Experimental and Theoretical Results - Case 8
(10.0 Inch Tube, PR=1.3982)

FREQUENCY (HZ)	EXPERIMENTAL AMPLITUDE RATIO	THEORETICAL AMPLITUDE RATIO	RELATIVE ERROR (PERCENT)	EXPERIMENTAL PHASE SHIFT (DEG)	THEORETICAL PHASE SHIFT (DEG)	RELATIVE ERROR (PERCENT)
0	1	1	0	0	0	0
10	.995	1.0001	-.51	-6.12	-7.4	-20.92
20	.993	1.0001	-.72	-11.8	-14.8	-25.42
30	.993	1.0001	-.72	-17.7	-22.3	-25.99
40	.995	.9996	-.46	-23.6	-29.8	-26.27
50	1	.9982	.18	-29.7	-37.5	-26.26
60	1	.9954	.46	-36.2	-45.2	-24.86
70	1.01	.9908	1.90	-42.6	-53	-24.41
80	1.01	.9839	2.58	-49.6	-68.8	-22.58
90	1.01	.9743	3.53	-57	-68.7	-20.53
100	.996	.9618	3.43	-64.3	-76.7	-19.28
110	.979	.9463	3.34	-71.8	-84.6	-17.83
120	.953	.9279	2.63	-79.4	-92.6	-16.62
130	.921	.9069	1.53	-86.3	-100	-15.87
140	.881	.8837	-.31	-93.6	-108	-15.38
150	.837	.8588	-2.60	-100	-116	-16.00
160	.792	.8327	-5.14	-107	-123	-14.95
170	.746	.806	-8.04	-113	-131	-15.93
180	.698	.7791	-11.62	-119	-138	-15.97
190	.663	.7523	-13.47	-123	-145	-17.89
200	.624	.7259	-16.33	-128	-152	-18.75

Table 21. Comparison of Experimental and Theoretical Results - Case 9
(10.0 Inch Tube, PR=1.8349)

FREQUENCY (HZ)	EXPERIMENTAL AMPLITUDE RATIO	THEORETICAL AMPLITUDE RATIO	RELATIVE ERROR (PERCENT)	EXPERIMENTAL PHASE SHIFT (DEG)	THEORETICAL PHASE SHIFT (DEG)	RELATIVE ERROR (PERCENT)
0	1	1	0	0	0	0
10	.995	1.0025	-.75	-4.85	-4.8	1.03
20	.999	1.0098	-1.08	-9.35	-9.66	-3.32
30	1.01	1.022	-1.19	-13.8	-14.6	-5.80
40	1.02	1.0386	-1.82	-18.6	-19.8	-6.45
50	1.04	1.0592	-1.85	-23.5	-25.3	-7.66
60	1.07	1.0831	-1.22	-28.8	-31.1	-7.99
70	1.1	1.109	-.82	-34.7	-37.3	-7.49
80	1.13	1.1353	-.47	-41.3	-43.9	-6.30
90	1.16	1.1595	.04	-48.3	-51	-5.59
100	1.18	1.1788	.10	-55.9	-58.5	-4.65
110	1.19	1.19	0	-64.2	-66.5	-3.58
120	1.19	1.1902	-.02	-72.7	-74.8	-2.89
130	1.17	1.1776	-.65	-81.8	-83.2	-1.71
140	1.13	1.1521	-1.96	-90.4	-91.6	-1.33
150	1.07	1.1149	-4.20	-98.9	-99.8	-.91
160	1.01	1.069	-5.84	-106	-108	-1.89
170	.943	1.0175	-7.90	-113	-115	-1.77
180	.884	.9638	-9.03	-120	-122	-1.67
190	.814	.9104	-11.84	-125	-129	-3.20
200	.757	.8591	-13.49	-130	-135	-3.85

Table 22. Comparison of Experimental and Theoretical Results - Case 9
(18.0 Inch Tube, PR=1.3982)

FREQUENCY (HZ)	EXPERIMENTAL AMPLITUDE RATIO	THEORETICAL AMPLITUDE RATIO	RELATIVE ERROR (PERCENT)	EXPERIMENTAL PHASE SHIFT (DEG)	THEORETICAL PHASE SHIFT (DEG)	RELATIVE ERROR (PERCENT)
0	1	1	0	0	0	0
10	.995	1.0000	-.58	-6.12	-6.29	-2.78
20	.993	1.003	-1.01	-11.8	-12.3	-4.24
30	.993	1.0064	-1.35	-17.7	-19.1	-7.91
40	.995	1.0104	-1.55	-23.6	-25.6	-8.47
50	1	1.0142	-1.42	-29.7	-32.4	-9.09
60	1	1.017	-1.70	-36.2	-39.3	-8.56
70	1.01	1.0176	-.75	-42.6	-46.4	-8.92
80	1.01	1.0149	-.49	-49.6	-53.7	-8.27
90	1.01	1.0077	.23	-57	-61.2	-7.37
100	.996	.9953	.07	-64.3	-68.8	-7.00
110	.979	.9771	.19	-71.8	-76.4	-6.41
120	.953	.9534	-.04	-79.4	-84	-5.79
130	.921	.9246	-.39	-86.3	-91.5	-6.03
140	.881	.8917	-1.21	-93.6	-98.8	-5.56
150	.837	.8559	-2.26	-100	-106	-6.00
160	.792	.8185	-3.35	-107	-113	-5.61
170	.746	.7808	-4.66	-113	-119	-5.31
180	.698	.7436	-6.53	-119	-125	-5.04
190	.663	.7077	-6.74	-123	-131	-6.50
200	.624	.6736	-7.95	-128	-137	-7.03

Table 23. Comparison of Experimental and Theoretical Results - Case 10
(10.0 Inch Tube, PR=1.8349)

FREQUENCY (HZ)	EXPERIMENTAL AMPLITUDE RATIO	THEORETICAL AMPLITUDE RATIO	RELATIVE ERROR (PERCENT)	EXPERIMENTAL PHASE SHIFT (DEG)	THEORETICAL PHASE SHIFT (DEG)	RELATIVE ERROR (PERCENT)
0	1	1	0	0	0	0
10	.995	1.0025	-.75	-4.85	-5.02	-3.51
20	.999	1.0099	-1.09	-9.35	-10.1	-8.02
30	1.01	1.0222	-1.21	-13.8	-15.3	-10.87
40	1.02	1.0389	-1.85	-18.6	-20.8	-11.83
50	1.04	1.0597	-1.89	-23.5	-26.4	-12.34
60	1.07	1.0836	-1.27	-28.8	-32.5	-12.85
70	1.1	1.1095	-.06	-34.7	-38.9	-12.10
80	1.13	1.1356	-.50	-41.3	-45.7	-10.65
90	1.16	1.1596	.03	-48.3	-53	-9.73
100	1.18	1.1786	.12	-55.9	-60.8	-8.77
110	1.19	1.1896	.03	-64.2	-68.9	-7.32
120	1.19	1.19	0	-72.7	-77.3	-6.33
130	1.17	1.1782	-.70	-81.8	-85.9	-5.61
140	1.13	1.1541	-2.13	-92.4	-94.4	-4.42
150	1.07	1.1192	-4.60	-98.9	-103	-4.15
160	1.01	1.0761	-6.54	-106	-111	-4.72
170	.943	1.0279	-9.00	-113	-118	-4.42
180	.884	.9777	-10.60	-120	-126	-5.00
190	.814	.9277	-13.97	-125	-132	-5.60
200	.757	.8798	-16.22	-130	-139	-6.92

Table 24. Comparison of Experimental and Theoretical Results - Case 10
(10.0 Inch Tube, PR=1.3982)

FREQUENCY (HZ)	EXPERIMENTAL AMPLITUDE RATIO	THEORETICAL AMPLITUDE RATIO	RELATIVE ERROR (PERCENT)	EXPERIMENTAL PHASE SHIFT (DEG)	THEORETICAL PHASE SHIFT (DEG)	RELATIVE ERROR (PERCENT)
0	1	1	0	0	0	0
10	.995	1.0007	-.57	-6.12	-6.59	-7.68
20	.993	1.0028	-.99	-11.8	-13.2	-11.86
30	.993	1.0058	-1.29	-17.7	-19.9	-12.43
40	.995	1.0093	-1.44	-23.6	-26.8	-13.56
50	1	1.0126	-1.26	-29.7	-33.8	-13.88
60	1	1.0147	-1.47	-36.2	-41	-13.26
70	1.01	1.0145	-.45	-42.6	-48.4	-13.62
80	1.01	1.0111	-.11	-49.6	-56	-12.98
90	1.01	1.0033	.66	-57	-63.6	-11.58
100	.996	.9906	.54	-64.3	-71.4	-11.04
110	.979	.9725	.66	-71.8	-79.2	-10.31
120	.953	.9493	.39	-79.4	-87	-9.57
130	.921	.9214	-.04	-86.3	-94.7	-9.73
140	.881	.8899	-1.01	-93.6	-102	-8.97
150	.837	.856	-2.27	-100	-109	-9.00
160	.792	.8206	-3.61	-107	-116	-8.41
170	.746	.785	-5.23	-113	-123	-8.85
180	.698	.75	-7.45	-119	-130	-9.24
190	.663	.7162	-8.02	-123	-136	-10.57
200	.624	.6841	-9.63	-128	-142	-10.94

Table 25. Comparison of Experimental and Theoretical Results - Case 11
(10.0 Inch Tube, PR=1.8349)

FREQUENCY (HZ)	EXPERIMENTAL AMPLITUDE RATIO	THEORETICAL AMPLITUDE RATIO	RELATIVE ERROR (PERCENT)	EXPERIMENTAL PHASE SHIFT (DEG)	THEORETICAL PHASE SHIFT (DEG)	RELATIVE ERROR (PERCENT)
0	1	1	0	0	0	0
10	.995	1.0023	-.73	-4.85	-5.49	-13.20
20	.999	1.009	-1.00	-9.35	-11	-17.65
30	1.01	1.0202	-1.01	-13.8	-16.7	-21.01
40	1.02	1.0354	-1.51	-18.6	-22.5	-20.97
50	1.04	1.0542	-1.37	-23.5	-28.6	-21.70
60	1.07	1.076	-.56	-28.8	-34.9	-21.18
70	1.1	1.0998	.02	-34.7	-41.6	-19.88
80	1.13	1.1242	.51	-41.3	-48.6	-17.68
90	1.16	1.1475	1.08	-48.3	-56	-15.94
100	1.18	1.1676	1.05	-55.9	-63.7	-13.95
110	1.19	1.1825	.63	-64.2	-71.8	-11.84
120	1.19	1.19	0	-72.7	-80.1	-10.18
130	1.17	1.1888	-1.61	-81.8	-88.6	-8.31
140	1.13	1.1782	-4.27	-90.4	-97.2	-7.52
150	1.07	1.1587	-8.29	-98.9	-106	-7.18
160	1.01	1.1316	-12.04	-106	-114	-7.55
170	.943	1.0987	-16.51	-113	-122	-7.96
180	.884	1.0623	-20.17	-120	-130	-8.33
190	.814	1.0242	-25.82	-125	-137	-9.60
200	.757	.9859	-30.24	-130	-145	-11.54

Table 26. Comparison of Experimental and Theoretical Results - Case 11
(10.0 Inch Tube, PR=1.3382)

FREQUENCY (HZ)	EXPERIMENTAL AMPLITUDE RATIO	THEORETICAL AMPLITUDE RATIO	RELATIVE ERROR (PERCENT)	EXPERIMENTAL PHASE SHIFT (DEG)	THEORETICAL PHASE SHIFT (DEG)	RELATIVE ERROR (PERCENT)
0	1	1	0	0	0	0
10	.995	1.0004	-.54	-6.12	-7.19	-17.48
20	.993	1.0016	-.87	-11.8	-14.4	-22.03
30	.993	1.0032	-1.03	-17.7	-21.7	-22.68
40	.995	1.005	-1.01	-23.6	-29.1	-23.31
50	1	1.0063	-.63	-29.7	-36.6	-23.23
60	1	1.0066	-.66	-36.2	-44.2	-22.10
70	1.01	1.0051	.49	-42.6	-52	-22.07
80	1.01	1.0012	.87	-49.6	-59.8	-20.56
90	1.01	.9942	1.56	-57	-67.3	-18.95
100	.996	.9837	1.23	-64.3	-75.8	-17.88
110	.979	.9695	.97	-71.8	-83.8	-16.71
120	.953	.9517	.14	-79.4	-91.8	-15.62
130	.921	.9305	-1.03	-86.3	-99.8	-15.64
140	.881	.9065	-2.89	-93.6	-108	-15.38
150	.837	.8803	-5.17	-100	-115	-15.00
160	.792	.8527	-7.66	-107	-123	-14.95
170	.746	.8243	-10.50	-113	-130	-15.04
180	.690	.7958	-14.01	-119	-137	-15.13
190	.663	.7675	-15.76	-123	-144	-17.07
200	.624	.7399	-18.57	-128	-151	-17.97

Figures 70-73 show the results for Cases 1-4. These are the results from the initial optimization attempts using a coarse volume increment. The theoretical results obtained using the manufacturer's equivalent dimensions to model the ZOC transducer are shown also for reference. Cases 6-8 represent another set of optimizations using a coarse volume increment, but over slightly different length ranges. These results are shown in Figures 74-77. In Figures 78-81 the results are shown for Cases 5 and 9-11, which are the cases for the optimizations using a fine volume increment.

These curves show that, by itself, the optimization program is inadequate as a means of identifying the geometry required to provide the best comparison of theoretical and experimental data throughout the entire 200 hertz frequency range. The geometry which best satisfied the optimization criterion (Case 11) did not yield the best overall match with the experimental data. In fact, Figures 78-81 and the corresponding relative error values in Tables 13 and 14 shows that the geometry identified in Case 5 actually produces the best overall match. Therefore, the program itself did not completely isolate an optimum set of geometry as originally anticipated, but rather it identified several candidates from which the optimum could be selected.

Based on the results presented in Tables 5-26 and Figures 70-81, then, the ideal geometry for use in modelling the ZOC14 transducer in the NASA program is from Case 5, where the internal tube length is 8.7 cm, the internal tube diameter is 0.0865 cm, and the internal volume is 6E-5 cubic centimeters. These transducer dimensions produce the best overall match between the theoretical and experimental results. In Figures 82-85 the experimental data

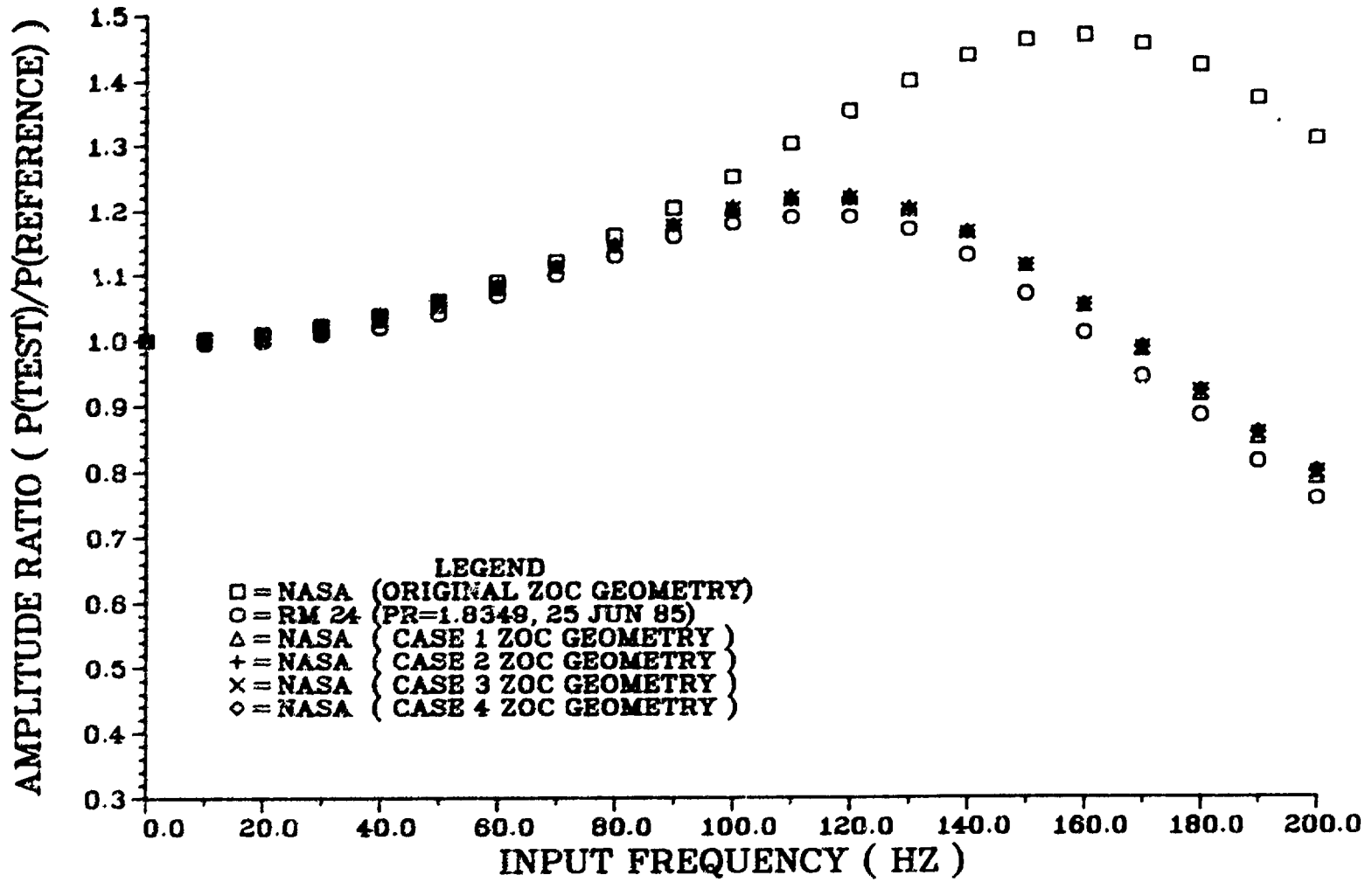

FIGURE 70. COMPARISON OF RM 24 EXPERIMENTAL DATA TO NASA PROGRAM FREQUENCY RESPONSE PREDICTIONS FOR A 10.0 IN. TUBE WITH .020 IN. ID

FIG70

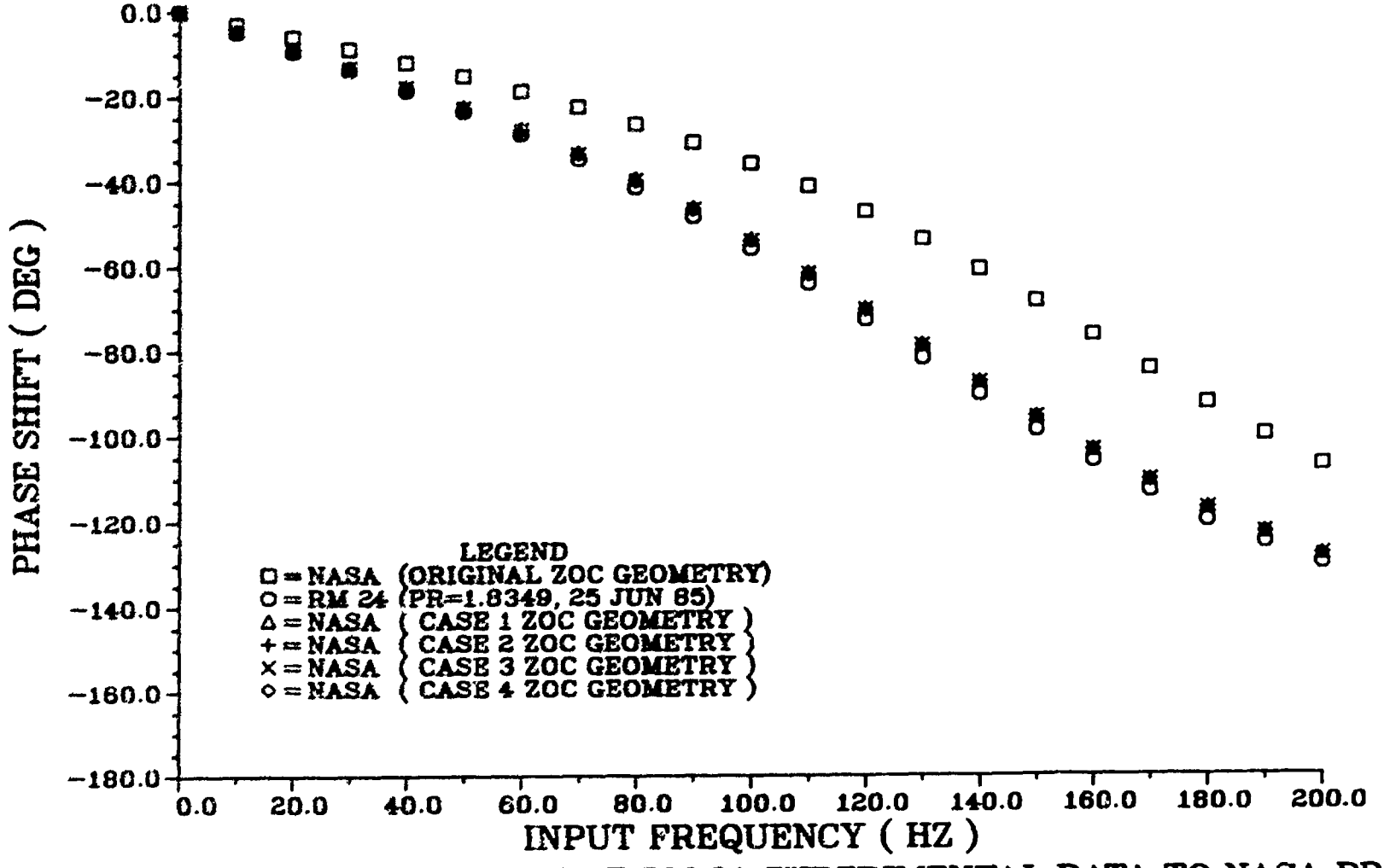

FIGURE 71. COMPARISON OF RM 24 EXPERIMENTAL DATA TO NASA PROGRAM FREQUENCY RESPONSE PREDICTIONS FOR A 10.0 IN. TUBE WITH .020 IN. ID

FIG71

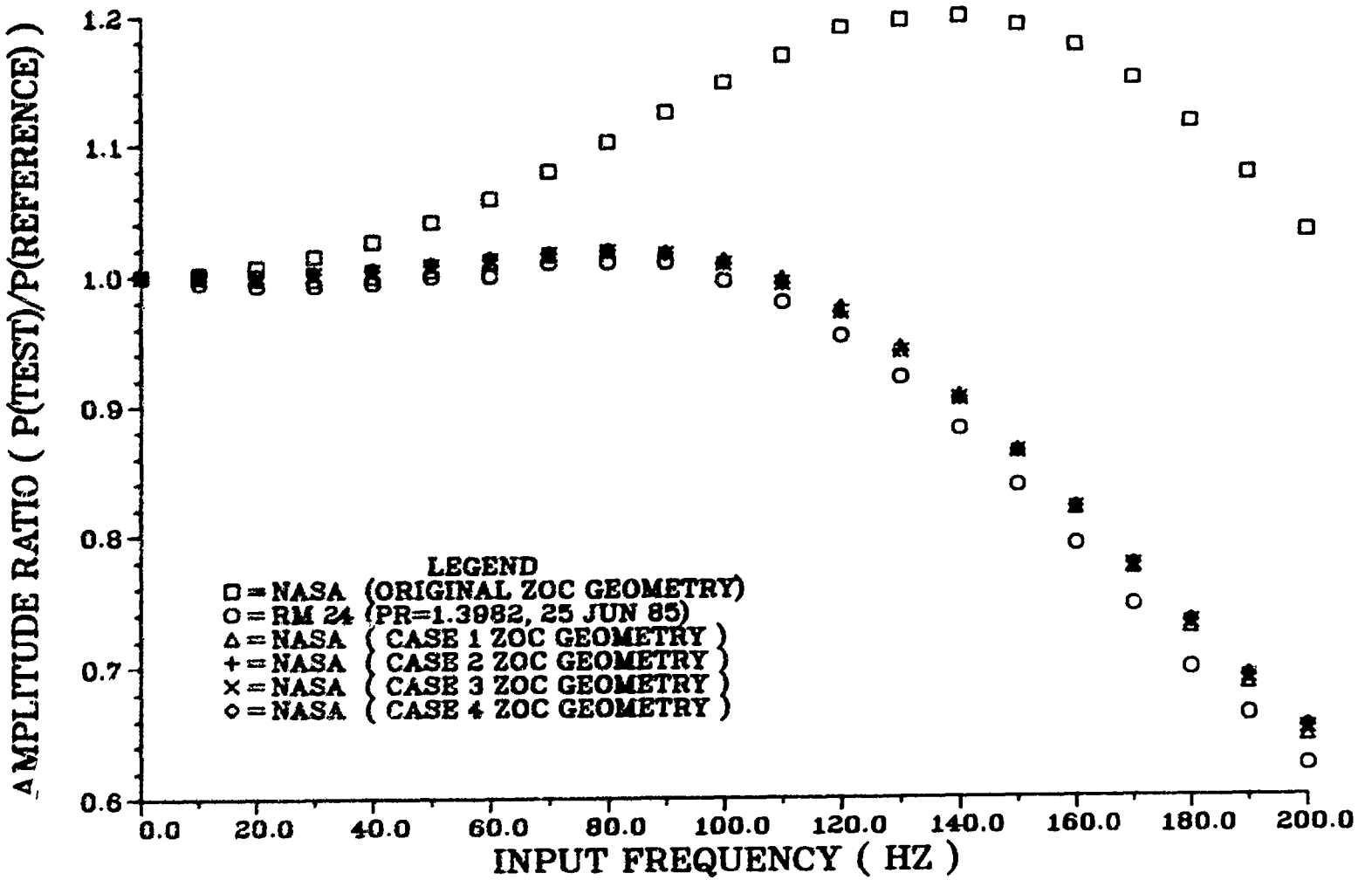

FIGURE 72. COMPARISON OF RM 24 EXPERIMENTAL DATA TO NASA PROGRAM FREQUENCY RESPONSE PREDICTIONS FOR A 10.0 IN. TUBE WITH .020 IN. ID

FIG72

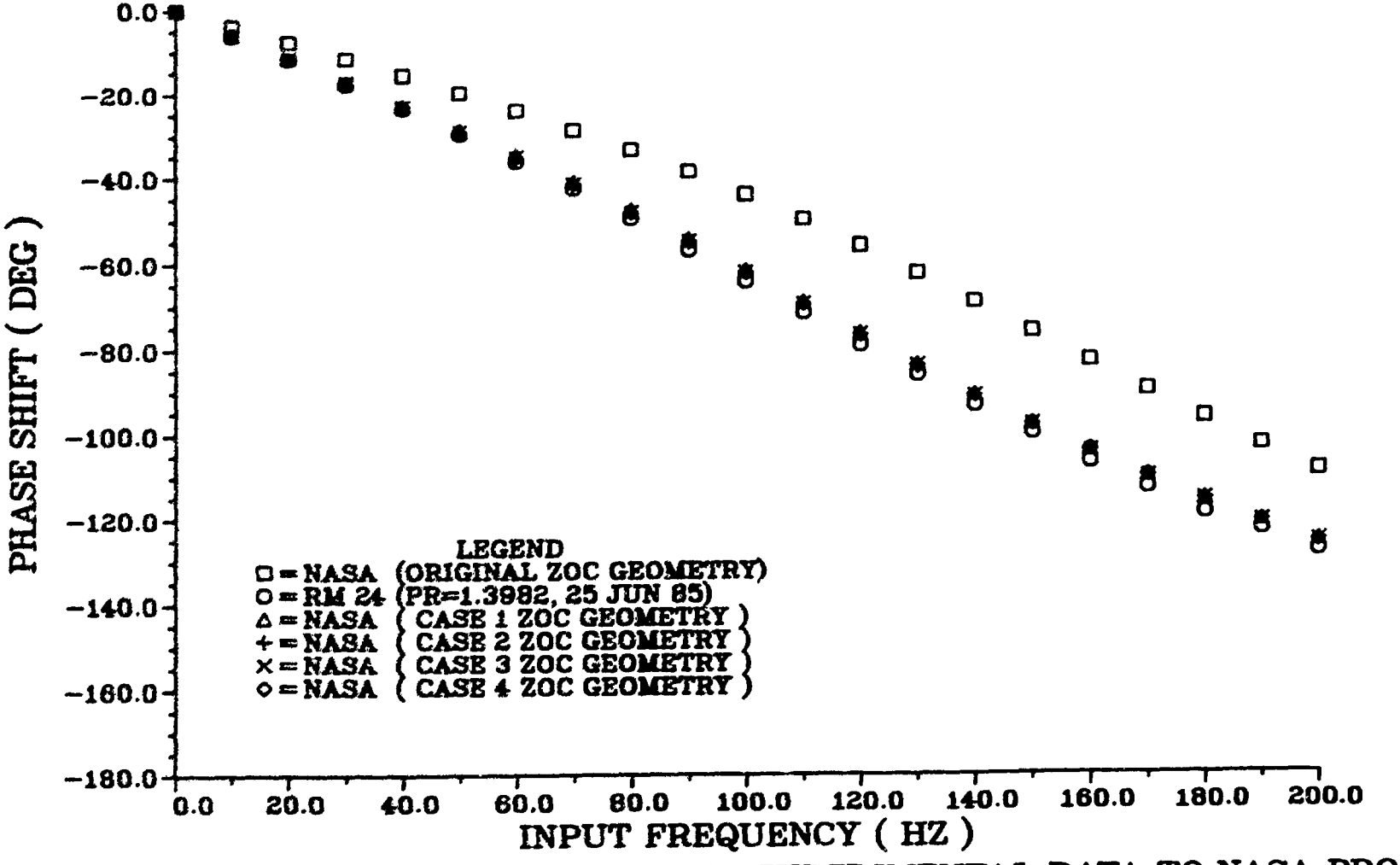

FIGURE 73. COMPARISON OF RM 24 EXPERIMENTAL DATA TO NASA PROGRAM FREQUENCY RESPONSE PREDICTIONS FOR A 10.0 IN. TUBE WITH .020 IN. ID

FIG73

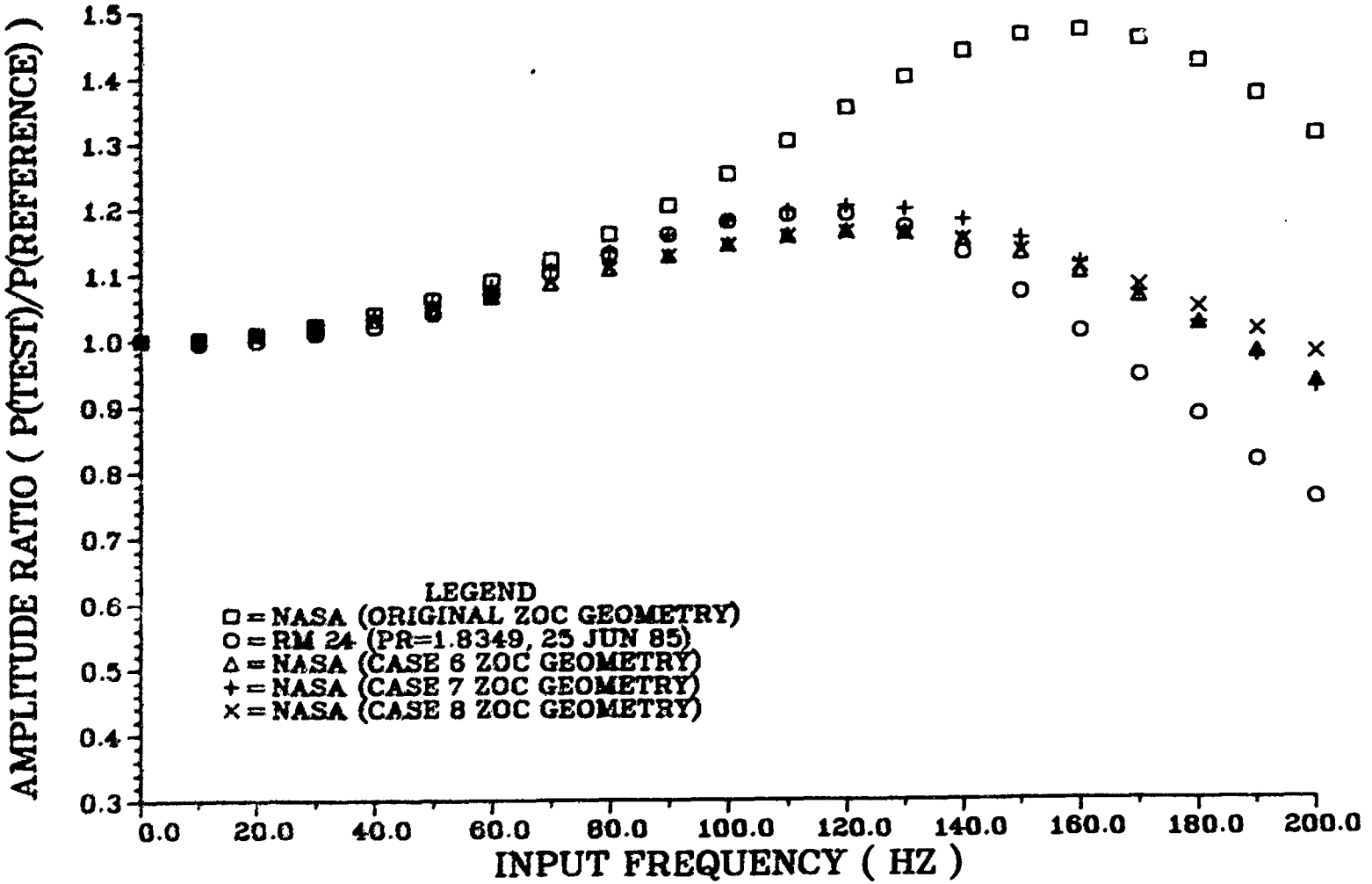

FIGURE 74. COMPARISON OF RM 24 EXPERIMENTAL DATA TO NASA PROGRAM FREQUENCY RESPONSE PREDICTIONS FOR A 10.0 IN. TUBE WITH .020 IN. ID

F1G74

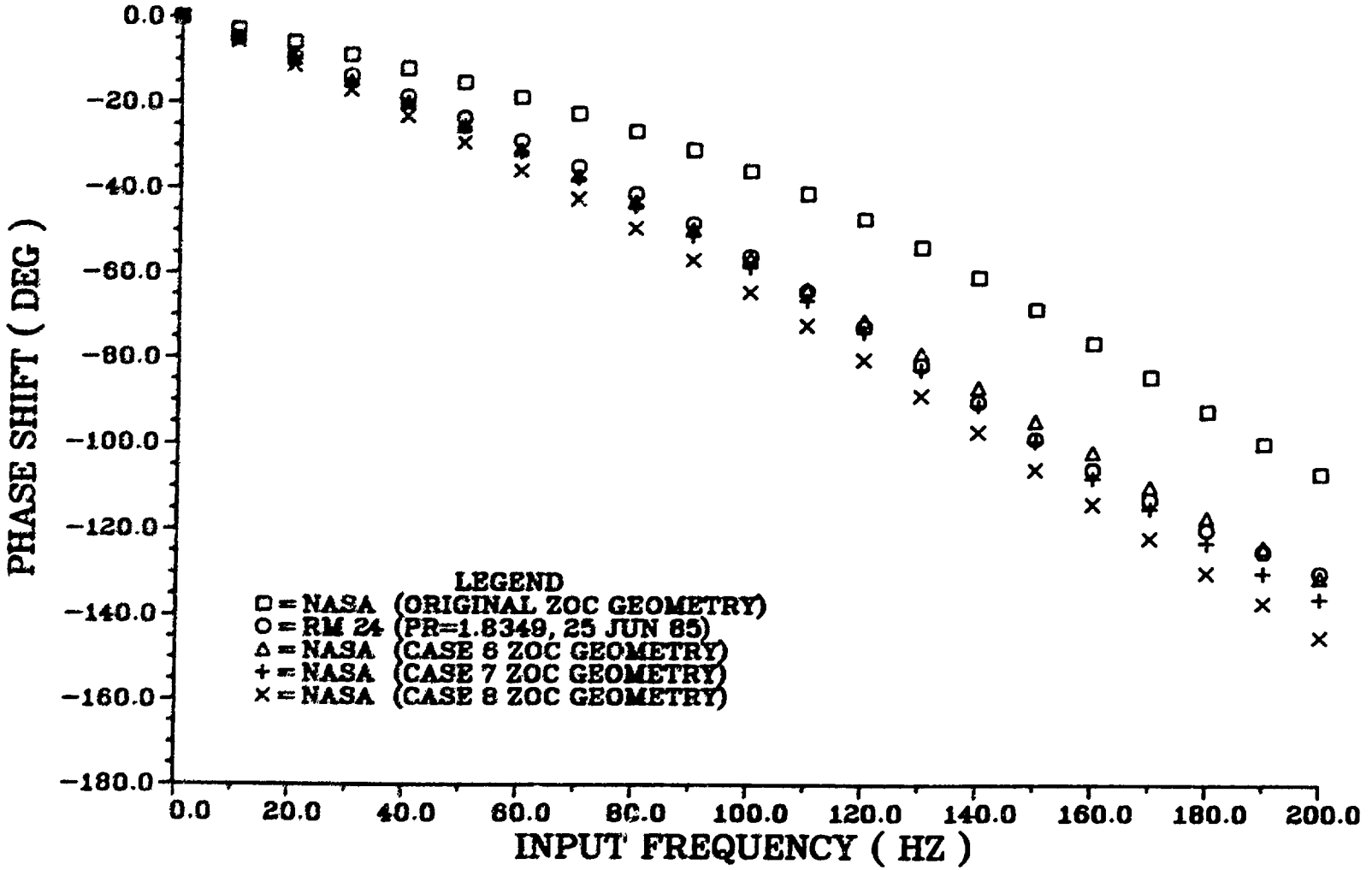

FIGURE 75. COMPARISON OF RM 24 EXPERIMENTAL DATA TO NASA PROGRAM FREQUENCY RESPONSE PREDICTIONS FOR A 10.0 IN. TUBE WITH .020 IN. ID

FIG75

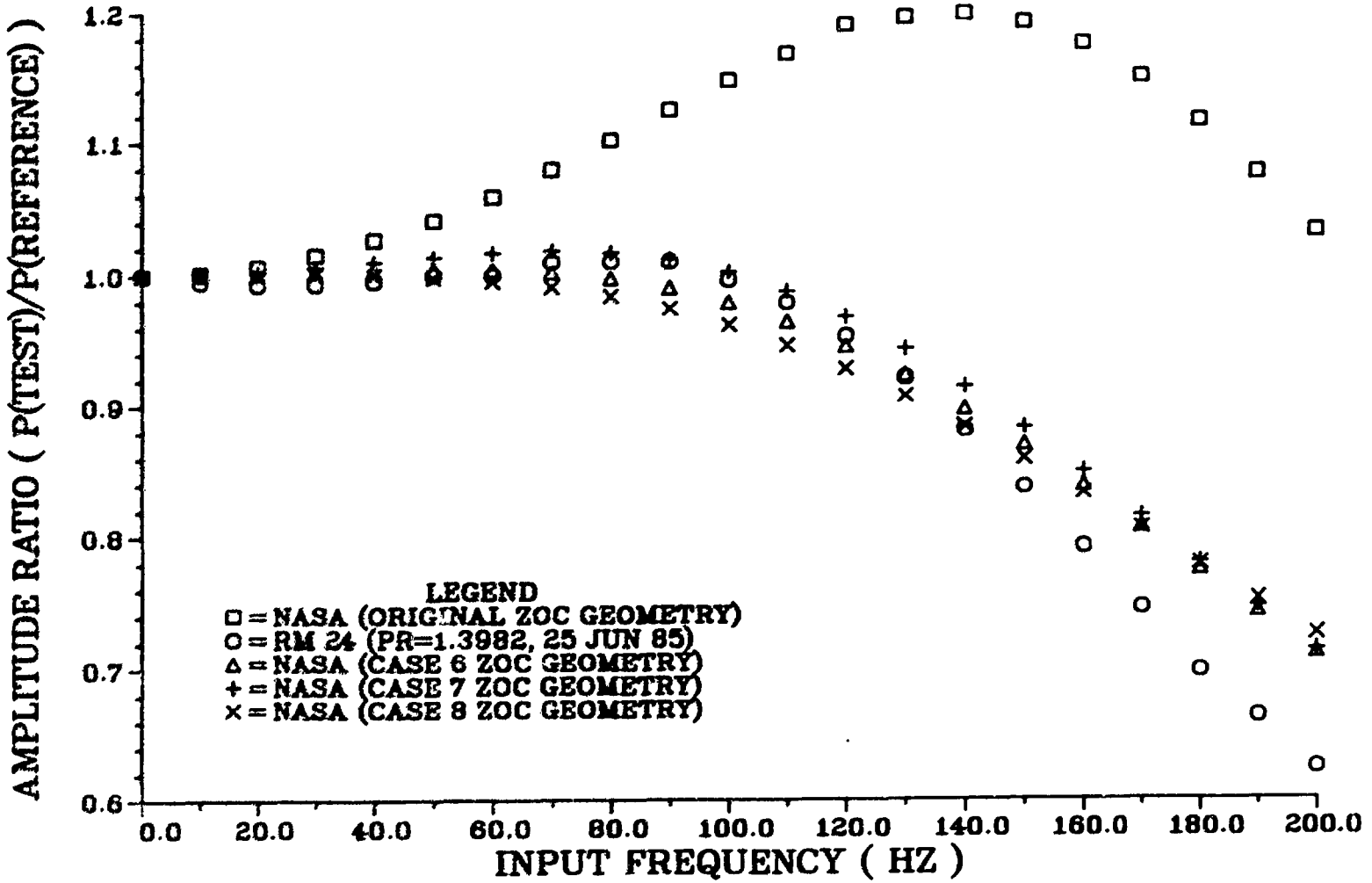

FIGURE 76. COMPARISON OF RM 24 EXPERIMENTAL DATA TO NASA PROGRAM FREQUENCY RESPONSE PREDICTIONS FOR A 10.0 IN. TUBE WITH .020 IN. ID

FIG76

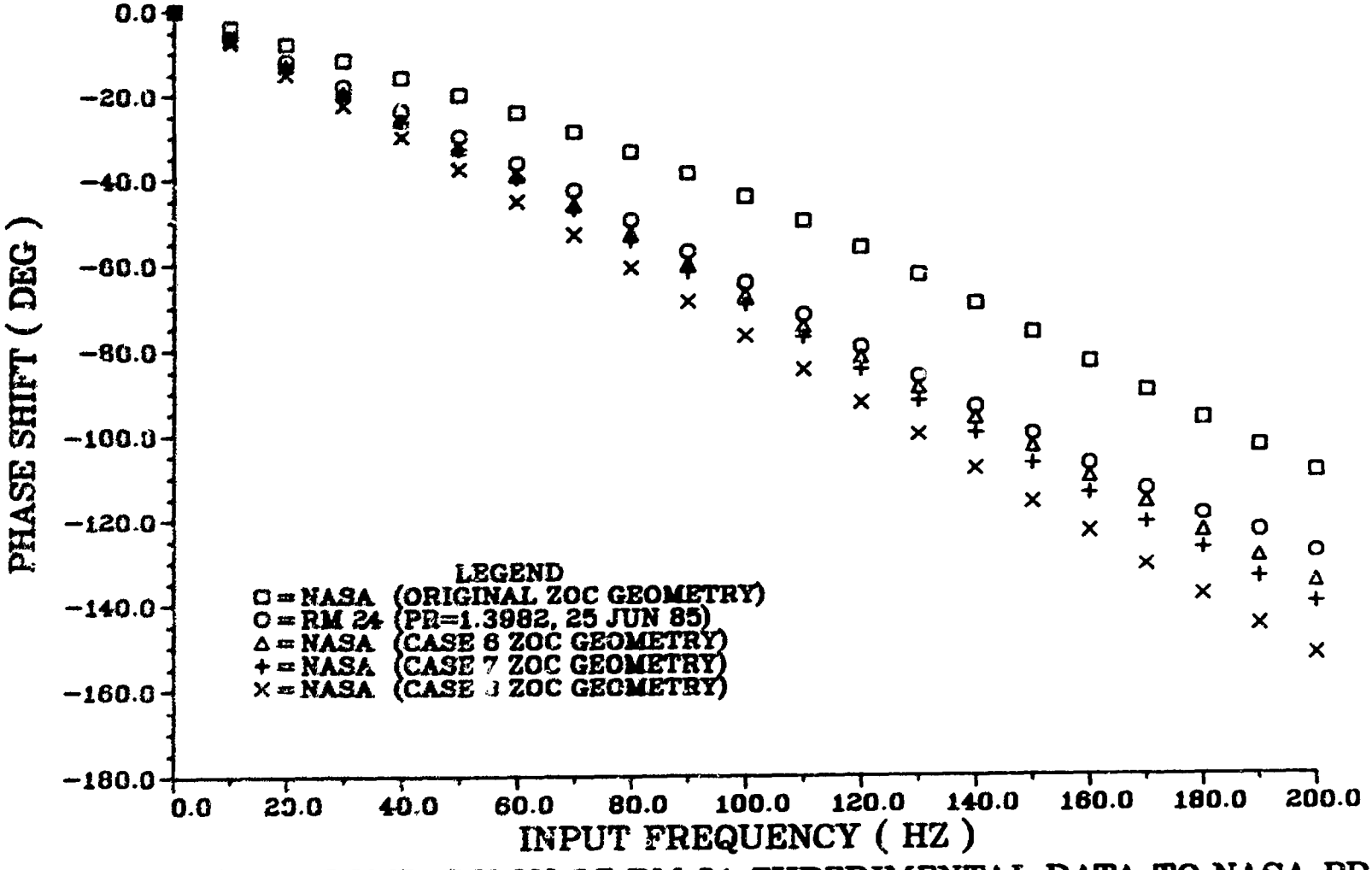

FIGURE 77. COMPARISON OF RM 24 EXPERIMENTAL DATA TO NASA PROGRAM FREQUENCY RESPONSE PREDICTIONS FOR A 10.0 IN. TUBE WITH .020 IN. ID

FIG77

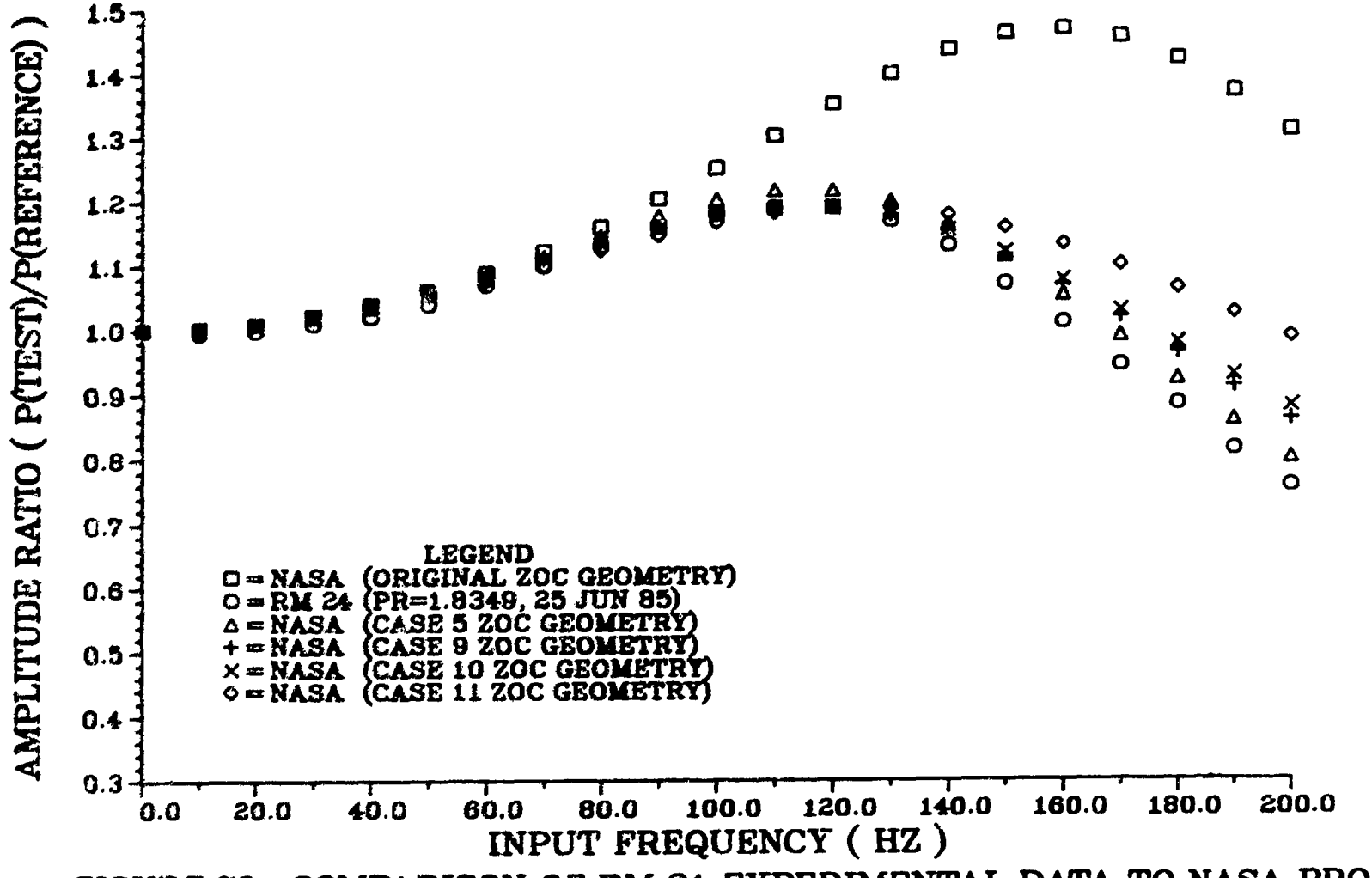

FIGURE 78. COMPARISON OF RM 24 EXPERIMENTAL DATA TO NASA PROGRAM FREQUENCY RESPONSE PREDICTIONS FOR A 10.0 IN. TUBE WITH .020 IN. ID

FIG78

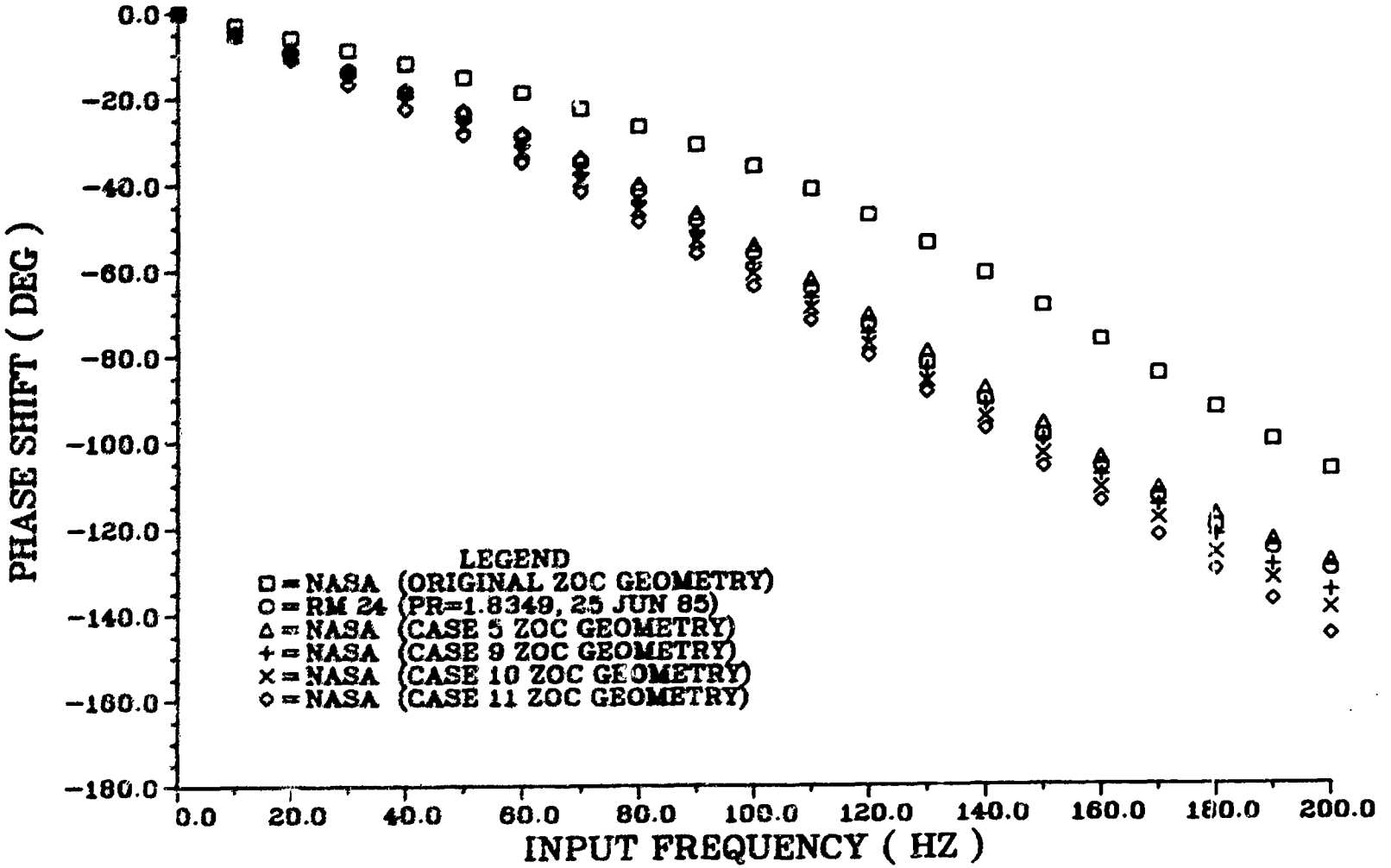

FIGURE 79. COMPARISON OF RM 24 EXPERIMENTAL DATA TO NASA PROGRAM FREQUENCY RESPONSE PREDICTIONS FOR A 10.0 IN. TUBE WITH .020 IN. ID

FIG79

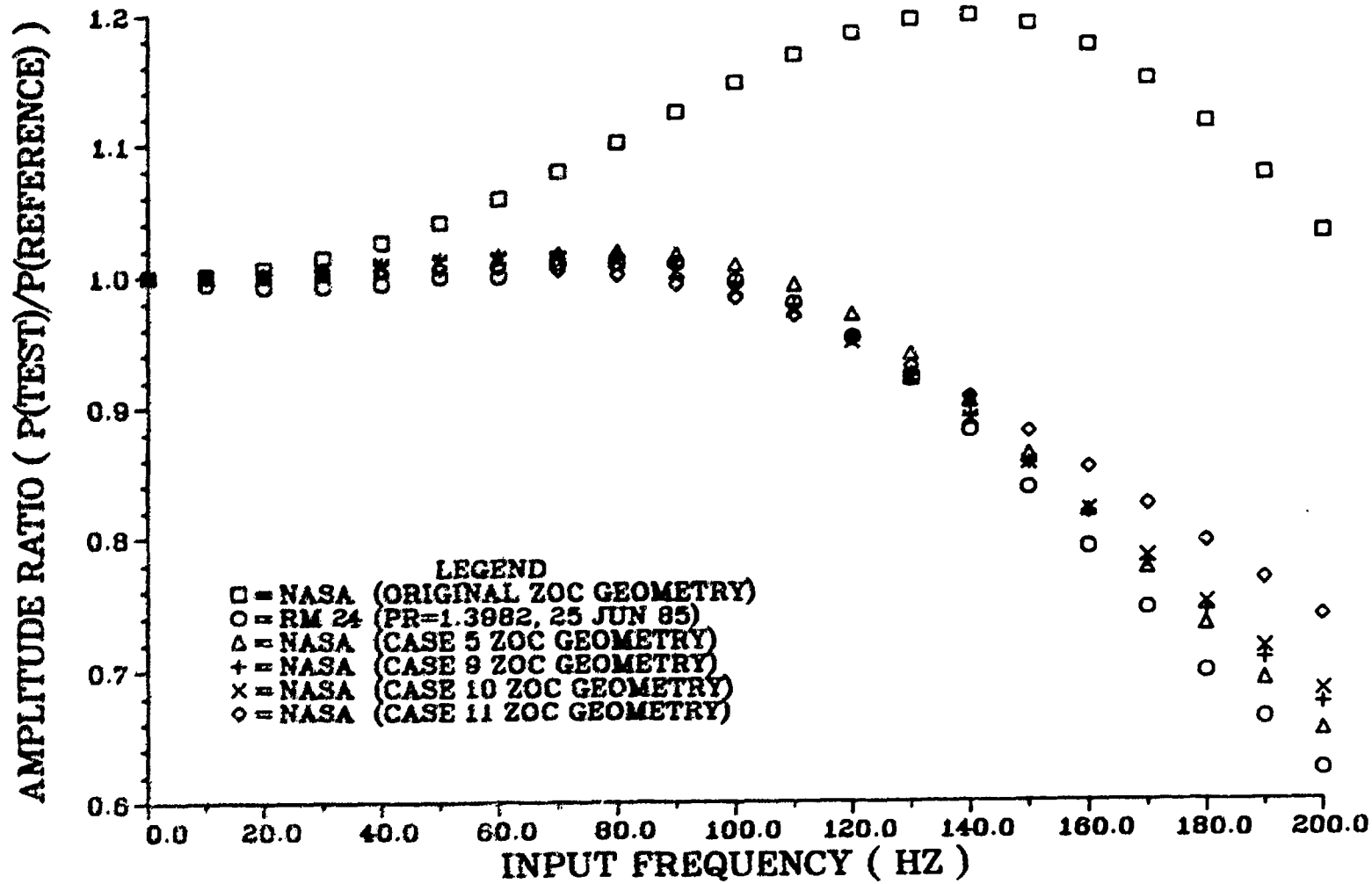

FIGURE 80. COMPARISON OF RM 24 EXPERIMENTAL DATA TO NASA PROGRAM FREQUENCY RESPONSE PREDICTIONS FOR A 10.0 IN. TUBE WITH .020 IN. ID

F1G80

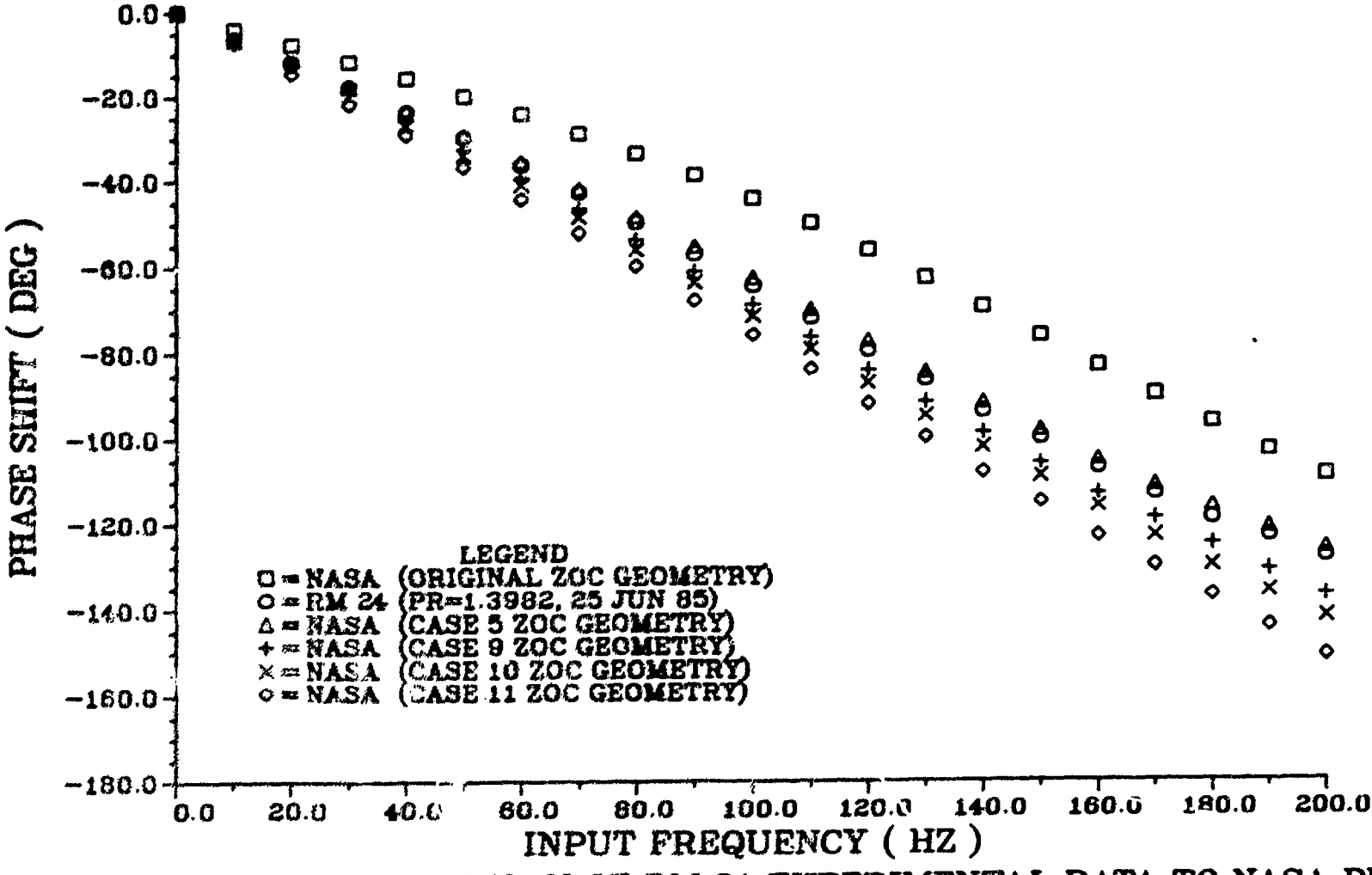

FIGURE 81. COMPARISON OF RM 24 EXPERIMENTAL DATA TO NASA PROGRAM FREQUENCY RESPONSE PREDICTIONS FOR A 10.0 IN. TUBE WITH .020 IN. ID

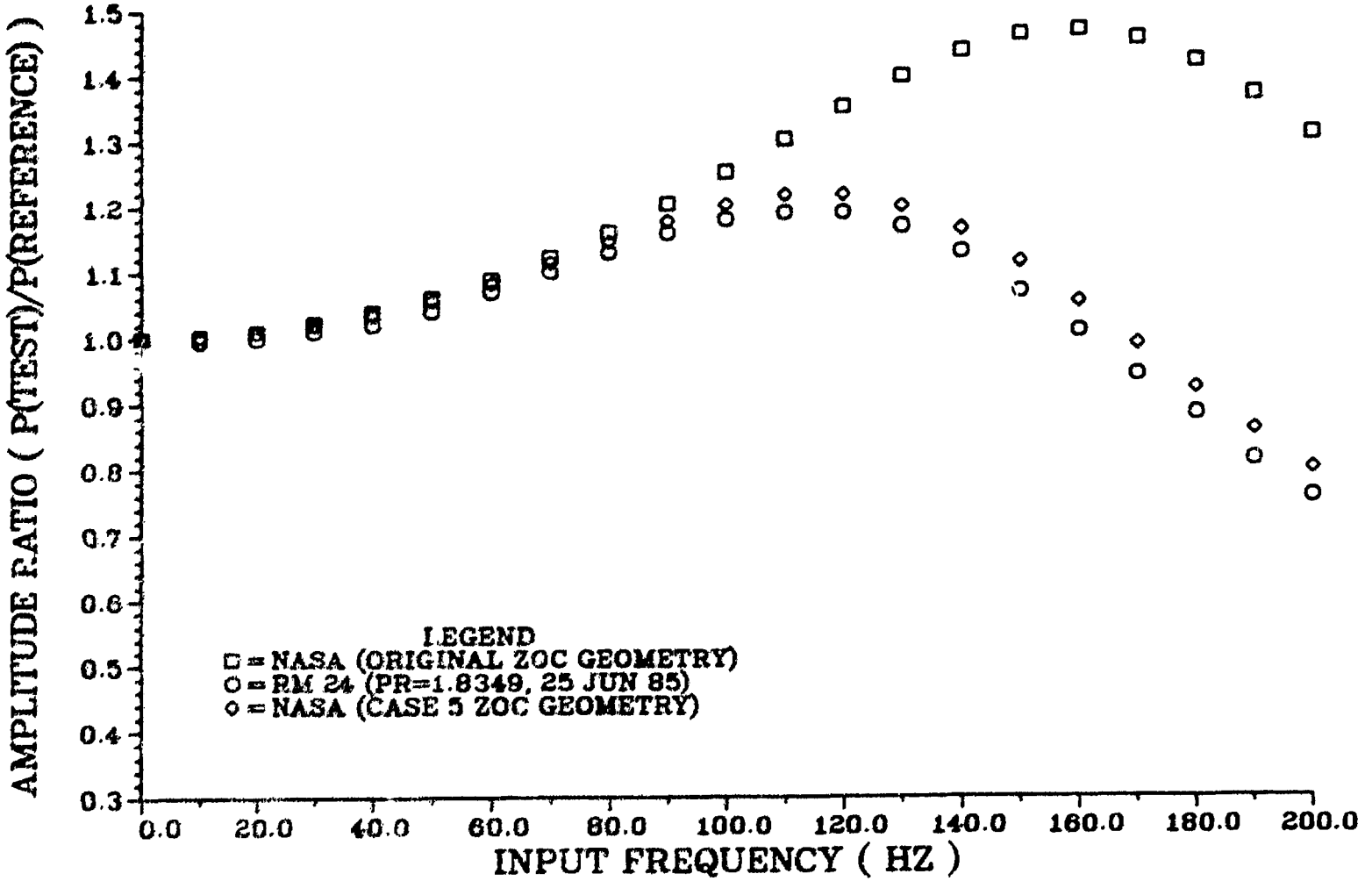

FIGURE 82. COMPARISON OF RM 24 EXPERIMENTAL DATA TO NASA PROGRAM FREQUENCY RESPONSE PREDICTIONS FOR A 10.0 IN. TUBE WITH .020 IN. ID

FIG82

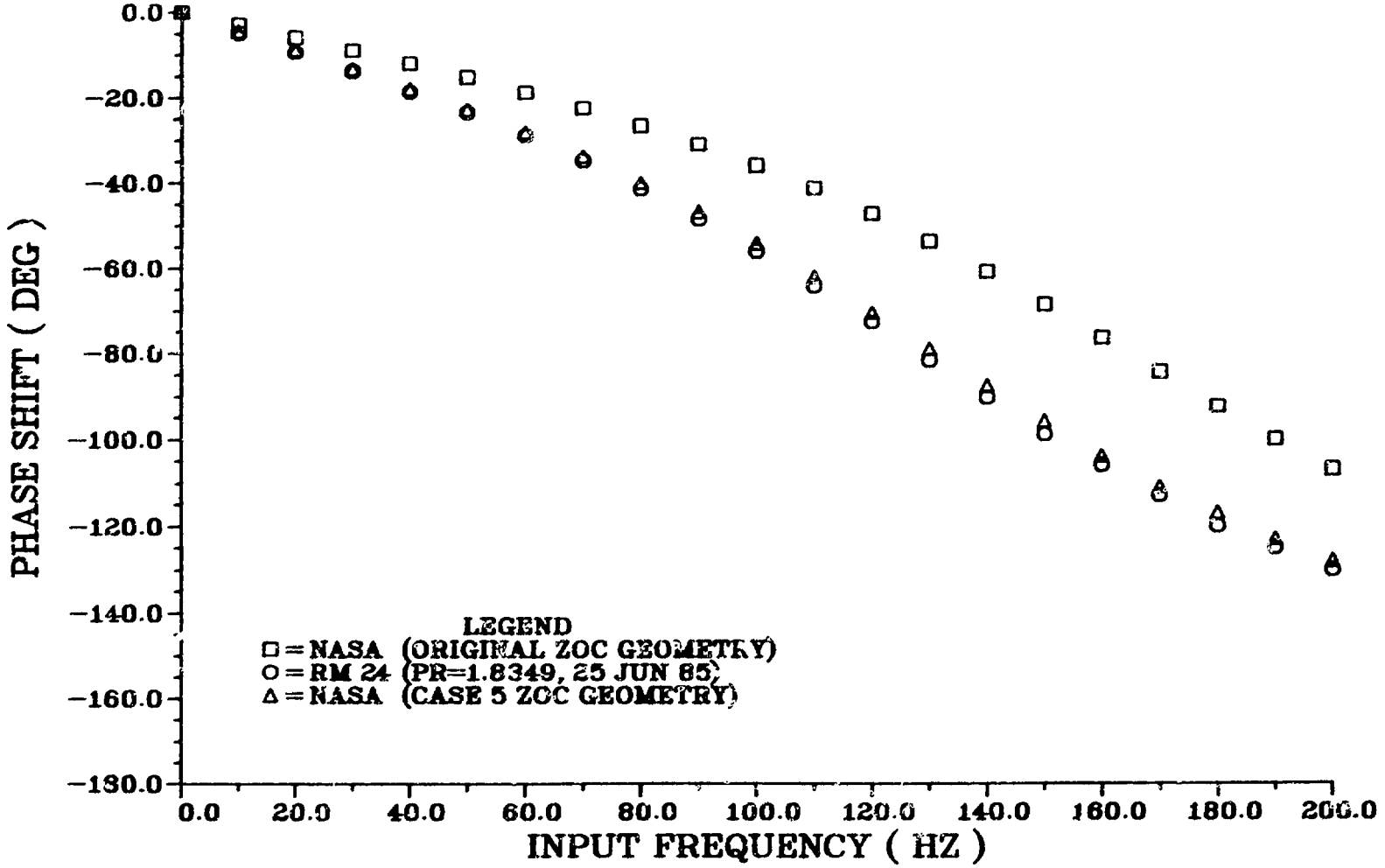

FIGURE 83. COMPARISON OF RM 24 EXPERIMENTAL DATA TO NASA PROGRAM FREQUENCY RESPONSE PREDICTIONS FOR A 10.0 IN. TUBE WITH .020 IN. ID

FIG83

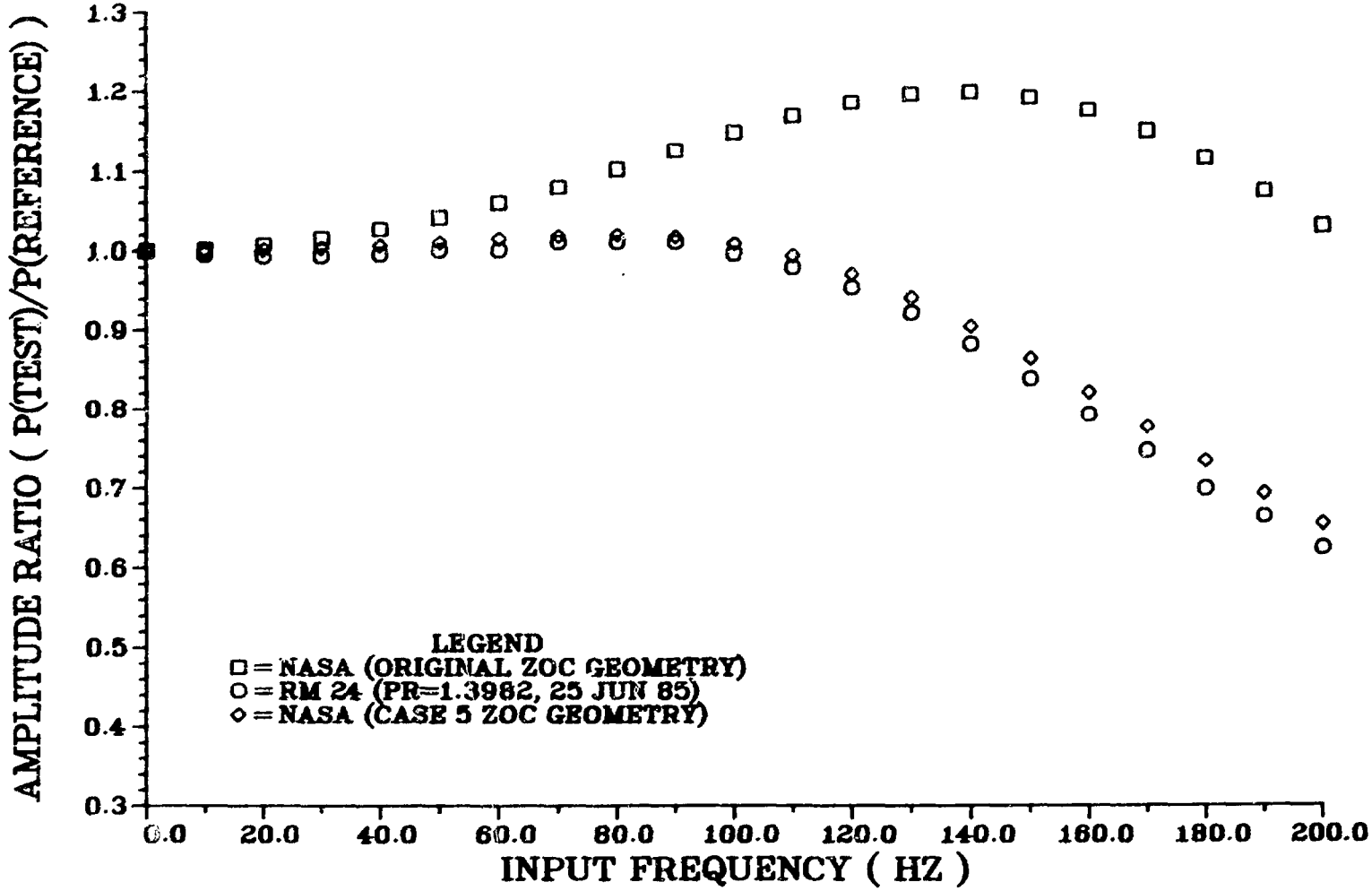

FIGURE 84. COMPARISON OF RM 24 EXPERIMENTAL DATA TO NASA PROGRAM FREQUENCY RESPONSE PREDICTIONS FOR A 10.0 IN. TUBE WITH .020 IN. ID

FIG84

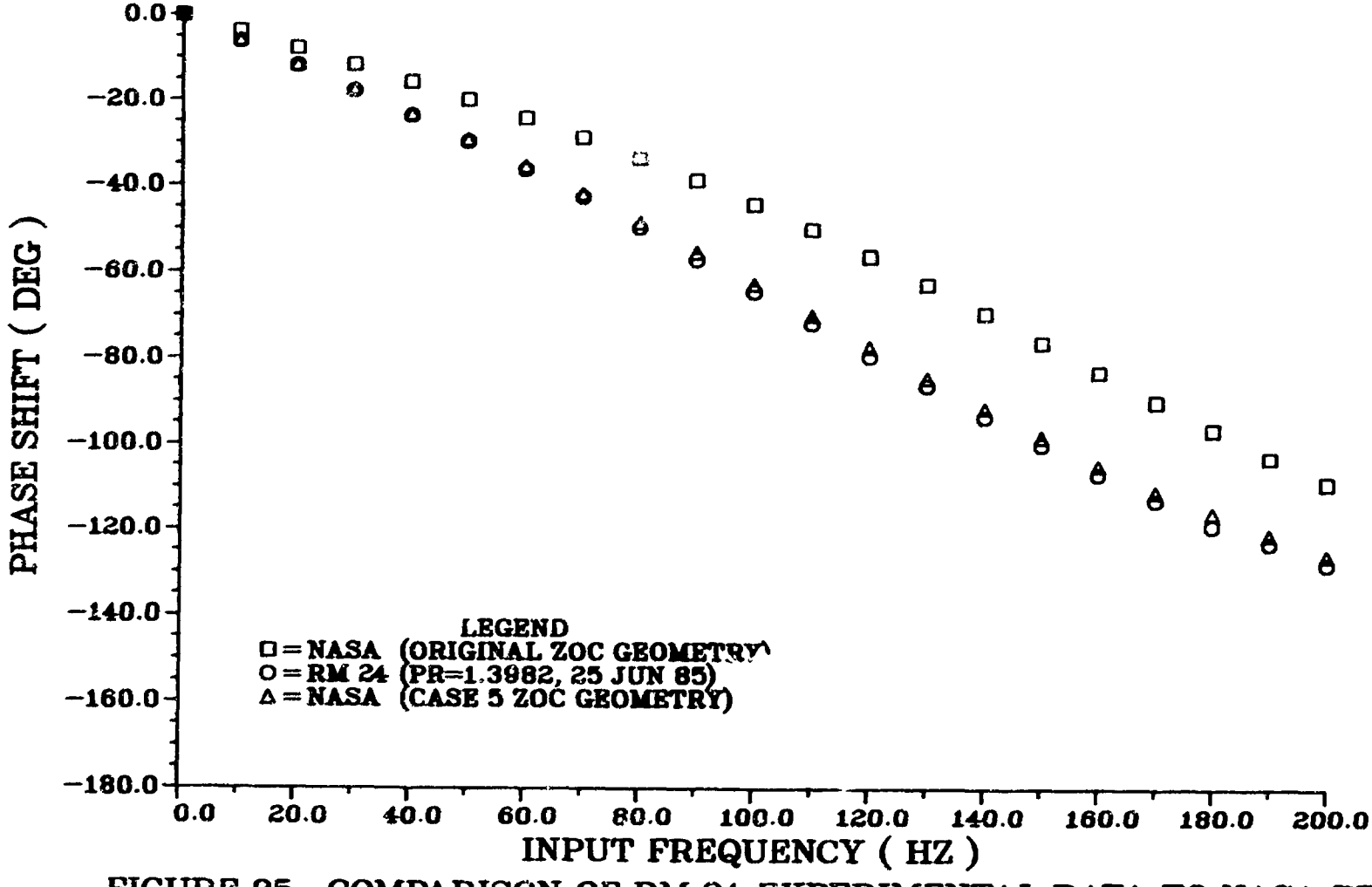

FIGURE 85. COMPARISON OF RM 24 EXPERIMENTAL DATA TO NASA PROGRAM FREQUENCY RESPONSE PREDICTIONS FOR A 10.0 IN. TUBE WITH .020 IN. ID

FIG85

for the 10.0-inch tube has been replotted to show the comparison with theoretical results based on the original and Case 5 geometry only. Tables 27 and 28 show the percent relative error associated with both sets of geometry.

With these dimensions identified for one test tube length, it was necessary to use them in comparisons with experimental data for other test tube lengths. Comparisons were made with the experimental data from the 15.0 and 16.375-inch tubes and these results are plotted in Figures 86-93. Again, the theoretical results are shown for both the original and the Case 5 geometry. The percent relative error is presented in Tables 29 and 30 for the 15.0 inch tube and in Tables 31 and 32 for the 16.375-inch tube.

The relative error shown in Tables 27-32 indicates that the Case 5 geometry works well for all three tube lengths tested. For the 10.0-inch tube with a pressure ratio of 1.8349, the maximum relative error between the experimental data and the theoretical results using the original geometry was 73 percent at 200 hertz. Using the Case 5 geometry the maximum relative error is reduced to less than 6 percent, as can be seen from Table 27. Similarly, with the original geometry the phase shift relative error ranged from approximately 20 to 40 percent, while with the Case 5 geometry the error ranges from only 2 to 10 percent. A similar trend can be seen in Table 28 for the 10.0-inch tube at a pressure ratio of 1.3982.

For the 15.0-inch tube at a pressure ratio of 1.8405, with the Case 5 geometry the maximum relative error in the amplitude ratio is just over 6 percent, compared to 55 percent with the original geometry. The maximum phase shift error is only 4 percent with the Case 5 geometry, as compared to 30 percent for the original geometry. Similar comparisons exist for the 15.0-inch tube with a pressure ratio of 1.3964, as shown in Table 30.

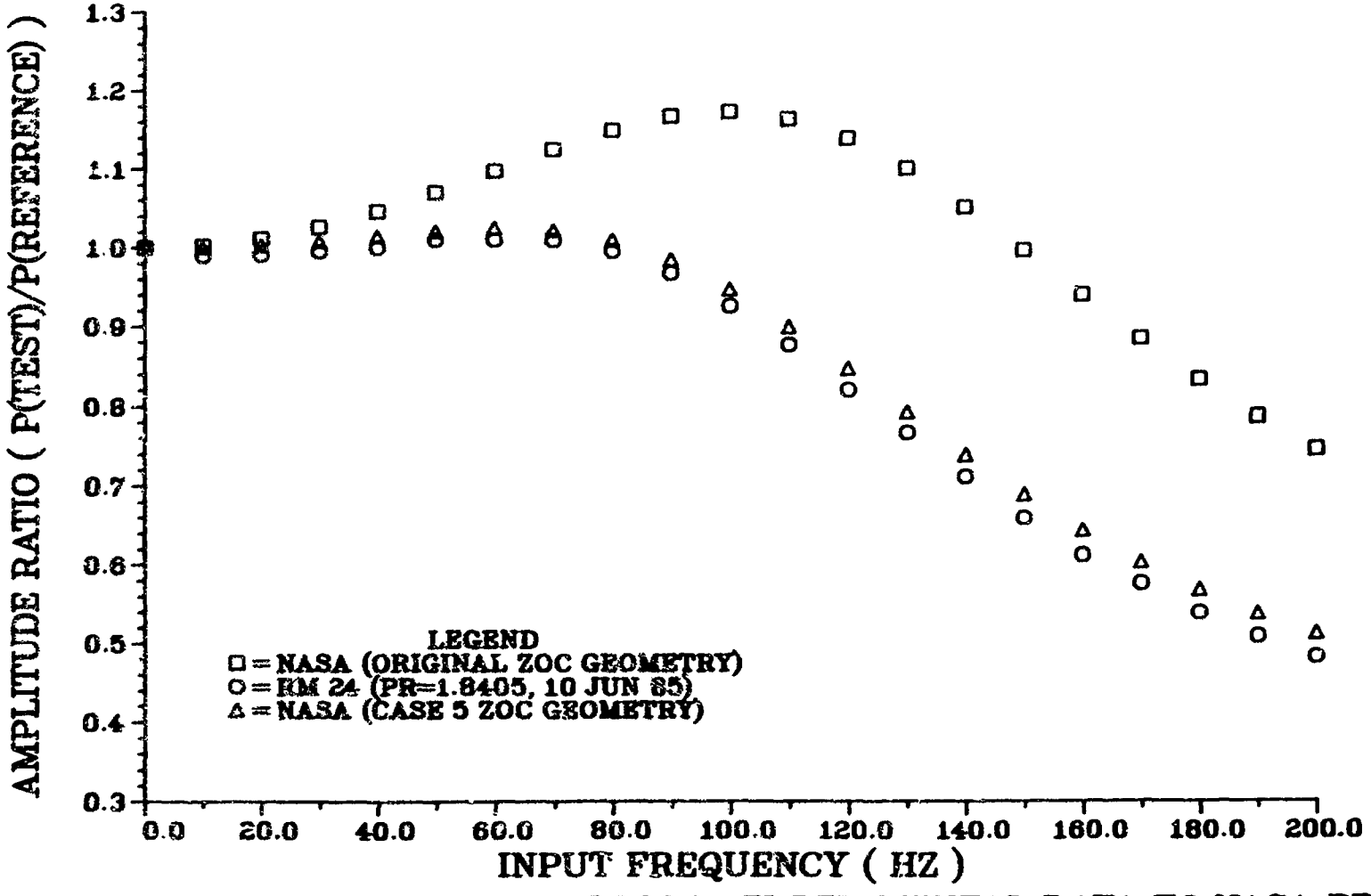

FIGURE 86. COMPARISON OF RM 24 EXPERIMENTAL DATA TO NASA PROGRAM FREQUENCY RESPONSE PREDICTIONS FOR A 15.0 IN. TUBE WITH .020 IN. ID

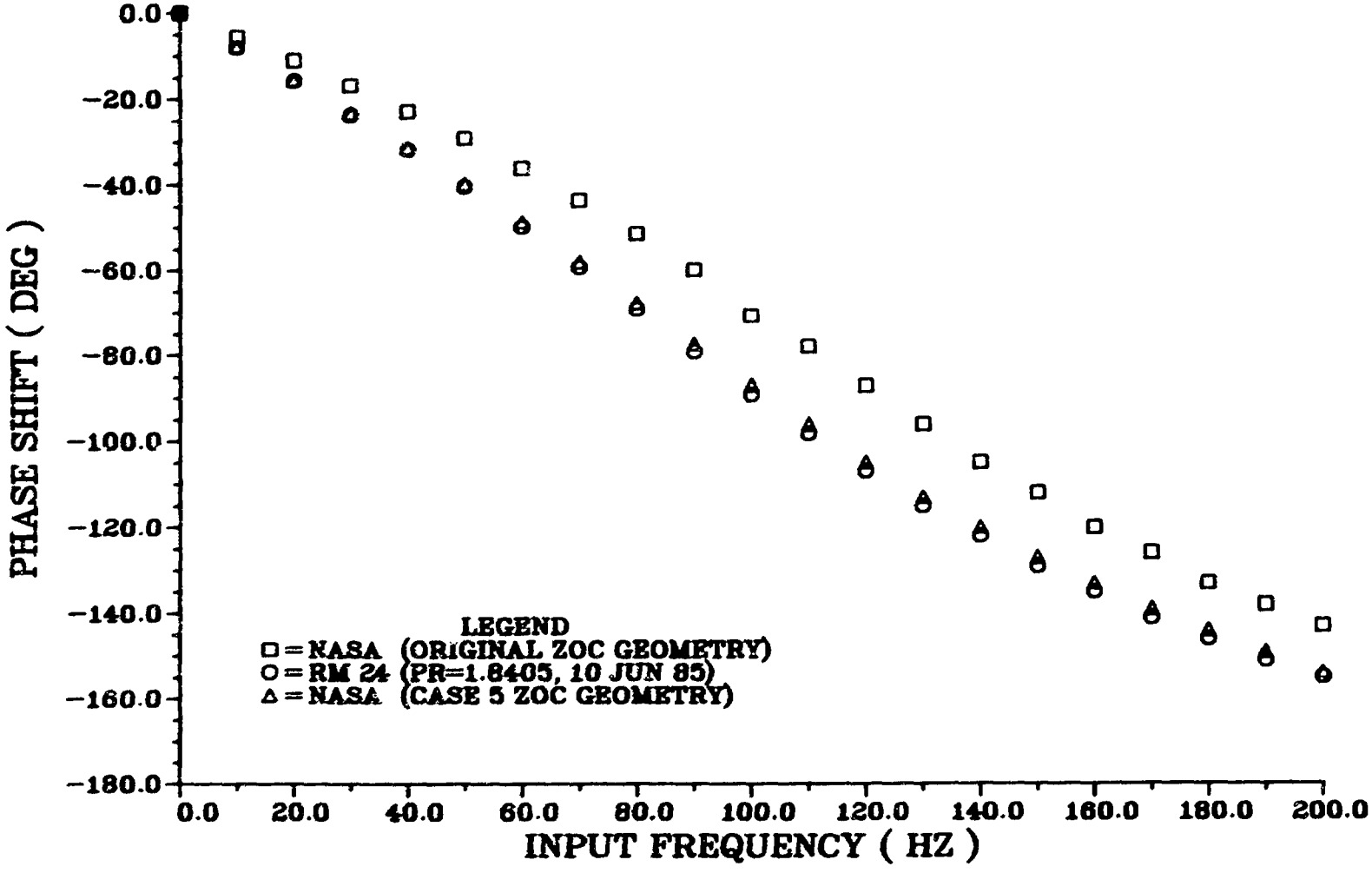

FIGURE 87. COMPARISON OF RM 24 EXPERIMENTAL DATA TO NASA PROGRAM FREQUENCY RESPONSE PREDICTIONS FOR A 15.0 IN. TUBE WITH .020 IN. ID

FIG87

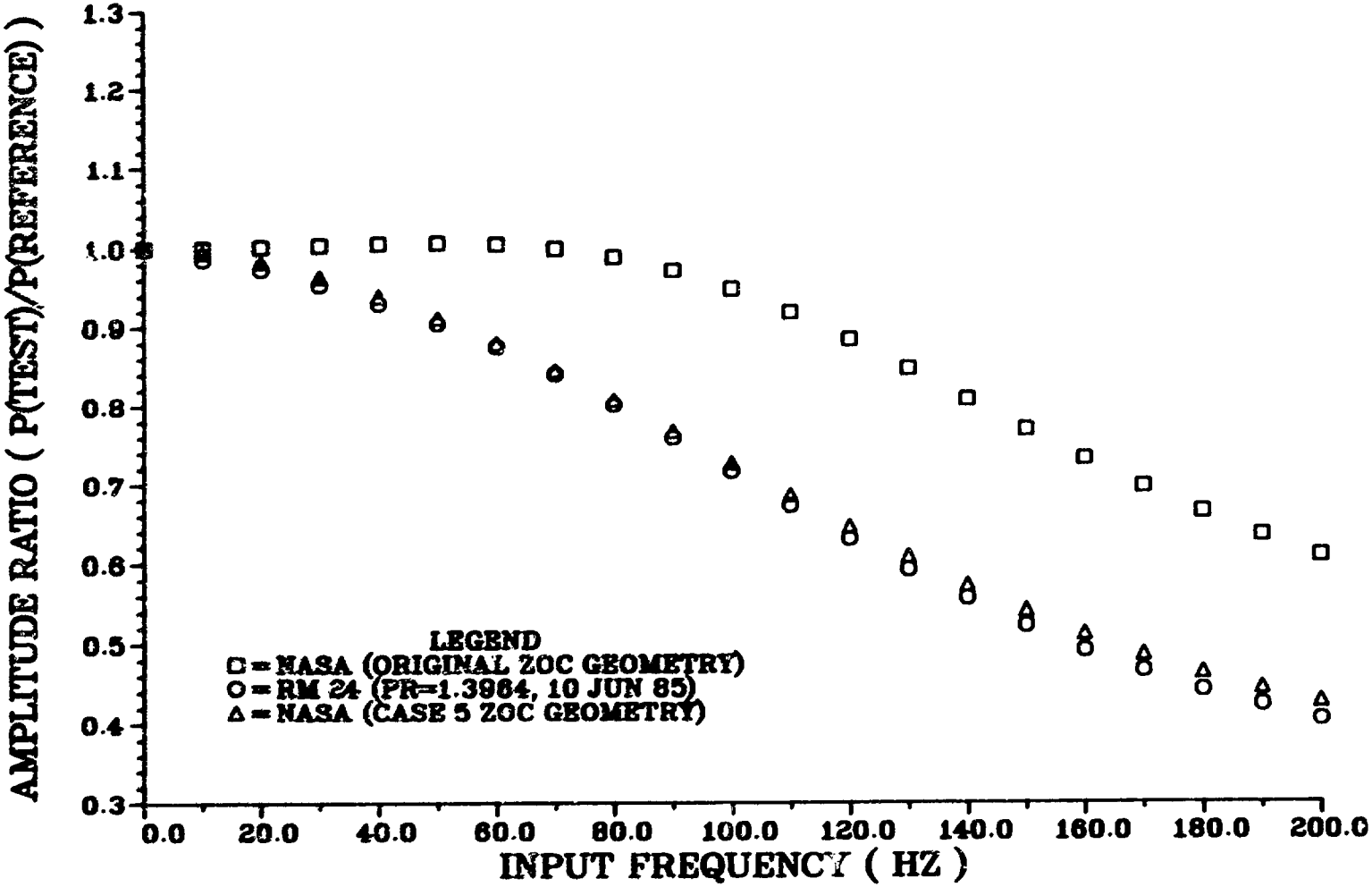

FIGURE 88. COMPARISON OF RM 24 EXPERIMENTAL DATA TO NASA PROGRAM FREQUENCY RESPONSE PREDICTIONS FOR A 15.0 IN. TUBE WITH .020 IN. ID

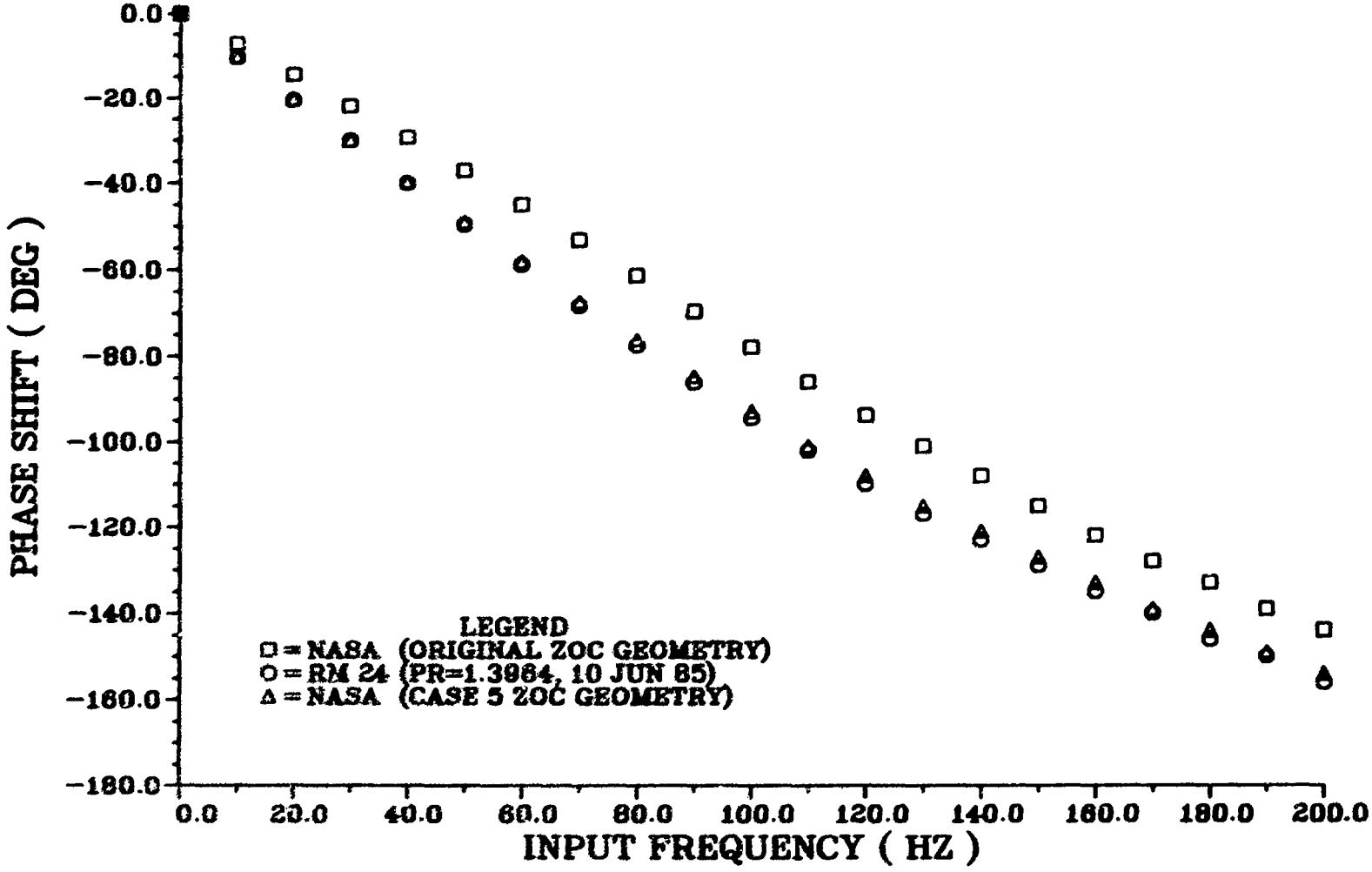

FIGURE 89. COMPARISON OF RM 24 EXPERIMENTAL DATA TO NASA PROGRAM FREQUENCY RESPONSE PREDICTIONS FOR A 15.0 IN. TUBE WITH .020 IN. ID

FIG89

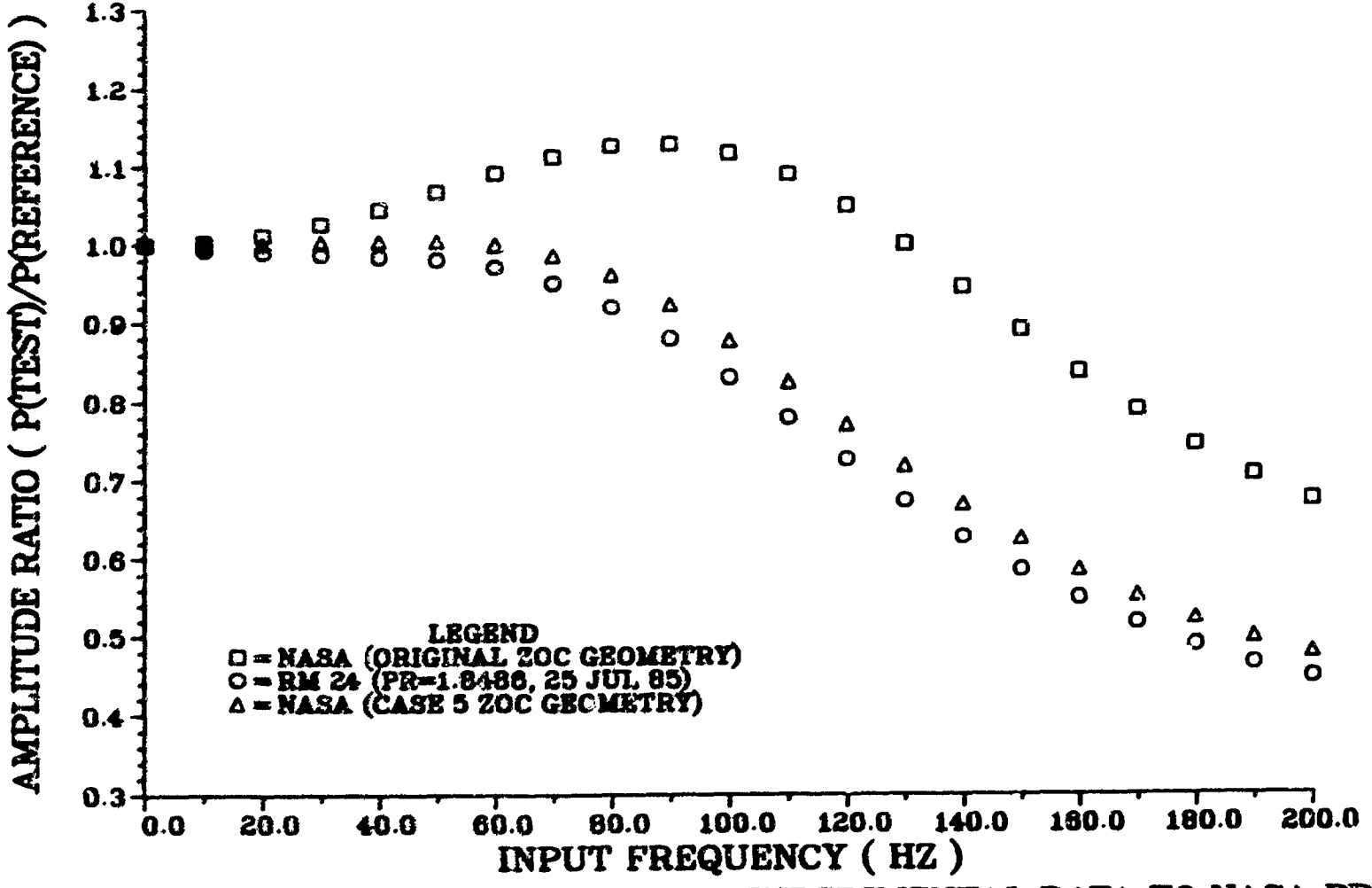

FIGURE 90. COMPARISON OF RM 24 EXPERIMENTAL DATA TO NASA PROGRAM FREQUENCY RESPONSE PREDICTIONS FOR A 16.38 IN. TUBE WITH .020 IN. ID

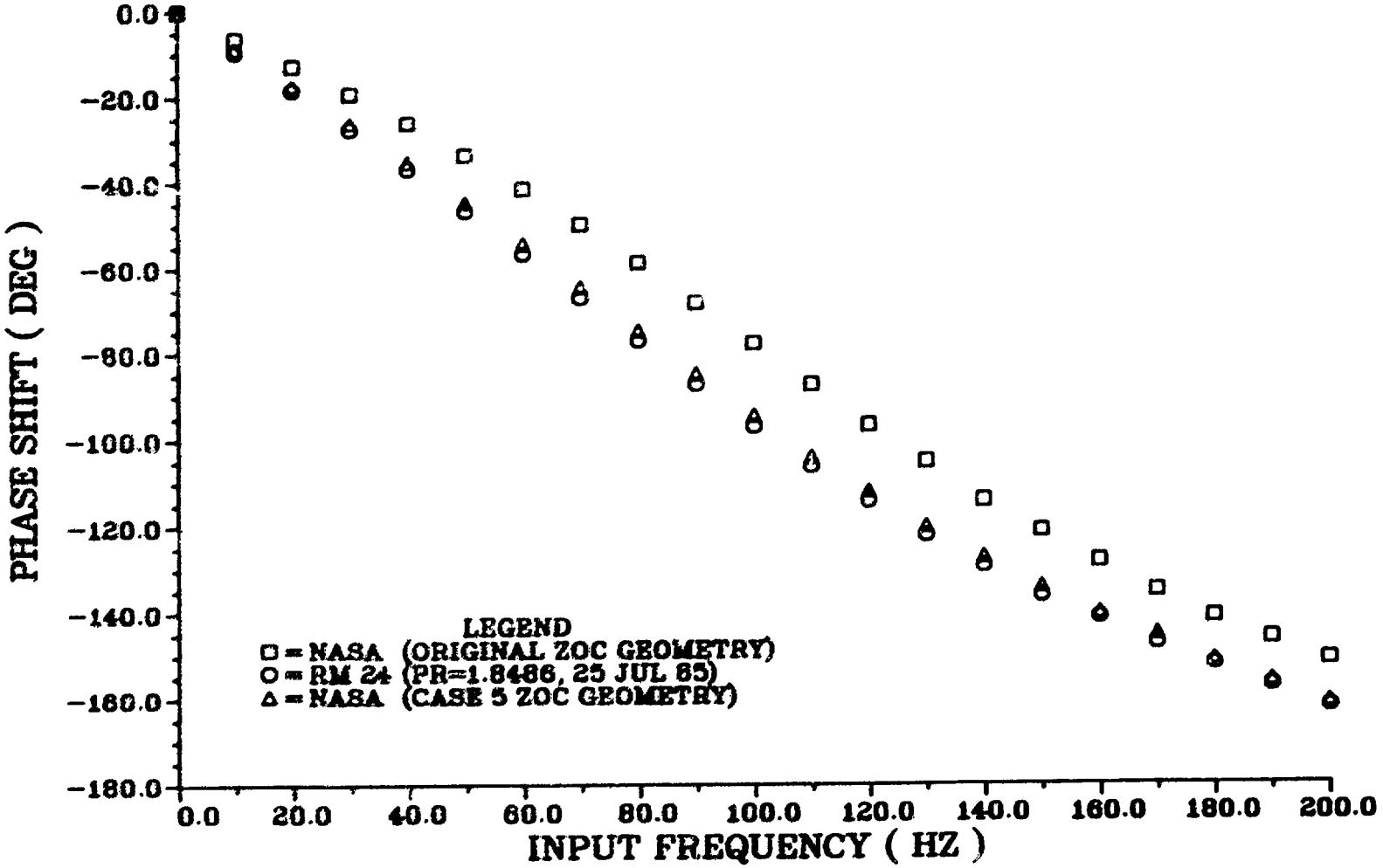

FIGURE 91. COMPARISON OF RM 24 EXPERIMENTAL DATA TO NASA PROGRAM FREQUENCY RESPONSE PREDICTIONS FOR A 16.38 IN. TUBE WITH .020 IN. ID

FIG91

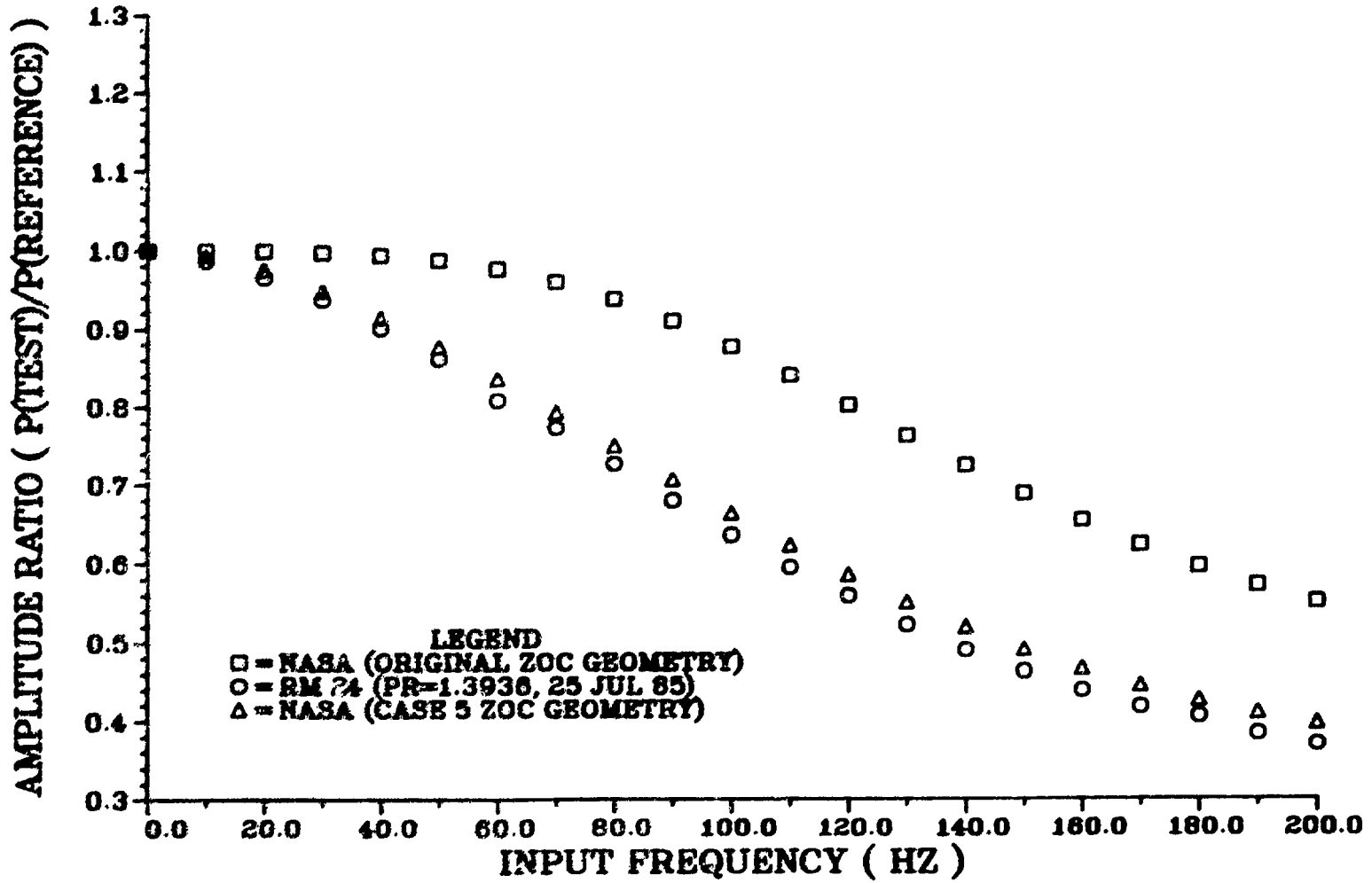

FIGURE 92. COMPARISON OF RM 24 EXPERIMENTAL DATA TO NASA PROGRAM FREQUENCY RESPONSE PREDICTIONS FOR A 16.38 IN. TUBE WITH .020 IN. ID

FIG92

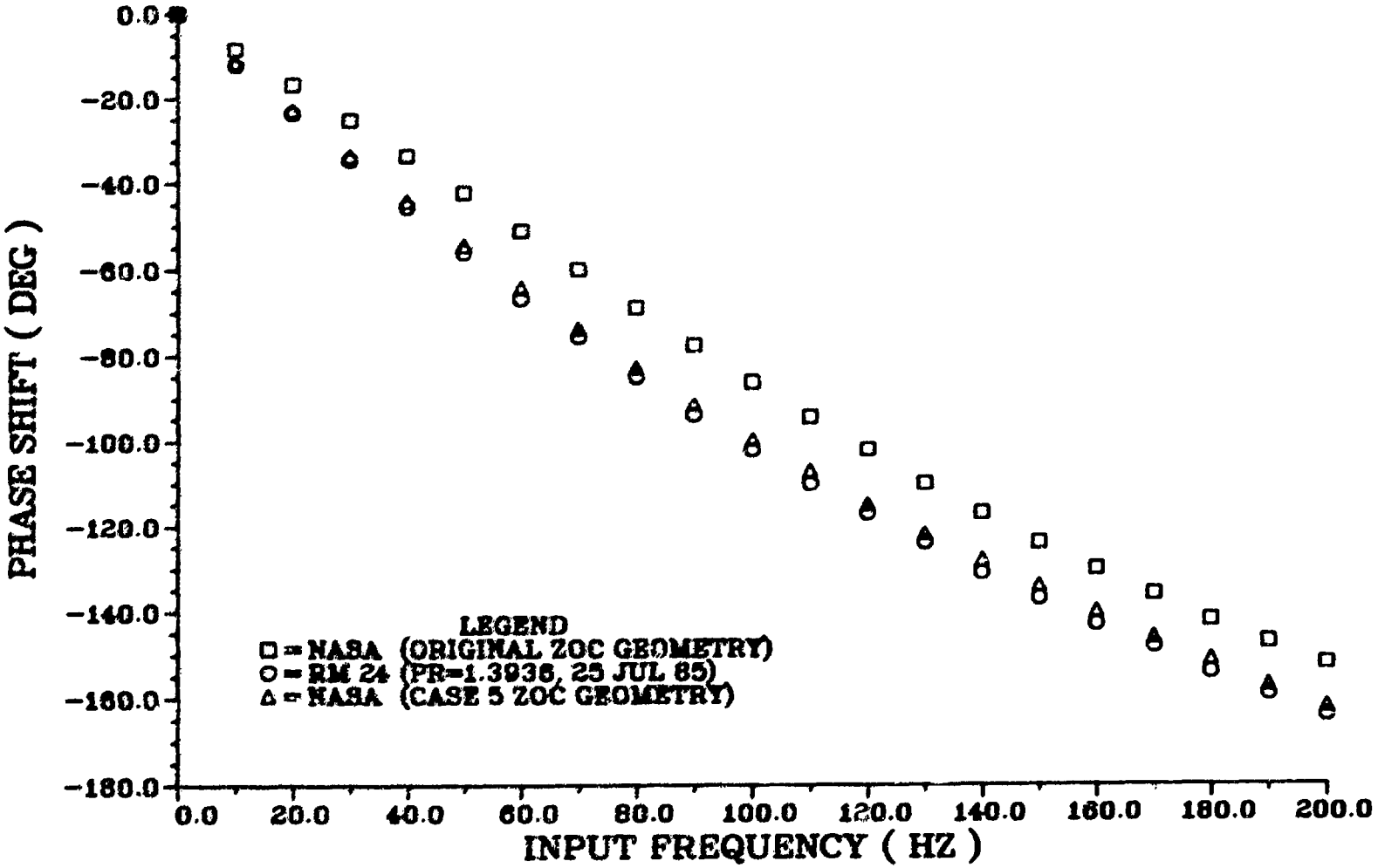

FIGURE 93. COMPARISON OF RM 24 EXPERIMENTAL DATA TO NASA PROGRAM FREQUENCY RESPONSE PREDICTIONS FOR A 16.38 IN. TUBE WITH .020 IN. ID

Table 27. Comparison of Experimental and Theoretical Results
(12.8 Inch Tube, M=1.8349)

FREQUENCY (HZ)	EXPERIMENTAL AMPLITUDE RATIO	THEORETICAL AMPLITUDE RATIO (Original Geometry)	RELATIVE ERROR (PERCENT)	THEORETICAL AMPLITUDE RATIO (Case 2 Geometry)	RELATIVE ERROR (PERCENT)	EXPERIMENTAL PHASE SHIFT (DEG)	THEORETICAL PHASE SHIFT (Original Geometry) (DEG)	RELATIVE ERROR (PERCENT)	THEORETICAL PHASE SHIFT (Case 5 Geometry) (DEG)	RELATIVE ERROR (PERCENT)
0	1	1	0	1	0	0	0	0	0	0
10	.935	1.0074	-.74	1.0039	-.63	-4.05	-2.91	40.00	-4.4	9.26
20	.979	1.0094	-2.04	1.000	-.90	-9.35	-5.04	37.54	-8.01	5.78
30	1.03	1.0234	-1.11	1.0105	-.88	-13.0	-8.05	35.07	-13.3	3.62
40	1.02	1.0386	-1.62	1.0252	-1.49	-18.6	-12	35.48	-17.9	3.76
50	1.04	1.0609	-2.01	1.027	-1.63	-23.5	-15.2	35.32	-22.8	2.98
60	1.07	1.0887	-1.75	1.0812	-1.29	-28.8	-18.7	35.07	-28	2.78
70	1.1	1.1427	-2.81	1.1141	-1.28	-34.7	-22.4	35.45	-33.7	2.88
80	1.13	1.1606	-2.73	1.1463	-1.44	-41.3	-26.5	35.84	-39.9	3.39
90	1.16	1.2042	-3.84	1.177	-1.47	-48.3	-30.9	36.02	-46.7	3.31
100	1.18	1.2523	-6.13	1.1922	-1.88	-55.9	-35.8	35.56	-54.1	3.22
110	1.19	1.3036	-9.46	1.217	-2.23	-64.2	-41.2	35.83	-62.1	3.27
120	1.19	1.3529	-13.93	1.217	-2.27	-72.7	-47.2	35.08	-70.5	3.03
130	1.17	1.3995	-19.62	1.1954	-2.51	-81.6	-53.8	34.23	-79.1	3.30
140	1.13	1.4377	-27.22	1.164	-2.81	-90.4	-60.9	32.63	-87.7	2.99
150	1.07	1.4625	-36.64	1.1127	-4.00	-98.9	-68.5	30.74	-95.9	3.03
160	1.03	1.4673	-43.48	1.0504	-4.30	-106	-76.5	27.83	-104	1.89
170	.943	1.4353	-54.37	.985	-4.77	-113	-84.5	25.22	-111	1.77
180	.886	1.4232	-60.06	.9252	-4.32	-120	-92.5	22.92	-117	2.53
190	.813	1.3711	-68.53	.8560	-5.50	-125	-100	20.00	-123	1.60
200	.757	1.3056	-72.00	.7993	-5.67	-130	-107	17.69	-128	1.54

Table [illegible]. Comparison of Experimental and Theoretical Results
(10.0 Inch Tube, Air, [illegible])

FREQUENCY (HZ)	EXPERIMENTAL AMPLITUDE RATIO	THEORETICAL AMPLITUDE RATIO (Original Geometry)	RELATIVE ERROR (PERCENT)	THEORETICAL AMPLITUDE RATIO (Case 5 Geometry)	RELATIVE ERROR (PERCENT)	EXPERIMENTAL PHASE SHIFT (DEG)	THEORETICAL PHASE SHIFT (Original Geometry) (DEG)	RELATIVE ERROR (PERCENT)	THEORETICAL PHASE SHIFT (Case 5 Geometry) (DEG)	RELATIVE ERROR (PERCENT)
0	1	1	0	1	0	0	0		0	0
10	.995	1.0037	-.17	1.0002	-.52	-6.12	-3.81	37.75	-5.76	5.88
20	.993	1.0087	-1.36	1.001	-.81	-11.8	-7.66	35.08	-11.5	2.54
30	.993	1.013	-2.22	1.0026	-.95	-17.7	-11.6	34.46	-17.3	2.26
40	.975	1.0264	-3.78	1.0057	-1.00	-23.6	-15.4	33.90	-23.2	1.69
50	1	1.0410	-4.16	1.0077	-.57	-29.7	-19.8	33.33	-29.2	1.68
60	1	1.0291	-5.95	1.0102	-1.42	-36.2	-24.1	33.43	-35.4	2.21
70	1.01	1.0794	-6.87	1.018	-.75	-42.6	-28.7	32.63	-41.8	1.88
80	1.02	1.1016	-9.07	1.0172	-.94	-49.6	-33.5	32.46	-48.5	2.22
90	1.01	1.1245	-11.36	1.0163	-.68	-57	-38.7	32.11	-55.4	2.81
100	.956	1.1475	-15.21	1.0065	-2.06	-64.3	-44.2	31.26	-62.6	2.64
110	.979	1.1667	-19.33	.9931	-1.44	-71.8	-50	30.36	-69.9	2.65
120	.923	1.1849	-24.21	.9781	-1.79	-79.4	-56.2	29.22	-77.2	2.77
130	.851	1.1952	-29.86	.9399	-2.05	-86.3	-62.7	27.35	-84.5	2.09
140	.801	1.1982	-36.00	.9035	-2.37	-93.6	-69.4	25.85	-91.5	2.24
150	.837	1.1916	-42.37	.8629	-3.09	-100	-76.2	23.80	-98.2	1.80
160	.792	1.1754	-48.37	.8190	-3.51	-107	-83.1	22.34	-105	1.87
170	.746	1.1493	-54.05	.7961	-4.03	-113	-89.9	20.44	-111	1.77
180	.698	1.1154	-59.00	.7332	-5.04	-119	-96.5	18.91	-116	2.
190	.643	1.0754	-62.80	.6922	-4.40	-123	-103	16.26	-121	1.63
200	.624	1.0315	-65.30	.6537	-4.76	-128	-109	14.84	-126	1.56

Table 25. Comparison of Experimental and Theoretical Results
(15.0 Inch Tube, PR=1.0485)

FREQUENCY (HZ)	EXPERIMENTAL AMPLITUDE RATIO	THEORETICAL AMPLITUDE RATIO (Original Geometry)	RELATIVE ERROR (PERCENT)	THEORETICAL AMPLITUDE RATIO (Case 5 Geometry)	RELATIVE ERROR (PERCENT)	EXPERIMENTAL PHASE SHIFT (DEG)	THEORETICAL PHASE SHIFT (Original Geometry) (DEG)	RELATIVE ERROR (PERCENT)	THEORETICAL PHASE SHIFT (Case 5 Geometry) (DEG)	RELATIVE ERROR (PERCENT)
0	1	1	0	1	0	0	0	0	0	0
10	.99	1.003	-1.23	1.0047	-1.08	-8.0	-5.47	31.71	-7.69	4.00
20	.991	1.0118	-2.19	1.0031	-1.22	-15.7	-11	23.94	-15.4	1.91
30	.975	1.0264	-3.16	1.0078	-1.29	-23.7	-16.6	23.11	-23.2	2.11
40	1	1.0464	-4.64	1.0144	-1.44	-31.0	-22.8	21.30	-31.3	1.57
50	1.01	1.0797	-6.01	1.0212	-1.51	-40.3	-29.1	27.79	-39.7	1.49
60	1.01	1.098	-6.71	1.0252	-1.51	-49.7	-36	27.77	-48.6	2.21
70	1.01	1.1253	-11.45	1.0227	-1.76	-59.1	-43.4	26.57	-57.9	2.03
80	.996	1.1583	-15.69	1.0053	-1.40	-69	-51.3	25.65	-67.6	2.03
90	.960	1.1657	-20.61	.9947	-1.73	-79.1	-59.4	24.49	-77.3	2.28
100	.926	1.1739	-25.72	.9473	-2.00	-89.1	-70.6	30.76	-86.9	2.47
110	.877	1.1643	-32.76	.9005	-2.63	-98.3	-77.9	28.75	-96.2	2.14
120	.82	1.1354	-38.95	.847	-3.29	-103	-87.1	18.60	-105	1.87
130	.766	1.1006	-41.66	.7921	-3.41	-115	-96.1	16.43	-113	1.74
140	.711	1.0531	-47.83	.7346	-3.48	-122	-105	13.93	-120	1.64
150	.628	.996	-51.14	.6607	-4.21	-129	-112	13.18	-127	1.55
160	.612	.9295	-53.51	.6435	-5.75	-135	-120	11.11	-133	1.48
170	.576	.8845	-53.56	.6014	-4.36	-141	-127	10.64	-139	1.42
180	.539	.8332	-54.58	.5604	-5.45	-146	-133	8.98	-144	1.37
190	.509	.7867	-54.56	.5353	-5.76	-151	-138	8.61	-149	1.32
200	.463	.7453	-54.11	.5126	-6.13	-155	-143	7.74	-154	.65

Table 10. Comparison of Experimental and Theoretical Results
(1.8 Inch Tube, PR=1.1564)

FREQUENCY (Hz)	EXPERIMENTAL AMPLITUDE RATIO	DIRECTICAL AMPLITUDE RATIO (Original Geometry)	RELATIVE ERROR (PERCENT)	THEORETICAL AMPLITUDE RATIO (Case 5 Geometry)	RELATIVE ERROR (PERCENT)	EXPERIMENTAL PHASE SHIFT (DEG)	THEORETICAL PHASE SHIFT (Original Geometry) (DEG)	RELATIVE ERROR (PERCENT)	THEORETICAL PHASE SHIFT (Case 5 Geometry) (DEG)	RELATIVE ERROR (PERCENT)
0	1	1	0	1	0	0	0	0	0	0
10	.986	1.0000	-1.46	.9926	-.97	-10.5	-7.2	30.10	-10.1	1.94
20	.973	1.0002	-2.88	.9832	-1.85	-20.4	-14.4	29.41	-20.1	1.47
30	.956	1.0004	-5.28	.9641	-1.86	-30	-21.8	27.33	-29.9	.33
40	.931	1.0006	-8.18	.94	-.97	-35.0	-29.3	26.57	-39.6	.75
50	.905	1.0073	-11.20	.932	-.77	-49.5	-37	25.25	-49	1.91
60	.875	1.0057	-14.81	.8884	-.58	-58.8	-44.9	23.54	-58.2	1.02
70	.841	1.0081	-18.92	.8455	-.54	-68.2	-53	22.29	-67.3	1.32
80	.802	.9813	-22.35	.8078	-.72	-77.4	-61.2	20.92	-76.1	1.68
90	.76	.9722	-27.92	.7679	-.96	-86.1	-69.5	19.28	-84.6	1.74
100	.717	.9647	-32.32	.7269	-1.38	-94.4	-77.8	17.58	-92.8	1.69
110	.673	.9192	-36.58	.686	-1.93	-102	-85.9	15.78	-101	.98
120	.631	.885	-40.25	.6463	-2.42	-110	-93.8	14.73	-108	1.82
130	.593	.8476	-42.93	.6086	-2.63	-117	-101	13.68	-115	1.71
140	.557	.8087	-45.19	.5735	-2.58	-123	-108	12.18	-121	1.63
150	.523	.77	-47.23	.5416	-3.54	-129	-115	10.85	-127	1.55
160	.493	.7335	-48.88	.5128	-4.23	-135	-122	9.63	-133	1.48
170	.467	.6973	-49.31	.4871	-4.38	-140	-128	8.57	-139	.71
180	.442	.6647	-50.35	.4645	-5.05	-146	-133	8.90	-144	1.37
190	.424	.6353	-49.83	.4448	-4.91	-150	-139	7.33	-149	.67
200	.405	.6089	-50.35	.4277	-5.60	-156	-144	7.69	-154	1.28

Table [illegible]. Comparison of Experimental and Theoretical Results
([illegible].375 Inch Tube, [illegible])

FREQUENCY (HZ)	EXPERIMENTAL AMPLITUDE RATIO	THEORETICAL AMPLITUDE RATIO (Original Geometry)	RELATIVE ERROR (PERCENT)	THEORETICAL AMPLITUDE RATIO (Case 5 Geometry)	RELATIVE ERROR (PERCENT)	EXPERIMENTAL PHASE SHIFT (DEG)	THEORETICAL PHASE SHIFT (Original Geometry) (DEG)	RELATIVE ERROR (PERCENT)	THEORETICAL PHASE SHIFT (Case 5 Geometry) (DEG)	RELATIVE ERROR (PERCENT)
0	1	1	0	1	0	0	0	0	0	0
10	.996	1.003	-.93	1.0003	-.61	-9.37	-6.24	33.40	-8.65	7.68
20	.991	1.0[illegible]19	-2.11	1.0061	-.98	-18.3	-12.6	31.15	-17.3	5.46
30	.986	1.0[illegible]	[illegible]	1.0021	-1.45	-27.5	-19.2	30.18	-26.1	5.09
40	.985	1.[illegible]	[illegible]	1.0042	-1.95	-36.7	-26	25.16	-35.1	4.36
50	.981	1.[illegible]	[illegible]	1.0054	-2.73	-46.5	-33.4	28.17	-44.5	4.30
60	.971	1.0915	[illegible]	.9934	-2.92	-56.5	-41.2	27.08	-54.2	4.07
70	.95	1.1123	-17.05	.9856	-3.75	-66.8	-49.6	25.75	-64.3	3.74
80	.92	1.126	-25.46	.9644	-4.33	-77	-58.6	23.98	-74.6	3.12
90	.84	1.128	[illegible]	.9335	-4.94	-87.1	-68	21.93	-81.7	2.76
100	.831	1.1149	-36.48	.8771	-5.52	-96.8	-77.6	19.83	-94.4	2.48
110	.779	1.0698	-35.98	.8247	-5.87	-106	-87.2	17.74	-104	1.89
120	.725	1.0494	-44.25	.7706	-6.12	-114	-96.6	15.26	-112	1.75
130	.672	.9976	-48.53	.7376	-6.63	-122	-105	13.93	-120	1.64
140	.627	.965	-50.72	.6626	-6.63	-129	-114	11.63	-127	1.55
150	.583	.8830	-52.18	.6244	-6.74	-136	-121	11.03	-134	1.47
160	.549	.8369	-52.44	.5855	-6.65	-141	-128	9.22	-140	.71
170	.517	.7882	-52.46	.5578	-6.73	-147	-135	8.16	-145	1.36
180	.489	.7446	-52.27	.5231	-6.97	-152	-141	7.24	-151	.66
190	.463	.7054	-51.51	.4972	-7.31	-157	-146	7.01	-156	.64
200	.447	.6729	[illegible]	.4709	-7.14	-162	-151	6.79	-161	.62

Table XI. Comparison of Experimental and Theoretical Results
(16.375 Inch Tube, PW=1.39363)

FREQUENCY (Hz)	EXPERIMENTAL AMPLITUDE RATIO	THEORETICAL AMPLITUDE RATIO (Original Geometry)	RELATIVE ERROR (PERCENT)	THEORETICAL AMPLITUDE RATIO (Case 5 Geometry)	RELATIVE ERROR (PERCENT)	EXPERIMENTAL PHASE SHIFT (DEG)	THEORETICAL PHASE SHIFT (Original Geometry) (DEG)	RELATIVE ERROR (PERCENT)	THEORETICAL PHASE SHIFT (Case 5 Geometry) (DEG)	RELATIVE ERROR (PERCENT)
0	1	1	0	1	0	0	0	0	0	0
10	.987	.9956	-1.38	.9936	-.67	-12.1	-6.27	31.65	-11.4	5.75
20	.966	.9911	-2.63	.9754	-.97	-23.4	-16.6	29.06	-22.7	2.99
30	.927	.9773	-6.44	.949	-1.17	-34.5	-25	27.54	-33.6	2.61
40	.901	.9537	-10.29	.9163	-1.48	-45.4	-33.5	26.21	-44.2	2.64
50	.851	.9031	-10.65	.8765	-1.88	-55.3	-42.2	24.51	-54.4	2.68
60	.8088	.8352	-10.82	.8257	-2.43	-66.7	-51	23.54	-64.2	3.75
70	.773	.7681	-24.28	.7631	-2.68	-75.5	-59.9	20.66	-73.7	2.38
80	.727	.9138	-25.82	.7436	-3.11	-84.8	-68.8	18.87	-82.8	2.36
90	.68	.9101	-33.68	.7061	-2.84	-93.8	-77.5	17.38	-91.4	2.56
100	.636	.8771	-37.91	.6636	-4.34	-102	-86.1	15.59	-99.6	2.35
110	.5925	.8484	-43.24	.6211	-4.72	-110	-94.4	14.18	-107	2.73
120	.5579	.8015	-43.35	.5852	-4.78	-117	-102	12.82	-115	1.71
130	.5172	.7522	-46.02	.5506	-5.48	-124	-110	11.29	-122	1.61
140	.493	.7239	-47.73	.5193	-5.98	-131	-117	10.69	-128	2.29
150	.4651	.6875	-48.49	.4913	-6.11	-137	-124	9.49	-134	2.19
160	.4339	.6539	-48.95	.4667	-6.31	-143	-130	9.09	-140	2.10
170	.4118	.6221	-49.11	.4451	-6.53	-148	-136	8.11	-146	1.35
180	.4006	.5996	-49.69	.4267	-6.18	-154	-142	7.79	-151	1.95
190	.3864	.5719	-48.93	.4109	-7.01	-159	-147	7.55	-157	1.26
200	.37	.5509	-48.89	.3975	-7.43	-164	-152	7.32	-162	1.22

In addition, Tables 31 and 32 show that the maximum relative error in amplitude ratio and phase shift for the 16.375-inch tube is about 7.5 percent. Again, this is a significant reduction in the relative error compared to the results with the original geometry.

Therefore, given the excellent correlation between the experimental data and the theoretical results using the Case 5 geometry, it is recommended that these dimensions be used to model the ZOC transducer in the NASA program when it is used for the reduction of data acquired in the CRF/F100 test.

SECTION VI

DISCUSSION AND CONCLUSIONS

The objectives of this study were successfully achieved through the experimental work described in this report. Accurate transfer functions were determined experimentally for several lengths of 0.020-inch-inside-diameter tubing over a frequency range of 0 to 200 hertz, and these data were used to determine the accuracy with which the NASA program could predict the amplitude response and phase shift for a given 0.020-inch-inside-diameter tube. These comparisons of experimental and theoretical results indicated that the NASA program can predict the frequency response behavior of 0.020-inch-inside-diameter tubes fairly accurately provided the pressure transducer in the system can be modelled precisely. To that end, an accurate model of the ZOC14 pressure transducer was developed as part of this effort.

Based on the results of this study the NASA program is recommended for use in the CRF/F100 test program as a tool for estimating the frequency response behavior of the close-coupled pressure instrumentation. Several conclusions from the experimental work should be considered when estimating the frequency response behavior, however.

1. The theory can only provide an estimate of the frequency response since its predictions are based on a sinusoidal dynamic pressure input, which is an ideal case that probably won't be realized in the F100 rotating stall environment.

2. The correlation of the experimental data with theoretical predictions is excellent for the cases tested. However, limitations of the experimental apparatus prevented the acquisition of experimental data over the full range of temperatures and pressures expected in the close-coupled instrumentation tubes during F100 testing. Therefore, in many instances, to estimate the frequency response behavior it will be necessary to assume that the observed correlation of experimental data and theoretical predictions from a few experiments can be applied universally.

3. The results of the study indicate the Bergh-Tijdeman theory, as implemented in the NASA program, can predict the amplitude response of a 0.020-inch-inside-diameter tube within 3 to 12 percent of the experimental value. The phase shift can be predicted within 6 to 14 degrees. Both tube length and mean tube pressure affect this correlation. In general, the percentage difference between experimental data and theoretical prediction is smaller for shorter tube lengths and lower mean pressures. Also, the tendency is for the discrepancy between experimental and theoretical values of amplitude ratio and phase shift to widen with increasing frequency. For example, the worst correlation of experimental and theoretical values would occur in the longest tube length at the highest mean pressure level, and at the highest frequency.

4. The theoretical predictions for amplitude ratio are consistently greater than the experimental values, while predicted phase shift values are consistently less than the experimental values.

5. For a given mean tube pressure level, changes in the dynamic pressure level over a range of 130 to 175 dB (.009 to 1.45 psi) had no significant impact on the frequency response behavior of the tubes.

6. Smooth radius bends in the tubing had no affect on the frequency response behavior.

7. The manufacturer's specifications for the ZOC14 pressure transducer internal dimensions are inadequate for modelling the transducer in the NASA program. An optimum set of internal geometry to be used for modelling the ZOC was determined. These values, which should be used for estimating the frequency response of the CRF/F100 instrumentation tubes, are: internal tube length, 8.7 cm; internal tube diameter, 0.0865 cm; and internal termination volume, 6E-5 cubic cm.

REFERENCES

1. Bergh, H., Tijdeman, H., "Theoretical and Experimental Results for the Dynamic Response of Pressure Measuring Systems," Report NLR-TR-F.238, National Aero- and Astronautical Research Institute, Amsterdam, January 1965.

2. Nyland, Ted W., England, David R., Anderson, Robert C., "On the Dynamics of Short Pressure Probes: Some Design Factors Affecting Frequency Response," NASA TN D-6151, NASA Lewis Research Center, Cleveland, Ohio, February 1971.

3. Gerlach, C. Richard, Johnson, James E., Astleford, William J., "Instrumentation for Monitoring Dynamic Flow Parameters in Engines," AFAPL-TR-70-14, Air Force Aero Propulsion Laboratory, Wright-Patterson Air Force Base, Dayton, Ohio, March 1970.

4. Chapin, William G., "Dynamic Pressure Measurements Using An Electronically Scanned Pressure Module," NASA TM-84650, NASA Langley Research Center, Hampton, Virginia, 1983.

5. Irwin, H.P.A.H., Cooper, K.R., "Correction of Distortion in Fluctuating Pressure Measurements," LTR-LA-222, National Research Council Canada, National Aeronautical Establishment, Ottawa, Canada, February 1980.

6. Ostdiek, Francis R., "A Cascade in Unsteady Flow," AFAPL-TR-76-115, Air Force Aero Propulsion Laboratory, Wright-Patterson Air Force Base, Dayton, Ohio, December 1976.

7. 6086 Multichannel Signal Processor User Manual, ZONIC Corporation, Milford, Ohio, 1984.

Appendix A

FORTRAN Steering Program and NASA Subroutines

This appendix contains a listing of the FORTRAN steering program, for a typical set of inputs, and the NASA subroutines used to calculate the theoretical amplitude ratio and phase shift for a given tube/volume combination.

```
          COMPILER OPTIONS - NAME= MAIN,OPT=00,LINECNT=60,SIZE=0000K,
                             SOURCE,EBCDIC,NOLIST,NODECK,LOAD,MAP,NOEDIT,ID,NOXREF
ISN 0002            DIMENSION D(10),XL(10),V(10),DVDP(10),P(10),RHO(10),VIS(10)
                   2,HZ(1000),AMATIC(1000),PHASE(1000),DC(1000)
ISN 0003            COMMON/GEOMTY/D(10),XL(10),V(10),DVDP(10)
ISN 0004            COMMON/THERMC/GAMMA,P(10),RHO(10),VIS(10),AMPRES
ISN 0005            COMMON/POLY1/ATERMS,B(1000),C(1000),DC(1000)
                    C
                    C     THIS VERSION CORRESPONDS TO THE AAMRL EXPERIMENTAL SETUP.
                    C     THE INSERTION LENGTH OF THE TUBE HAS BEEN ACCOUNTED FOR.
                    C
ISN 0006            N=2
ISN 0007            DF=10.0
ISN 0008            GAMMA=1.4
ISN 0009            PR=1.0
ISN 0010            TR=1.00566
ISN 0011            FIRSTL=25.4
ISN 0012            TREF=530.
ISN 0013            T=TR*TREF
ISN 0014            PREF=985238.55
ISN 0015            AMPRES=PREF*PR
ISN 0016            VIS(1)=.000182*(T/531.)**1.5*(729./(T+198.))
ISN 0017            RHO(1)=1.2046E-3*PR/TR
ISN 0018            FRMAX=0.
ISN 0019            DO 12 I=1,10
ISN 0020            RHO(I)=RHO(1)
ISN 0021            VIS(I)=VIS(1)
ISN 0022            P(I)=.70
ISN 0023            D(I)=0.
ISN 0024            XL(I)=0.
ISN 0025            DVDP(I)=0.
ISN 0026            V(I)=0.
ISN 0027       12   CONTINUE
ISN 0028            PI=3.14159
                    C
                    C  THIS CASE FOR A DRUCK TEST TRANSDUCER.
                    C
ISN 0029            V(1)=0.0
ISN 0030            V(2)=2.0E-5
ISN 0031            D(1)=.0500
ISN 0032            D(2)=.10414
ISN 0033            XL(1)=FIRSTL
ISN 0034            XL(2)=1.20e5
ISN 0035            DVDP(1)=0.
ISN 0036            DVDP(2)=0.
ISN 0037            FREQ=0.
ISN 0038            WRITE(6,7)
ISN 0039          7 FORMAT(/,1X,'ATMOSPHERIC CHAMBER PRESSURE WITH 175 DB RMS'
                   2' PRESSURE LEVEL')
ISN 0040            WRITE(6,8)
ISN 0041          8 FORMAT(1H1,' THE TUBING SYSTEM CONSISTS OF THE FOLLOWING')
ISN 0042            DO 14 I=1,N
ISN 0043         14 WRITE(6,9)I,D(I),XL(I),V(I)
ISN 0044          9 FORMAT(I3,' D=',F10.6,' XL=',F10.4,' V=',F10.6)
ISN 0045            WRITE(6,10)
ISN 0046            DO 100 K=1,10
ISN 0047            FREQ=FREQ+DF
ISN 0048            CALL AMPPHS(FREQ,A,PA,I,N)
```

```
ISN 0049            WRITE(6,11) FREQ,A,PA
ISN 0050      100   CONTINUE
ISN 0051       10   FORMAT(///1H ,' FREQUENCY   AMP RATIO     PHASE ')
ISN 0052       11   FORMAT(2F10.4,F12.4)
ISN 0053            STOP
ISN 0054            END
```

```
         COMPILER OPTIONS - NAME= MAIN,OPT=00,LINECNT=60,SIZE=0000K,
                            SOURCE,EBCDIC,NOLIST,NODECK,LOAD,MAP,NOEDIT,ID,NOXREF
ISN 0002            SUBROUTINE AMPPHS(FREQ,A,PA,I,J)                          00000010
                    C                                                         00000020
                    C                                                         00000030
                    C    THIS ROUTINE CALCULATES THE AMPLITUDE RATIO (A) P(I)/P(0)  00000040
                    C AND PHASE ANGLE (PA)  FOR A SERIES CONNECTION OF  TUBE-VOLUME  00000050
                    C SYSTEMS GIVEN FREQUENCY 'FREQ'.                         00000060
                    C    THE SYSTEM GEOMETRY IS ENTERED THROUGH COMMON BLOCK /GEOMTY/.  00000070
                    C    THE THERMODYNAMIC CONDITIONS ARE ENTERED THROUGH COMMON BLOCK  00000080
                    C   1/THERMO/.                                            00000090
                    C                                                         00000100
                    C                                                         00000110
ISN 0003            DIMENSION PRATIO(10)                                      00000120
ISN 0004            COMMON/GEOMTY/D(10),XL(10),V(10),DVDP(10)                 00000130
ISN 0005            COMMON/THERMC/GAMMA,P(10),RHO(10),VIS(10),AMPRES          00000140
ISN 0006            COMMON/XFREQ/FREQ1
ISN 0007            COMPLEX  PRATIO,RECURS                                    00000150
ISN 0008            FREQ1 = FREQ                                              00000160
ISN 0009            RECURS = 1.0                                              00000170
ISN 0010            DO 10  M=1,10                                             00000180
ISN 0011       10     PRATIO(M) = 0.0                                         00000190
ISN 0012            N = J                                                     00000200
                    C                                                         00000210
                    C CALCULATE SUCCESSIVE PRESSURE RATIOS                    00000220
                    C                                                         00000230
ISN 0013            DO 20  K=1,N                                              00000240
ISN 0014       20   CALL RATIO(PRATIO,J+1-K,J)                                00000250
                    C                                                         00000260
                    C CALCULATE REQUIRED RATIO BY MULTIPLYING APPROPRIATE PRESSURE RATIOS  00000270
                    C                                                         00000280
ISN 0015            DO30 K = 1,N
ISN 0016       30   RECURS = RECURS*PRATIO(K)                                 00000300
ISN 0017            A= CABS(RECURS)                                           00000310
ISN 0018            PA= ATAN2(AIMAG(RECURS),REAL(RECURS))                     00000320
                    C                                                         00000330
                    C CONVERT RADIANS TO DEGREES                              00000340
                    C                                                         00000350
ISN 0019            PA= PA*57.2957795                                         00000360
ISN 0020            IF(PA.GT.0.0) PA =-360.+PA                                00000370
ISN 0022            RETURN                                                    00000380
ISN 0023            END                                                       00000390
```

```
          COMPILER OPTIONS - NAME= MAIN,OPT=00,LINECNT=60,SIZE=0000K,
                             SOURCE,EBCDIC,NOLIST,NODECK,LOAD,MAP,NOEDIT,ID,NOXREF
ISN 0002            SUBROUTINE RATIO(PRATIO,J,K)                                    00000420
                    C                                                               00000430
                    C                                                               00000440
                    C     THIS PROGRAM CALCULATES THE PRESSURE RATIO P(J)/P(J-1).   00000450
                    C                                                               00000460
                    C                                                               00000470
ISN 0003            DIMENSION PRATIO(10),VRATIO(10),CORRCT(10)
ISN 0004            COMMON/GEOMTY/D(10),XL(10),V(10),DVDP(10)                       00000490
ISN 0005            COMMON/THERMO/GAMMA,P(10),RHO(10),VES(10),AMPRES                 0000050
ISN 0006            COMMON/XFREQ/FREQ                                               00000510
ISN 0007            COMPLEX PHI,JRAT,POLY,POLRAT,CCOSH,CSINH,PRATIO,TERM1,TERM2,TERM3,00000520
                   1TPHI1,TPHI2,JRATIO
ISN 0008            PI = 3.1415927                                                  00000540
ISN 0009            VRATIO(J) = V(J)/(PI*D(J)**2*XL(J)/4.)                          00000550
ISN 0010            RFREQ = 2.*PI*FREQ                                              00000560
ISN 0011            IF(V(J).NE.0.0)GOTO1                                            00000570
ISN 0013            CORRCT(J) = 1.0                                                 00000580
ISN 0014            GOTO3                                                           00000590
ISN 0015          1 CORRCT(J) = 1.0 + (DVDP(J)* AMPRES/V(J))
ISN 0016          3 CONTINUE                                                        00000610
ISN 0017            IF(J.EQ.K) GO TO 5                                              00000620
ISN 0019            POLRAT = CSQRT(POLY(J)/POLY(J+1))                               00000630
ISN 0020            RHORAT = SQRT(RHO(J+1)/RHO(J))                                  00000640
ISN 0021            VOLRAT = D(J+1)**2/D(J)**2)                                     00000650
ISN 0022            TPHI2 = PHI(J+1)                                                00000660
ISN 0023            JRAT = CSQRT(                                                   00000670
                   1(1.0,0.0)+(CMPLX(0.0,-(RFREQ*D(J+1)**2*RHO(J+1)/                00000680
                   2( 4.0*V(S(J+1))))))/                                           00000690
                   3(1.0,0.0)+(CMPLX(0.0,-(RFREQ*D(J  )**2*RHO(J  )/               00000700
                   4( 4.0*V(S(J  ))))))                                            00000710
ISN 0024          5 TPHI1 = PHI(J)                                                  00000720
ISN 0025            TERM1 = CCOSH(TPHI1*XL(J))                                      00000730
ISN 0026            TERM2 = VRATIO(J)*CORRCT(J)*XL(J)*TPHI1*POLY(J)*CSINH(TPHI1*XL(J))00000740
ISN 0027            IF(J.EQ.K) GO TO 2                                              00000750
ISN 0029            TERM3 = ((CSINH(TPHI1*XL(J))/CSINH(TPHI2*XL(J+1)))*             00000760
                   1        VOLRAT*RHORAT*JRAT*POLRAT*                             00000770
                   2        (CCOSH(TPHI2*XL(J+1))-PRATIO(J+1))                     00000780
ISN 0030            GOTO6                                                           00000790
ISN 0031          2 TERM3 = CMPLX(0.0,0.0)                                          00000800
ISN 0032          6 CONTINUE                                                        00000810
ISN 0033            PRATIO(J) = 1.0/(TERM1+TERM2+TERM3)                             00000820
ISN 0034            RETURN                                                          00000830
ISN 0035            END                                                             00000840
```

```
         COMPILER OPTIONS - NAME= MAIN,OPT=00,LINECNT=60,SIZE=0000K,
                            SOURCE,EBCDIC,NOLIST,NODECK,LOAD MAP,NOEDIT,ID,NOXREF
ISN 0002                    COMPLEX FUNCTION JRATIO(CARG)                          00000870
                    C                                                              00000880
                    C                                                              00000890
                    C  THIS ROUTINE CALCULATES THE RATIO OF THE BESSEL FUNCTION OF THE  00000900
                    C FIRST KIND, ORDER 2 TO THE BESSEL FUNCTION OF THE FIRST KIND.    00000910
                    C ORDER 0 WITH COMPLEX ARGUMENT.                               00000920
                    C                                                              00000930
ISN 0003                    COMPLEX FM,QSUM,PSUM,XPSUM(2),XQSUM(2),XJ(2),RATIO,XX,Y  00000940
                           1Y,Z                                                    00000950
ISN 0004                    COMPLEX J2,J0,JRATIO,CARG
ISN 0005                    COMMON /SI/X,Y,PSUM,QSUM                               00000970
ISN 0006                    COMMON /SMN/M/FM                                       00000980
ISN 0007                    DATA PI/3.1415927/,M/-1/,Z/(0.0,1.0)/                  00000990
ISN 0008                    IF(REAL(CARG).GT.30.0) GO TO 40                        00001000
                    C                                                              00001010
                    C   IF THE REAL PART OF THE ARGUMENT IS GREATER THAN 30 USE IS MADE OF  00001020
                    C HANKELS ASYMPTOTIC EXPANSION (SEE NBS HANDBOOK OF MATHEMATICAL    00001030
                    C FUNCTIONS AMS NO.55) TO CALCULATE THE BESSEL FUNCTION RATIO. THE P  00001040
                    C AND Q COEFFICIENTS USED IN THE EXPANSIONS ARE CALCULATED USING THE  00001050
                    C SERIES SUBROUTINE.                                           00001060
                    C                                                              00001070
ISN 0010                    GO TO 20                                               00001080
ISN 0011            40      X = REAL(CARG)                                         00001090
ISN 0012                    Y = -X                                                 00001100
ISN 0013                    DO 2 J=1,2                                             00001110
ISN 0014                    M = M + J                                              00001120
ISN 0015                    XI = FLOAT(M)                                          00001130
ISN 0016                    FM = CMPLX(XI,0.0)                                     00001140
ISN 0017                    CALL SERIES                                            00001150
ISN 0018                    XPSUM(J) = PSUM                                        00001160
ISN 0019            2       XQSUM(J) = QSUM                                        00001170
ISN 0020                    DO 3 K=1,2                                             00001180
ISN 0021                    A = X + (0.75 - FLOAT(K))*PI                           00001190
ISN 0022                    XX = XPSUM(K) * COS(A)  - XQSUM(K)  * SIN(A)           00001200
ISN 0023                    YY = (XPSUM(K) * SIN(A) + XQSUM(K)  * COS(A))  * Z     00001210
ISN 0024            3       XJ(K) = XX + YY                                        00001220
ISN 0025                    RATIO = XJ(2) / XJ(1)                                  00001230
ISN 0026                    JRATIO = RATIO                                         00001240
ISN 0027                    M = -1                                                 00001250
ISN 0028                    GO TO 30                                               00001260
ISN 0029            20      CALL ZEBESI(J0,0,CARG)                                 00001270
ISN 0030                    CALL ZEBESI(J2,2,CARG)                                 00001280
ISN 0031                    JRATIO = J2/J0                                         00001290
ISN 0032            30      CONTINUE                                               00001300
ISN 0033                    RETURN                                                 00001310
ISN 0034                    END                                                    00001320
```

```
        COMPILER OPTIONS - NAME= MAIN,OPT=00,LINECNT=60,SIZE=0000K,
                           SOURCE,EBCDIC,NOLIST,NODECK,LOAD,MAP,NOEDIT,ID,NOXREF
ISN 0002            SUBROUTINE SERIES                                          00001360
                C                                                              00001370
                C                                                              00001380
                C    THIS ROUTINE CALCULATES THE VALUE OF THE SERIES NEEDED FOR 00001390
                C HANKELS ASYMPTOTIC EXPANSION                                 00001400
                C                                                              00001410
                C   IN CALCULATING P(J) AND Q(J) NUMBERS WITH EXPONENTS LESS THAN -38 00001420
                C MAY OCCUR.  THIS PROGRAM USES A BUILT-IN ROUTINE WHICH SETS P(J) 00001430
                C AND/OR Q(J) EQUAL TO ZERO WHENEVER THESE SMALL NUMBERS OCCUR. 00001440
                C                                                              00001450
                C                                                              00001460
                C                                                              00001470
ISN 0003            COMPLEX Z,ML,PSUM,QSUM,FM,P(50),Q(50)                      00001480
ISN 0004            COMMON/S1/X,Y,PSUM,QSUM                                    00001490
ISN 0005            COMMON /FMMAP/FM                                           00001500
ISN 0006            PSUM = (0.,0.)                                             00001510
ISN 0007            QSUM = (0.,0.)                                             00001520
ISN 0008            MU =4.*FM**2                                               00001530
ISN 0009            Z =  CMPLX(X,Y)                                            00001540
ISN 0010            DO 100 J=1,50                                              00001550
ISN 0011            N = J-1                                                    00001560
ISN 0012            FN = N                                                     00001570
ISN 0013            IF(N .NE. 0) GO TO 30                                      00001580
ISN 0015        20  P(J) =(1.,0.)                                              00001590
ISN 0016            Q(J) = (MU-1.)/(8.*Z)                                      00001600
ISN 0017            GO TO 90                                                   00001610
ISN 0018        30  FN2 = 2.*FN                                                00001620
ISN 0019            FN4 = 2.*FN2                                               00001630
ISN 0020            FN21 = FN2 * 1.                                            00001640
ISN 0021            FN41 = 2.*FN21                                             00001650
ISN 0022            IF(CABS(P(J-1)).EQ.0.) GO TO 50                            00001660
ISN 0024            P(J) = -((MU-(FN4-3.)**2)/(64.*(FN2-1.)*FN2))*((MU-(FN4-1.)**2)/Z 00001670
                   $**2)*P(J-1)
ISN 0025            IF (J .GT. 2 .AND. CABS(P(J)) .GT. CABS(P(J-1)) ) P(J) = (0.,0.) 00001690
ISN 0027            GO TO 55                                                   00001700
ISN 0028        50  P(J) = (0.,0.)                                             00001710
ISN 0029        55  IF(CABS(Q(J-1)).EQ.0.) GO TO 80                           00001720
ISN 0031            Q(J) = -((MU-(FN41-3.)**2)/(64.*FN2*FN21))*((MU-(FN41-1.)**2)/Z 00001730
                   $**2)*Q(J-1)
ISN 0032            IF (J .GT. 2 .AND. CABS(Q(J)) .GT. CABS(Q(J-1)) ) Q(J) = (0.,0.) 00001750
ISN 0034            GO TO 90                                                   00001760
ISN 0035        80  Q(J) = (0.,0.)                                             00001770
ISN 0036        90  PSUM = P(J)+PSUM                                           00001780
ISN 0037            QSUM = Q(J)+QSUM                                           00001790
ISN 0038            IF(CABS(P(J)).EQ.0. .AND. CABS(Q(J))  .EQ. 0.) GO TO 110   00001800
ISN 0040        100 CONTINUE                                                   00001810
ISN 0041        110 CONTINUE                                                   00001820
ISN 0042            RETURN                                                     00001830
ISN 0043            END                                                        00001840
```

```
        COMPILER OPTIONS - NAME= MAIN,OPT=00,LINECNT=60,SIZE=0000K,
                           SOURCE,EBCDIC,NOLIST,NODECK,LOAD,MAP,NOEDIT,ID,NOXREF
ISN 0002            SUBROUTINE ZEEBES(J,N,Z)                                    000C1870
                    C                                                           000C1880
                    C   THIS ROUTINE CALCULATES THE VALUE OF THE BESSEL FUNCTION OF THE   000C1890
                    C FIRST KIND OF INTEGER ORDER. THE ARGUMENT IS OF THE FORM   00001900
                    C C(1 - SQRT(-1)) WHERE C IS A REAL CONSTANT LESS THAN 30 .  00001910
                    C                                                           000C1920
                    C                    J...BESSEL FUNCTION VALUE              00001930
                    C                    N....BESSEL FUNCTION ORDER             00001940
                    C                    Z...BESSEL FUNCTION ARGUMENT           000C1950
                    C                                                           000C1960
                    C                                                           000C1970
ISN 0003            COMPLEX J,Z                                                 000C1980
ISN 0004            DOUBLE PRECISION DFN,T,R(2),C,DK,D,B
ISN 0005            D = REAL(Z)                                                 00002000
ISN 0006            C = D * 1.41421356237309500                                 00002010
ISN 0007            CR = D                                                      00002020
ISN 0008            DFN = FLOAT(N)                                              00002030
ISN 0009            IF(N.NE.2) GO TO 1                                          00002040
ISN 0011            T = 5.D-1                                                   00002050
ISN 0012            GO TO 2                                                     00002060
ISN 0013       1    T = 1.00                                                    00002070
ISN 0014       2    R(1) = T                                                    00002080
ISN 0015            R(2) = 0.00                                                 00002090
ISN 0016            C = (C**2.) / 4.00                                          00002100
ISN 0017            DK = 0.00                                                   00002110
ISN 0018            I = 1                                                       00002120
ISN 0019            M = 0                                                       00002130
ISN 0020       5    DK = DK + 1.00                                              00002140
ISN 0021            T = T * C / ((DK)*(DK+DFN))                                 00002150
ISN 0022            I = I + 1                                                   00002160
ISN 0023            IF (T.LT.DABS(R(I))*1.D-8)) GO TO 7                         00002170
ISN 0025            M = M + 1                                                   00002180
ISN 0026            B = 1.00                                                    00002190
ISN 0027            IF(M.GT.1) B = -1.00                                        00002200
ISN 0029            IF(M.EQ.3) M = -1                                           00002210
ISN 0031            R(I) = R(I) + B * T                                         00002220
ISN 0032            IF(I.EQ.2) I = 0                                            00002230
ISN 0034            GO TO 5                                                     00002240
ISN 0035       7    AR= R(1)                                                    00002250
ISN 0036            AI = R(2)                                                   00002260
ISN 0037            IF(N.NE.2) GO TO 8                                          00002270
ISN 0039            RI = (-1.) * R(1) * C                                       00002280
ISN 0040            AR =R(2) * C                                                00002290
ISN 0041       8    J = CMPLX(AR,RI)                                            00002300
ISN 0042            RETURN                                                      00002310
ISN 0043            END                                                         00002320
```

```
        COMPILER OPTIONS - NAME=  MAIN,OPT=00,LINECNT=60,SIZE=0000K,
                           SOURCE,EBCDIC,NOLIST,NODECK,LOAD,MAP,NOEDIT,ID,NOXREF
  ISN 0002            COMPLEX FUNCTION PHI(J)
                C
                C        THIS PROGRAM CALCULATES A FUNCTION PHI WHICH IS AN
                C     ATTENUATION PARAMETER.
  ISN 0003            COMMON/GEOPTY/D(10),XL(10),V(10),DVDP(10)
  ISN 0004            COMMON/THERMO/GAMMA,P(10),RHO(10),VIS(10),AMPRES
  ISN 0005            COMMON/XFREQ/FREQ
  ISN 0006            COMPLEX POLY,PHI,JRATIO
  ISN 0007            SN = 6.283185*FREQ*D(J)**2*RHO(J)/VIS(J)
  ISN 0008            PHI=6.2831854*FREQ*SQRT(RHO(J)/(GAMMA*AMPRES))*
                     P        CSQRT(1./JRATIO(CSQRT(CMPLX(0.0,-(SN/4.0)))))*
                     P        CSQRT(GAMMA/POLY(J))
  ISN 0009            RETURN
  ISN 0010            END
```

```
        COMPILER OPTIONS - NAME= MAIN,OPT=00,LINECNT=60,SIZE=0000K,
                           SOURCE,EBCDIC,NOLIST,NODECK,LOAD,MAP,NOEDIT,ID,NOXREF
ISN 0002            COMPLEX FUNCTION POLY(J)                                    00002530
                    C                                                           00002540
                    C       THIS ROUTINE CALCULATES A POLYTROPIC COEFFICIENT     00002550
                    C     (LABELED 'N' IN BERGH AND TIDJEMAN)                   00002560
                    C                                                           00002570
ISN 0003            COMMON/GEOMTY/D(10),XL(10),V(10),DVDP(10)                   00002580
ISN 0004            COMMON/THERMO/GAMMA,P(10),RHO(10),VIS(10),AMPRES            00002590
ISN 0005            COMMON/XFREQ/FREQ                                           00002600
ISN 0006            COMPLEX JRATIO,CARG,POLY                                    00002610
ISN 0007            SN = 6.2831854*FREQ*D(J)**2*RHO(J)/VIS(J)                   00002620
ISN 0008            ARG = P(J)*SN/4.                                            0000263
ISN 0009            CARG=  CSQRT(CMPLX(0.0,-ARG))                               00002640
ISN 0010            POLY=1.0/(1.0+((GAMMA-1.0)/GAMMA)*JRATIO(CARG))             00002650
ISN 0011            RETURN                                                      00002660
ISN 0012            END                                                         00002670
```

```
LEVEL 21.8 ( JUN 74 )                    OS/360  FORTRAN H                    DATE  85.339/16.54.23

          COMPILER OPTIONS - NAME=  MAIN,OPT=00,LINECNT=60,SIZE=0000K,
                             SOURCE,EBCDIC,NOLIST,NODECK,LOAD,MAP,NOEDIT,ID,NOXREF
  ISN 0002            COMPLEX FUNCTION CCOSH(ARG)                          00002700
  ISN 0003            COMPLEX ARG,CCOSH                                    00002710
  ISN 0004            CCOSH = (CEXP(ARG)+CEXP(-ARG))/2.0
  ISN 0005            RETURN                                               00002730
  ISN 0006            END                                                  00002740
```

```
          COMPILER OPTIONS - NAME= MAIN,OPT=00,LINECNT=60,SIZE=0000K,
                             SOURCE,EBCDIC,NOLIST,NODECK,LOAD,MAP,NOEDIT,ID,NOXREF
ISN 0002            COMPLEX FUNCTION CSINH(ARG)                                  00002780
ISN 0003            COMPLEX ARG,CSINH                                            00002790
ISN 0004            CSINH= (CEXP(ARG)-CEXP(-ARG))/2.0                            00002800
ISN 0005            RETURN                                                       00002810
ISN 0006            END                                                          00002820
```

Appendix B

Pressure Transducer Calibrations

The ZOC and DRUCK pressure transducers used in this project were calibrated on the bench using an AMETEK RK-300 dead weight tester, connected as shown in Figure B-1. For the ZOC transducer it was necessary to apply compressed nitrogen at 80 psig to the CAL CTL port to switch the transducer into the "calibrate" mode. The transducers were calibrated with the same amplifier/signal conditioning units used during the experiments.

Three transducers were used in the project--one 0 to 5 psig ZOC and two 0 to 15 psig DRUCK transducers. DRUCK transducer SN10135 was used as the reference transducer in all experiments, while SN12625 was used as a test transducer in those experiments requiring a DRUCK. The ZOC and DRUCK SN10135 were calibrated twice during the project, while DRUCK SN12625 was calibrated only once. The resulting calibration curves are shown in Figures B-2 through B-6 and the calibration data are listed in Tables B-1 and B-2.

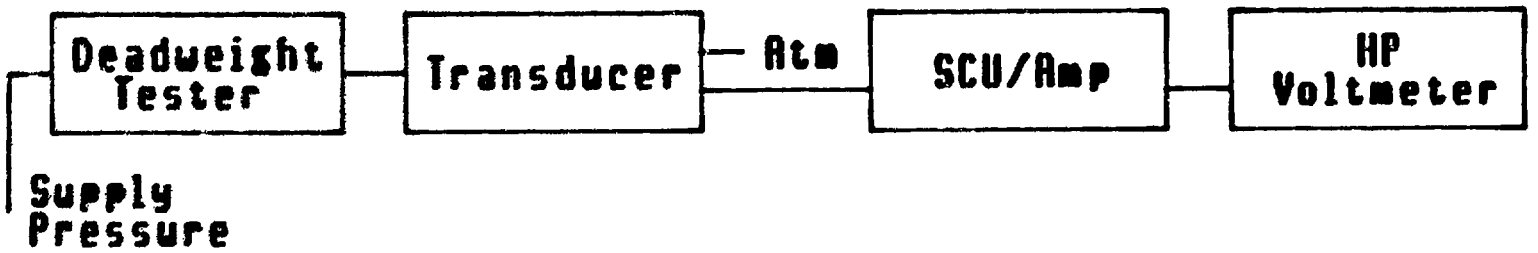

Figure B-1. Transducer Calibration Setup

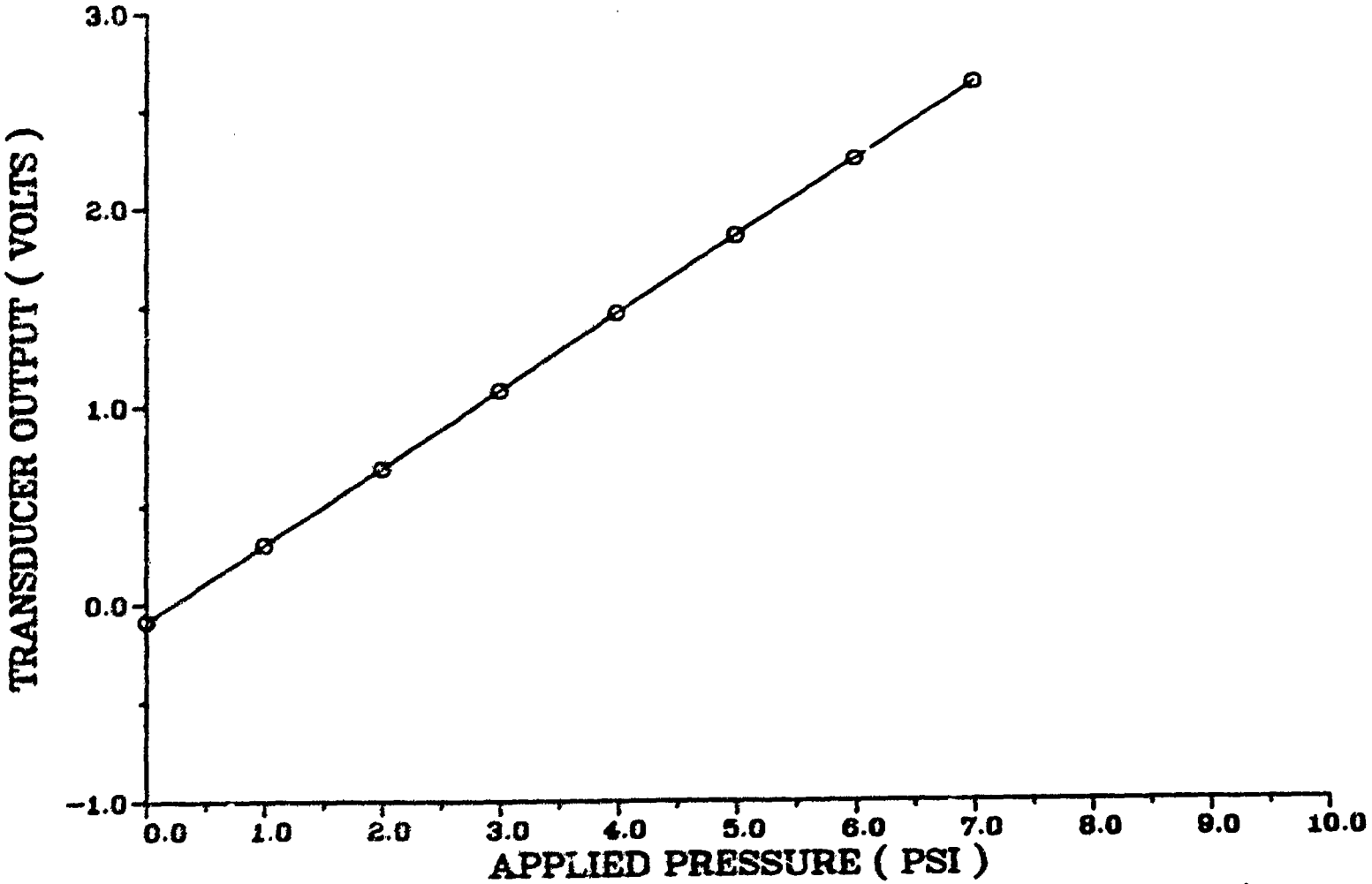

FIGURE B-2. ZOC 14 TRANSDUCER CALIBRATION CURVE (4 MAR 85)

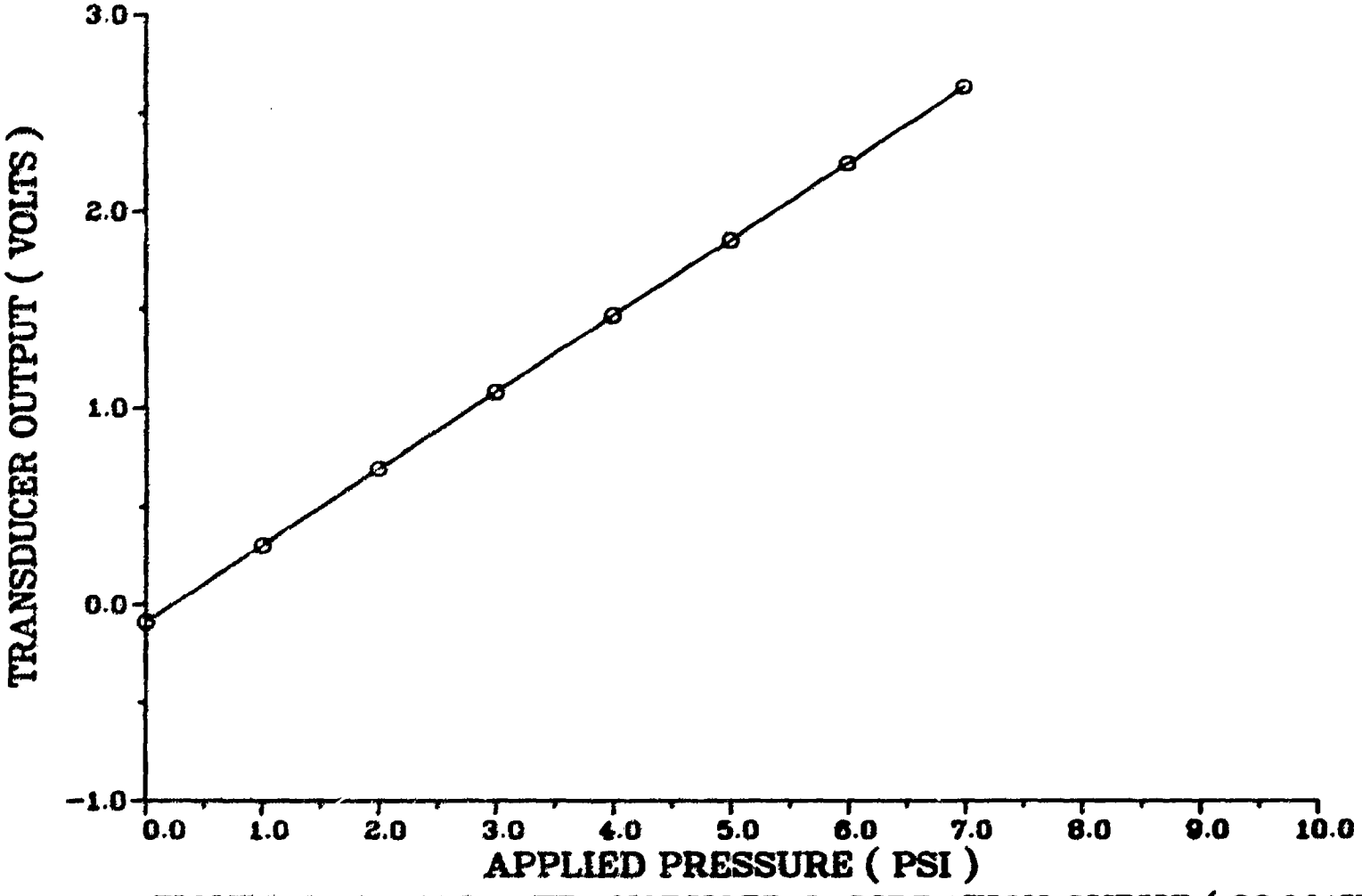

FIGURE B-3. ZOC14 TRANSDUCER CALIBRATION CURVE (22 MAY 85)

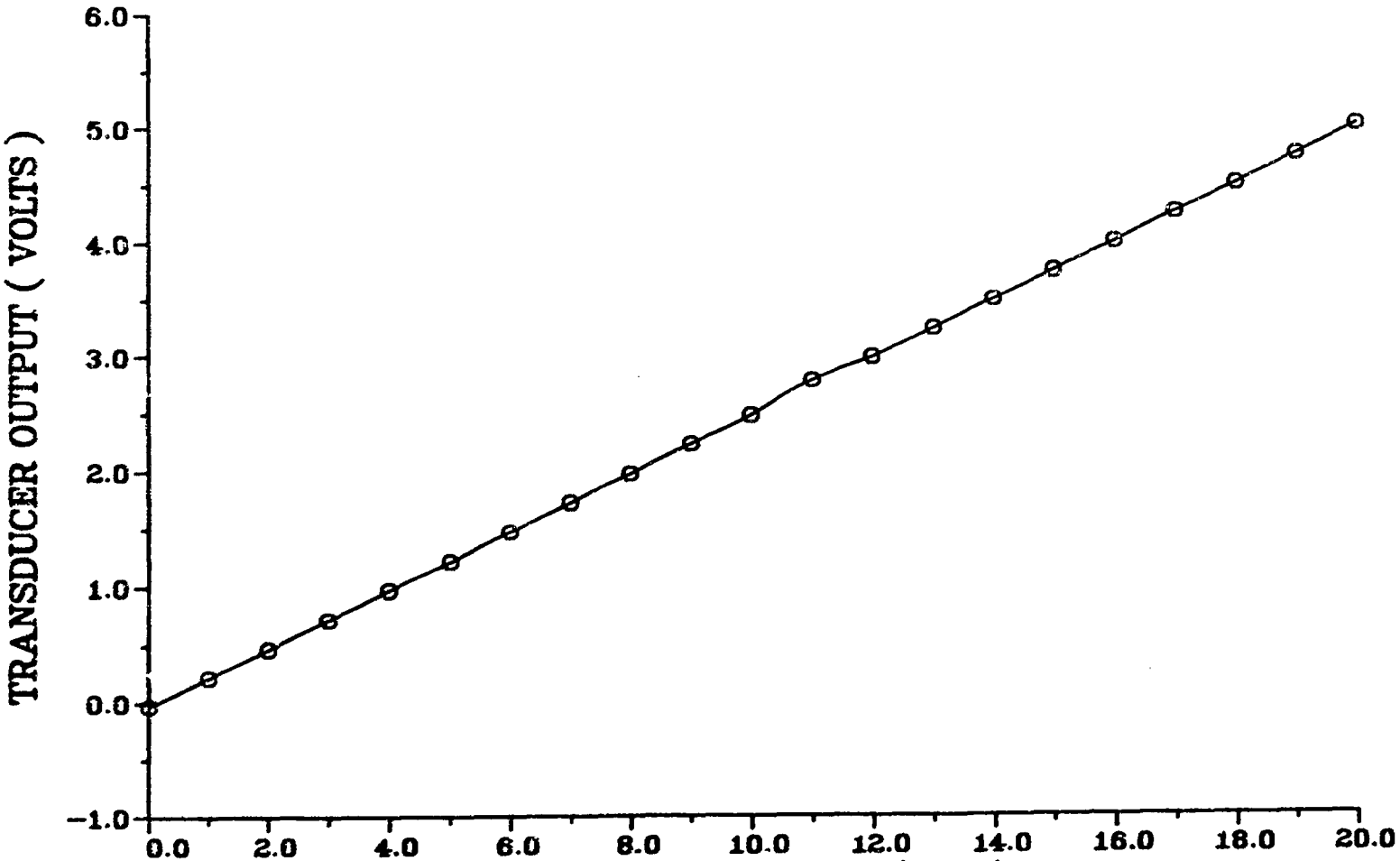

FIGURE B–4. DRUCK TRANSDUCER CALIBRATION CURVE (4 MAR 85)
(SN 10135)

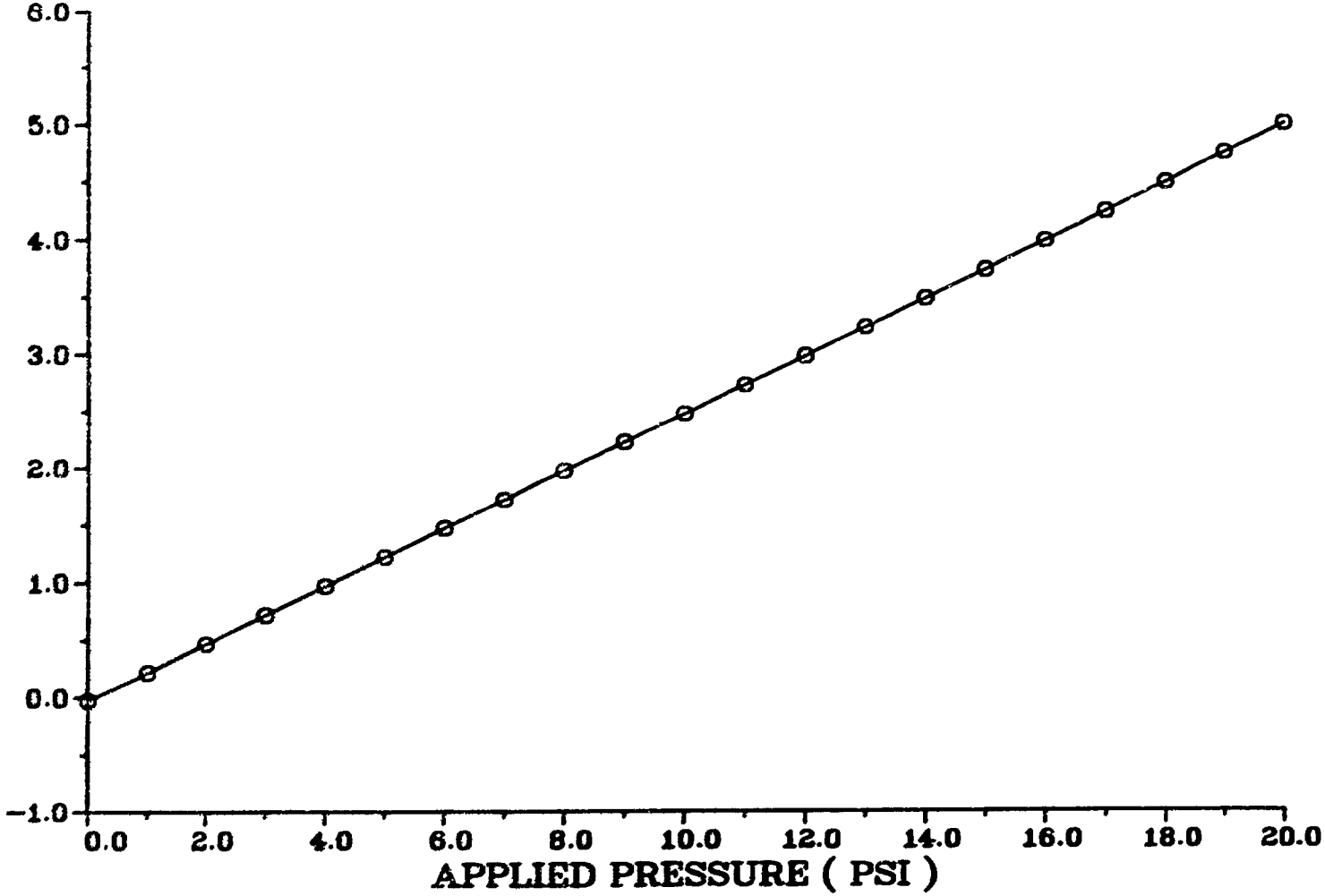

FIGURE B-5. DRUCK TRANSDUCER CALIBRATION CURVE (22 MAY 85)
(SN 10135)

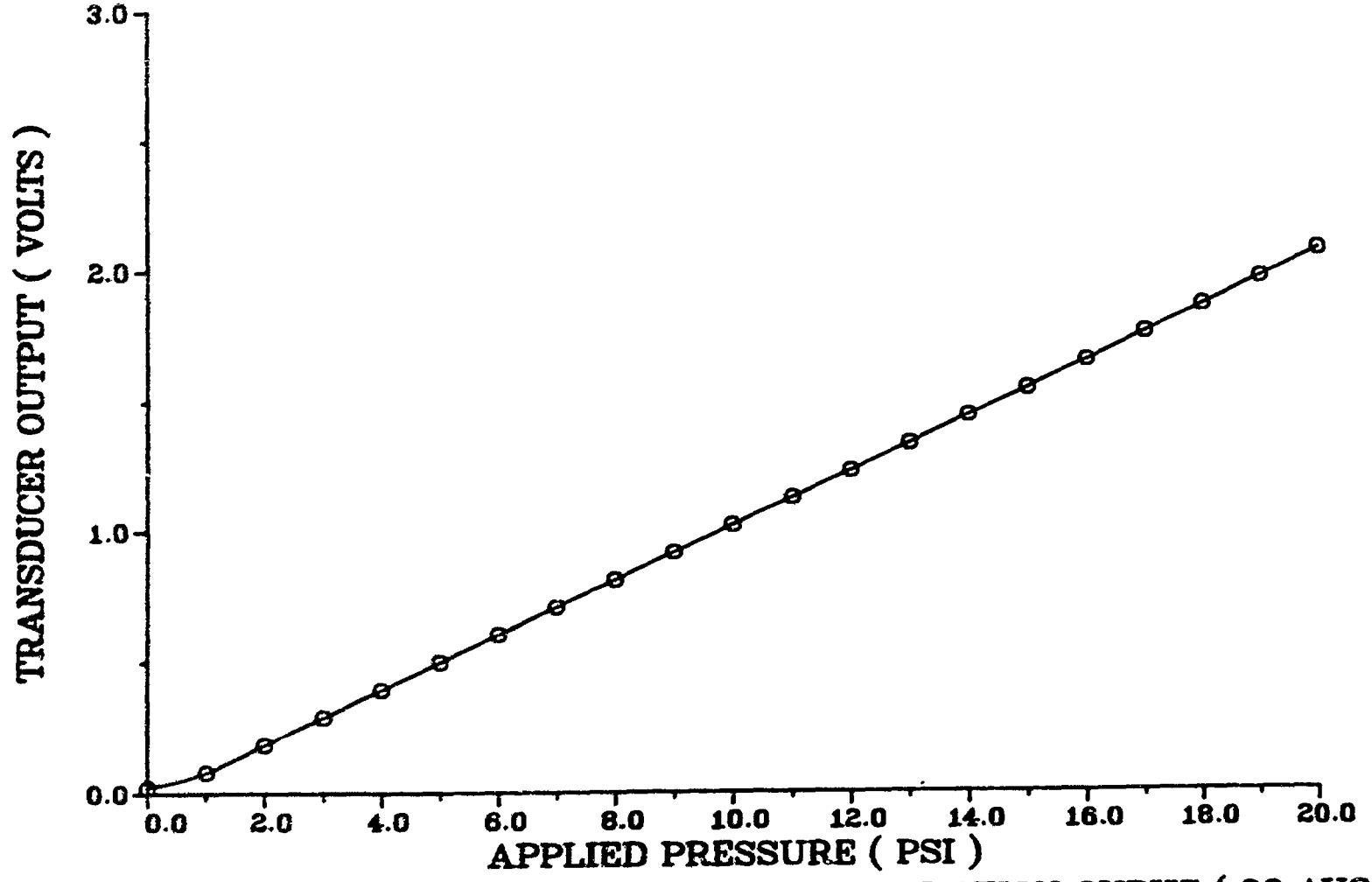

FIGURE B-6. DRUCK TRANSDUCER CALIBRATION CURVE (30 AUG 85)
(SN 12625)

Table B-1. ZOC Transducer Calibration Data

Applied Pressure (psig)	(1) 4 Mar 85 Transducer Output (Volts)	(2) 22 May 85 Transducer Output (Volts)
0	-87.0 (E-3)	-78.1(E-3)
1.0	0.3019	0.3132
2.0	0.6905	0.7045
3.0	1.0789	1.0957
4.0	1.4675	1.4872
5.0	1.8555	1.8788
6.0	2.2452	2.2703
7.0	2.6333	2.6614

(1) $f(x) = A1 + A2*x$

$A1 = -0.0869$
$A2 = 0.3886$

(2) $f(x) = A1 + A2*x$

$A1 = -0.0783$
$A2 = 0.3914$

Table B-2. DRUCK Transducer Calibration Data

Applied Pressure (psig)	SN 10135 (1) 4 Mar 85 Transducer Output (Volts)	SN 10135 (2) 22 May 85 Transducer Output (Volts)	SN 12625 (3) 30 Aug 85 Transducer Output (Volts)
0	-0.0295	-0.0256	0.0219
1.0	0.2211	0.2180	0.0824
2.0	0.4718	0.4683	0.1865
3.0	0.7224	0.7186	0.2907
4.0	0.9732	0.9691	0.3949
5.0	1.2242	1.2194	0.4992
6.0	1.4750	1.4699	0.6034
7.0	1.7250	1.7203	0.7076
8.0	1.9760	1.9710	0.8111
9.0	2.2268	2.2213	0.9161
10.0	2.4771	2.4715	1.0203
11.0	2.7286	2.7218	1.1247
12.0	2.9792	2.9731	1.2288
13.0	3.2303	3.2244	1.3331
14.0	3.4812	3.4740	1.4374
15.0	3.7321	3.7246	1.5417
16.0	3.9831	3.9755	1.6462
17.0	4.2340	4.2259	1.7504
18.0	4.4850	4.4768	1.8547
19.0	4.7361	4.7276	1.9591
20.0	4.9865	4.9775	2.0631

(1) $f(x) = A1 + A2*x$

$A1 = -0.0301$
$A2 = 0.2508$

(2) $f(x) = A1 + A2*x$

$A1 = -0.0318$
$A2 = 0.2504$

(3) $f(x) = A1 + A2*x$

$A1 = -0.0144$
$A2 = 0.1037$

Appendix C

ZOC Optimization FORTRAN Steering Program

This appendix contains a listing of the steering program written to determine the optimum internal dimensions for the ZOC14 transducer to be used in the NASA program.

```
         COMPILER OPTIONS - NAME=  MAIN,OPT=00,LINECNT=60,SIZE=0000K,
                          SOURCE,EBCDIC,NOLIST,NODECK,LOAD,MAP,NOEDIT,ID,NOXREF
ISN 0002            DIMENSION D(10),XL(10),V(10),DVDP(10),P(10),RHO(10),VIS(10)
                   C,HZ(1000),ARATIO(1000),PHASE(1000),DC(1000)
ISN 0003            COMMON/GEOMTY/D(10),XL(10),V(10),DVDP(10)
ISN 0004            COMMON/THERMC/GAMMA,P(10),RHO(10),VIS(10),AMPRES
                C
                C     THIS IS DATA SET LARRY3.CNTL
                C
ISN 0005            REAL MINERR,MAXFRE,INCVOL,INCXL2,INCDIA,MINDF,LENMIN,LMINDF
ISN 0006            LOGICAL COARSE
                C
                C  INITIALIZE VARIABLES
                C
ISN 0007               N=1
ISN 0008               PR=1.8345
ISN 0009               TR=1.00566
ISN 0010               PREF=9859E7C.95
ISN 0011               XL(1)=25.4
ISN 0012               D(1)=.05CE
ISN 0013               V(1)=0.0665
ISN 0014               XL(2)=6.25
ISN 0015               D2INIT=.0005
ISN 0016               D(2)=D2INIT
ISN 0017               VINIT=1.CE-5
ISN 0018               V(2)=VINIT
ISN 0019               RM24AR=1.15
ISN 0020               RM24FR=12C.0
ISN 0021               COARSE=.TRUE.
ISN 0022            DF=10.0
ISN 0023            GAMMA=1.4
ISN 0024            TREF=53C.C
ISN 0025            T=TR*TREF
ISN 0026            AMPRES=PREF*PR
ISN 0027            VIS(1)=.0001824*(T/531.)**1.5*(729./(T+198.))
ISN 0029            RHO(1)=1.2C4SE-3*PR/TR
ISN 0029                  DO 10 I=1,10
ISN 0030                     RHO(I)=RHO(1)
ISN 0031                     VIS(I)=VIS(1)
ISN 0032                     P(I)=.70
ISN 0033                     DVDP(I)=C.
ISN 0034         10 CONTINUE
ISN 0035            PI=3.14159
ISN 0036            F=E.=0.
ISN 0037            AMPEAK=C.
ISN 0038            MINERR=100.
ISN 0039            MINDF=1000.
ISN 0040            FREQER=100.
ISN 0041            INCXL2=0.25
ISN 0042            INCVOL=5.0E-7
ISN 0043            INCDIA=5.0E-3
ISN 0044            XL2MAX=12SC
ISN 0045            DIAMAX=.1J6C
ISN 0046            VMAX=.1C
ISN 0047            FAC=1.0
ISN 0048            INCJ=2
                C
                C  CONVERT LENGTHS, DIAMETERS, AND PRESSURES TO ENGLISH UNITS FOR THE
```

```
                C  BANNER PAGE PRINTOUT.
                C
ISN 0049            EUXL1=XL(1)/2.54
ISN 0050            EUD1=D(1)/2.54
ISN 0051            EUV2=V(2)/2.54**3
ISN 0052            EUXL2=XL(2)/2.54
ISN 0053            EUD2=D(2)/2.54
ISN 0054            EUPREF=PREF*145.04E-7
ISN 0055            EUXLMX=XL2MAX/2.54
ISN 0056            EUDIMX=DIAMAX/2.54
ISN 0057            EUVMAX=VMAX/2.54**3
                C
                C  PRINT A HEADER PAGE CONTAINING THE SETUP INFORMATION.
                C
ISN 0058            WRITE(6,100)EUXL1,XL(1),EUD1,D(1),PR,TR,EUPREF,
                   &PREF,EUVMAX,VMAX,EUXL2,EUXLMX,XL(2),XL2MAX,EUD2,
                   &EUDIMX,D(2),DIAMAX
                C
                C  PRINT COLUMN HEADERS FOR THE OUTPUT PAGE.
                C
ISN 0059            30 IF (N .EQ. 1) WRITE(6,500)
ISN 0061               IF (N .NE. 1) WRITE(6,200)
                C
                C  DO THE CALCULATIONS BY CALLING AMPPHS OVER A 200 HZ FREQUENCY RANGE
                C  FOR A GIVEN VOLUME, THEN INCREMENTING THE VOLUME AND REPEATING
                C  THROUGHOUT THE ENTIRE VOLUME RANGE.  THESE CALCULATIONS WILL FIND THE
                C  VALUE AND FREQUENCY FOR THE MAXIMUM AMPLITUDE RATIO PEAK AND COMPARE
                C  THIS INFORMATION TO THE VALUES OBTAINED EXPERIMENTALLY.  THE RELATIVE
                C  ERROR BETWEEN THE TWO VALUES OF PEAK AMPLITUDE RATIO IS DETERMINED
                C  ALONG WITH THE DIFFERENCE BETWEEN THE TWO FREQUENCIES AT WHICH THESE
                C  PEAKS OCCUR.
                C
ISN 0063            6 FREQ=FREQ+CF
ISN 0064              IF(FREQ .GT. 200.) GO TO 2
ISN 0066              CALL AMPPHS(FREQ,A,PA,I,N)
ISN 0067              IF(A .GT. ARPEAK) GO TO 4
ISN 0069              GO TO 6
                C
ISN 0070            4 ARPEAK=A
ISN 0071              MAXFRE=FREQ
ISN 0072              GO TO 6
                C
ISN 0073            2 AREER=RELERR(ARPEAK,RM24AR)
ISN 0074              DELTAF=ABS(MAXFRE-RM24FR)
ISN 0075              IF (DELTAF .LE. MINDF) GO TO 22
ISN 0077           23 IF (AREER .LT. MINERR) GO TO 8
ISN 0079              GO TO 14
                C
ISN 0080           22 IF (DELTAF .LT. MINDF  .OR.  AREER .LT. FREQER) GO TO 36
ISN 0082              GO TO 23
                C
ISN 0083           36 MINDF=DELTAF
ISN 0084              VMINDF=V(N)
ISN 0085              DMINDF=D(N)
ISN 0086              LMINDF=XL(N)
ISN 0087              FREQER=AREER
ISN 0088              GO TO 28
                C
```

```
C  PRINT THE RESULTS FOR THIS VOLUME, DIAMETER, AND LENGTH
C
ISN 0089        14 WRITE(6,300)C(N),XL(N),V(N),ARPEAK,MAXFRE,ARERR,DELTAF
C
C  INCREMENT THE VOLUME AND REPEAT
C
C  SKIP THE VOLUME INCREMENT SECTION IF THIS IS A SINGLE TUBE/
C  VOLUME SYSTEM (N=1)
C
ISN 0090           IF (N .EQ. 1) GO TO 18
C
C  CHECK TO SEE IF THE VOLUME INCREMENT IS COARSE OR FINE AND BRANCH
C  TO THE APPROPRIATE LOCATION
C
ISN 0092           IF (COARSE) GO TO 24
C
C  THIS IS THE LOOP FOR A FINE VOLUME INCREMENT
C
ISN 0094           V(N)=V(N)+INCVOL
ISN 0095           IF (V(N) .GT. VMAX) GO TO 12
ISN 0097           FREQ=0.
ISN 0098           ARPEAK=0.
ISN 0099           GO TO 6
C
C  THIS IS THE COARSE VOLUME INCREMENT FOR ALL PASSESEXCEPT THE FIRST
C
ISN 0100        24 J=J+INCJ
ISN 0101           IF (J .GT. 10) GO TO 34
ISN 0103           V(N)=VINIT*FAC*FLOAT(J)
ISN 0104           IF (V(N) .GT. VMAX) GO TO 12
ISN 0106           FREQ=0.
ISN 0107           ARPEAK=0.
ISN 0108           GO TO 6
ISN 0109        34 FAC=FAC*10.
ISN 0110           J=0
ISN 0111           GO TO 24
C
ISN 0112         8 MINERR=ARERR
ISN 0113           VOLMIN=V(N)
ISN 0114           FREMIN=MAXFRE
ISN 0115           DIAMIN=C(N)
ISN 0116           LENMIN=XL(N)
ISN 0117           GO TO 14
C
C  PRINT THE MINIMUM RELATIVE ERROR, THE VOLUME ASSOCIATED WITH THE
C  MINIMUM ERROR, AND THE FREQUENCY FOR THE MINIMUM ERROR AFTER
C  SWEEPING THROUGH THE ENTIRE RANGE OF VOLUMES
C
C  INCREMENT THE DIAMETER
C
ISN 0118        12 C(N)=C(N)+INCDIA
ISN 0119           IF(C(N) .GT. DIAMAX) GO TO 16
ISN 0121           FREQ=0.
ISN 0122           ARPEAK=0.
ISN 0123           V(N)=VINIT
ISN 0124           J=0
ISN 0125           FAC=1.0
ISN 0126           GO TO 30
```

```
C
C  INCREMENT XL(N) AND REPEAT THE PROCESS
C
ISN 0127        16 XL(N)=XL(N)+INCXL2
ISN 0128           IF (XL(N) .GT. XL2MAX) GO TO 26
ISN 0130           FREQ=0.
ISN 0131           ARPEAK=0.
ISN 0132           V(N)=VINIT
ISN 0133           D(N)=D2INIT
ISN 0134           J=0
ISN 0135           FAC=1.0
ISN 0136           GO TO 30
ISN 0137        26 WRITE(6,600)MINDF,VMINDF,DMINDF,LMINDF,FREQER
ISN 0138        18 WRITE(6,400)MINERR,FREMIN,VOLMIN,DIAMIN,LENMIN
C
C  IF N=1, INCREMENT N, REINITIALIZE VARIABLES AND REPEAT FOR THE
C  NEXT TUBE/VOLUME SYSTEM
C
ISN 0139           IF (N .NE. 1) GO TO 20
ISN 0141           N=N+1
ISN 0142           D(N)=D2INIT
ISN 0143           V(N)=VINIT
ISN 0144           V(1)=0.0
ISN 0145           FREQ=0.
ISN 0146           ARPEAK=0.
ISN 0147           MINERR=1000.
ISN 0148           MINDF=1000.
ISN 0149           FREQER=1000.
ISN 0150           J=0
ISN 0151           GO TO 30
C
C  FORMAT SECTION
C
ISN 0152        100 FORMAT(///,T50,32('*'),/,T50,'*',1X,'ZCC MODELLING PROGRAM OUTPUT'
                   &,1X,'*',/,T50,32('*'),///,T51,'INPUT DATA AND TEST CONDITIONS',/,
                   &1H+,T51,30('_'),///,T35,'TEST TUBE LENGTH - ',F4.1,1X,'IN.',2X,
                   &'(',F4.1,' CM)',///,T35,'TEST TUBE DIAMETER - ',F5.3,' IN.',
                   &'  (',F6.4,' CM)',///,T35,'PR - ',F6.4,//,T35,'TR - ',F7.5,//,T35,
                   &'REFERENCE PRESSURE - ',F6.3,' PSI','  (',F10.2,' DYNE/SQ. CM)',
                   &///,T54,'ZCC MODELLING PARAMETERS',/,1H+,T54,24('_'),//,T35,
                   &'ZCC INTERNAL VOLUME - 0.0 TO ',F6.4,' CU. IN.','  (',F6.4,' CU.',
                   &' CM)',//,T35,'ZCC INTERNAL TUBING DIMENSIONS',//,T40,'LENGTH -',
                   &F7.4,' TO ',F7.4,' IN.','  (',F9.6,' TO ',F9.6,' CM)',//,T40,
                   &'DIAMETER - ',F9.6,' TO ',F9.6,' IN.','  (',F9.6,' TO ',F9.6,
                   &' CM)',/,1H1)
C
ISN 0153        200 FORMAT(///,T3,'ZCC DIAMETER',4X,'ZCC LENGTH',4X,'ZCC VOLUME',4X,
                   &'PEAK AMPLITUDE RATIO',4X,'FREQUENCY FOR PEAK AR',4X,
                   &'RELATIVE ERROR',4X,'DELTA FREQUENCY',//,T6,'( CM )',T21,'( CM )',
                   &T33,'( CU. CM )',T76,'( HZ )',T103,'( % )',T117,'( HZ )',/)
C
ISN 0154        300 FORMAT(T4,F10.7,T20,F10.7,T34,F10.7,T53,F6.4,T77,F8.4,T98,F8.4,
                   &T116,F8.4)
C
ISN 0155        400 FORMAT(//,1X,'THE MINIMUM RELATIVE ERROR IS ',12X,F10.5,/,1X,
                   &'THE FREQUENCY FOR MINIMUM RELATIVE ERROR IS ',F8.3,/,1X,
                   &'THE VOLUME FOR MINIMUM RELATIVE ERROR IS ',3X,F9.6,/,1X,
                   &'THE DIAMETER FOR MINIMUM RELATIVE ERROR IS ',1X,F10.7,/,1X,
```

```
     &'THE LENGTH FOR MINIMUM RELATIVE ERROR IS ',3X,F10.7)
C
ISN 0156      500 FORMAT(///,13,'TUBE DIAMETER',4X,'TUBE LENGTH',4X,'ZOL VOLUME',4X,
     &'PEAK AMPLITUDE RATIO',4X,'FREQUENCY FOR PEAK AR',4X,
     &'RELATIVE ERROR',4X,'DELTA FREQUENCY',/,T6,'( CM )',T21,'( CM )',
     &T33,'( CU. CM )',T78,'( HZ )',T100,'( % )',T117,'( HZ )',/)
C
ISN 0157      600 FORMAT(//,1X,'THE MINIMUM FREQUENCY DIFFERENCE IS ',20X,F12.6,/,
     &1X,'THE VOLUME FOR MINIMUM FREQUENCY DIFFERENCE IS ',8X,F10.7,/,
     &1X,'THE DIAMETER FOR MINIMUM FREQUENCY DIFFERENCE IS ',6X,F10.7,/,
     &1X,'THE LENGTH FOR MINIMUM FREQUENCY DIFFERENCE IS ',6X,F10.7,/,
     &1X,'THE RELATIVE ERROR FOR MINIMUM FREQUENCY DIFFERENCE IS ',
     &F10.5)
C
ISN 0158        20 STOP
ISN 0159           END
```


U.S. Government Printing Office: 1990—748-056/24263